ALMA MATER STUDIORUM –UNIVERSITÀ DI BOLOGNA

DOTTORATO DI RICERCA IN

IL FUTURO DELLA TERRA, CAMBIAMENTI CLIMATICI E SFIDE SOCIALI

Ciclo 35

Settore Concorsuale: 04/A4 - GEOFISICA

Settore Scientifico Disciplinare: GEO/10 - GEOFISICA DELLA TERRA SOLIDA

ANALYSIS OF EARTHQUAKES PREDICTABILITY

Presentata da: Emanuele Biondini

Coordinatore Dottorato
Silvana Di Sabatino

Supervisore
Paolo Gasperini

Esame finale anno 2023

Abstract

Deterministic earthquake prediction has proven to be an extremely complex problem for scientists. Improving the ability to predict earthquakes is one of the major challenges for Seismology and a key goal for the protection of properties, infrastructure, and people inhabiting Earth's areas characterized by high seismic risk. Full knowledge and understanding of the phenomenon are necessary for earthquake predictions to be reliable. However, this poses a nontrivial problem for the scientific community since strong earthquakes are relatively rare compared to other natural phenomena and occur at inaccessible depths. In this thesis, the development, application, and comparison of both deterministic and probabilistic forecasting methods is shown.

Regarding the deterministic approach, the implementation of an alarm-based method using the occurrence of strong (fore)shocks, widely felt by the population, as a precursor signal is described. This model is then applied for retrospective prediction of Italian earthquakes of magnitude M≥5.0,5.5,6.0, occurred in Italy from 1960 to 2020. Retrospective forecasting performance is evaluated using tests and statistics recognized in the literature and specific for deterministic alarm-based models.

Regarding probabilistic models, this thesis focuses mainly on the EEPAS (Every Earthquake a Precursor According to Scale) and ETAS (Epidemic Type Aftershock Sequence) models. Although the EEPAS model has been previously applied and tested for some regions of the world, it has never been applied for the forecast of Italian earthquakes. Therefore, in this thesis, the EEPAS model is applied to the retrospective forecast of Italian shallow earthquakes of magnitude M≥5.0 using a new software developed in MATLAB. The retrospective forecasting performance of the treated probabilistic models was compared with that of other models both time dependent and time independent using the new CSEP tests based on the negative

binomial distribution. The EEPAS and ETAS models applied for forecasting Italian earthquakes show different characteristics. In particular, the EEPAS and ETAS models seem to have better forecasting performance in the long and short period, respectively.

The deterministic model based on the occurrence of strong (fore)shocks (called FORE) is compared with the EEPAS and ETAS models using the alarm-based deterministic approach. The comparison and evaluation analyses show that all models overperform a random forecasting model. However, evaluation of relative performance suggests better forecasting power for the ETAS and FORE models.

To realistically evaluate the forecasting performance of all models, however, prospective tests should be conducted. One of the main problems that emerged during the development of this thesis is the lack of objective prospective CSEP tests for evaluating deterministic models and comparing them with probabilistic ones.

Contents

Chapter 1

Introduction on main characteristics of earthquakes and properties of occurrence

Earthquakes have affected the Earth since the formation of the solid crust 4 billion years ago and have plagued humanity since the construction of the first village. Earthquakes, most caused by the movement of tectonic plates that have characterized every step in the formation of mountain ranges, oceans, and continental drift, are evidence of the dynamism of planet Earth (Marshak, 2004).

1.1 Elastic rebound theory

Earthquakes are rapid movement of the Earth due to a sudden release of potential deformation energy by the lithosphere. An earthquake is therefore the consequence of the breaking of rocks and is felt through the shaking of the ground. The mechanism of earthquake generation can be explained by the elastic rebound model proposed by Reid (1910) from the observation of geodetic data and information analyzed during and after the 1906 San Francisco earthquake of magnitude 7.8. According to the elastic rebound model, lithospheric rocks react elastically when subjected to differential stress. When the applied deformation stress exceeds the failure load, the rocks fail along one or more fault surface, i.e., a surface of weakness. When a failure occurs, the rocks suddenly readjust to reach a new potential state. The rock blocks, separated from the fault surface, continue their relative readjustment for a variable time frame until a new equilibrium condition is reached (Fig. 1.1). The sudden rearrangement of the rock volumes involved produces seismic waves that propagate in space and time as spherical wave fronts. Elastic rebound theory (Reid, 1910) assumes that rocks rupture and subsequent propagation of seismic waves begins at a certain time (origin time $t(0)$) and at a certain nucleation point in space (hypocenter) located at a certain depth along the fault plane. Analysis of most

destructive earthquakes shows that they generally occur at a depth of less than 50 km, although they can be deeper, where past earthquakes have already weakened the brittle rocks that constitute an active fault or in parts of cold lithosphere in subductuon zones, where the brittle-ductile transition is deeper than in a normal geothermal gradient. Estimation of hypocentral parameters requires a seismic network consisting of stations capable of recording arrival times and oscillations induced by seismic waves. The analysis of the arrival time of seismic waves generated by an earthquake from several stations makes it possible to estimate the latitude, longitude, depth, and origin time of the recorded earthquake.

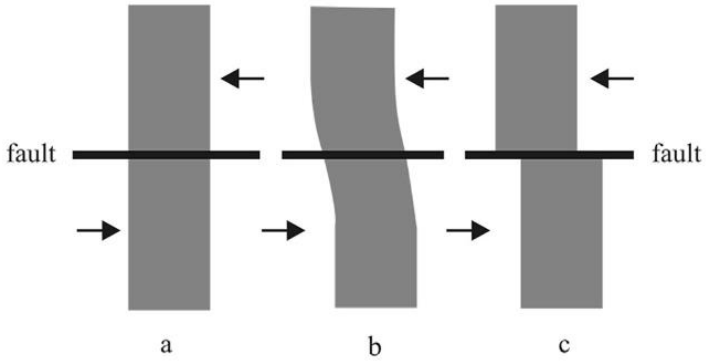

a–No slip potential accumulation

b– Interseismic slip potential accumulation (fault locking)

c– Coseismic slip potential release

Figure 1.1: Elastic rebound theory (Wei et al., 2015).

1.2 Seismic catalogues

Seismic catalogs represent one of the essential products made available by the agencies that manage, monitor, and analyze data deriving from seismic networks. A seismic network consists of instruments capable of recording waveforms and of other equipment able to process data related to the occurrences of seismic events (Fig. 1.2). Seismic catalog contains parametric information of earthquakes (latitude, longitude, depth, magnitude, and sometimes additional information such as focal mechanism)

that are recorded for a certain region. Such datasets are extremely important for analysis and research on seismicity patterns and seismic risk. However, each seismicity catalogue is the product of complex procedures that begin with the configuration of the seismic network, the choice of sensors and software to process the data, and the choice of a localization procedure and magnitude scale. The human-chosen computational tools and defined processing steps, combined with the spatial and temporal heterogeneity of the seismic network and seismicity, make catalogues inherently heterogeneous (Woessner et al., 2010). Seismic catalogues can be classified into different types (pre-historic, historic, and instrumental). Pre-historic seismic catalogues are based on geological information obtained by campaign observations and contain information on earthquakes that may have occurred even in past millennia. Historic seismic catalogues are based on information collected by historical archives that describe macro-seismic effects of earthquakes on population or buildings. By regression analysis of the observed intensity field it is possible to trace the location, origin time and magnitude of historical earthquakes with some reliability (Gasperini et al., 1999; Rovida et al., 2020, 2022). The instrumental seismic catalogs are datasets derived from primary instrumental data produced by seismologists who are able to process the data and record the occurrence of earthquakes and the related hypocentral parameters (origin time, longitude, latitude and depth) and magnitude (Woessner et al., 2010).

1.3 Magnitude scales

Since the development of the first magnitude scales by Richter (1935), different magnitude scales with different definitions and characteristics have been proposed (Lay and Wallace, 1995). The use of one or the other depends on the characteristics of a seismic network. One of the most used magnitude scale of greatest use is the local magnitude M_L, defined by Richter (1935). It is given by the ratio of the decimal logarithm of the maximum amplitude A (expressed in mm) recorded by a Wood-

Anderson torsion seismometer with a period of $0.8\,seconds$ and the maximum amplitude that the same instrument would have recorded for a standard earthquake A_0 (i.e. an earthquake of magnitude $M_L = 0$ which at $100\,km$ from the epicenter produces an amplitude of $10^{-3}\,mm$). For earthquakes occurring at different distances it is necessary to introduce corrections to scale A_0 relative to the effective distance from the station. These corrections consider the amplitude attenuation due to geometric spreading (Richter, 1935; Gutenberg and Richter, 1942; Jennings and Kanamori, 1983; Hutton and Boore, 1987; Di Stanza and Console, 2002; Gasperini, 2002; Lolli et al., 2015). Further corrections are applied considering that modern seismometers with different amplification and damping characteristics are currently used to estimate the local magnitude. Modern instruments can emulate the Wood-Anderson seismometers (synthesized Wood-Anderson) through adjustments. Other magnitude scales have been defined (Gutenberg and Richter, 1956) such as the body wave magnitude m_b based on the amplitude of body waves (P and S) and the surface wave magnitude M_S based on the amplitude of surface waves (Love and Rayleigh waves). However, these two magnitude scales are not appropriate for strong earthquakes because they tend to saturate for high magnitudes ($m_b > 5.0$, $M_S > 8$). Therefore, some of the earthquakes recorded in catalogs with such magnitude scales may have higher energy than reported (Woessner et al., 2010). The magnitude scale m_D (duration magnitude) is based on the duration of the phenomenon (Eaton, 1992), that is the time interval between the recording of the first pulse and the return to the background signal. Therefore, m_D does not depend on the amplitude of the peaks recorded by the seismograph, but on the duration of the phenomenon estimated by the seismogram. The duration magnitude is generally used to attribute the magnitude to low or medium earthquakes that occur locally or regionally and can be used in cases where the exact calibration of seismometers is not known. The definitions of the previous magnitude scales are purely empirical. Moreover, it has been observed that they tend to underestimate or overestimate the true magnitude. This depends on the physical characteristics of the instruments used for seismic wave

recordings. In fact, seismographs can record seismic waves in a certain frequency range. Earthquakes, produce seismic waves even at very low frequency, which cannot be correctly recorded by seismometers. This phenomenon increases with the energy released by the earthquake, so high magnitudes may be underestimated.

The introduction of the seismic moment magnitude Mw by Hanks and Kanamori (1979), made it possible to relate the magnitude with the physics of the phenomenon. Moment magnitude is based on the elastic rebound theory (Reid, 1910) under which a couple of forces applied symmetrically on the two blocks of a fault generates a torsional moment (seismic moment). In addition, from the relationship between Mw and seismic moment, it is possible to empirically estimate the parameters like the length, width, and area of the fault, and the co-seismic displacement. Wells and Coppersmith (1994) showed consistency between the estimation of these parameters and observations.

1.4 Heterogeneity of seismic catalogues

The data logging capacity of a seismic network (Fig. 1.2) depends strongly on the density and number of stations in the area, their operating status, logging characteristics and the degree of connection with data processing headquarters. The choice of using a certain magnitude scale rather than another depends on the characteristics of the network. Often different definitions of magnitude may be used for a single network. This inevitably leads to heterogeneous seismic catalogs. This heterogeneity produces artefacts in the analysis of the statistical distribution of magnitudes and in other uses of seismic catalogues, such as the application and testing of seismicity models. Therefore, variations in the measured rate of seismicity can result from both natural and man-made causes. It is important to differentiate them as much as possible to identify significant and real rate changes in seismicity studies (Habermann, 1987; Matthews and Reasenberg, 1988). Man-made changes can

be caused by transitions of a seismic network, which include changes in station coverage, type of magnitude reported, improved seismic wave attenuation models, instrumentation, and automation (e.g., analog, and digital data processing waveform). Such changes occasionally become apparent and can be noticed by analyzing systematic temporal variations in the magnitude-frequency distribution of earthquakes (Habermann, 1982). Heterogeneities are not only related to individual seismic catalogs, but different catalogs produced by different networks are heterogeneous with respect to each other. In fact, although the local M_L magnitude is most commonly used, it is not directly comparable across different seismic catalogs because the estimation considers local characteristics and may involve the use of different techniques. However, heterogeneities are also related to the different methods of estimating hypocentral parameters.

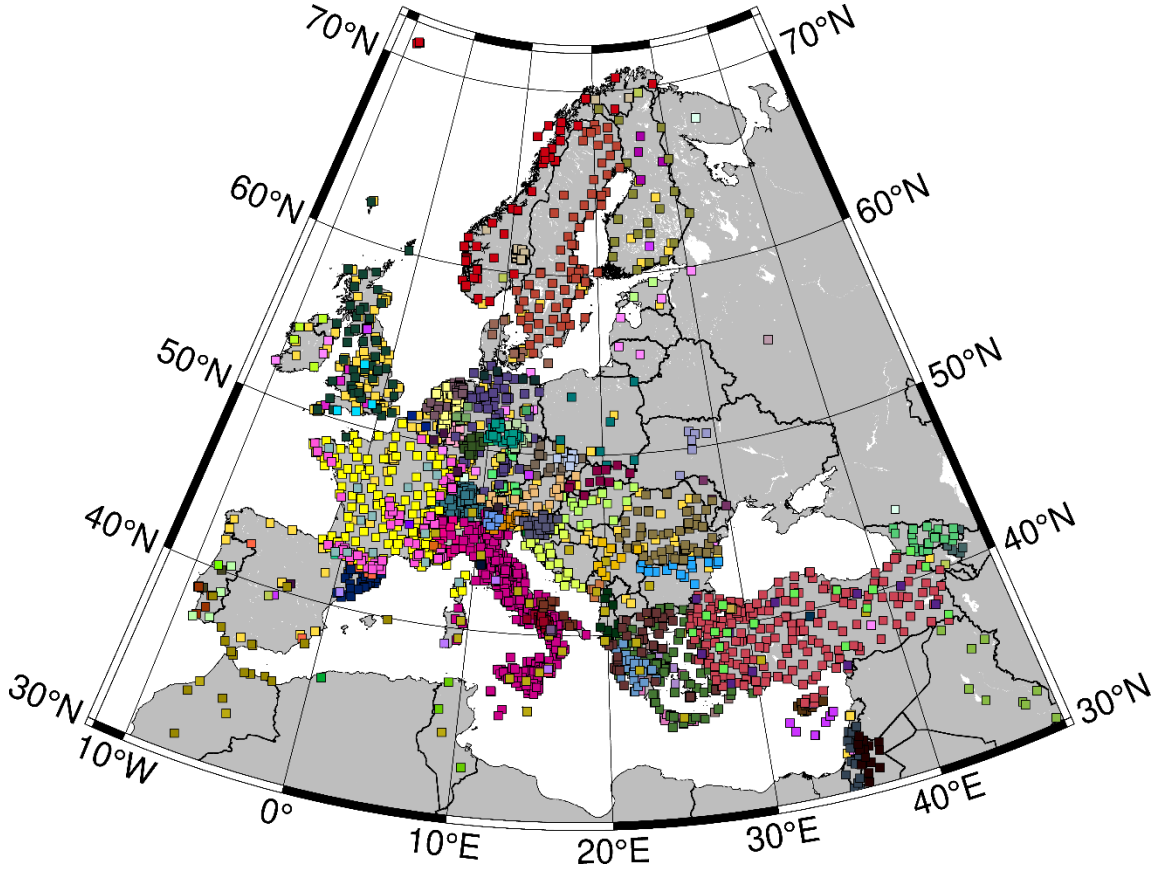

Figure 1.2: Map of seismic networks present in the Euro-Mediterranean region indicated with different colors. Data on seismic stations are available on the web services of IRIS (Incorporated Research Institutions for Seismology, https://www.iris.edu/hq/).

1.5 Properties of occurrence of earthquakes

Analysis of data recorded from long-term seismic catalogs makes it possible to observe and analyze the typical occurrence behavior of earthquakes such as the relationship between high-magnitude and low-magnitude earthquakes, spatiotemporal clustering, or the behavior of seismicity before or after a strong earthquake.

1.5.1 Earthquakes as a Poisson point processes

Earthquakes are represented in space and time as points marked by their magnitude. This allows us to consider earthquakes as point processes. Point processes are widely used in probability theories to model spatiotemporal data (Daley and Vere-Jones, 2008) and are widely used in many disciplines such as ecology, epidemiology, geography, telecommunications, and others. Mathematically, a point process is a countable set of points randomly distributed in a certain space-time domain (Fig. 1.3), therefore, it can be considered as a stochastic model that defines probabilistic rules for the occurrence of points (e.g., earthquakes) in time and space (Zhuang et al., 2012). In fact, if we compress the time axis of the seismograph to view all earthquake records on a large time scale, the waveforms of each strong earthquake become independent pulses randomly distributed over time (Zhuang et al., 2012). The hypothesis of complete temporal randomness assumes that the number of events in each time window follows the Poisson distribution with a certain expected number of events λ in the unit of time. A stationary Poisson process is usually considered a fundamental assumption of many probabilistic seismic hazard analysis (Cornell, 1968). However, in the short-medium term earthquakes tend to occur in clusters and strong earthquakes are always followed by aftershocks that have some relation to the mainshock. Analysis of clustered seismic events has shown that in global (Aki, 1956) or local (Knopoff, 1964) catalogs the events of the main sequences are significantly non-poissonian. This conclusion is important for earthquake forecasting, since the

demonstration of non-randomness in earthquake catalogs gives hope that a basis can be found for predicting the timing of occurrence by decoding the sequential message in the list of events. Gardner and Knopoff (1974) investigated seismicity in Southern California after removal of the aftershock clusters founding Poissonian behavior.

Considering $N(a,b)$ as the number of earthquakes of a point process occurred in a certain temporal window $t(a,b)$, the processes can be considered as Poissonian if:

i) The number of events m and k occurring in disjoint temporal windows are independent.

$$P\{N(a,b)=m, \quad N(c,d)=k\} = P\{N(a,b)=m\}\,P\{N(c,d)=k\} \tag{1.1}$$

ii) The probability distribution of N events occurring in a certain time window depend only on its length.

iii) The probability of two or more events occurring simultaneously is considered negligible i.e., two or more events cannot occur simultaneously.

The Poisson process is considered stationary or homogeneous if the probability that N events occurring within a certain time window of τ extent, follow the Poisson distribution

$$P\{N(a,a+\tau)=k\} = \frac{(\lambda\tau)^k}{k!}\exp(-\lambda\tau) \tag{1.2}$$

where λ is the average rate of occurrence in an interval of unit length and λ is constant in time. A non-stationary Poisson process is instead characterized by a time dependent rate $\lambda(t)$. Therefore, in this case, the probability distribution of N events in each time window depends on the $\lambda(t)$ and the processes cannot be stationary. In a non-stationary Poisson process, the expected number of events for a certain time window of length $[t_1, t_2[$ is given by

$$\Lambda(t_1,t_2) = \int_{t_1}^{t_2}\lambda(t)dt \tag{1.3}$$

and the probability to observe k events in the time interval $[t_1, t_2[$ is given by

$$P\{N(t_1,t_2]=k\} = \frac{[\Lambda(t_1,t_2)]^k}{k!}\exp[-\Lambda(t_1,t_2)]\,. \tag{1.4}$$

The nonstationary Poisson process can be used as an alternative to the stationary Poisson model when an apparent trend or seasonality is visible in the data (Zhuang et al., 2012).

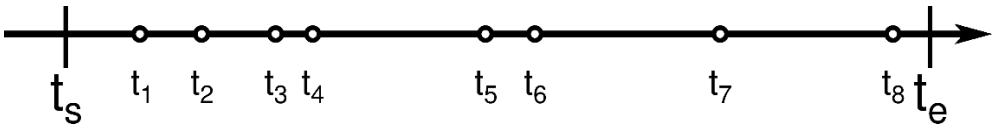

Figure 1.3: Sequence of ordered points within a given time window.

1.5.2 Maximum Likelihood Estimation (MLE) for a Poisson point process

Given an observed point process containing N events occurring at times $t = \{t_1, t_2, \dots, t_n\}$ within a given time interval $[t_s, t_e[$ (fig. 1.3), each $i-th$ time of occurrence can be taken as an infinitesimal interval $\tau_i = [t_i,\ t_i + \delta t[$. The likelihood function (Akaike, 1998; Myung, 2003) is determined by the joint probability to observe each $i-th$ event in the time interval τ_i and to not observe any event in the time range $]\, t_i,\ t_{i+1}[$. Considering a non-stationary Poisson process characterized by an intensity function $\lambda(t)$, the probability to observe an event in τ_i is given by

$$P\{n(\tau_i) = 1\} \approx \lambda(t_i)\delta t + o(\delta t) \tag{1.5}$$

and the probability to observe zero events in the time range $]t_i,\ t_{i+1}[$ is given by

$$P\{n(\, t_{i-1}\, , t_i) = 0\} = \exp\left[-\int_{t_i}^{t_{i+1}} \lambda(t)\, dt\right]. \tag{1.6}$$

Such probabilities can be derived from eqs. 1.2 and 1.4. Considering that in a Poisson process the occurrence of events are assumed disjoint, the likelihood function is equal to

$$L(t_i; N) = \prod_{i=1}^{N} [\lambda(t_i)\delta t] \prod_{i=1}^{N-1} \exp\left[-\int_{t_i}^{t_{i+1}} \lambda(t)\, dt\right] = \tag{1.7}$$

$$= (\delta t)^N \prod_{i=1}^{N} [\lambda(t_i)] \prod_{i=1}^{N-1} \exp\left[-\int_{t_i}^{t_{i+1}} \lambda(t)\, dt\right].$$

To simplify algebraical resolution, the application of the natural logarithm is preferable, and the log-likelihood function become:

$$logL(t_i;N) = \sum_{i=1}^{N} log[\lambda(t_i)\delta t] - \sum_{i=1}^{N-1} \int_{t_i}^{t_{i+1}} \lambda(t)\, dt = \tag{1.8}$$

$$= \mathrm{N}\log(\delta t) + \sum_{i=1}^{N} log[\lambda(t_i)] - \int_{t_s}^{t_e} \lambda(t)\, dt\ .$$

In many applications and in the literature (e.g. Ogata, 1983) the likelihood function is used to estimate the optimal parameters of a model that assumes a certain parametric probability distribution $p(x,\theta)$, given some observed data $x = \{x_1, \dots, x_n\}$. The optimal parameters are found by estimating the maximum of the likelihood function (MLE). Considering a set of function $cL(x,\theta)$ where c is a multiplicative constant, their maximum value is obtained for the same θ. For the MLE, the constant multiplicative term $(\delta t)^N$ in the equation (1.7) can be neglected and the equation to maximize is then:

$$L'(t_i;N) = \prod_{i=1}^{N} [\lambda(t_i)] \prod_{i=1}^{N-1} \exp\left[-\int_{t_i}^{t_{i+1}} \lambda(t)\, dt\right] \tag{1.9}$$

or if the log-likelihood is preferable:

$$logL'(N;t_s,t_e) = \sum_{i=1}^{N} log[\lambda(t_i)] - \int_{t_s}^{t_e} \lambda(t)\, dt\ . \tag{1.10}$$

1.5.3 Frequency-magnitude relationship of earthquake occurrence (The Gutenberg-Richter law)

The frequency-magnitude relationship of earthquakes, known as the Gutenber-Richter law (GR, Gutenberg and Richter, 1944) is an empirical relation that represents one of the foundations of modern seismology. The GR describes the occurrence of earthquakes in a certain space-time domain as a function of magnitude. In particular,

the number (N) of earthquakes decreases exponentially as the magnitude (M) increases according to the relationship:

$$Log_{10}[N(M)] = a - bM \tag{1.11}$$

$$N(M) = 10^{a-bM} \tag{1.12}$$

The a-value describes the overall level of seismicity in the region of interest. Its value therefore depends on the seismic characteristics of the area and catalog considered. The b-value represent the relative proportion between high and low magnitude seismic events. Generally, over long periods its value is around 1. High values of b ($b > 1$) indicate a high proportion of low-magnitude events in an earthquake dataset, and conversely ($b < 1$) indicates a high proportion of high-magnitude events. The commonly used forms for visualizing the magnitude-frequency relationship are the cumulative and incremental non-cumulative magnitude-frequency distribution (FMD) curves. The cumulative FMD described by the equation (1.12) is showed in Fig. 1.4 with light grey and red circles provide the number of earthquakes with $m > M$. On the other hand, the non-cumulative or incremental FMD, represented in the same figure by grey and light blue triangles provide the numbers of earthquake with a certain magnitude range. Usually, magnitudes are binned so their value is within the range $\left[M - \frac{dM}{2}, M + \frac{dM}{2}\right]$ where dM is the magnitude bin. The two parameters a-value and b-value, represent the number of earthquakes with magnitude $m \geq 0$ and the slope of the cumulative FMD, respectively. The exponential distribution (1.12) is in principle valid for each magnitude. However, seismic networks are not completely able to detect all earthquakes whose magnitude is lower than a certain M_{min}. As is evident in Fig. 1.4, for $m < M_{min}$ the FMD distributions deviate from the theoretical exponential distribution due to a lack of such events in the seismic catalogue.

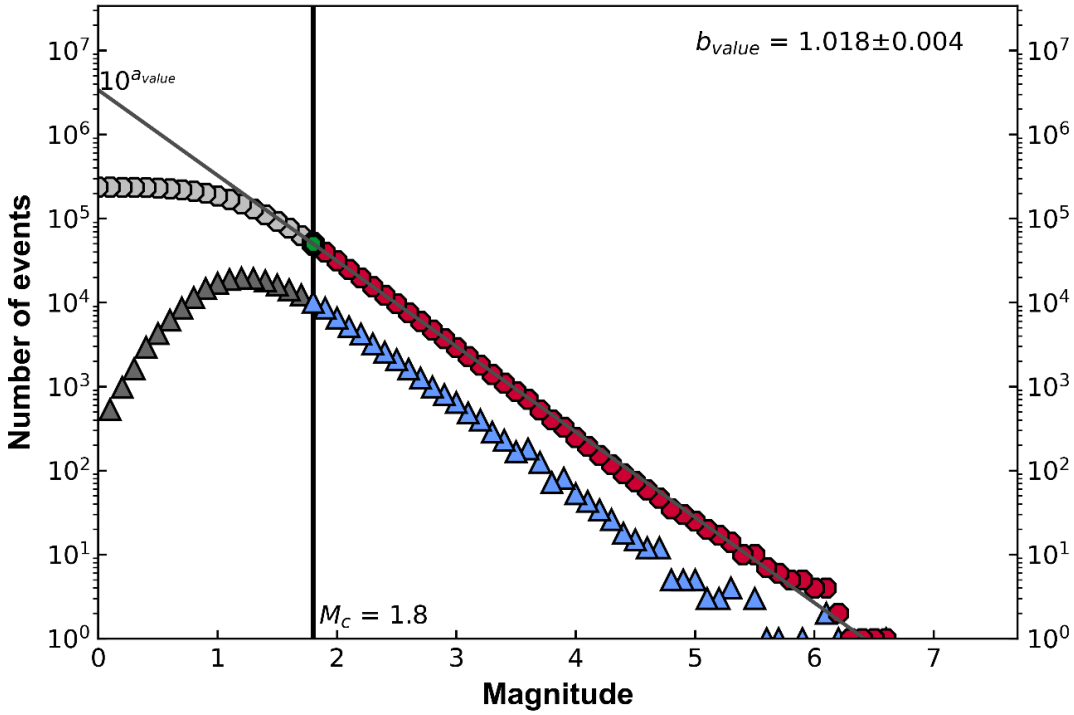

Figure 1.4: Cumulative (red dots) and non-cumulative (light blue triangles) frequency magnitude distribution (FMD) of Italian inland earthquakes reported by the Homogenized InstRUmental Seismic catalog (Lolli et al., 2020) for the period 2012-2022. As marked by gray dots and triangles, the FMD deviate from the exponential distribution for $m < M_{min}$ (indicated as completeness magnitude m_c).

1.5.4 The b-value Maximum Likelihood Estimation

The GR equations (1.11 and 1.12) can be also expressed in exponential form as:

$$\ln(N) = \alpha - \beta M \tag{1.13}$$

$$N(M) = e^{\alpha - \beta M} \tag{1.14}$$

Where $\alpha = \ln(10)\, a$ and $\beta = \ln(10)\, b$. Assuming that all recorded earthquakes are greater than a certain minimum magnitude M_{min}, the probability to detect an event of magnitude m is given by:

$$p(m|b) = \frac{N(m)}{\int_{M_{min}}^{+\infty} N(x)dx} = \frac{\exp(\alpha)\exp(-\beta m)}{\int_{M_{min}}^{+\infty} \exp(\alpha)\exp(-\beta x)\,dx} == \frac{\exp(-\beta m)}{-\frac{1}{\beta}\exp(-\beta x)\Big|_{M_{min}}^{+\infty}} \tag{1.15}$$

But $\lim_{x\to+\infty} -\beta^{-1}\exp(-\beta x) \to 0$ so the upper limit term of the integral is negligible, thus:

$$p(m|b) = \frac{\exp(-\beta m)}{\frac{1}{\beta}\exp(-\beta M_{min})} = \beta ex\, p[-\beta(m - M_{min})] \quad , \qquad M_{min} \leq m \tag{1.16}$$

or

$$p(m|b) = b\ log(10)\ 10^{-b(m-M_{min})}, \qquad M_{min} \leq m \tag{1.17}$$

Equations (1.16 and 1.17), however, unrealistically assume that earthquakes of any magnitude can be observed up to infinity (Bender, 1983). Considering the characteristics of the observational region a maximum magnitude threshold (M_{max}) can be fixed and from (1.15) we obtain:

$$p(m|b) = \frac{\beta\exp(-\beta m)}{\exp(-\beta M_{min}) - \exp(-\beta M_{max})} \quad , \qquad M_{min} \leq m \leq M_{max} \tag{1.18}$$

Equations (1.16) and (1.18) converge to the same value as the magnitude range becomes wider and usually, if $M_{min} \ll M_{max}$, the equations (1.16) or (1.17) are preferred.

Given a set of observed magnitudes that are statistically independent $m = \{m_1, m_2, \dots, m_i\}$ the likelihood function $L(m|b)$ is given by the product of each $i - th$ probability of observation (eq. 1.16 or 1.18). Therefore, the joint probability to observe the entire set of magnitudes m is given by:

$$L(m|b) = \prod_{i=1}^{n} p_i(m|b) \tag{1.19}$$

To simplify algebraical resolution, the application of the natural logarithm is preferable, and the log-likelihood estimation is given by:

$$logL(m|b) = \log\left[\prod_{i=1}^{n} p_i(m|b)\right] = \sum_{i=1}^{n} \log\big(p_i(m|b)\big) = \tag{1.20}$$

$$= \sum_{i=1}^{n} \log\big[b\ log(10)\ 10^{-b(m-M_{min})}\big] =$$

$$= \sum_{i=1}^{n} log[b\log(10)] - log\big[10^{-b(m-M_{min})}\big] =$$

$$= \sum_{i=1}^{n} log[b\log(10)] - \log(10)\, b(m_i - M_{min}) =$$

$$= n\ log[b\log(10)] + b\log(10)\left(n\ M_{min} - \sum_{i=1}^{n} m_i\right)$$

The optimal b-value is found using the MLE method (Aki, 1965), thus the derivative of $logL(b)$ is posed equal to 0.

$$\frac{d}{d\ b} logL(b) = 0 \tag{1.21}$$

$$\frac{d\ logL(b)}{d\ b} = \frac{n}{b} + n\ M_{min}\ \log(10) - \log(10)\sum_{i=1}^{n} m_i =$$

$$= \frac{1}{b\log(10)} + M_{min} - \frac{1}{n}\sum_{i=1}^{n} m_i = \frac{1}{b\log(10)} + M_{min} - \bar{m} = 0$$

The analytical solution of (1.21) was the formula proposed by Aki (1965)

$$b = \frac{\log_{10} e}{\bar{m} - M_{min}}. \tag{1.22}$$

where $\bar{m}$ is the mean value of the magnitude of the considered dataset. The equation proposed by Aki (1965) as described (1.22) assumes that magnitudes are a continuous quantity on the real number line. Although in principle this assumption is correct, magnitudes in seismic catalogs are generally given in incremental bins of finite width. The use of binned magnitudes requires the correction term $-\frac{dM}{2}$ in the original formula (Utsu, 1966) to avoid a bias in the b-value estimation

$$b = \frac{\log_{10} e}{\bar{m} - \left(M_{min} - \frac{dM}{2}\right)}, \qquad m \geq M_{min} \tag{1.23}$$

The standard deviation associated to the estimated b-value is given by the equation proposed by Shi and Bolt (1982):

$$\sigma_b = 2.30b^2\sqrt{\frac{\sum_{i=1}^{n}(m_i - \bar{m})^2}{n(n-1)}} \tag{1.24}$$

where n is the number of events used in estimating the b-value. Recently (van der Elst, 2021) demonstrated that the b-value of equation (1.23) obtained by the MLE (Aki, 1965) is only approximate, in particular for the discretized magnitudes. van der Elst (2021) proposed the exact equation:

$$b = \frac{1}{\log(10)\frac{dM}{2}} \coth^{-1}\left[\frac{1}{\frac{dm}{2}}\left(\bar{m} - M_{min} + \frac{dM}{2}\right)\right]. \quad (1.25)$$

1.5.5 Completeness magnitude

Even if the exponential distribution described by the GR (1.12) in principle should be followed by the FMD at each magnitude, they begin to diverge from the theorical distribution as the magnitudes become smaller. This is due to a lack of events in the dataset. This lack is due to the characteristic of the seismic network that is not able to detect all earthquakes with magnitude lower than a certain magnitude defined as completeness magnitude M_c. There are multiple causes for an earthquake to not being recorded:

i) The magnitude can be too small, and the signal detected is not distinguishable respect the background signal. In addition, if the magnitude is small and not detected by multiple stations, hypocenter parameters cannot be defined.

ii) Network operators willfully neglect events with low magnitude.

iii) Event occurs after a large earthquake and during a seismic sequence. In this case, the background noise increases and prevents the detection of minor seismic events. Usually, after a strong earthquake the magnitude of completeness increases for a certain time period in the spatial domain where the main quake occurred.

The M_c is therefore intended as the minimum magnitude beyond which 100% of earthquakes are detected by a seismic network (Rydelek and Sacks, 1989). A correct estimate of the M_c is essential because a too high estimated value leads to discard data that could be used. On the other hand, a too low value of M_c leads to the inclusion of incomplete data. The choice of an appropriate M_c has a direct impact on the GR parameters evaluation. Such parameters are widely used in seismic hazard studies (Wiemer et al., 2009) and in developing earthquakes forecasting models (e.g.

Wiemer and Schorlemmer, 2007; Gulia and Wiemer, 2019). The b-value tends to be underestimated if the dataset contains earthquakes with $m < M_c$ because the GR model does not fit data correctly. The GR can be then applied only in the complete part of the dataset ($m \geq M_c, fig.1.4$). To ensure GR validity and the correct assessment of related parameters, earthquakes with $m < M_c$ are discarded and in (1.23) M_{min} is substituted by M_c.

Most of methods used to assess the M_c are based on the validity of the GR. Because of its computational speed, a widely used technique for estimating M_c is the Maximum Curvature method (Wyss et al., 1999; Wiemer, 2000). This method consists in defining the point of maximum curvature by estimating the first derivative of the non-cumulative FMD curve. In practice, this matches the magnitude bin with the highest frequency of events in the FMD. Despite its easy applicability, is demonstrated that the Maximum Curvature method tends to underestimate the M_c of about 0.2 units (Woessner and Wiemer, 2005). In addiction if the non-cumulative FMD is gradually curved or with up and down in the curvature region Mc is underestimated and other more sophisticate techniques are recommended (see for example Roberts et al., 2015).

Another commonly used method to assess M_c is based on the stability of b-value (Cao and Gao, 2002). According to this method the completeness is estimated analyzing the stability of b-value in function of a cut-off magnitude. As the cut-off magnitude approaches the true M_c, the b-value approaches its true value and remain constant, forming a plateau. Other methods have been proposed in the literature (Rydelek and Sacks, 1989; Woessner and Wiemer, 2005; Amorese, 2007), each with its own characteristics. None of them has to be preferred, but they must be applied carefully to avoid incompleteness effects that could affect the b-value estimate.

1.5.6 Spatiotemporal variations in magnitude of completeness

Spatiotemporal variations in magnitude of completeness over the long term are due to the evolution (improvement) of the seismic network. Improvements in the seismic

network consist of the placement of new stations to enlarge the spatial coverage and thus the detection of seismic events. Usually, transition phases of a seismic network are well identified in seismic catalogs that show a clear change in Mc (Hutton et al., 2010). Long-term seismic catalogs are characterized by a decreasing Mc over time (Fig. 1.5). The analysis of Mc makes it possible to select a sub-dataset in which Mc does not change. If a more extended data set is required, in which Mc changes over time, the maximum Mc for the whole period is recommended. Short-term spatiotemporal variations are very common during seismic sequences of strong earthquakes in which the seismic noise is higher and prevents proper detection of weaker events. This causes a transient increase in the magnitude of completeness until the seismicity rate and seismic noise are diminished (Fig. 1.6).

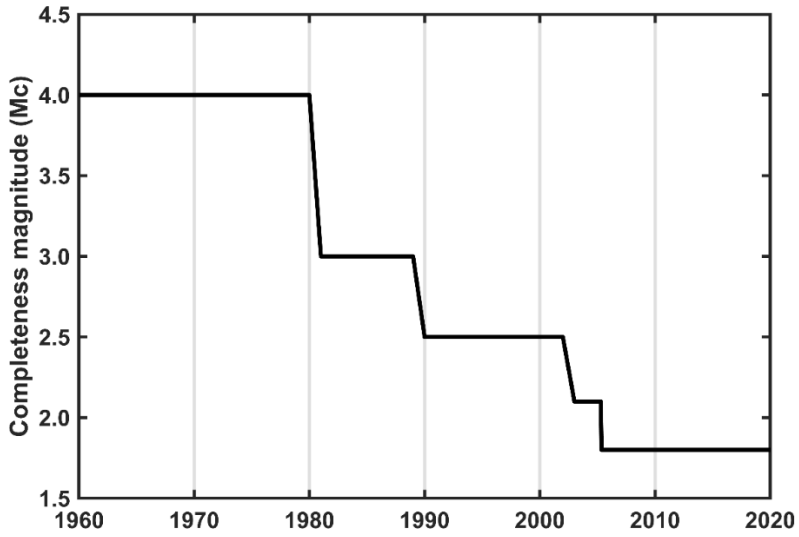

Figure 1.5: Temporal decrease of the Horus seismic catalog completeness magnitude as described in Lolli et al., (2020). As evident, periods of seismic network upgrades correspond to improvements (decreases) in completeness magnitude.

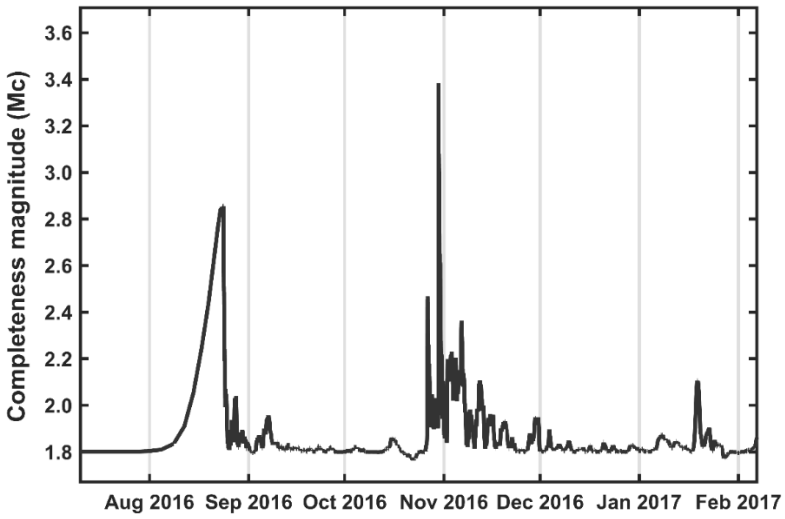

Figure 1.6: Temporary increases in the magnitude of completeness estimated during the Norcia earthquake sequence that started in October 2016 (Mw=6.5) within a radius of 50 km from the epicenter. An increase in completeness magnitude can also be observed in the same area due to the sequence that started with the Amatrice earthquake of 24 August 2016.

1.5.7 Clusters and aftershock sequences

As mentioned already, earthquakes tend to occur in clusters in space and time (fig. 1.7). This is evident after a strong shock in which numerous other earthquakes occur in the same area. However other clustering phenomena are common such as seismic swarms or foreshocks. Seismic swarms are characterized by a sequence of low to moderate magnitude earthquakes and with an unclear mainshock occurring in a certain area. The duration of these phenomena generally ranges from a few days to months, more rarely they can last even years (e.g. The Matsushiro earthquake swarm occurred from 1965 to 1967; Mogi, 1989). Despite the causes that trigger a mainshock (par. 1.1), such as stress transfers, the causes that produce seismic swarms can be of different nature. Tectonic stress causes a slow motion of a fault blocks generating seismic swarms. Other swarms are generated when magma or pressurized fluids crack and proceeds through rocks (Hainzl, 2004). Sometimes before the occurrence of a mainshocks minor shocks (foreshock) are observed in the

same area. These events can cluster in the area for which the mainshock will occur (Zhuang et al., 2019).

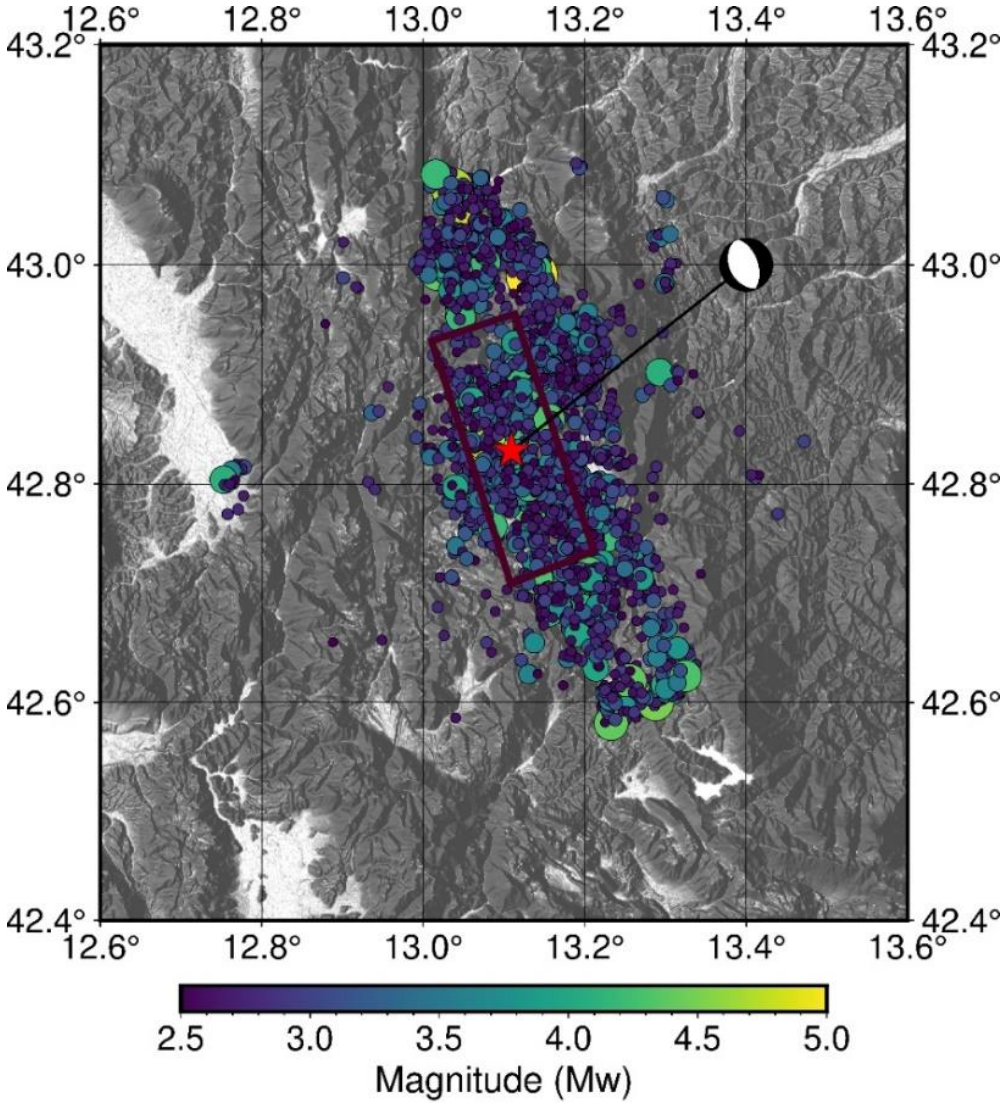

Figure 1.7: Map of seismicity around the epicenter of the Norcia earthquake that occurred on 30 October 2016. The mainshock of Mw=6.5 is indicated by the red star to which the focal mechanism is associated (according to the GCMT catalogue). The size and color of the dots representing successive earthquakes are defined according to their magnitude.

1.5.8 Omori-Utsu law

The occurrence of strong shocks is in general followed by aftershock sequences because of the relative readjustment of the rocks that constitutes the fault blocks. The number of aftershocks decay over time, and the sequence can be defined as finished when it is indistinguishable from the background seismicity. Omori (1894), analyzed the occurrences of aftershocks felt in Gifu following the Nobi earthquake ($M = 8$) that occurred in 1891 in central Japan and observed that their frequencies per unit of time were represented by the equation

$$n(t) = \frac{K}{t + c} \tag{1.26}$$

where t is the elapsed time since the mainshock, c is a temporal delay ranging from minutes to hours (or days) necessary to avoid the singularity at $t = 0$, and K is the productivity parameter that depends on both the mainshock magnitude and the completeness magnitude after the mainshock. If plotted in $log - log$ scale, the Omori's equation represents a straight line with slope -1 for $t \gg c$ (fig. 1.8). Utsu (1961) continued the work started by Omori by observing the occurrence of aftershocks that followed the mainshock of Nobi until 1969. Reporting the occurrences in the plot started by Omori (1894), Utsu (1961) noted that the sequence of aftershocks had continued for 80 years after the mainshock with a uniform decay, but the slope of the line was 1.05. Utsu (1961) already corrected the Omori's formula (1.17) adding the parameter p that consider the rate of decay:

$$n(t) = \frac{K}{(t + c)^p} \tag{1.27}$$

Successive observations on the occurrence of aftershocks showed that the parameter p can range from 0.8 to 1.6 (Hirano, 1924; Utsu, 1961; Mogi, 1962).

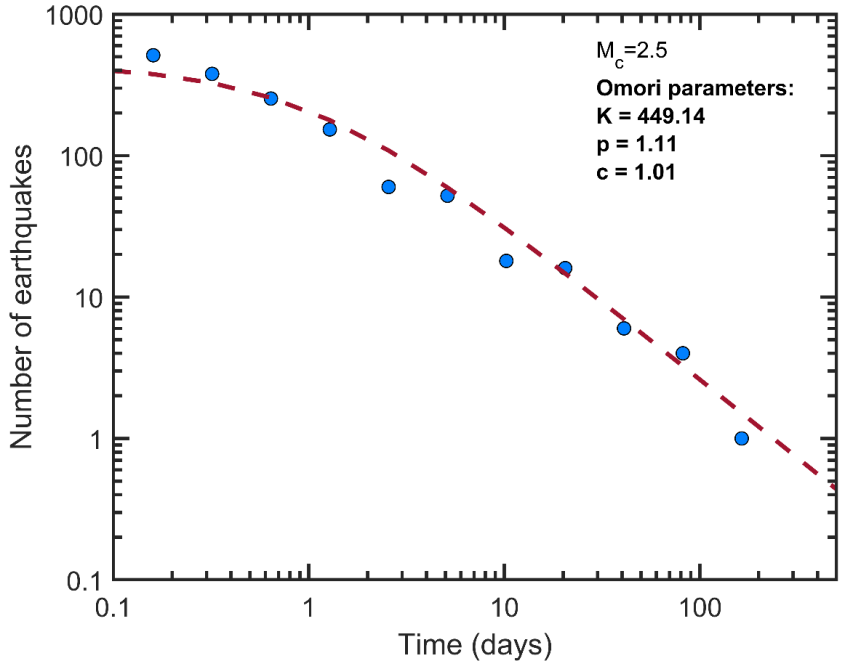

Figure 1.8: Decay of events of magnitude greater than 3 over time, following the Norcia earthquake of 30 October 2016 (blue dots). The red curve represents the decay obtained by the Omori-Utsu distribution.

1.5.9 Estimation of the parameters of Omori distribution

The estimation of parameters of the Omori-Utsu equation can be done through the MLE method (Ogata, 1983). Assuming a set of occurrence times of aftershock sequence, $\tau = \{t_1, \dots, t_n\}$, within the time interval $[t_s, t_e]$ with an intensity function $\lambda(t)$ given by the eq. (1.27), the log-likelihood function derived from eq. (1.10) is given by:

$$\log \mathrm{L}(\mathrm{K}, \mathrm{c}, \mathrm{p}; \tau) = \sum_{i=1}^{N} log\left[\frac{K}{(t_i + c)^p}\right] - \int_{t_s}^{t_e}\left[\frac{K}{(t + c)^p}\right] dt = \tag{1.28}$$

$$= \begin{cases} Nlog(K) - p\sum_{i=1}^{N}[\log(t_i + c)] - K[\log(\mathrm{t_e} + c) - \log(t_s + c)] & if\ p = 1 \\ Nlog(K) - p\sum_{i=1}^{N}[\log(t_i + c)] - \frac{K[(t_e + c)^{1-p} - (t_s + c)^{1-p}]}{1 - p} & if\ p \neq 1 \end{cases}$$

The MLE can be performed posing the partial derivatives with respect each parameter equal to 0. If $p \neq 1$:

$$\frac{\partial logL}{\partial K} = \frac{N}{K} - \frac{[(t_e + c)^{1-p} - (t_s + c)^{1-p}]}{(1-p)} = 0 \tag{1.29}$$

$$K = \frac{N(1-p)}{[(t_e + c)^{1-p} - (t_s + c)^{1-p}]} \tag{1.30}$$

$$\frac{\partial logL}{\partial c} = -p \sum_{i=1}^{N} \left[\frac{1}{t_i + c}\right] - k[(t_e + c)^{-p} - (t_s + c)^{-p}] = 0 \tag{1.31}$$

$$\frac{\partial logL}{\partial p} = -\sum_{i=1}^{N} [\log(t_i + c)] - \frac{K[(t_e + c)^{1-p} - (t_s + c)^{1-p}]}{(1-p)^2} + \frac{K[\log(t_e + c)\,(t_e + c)^{1-p} - \log(t_s + c)\,(t_s + c)^{1-p}]}{1-p} = 0 \tag{1.32}$$

Usually, for multi-parametric distributions, the log-Likelihood function $logL(\theta)$ is maximized numerically by a non-linear optimization algorithm. The standard error for the time distribution parameters can be derived from the variance-covariance matrix $J(\theta)^{-1}$ as the inverse of the Fisher information matrix (Ogata, 1983; Lolli and Gasperini, 2003):

$$J(\theta) = \int_{t_s}^{t_e} \left[\frac{1}{\lambda(\theta, t)} \left(\frac{\partial \lambda(\theta, t)}{\partial \theta}\right)^T \left(\frac{\partial \lambda(\theta, t)}{\partial \theta}\right)\right] \tag{1.33}$$

where for the distribution of Omori-Utsu:

$$J(K, c, p) = \begin{bmatrix} \frac{1}{K(c\ +\ t)^p} & \frac{-p}{(c\ +\ t)^{p\,+\,1}} & \frac{-log(c\ +\ t)}{(c\ +\ t)^p} \\ \frac{-p}{(c\ +\ t)^{p\,+\,1}} & \frac{kp^2}{(c\ +\ t)^{p\,+\,2}} & \frac{k\,p\,log(c\ +\ t)}{(c\ +\ t)^{p\,+\,1}} \\ \frac{-log(c\ +\ t)}{(c\ +\ t)^p} & \frac{k\,p\,log(c\ +\ t)}{(c\ +\ t)^{p\,+\,1}} & \frac{k\,log(c\ +\ t)^2}{(c\ +\ t)^p} \end{bmatrix} \tag{1.34}$$

The standard error (SE) for each parameter $\theta_{i_{th}}$ is computed as the square root of the corresponding diagonal element of $J(\theta)^{-1}$ (Ogata, 1978, 1983). Another similar approach to assess SEs consist in determine the square root of the diagonal of variance-covariance matrix computed as the inverse of the Hessian matrix for log-likelihood function at the maximum (Ogata, 1988; Lolli et al., 2009).

For data reported in fig. 1.8

Standard errors computed using $J(\boldsymbol{\theta})^{-1}$ method	**Standard errors computed using $H(\boldsymbol{\theta})^{-1}$ method**
$J(K,c,p) = \begin{bmatrix} 0.008 & -0.983 & -7.648 \\ -0.983 & 256.804 & 389.843 \\ -7.648 & 389.843 & 10107.308 \end{bmatrix}$	$H(K,c,p) = \begin{bmatrix} 0.01 & -0.457 & -16.926 \\ -0.457 & 57.948 & 325.755 \\ -16.926 & 325.755 & 36520.982 \end{bmatrix}$
$J(K,c,p)^{-1} = \begin{bmatrix} 3441.229 & 9.794 & 2.226 \\ 9.794 & 0.032 & 0.006 \\ 2.226 & 0.006 & 0.002 \end{bmatrix}$	$H(K,c,p)^{-1} = \begin{bmatrix} 3452.413 & 19.222 & 1.429 \\ 19.222 & 0.125 & 0.008 \\ 1.429 & 0.008 & 0.001 \end{bmatrix}$
$std(K) = 58.66;\ \ std(c) = 0.18;$	$std(K) = 58.75;\ \ std(c) = 0.35;$
$std(p) = 0.04;$	$std(p) = 0.03;$

Chapter 2

Predictability and forecastability of earthquakes

"Major natural disasters call for a change of mentality that obliges us to abandon the logic of pure consumerism and promote respect for creation" (Albert Einstein).

2.1 Seismic risk

The occurrence of earthquakes in regions, cities and densely populated areas poses enormous risks that can threaten the national prosperity and the social welfare (Jordan, 2009). Urban seismic risk quantification is a complex problem that requires a detailed knowledge of the environment, infrastructures and understanding of seismic phenomena as well as the human behavior under dangerous situations. The estimation of seismic risk can be improved through the international collaboration of scientist and engineers analyzing and developing building engineering strategies. Indeed, during a strong seismic event, one of the greatest sources of risk to the population is the damage or collapse of buildings or infrastructure. The seismic risk is a forecast of damage to society, usually expressed in terms of casualties or economic losses, which would be caused by a future seismic event in a certain space-time domain. Its assessment depends on three parameters: the hazard (H) that is an intrinsic characteristic of a region, the exposure (E) of the community, and vulnerability (V). In some cases, the population who are aware of the danger in their territory are prepared for disasters and the capability to respond and restore earthquake dagame is faster (Fig. 2.1). This capability is called resilience (r) which reduces the global risk (Jordan, 2009) as follows:

$$Risk = \frac{H * E * V}{r} \tag{2.1}$$

The implicit goal of earthquake risk analysis is to assess the areas that could be affected by the worst consequences caused by a destructive earthquake and to inform policy makers who are involved in risk reduction.

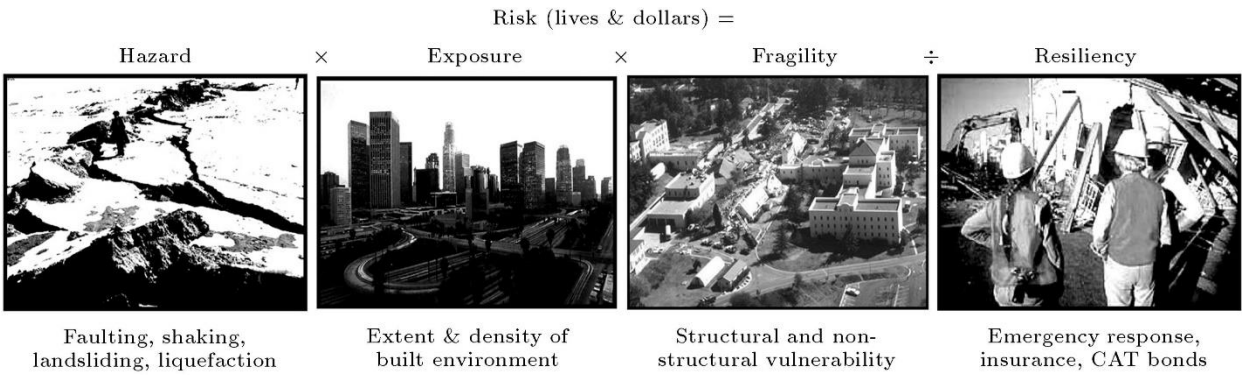

Figure 2.1: The risk equation (Jordan, 2009).

2.1.1 Hazard and hazard map

The hazard is the first term of the risk equation (eq. 2.1) and is qualitatively different from the others. In fact, the hazard cannot be reduced. Indeed, the primary hazard related to the breaking of rocks and the resulting ground shaking generated by the passage of seismic waves is a characteristic feature of the involved area. Earthquakes involve high forces and energies that cannot be controlled by humans. The hazard estimated as the probability to exceeding a fixed level of ground shaking obtained by the analysis of frequencies of previous seismic events, cannot be managed. In addition, the Hazard should also consider the probability of secondary events (Jordan, 2009) generated by an earthquake such as tsunami, liquefaction of soil, mud volcanoes etc. An adequate seismogenesis characterization combined with a historical seismic catalog and a relationship describing the attenuation of the seismic wave with the distance from the source area can be used to estimate the probability for a certain ground motion. Starting from this information is possible to define the hazard map. The main aims of this latter are to inform the policy makers and the population about the characteristic of the territory and making regulation for the construction or upgrade of buildings. For Italy the National Institute of Geophysics

and Vulcanology (INGV) developed a seismic hazard map (Fig. 2.2) that is periodically reviewed and updated with new information. A Seismic hazard map generally plots the peak horizontal ground acceleration with a certain probability of exceedance in 50 years (10% for the INGV hazard map).

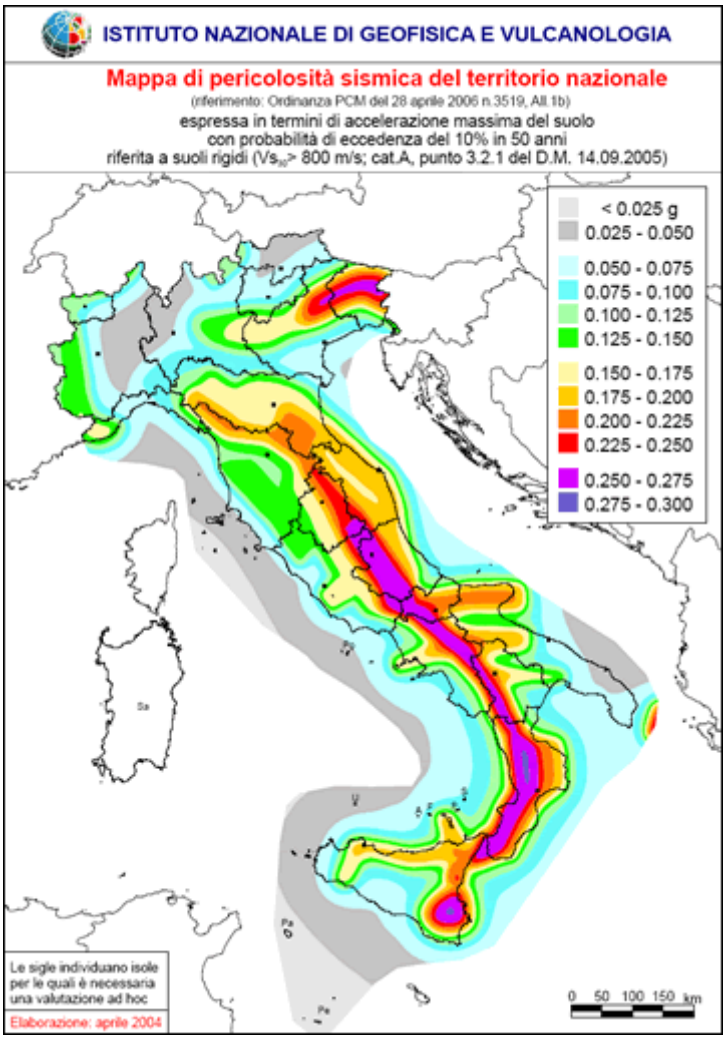

Figure 2.2: Seismic hazard map of Italy developed by the INGV and with the hazard expressed in terms of horizontal pick ground acceleration with probability of 10% in 50 years.

2.1.2 Exposure and vulnerability

The presence of cities or villages in areas potentially subject to natural hazards constitutes the exposure. The exposure to the hazard can be reduced using policies that regulate the construction of new buildings and new infrastructures near active faults or potentially dangerous areas (Armstrong, 2001). The susceptibility of

infrastructure to damage following a certain level of ground shaking constitutes vulnerability. One effective strategy to reduce the vulnerability is to operate on the fragility of the buildings through regulations that establish severe earthquake-resistant construction criteria for new buildings and improving the already existing buildings resistance to the indicted shear stress caused by the seismic waves (Jordan, 2009).

2.1.3 Resilience

The resilience is the response of the community involved to the injury suffered. If the population is adequately prepared to suffer a certain type of damage it has the time to prepare appropriate actions to repair the damage suffered (Jordan, 2009). Community resilience can be improved through public and private sector preparedness for response in the face of an emergency. The greater the community's preparedness for a certain type of damage, the lower the risk associated with it. Achieving high levels of resilience requires the co-participation of all levels of government by improving coordination and cooperation in the case of an emergency (Perry et al., 2008). An additional aspect that should not be underestimated is education to the community of hazards characteristic of a given area to improve the preparedness of the population for the occurrence of the damaging phenomenon such as a strong earthquake (Perry et al., 2008).

2.2 Earthquakes predictability

Earthquake prediction has proven to be a very intricate issue for seismologist and the improvements in this field were slower than for other natural phenomena (Jordan, 2009). Indeed, one of the main problems is that it is currently not possible to directly observe what exactly happens at the exact moment an earthquake is generated, because it occurs in the interior of the planet at depths not yet accessible.

Furthermore, the state of stress acting on a fault or fault system as well as the limit stress before the rocks failure cannot be directly observed and measured (Wyss, 2001). A valid earthquake prediction should be able to specify the location, time, and magnitude, within a certain limit of uncertainty. Such information should be also coupled with a high probability that a certain earthquake will occur (Allen, 1976). An efficient earthquake prediction method could be important in saving many lives and in mitigating the economic damages caused by a strong and destructive earthquake. An effective prediction could be used by the civil protection service to alert the community and prepare countermeasure for the impending danger allowing adequate preparation of the population involved. For risk reduction it is not possible to manage the seismic hazard of a region because depends on their seismotectonic features. The way for reduce risk and mitigate the effects of a strong earthquake is decreasing the seismic vulnerability and exposure. This is possible through prevention and an appropriate information campaign to raise community awareness of seismic risk. Earthquake prediction has been widely debated in recent decades. The most skeptical approach considers earthquakes as a random process in space and time and for this reason earthquakes are inherently unpredictable (Geller et al., 1997). On the other hand, according to the more optimistic approach, the predictability of earthquakes is difficult but not impossible and only through a better understanding of the phenomenon and the support of technology will this goal be achievable (Wyss, 2001).

2.2.1 The search for the "silver bullet"

In the second half of the 1970s, seismologists were optimistic that earthquakes could be predicted quickly. This wake of optimism came largely from the first successful prediction of the 7.8 magnitude Haicheng earthquake in China February 4, 1975 (Cicerone et al., 2009). Numerous phenomena such as geodetic deformation, groundwater level variation, chemistry and other properties were analyzed before

the mainshock occurrence. However, the precursor signal that played a key role in the warning was the increase in foreshock activity a few hours before. After the earthquake of magnitude 7.8 the city was seriously damaged but warning signal and the subsequent evacuation order saved the lives of thousands of residents. Although the prediction of the Haicheng earthquake was a blend of confusion, empirical analysis, intuitive judgment, and good deal of luck, it was an attempt to predict a major earthquake that for the first time did not end up with practical failure. The optimism inspired by this success was short-lived. The following year, on July 28, 1976, an earthquake of magnitude 7.6 struck the city of Tangshan, a thriving industrial city with approximately one million inhabitants, without warning. None of the precursors observed near Haicheng were observed this time. The earthquake caused at least 250,000 fatalities and 164,000 injured (Wang et al., 2006). The analysis of precursor signals related to the preparation process of strong earthquakes, the "silver bullets" as defined by (Jordan, 2006), continued for the next two decades, and in the 1990s, during the 25th General Assembly of the International Association of Seismology and Physics of the Earth's Interior (IASPEI) held in Istanbul, the idea of compiling a list of significant precursors was advanced. As precursor signal is intended a variation of a physical, chemical, or biological characteristic in a certain geographical region that could be related to the preparation process of a strong seismic event (Wyss, 1997). A precursor signal is defined as diagnostic if can predict with high probability the location, time, and the magnitude range of an impending seismic event with a small range of error (Wyss, 1991). In addition, it is necessary for the precursor signal to be strongly correlated with seismic activity and to be supported by accurate documentation describing the quality, characteristics, and result of observations before an earthquake. The evaluation procedure to assess the predictive capability of each proposed precursor signal (Fig. 2.3) has been more rigorous than a journal peer review because of the limited opportunity for independent testing (Wyss and Booth, 1997). During the first evaluation round, concluded in the early 1990s, the expert panel criticised the lack of a precise

definitions of the anomalies associated with the candidate precursor phenomena, a comprehensive explanation of the experiments conducted, or consideration of other possible origin of the anomalies. At the beginning of 1994 the list of candidate precursors was composed by five precursor signals derived from seismicity patterns (foreshocks and pre-shocks), ground water proprieties (Radon concentrations and temperature decrease in ground water) and crustal deformation (ground water rise) (Wyss, 1997).

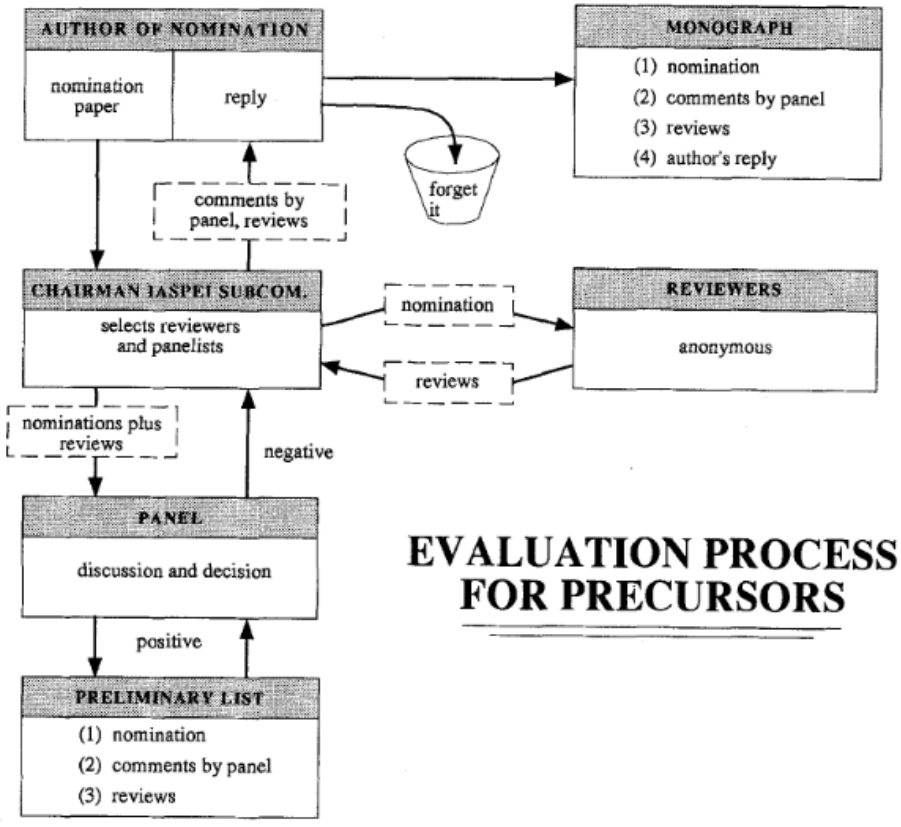

Figure 2.3: Review process used by the IASPEI Sub-commission on Earthquake Prediction to evaluate nominations for the IASPEI Preliminary List of Significant Precursors (Wyss, 1997).

Other proposed precursor signals include change in crustal strain rates, changes in seismic wave velocities, change in crustal electrical conductivity, change in Radon or other geochemical gasses concentration in ground water, in ground and air, ground water level fluctuations, thermal anomalies, precursor based on seismicity (Cicerone

et al., 2009). At the end of the 1990s, it was concluded that it was not sufficiently clear whether the phenomena proposed as significant precursor signals were understood to such a degree that they could be used for prediction. However, they represent a list of phenomena that were considered to show an above-average probability of being useful in earthquake prediction (Wyss and Booth, 1997).

Although the search for precursor diagnostic signals and the silver bullet approach proved to be fruitless (Kagan, 1997) the analyses on precursor signals have contributed to the improvement of knowledge of seismic phenomena, processes related to fault systems and seismic sources. Currently, technologies and instruments have improved considerably, and quality seismological, geodetic, and geophysical data are currently available for many regions of the world. These advances have improved the ability to analyze earthquake predictability. However, to check and analyze non seismic signals is necessary to install and maintain a specific network and wait a long time for the occurrence of damaging earthquakes. In contrast, most of the world's seismic regions have a seismological network that exists since dozens of years and continuously collects data. For this reason, signals based on seismicity or that can be derived from seismicity could be simpler to analyze and test.

2.2.2 Deterministic predictions

Deterministic predictions try to define the occurrence of future seismic events within a certain space-time domain. They are typically defined as deterministic affirmations according to a future earthquake will occur (or will not) in a certain subdomain of a geographical region, with a certain magnitude range and in a certain time window $(t, t + \Delta t)$. The deterministic prediction approach consists in the analysis over time and space of a precursor signals or seismicity patterns that could suggest with high probability the occurrence of an impending strong target earthquake. A target earthquake is defined as an event characterized by a magnitude above a certain identified threshold. An alarm of temporal duration Δt is triggered when a single

precursor phenomena or a certain combination of them is detected (Keilis-Borok, 2002). A target event to forecast is considered predicted if it occurs within the alarm space-time domain. An alarm is considered false alarm if no target earthquake occurs within the alarm domain (type I error, or false positive). If a target earthquake occurs outside any alarm space-time domain and in a sub-domain without any alarm is considered a failure to predict (type II error, false negative) (Fig. 2.4).

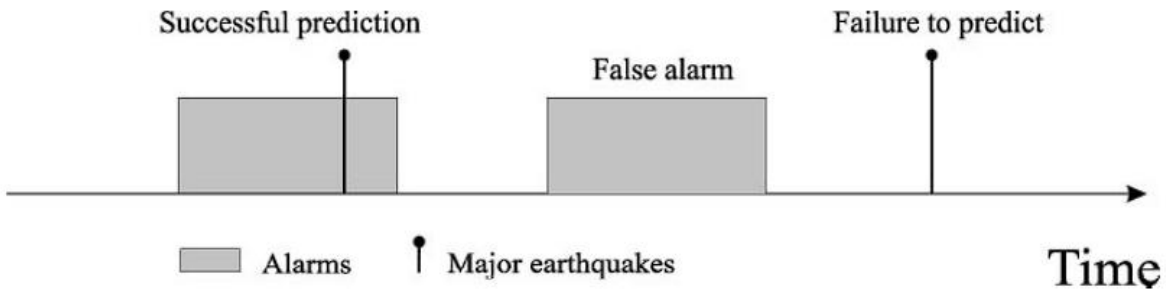

Figure 2.4: Possible outcome from alarm-based deterministic predictions (Keilis-Borok, 2002).

A deterministic forecast can also be performed using anti-alarm, an assertion that no target earthquake will occur within a certain space-time domain for which the anti-alarm has been issued (Molchan and Kagan, 1992). Even if the procedure to conduct deterministic prediction is developed and described in literature (Molchan and Kagan, 1992; Keilis-Borok, 2002; Zechar and Jordan, 2008), it is currently not yet possible to make reliable deterministic predictions of earthquakes because a diagnostic precursor observable before the majority of strong earthquakes (the "silver bullet") has not yet been found. In addition, often precursor phenomena are different for different earthquakes and the success of measuring some anomalous phenomenon before an earthquake usually depends on having a good scientific experiment operating in an area before, during and after an earthquake (Cicerone et al., 2009).

2.3 Probabilistic forecasts

Earthquake forecasting is an essential tool for earthquake risk reduction, and after the failure of the 'silver bullet' search in the 1980s-1990s, the approach has changed radically since the new century. In fact, currently seismologists prefer to speak about "earthquakes forecasting" instead of "earthquakes prediction". The difference is not only linguistic but requires changing the approach from deterministic prediction to statistic forecast. The probabilistic forecasts do not focus directly on the behavior of potentially precursive signals, but rather on the probability that a future target earthquake will occur in given space-time domain (Marzocchi and Lombardi, 2009; Jordan et al., 2011). Depending on the level of information used for their elaboration, the forecasts can be defined as time dependent and time independent. Time-independent forecasts assume earthquakes as Poissonian random processes in the long-term and the short-term seismicity is not considered for probability estimates. Probability estimates are made considering hypocenter of past earthquakes, active faults position, average time of recurrence, satellite, and tectonic data to assess the long-term seismic hazard (Jordan et al., 2011). Time-dependent forecasts, on the other hand, aim to define the time-dependent probability that a certain target earthquake will occur given the information $I(t)$ available at a certain instant t. Such information regard mainly the short and medium-term seismicity that can be obtained from seismic and geological catalogues in which the history of seismicity of a certain region, the characteristics of faults that have been activated over time triggering earthquakes, are recorded (Jordan et al., 2011).

2.3.1 Forecast time scale

Earthquake forecasts can be classified according to their time interval of validity in long, medium, and short term. Long-term forecasts generally define the time-

independent probability of occurrence over a time horizon of the order of a decade and are useful in seismic hazard assessment. This latter is necessary and essential both for the characterization of the territory and from the decision-making point of view to establish the regulations that define the guidelines for the construction of new buildings or the adaptation of existing ones. Medium-term forecasts provide probabilistic estimates on time scales of the order of a year and can be useful for preparing retrofitting operations of existing buildings. Short-term forecasts, on the other hand, provide probabilistic information on a daily, weekly, or monthly time scale (Fig. 2.5).

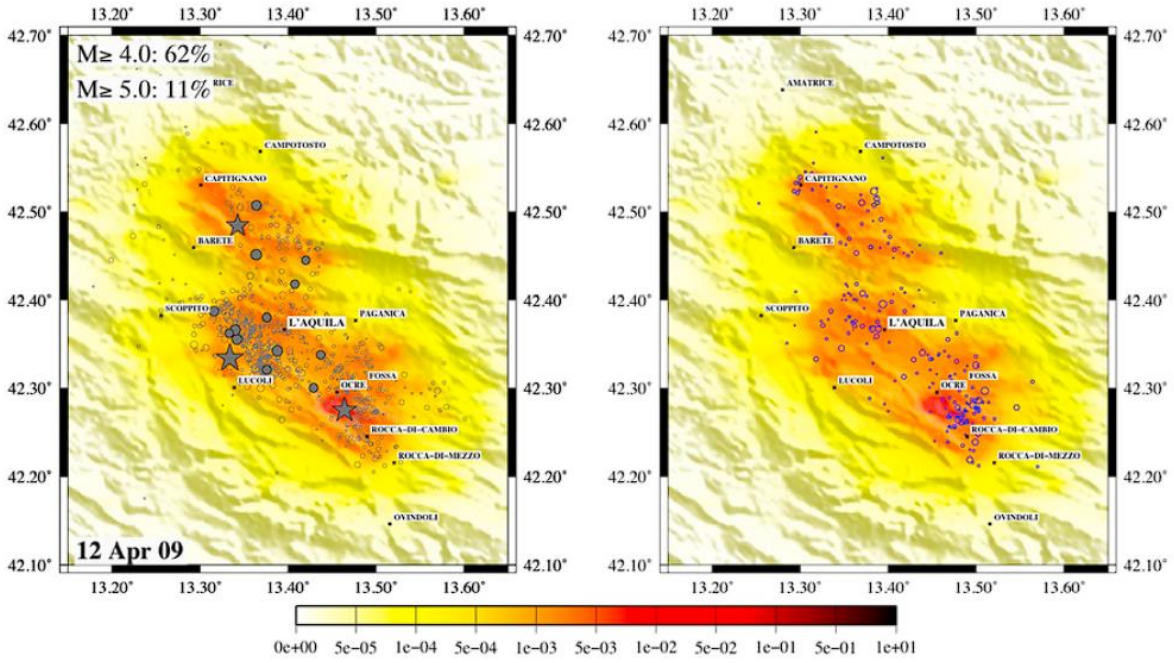

Figure 2.5: Map of expected number of events per square kilometer of magnitude greater than 4 for 12 April 2009 in the L'Aquila earthquake area (Marzocchi and Lombardi, 2009). The upper left corner shows the daily probability of having earthquakes of magnitude 4 and 5 or higher in the entire area. The forecasts on the left and right are the same. (Left) The map contains the past seismicity used by the model. (Right) The map contains earthquakes (blue dots) that occurred during the forecast time windows. The size of the dots is scaled with the magnitude.

Such forecasts are relevant, especially during periods of higher than usual seismicity (e.g., before a strong earthquake if it is preceded by foreshocks, or after a strong earthquake) where the population and decision-makers wish to receive information regarding the possibility of major seismic events to prepare immediate seismic risk mitigation operations (Marzocchi and Lombardi, 2009; Azarbakht et al., 2021). However, although the daily or weekly probability of a potentially destructive earthquake in a given area may increase by several orders of magnitude from the background value, after an intermediate earthquake or during a seismic sequence, it often remains in the range of a few percent. Such low probability values are difficult to use to prepare imminent and generalized mitigation procedures (Marzocchi et al., 2015), although they provide relevant information to civil protection authorities if properly communicated.

2.3.1 Operational earthquake forecasting (OEF)

The probability of occurrence of a certain target earthquake in each area does not remain constant over time but generally varies on a daily scale in correlation with seismicity. The purpose of operational earthquake forecasting (OEF) is to distribute authoritative information regarding variations in seismic risk over time, particularly in the short term, to assist communication and preparation of the population for a potential destructive earthquake (Jordan et al., 2014). The guidelines and status for the development of OEF were proposed and described by the International Commission for Earthquake Forecasting and for Civil Protection (ICEF) appointed by the Italian government following the L'Aquila earthquake. Underlying the guidelines for OEF described in the ICEF report (Jordan et al, 2011) and remarked, e.g., in Jordan et al., 2014, Woo and Marzocchi 2013, the two important principles that should guide OEF concern transparency and the separation of risk from hazard. According to the principle of transparency, authoritative information on future seismic activity should also be communicated in probabilistic terms with a certain

timeliness and frequency to all potential members of the public who wish to use it. The principle of separating risk from hazard, supports the dissemination of scientific information on future seismic activity independently of its application for seismic risk assessment and mitigation. The dissemination of OEF information in probabilistic terms therefore helps to separate hazard estimates and thus the role of scientists from that of public civil protection administrations. The sharing of probabilistic estimates produced by earthquake forecasting models recognized in the literature e.g. ETAS (Ogata, 1988) to a wide audience allows, under the guidance of civil protection administrations, to weigh decisions individually by assessing the costs and benefits of each seismic risk mitigation action (Woo and Marzocchi, 2014) (Fig. 2.6). A similar application of OEF was tested in New Zealand, where during the Canterbury and Cook Streit earthquake sequences, which occurred between 2011 and 2013, the population was informed of the increased danger in the short term. In particular, the population in the affected areas was allowed to undertake individual mitigation operations, including evacuation (Jordan et al., 2014).

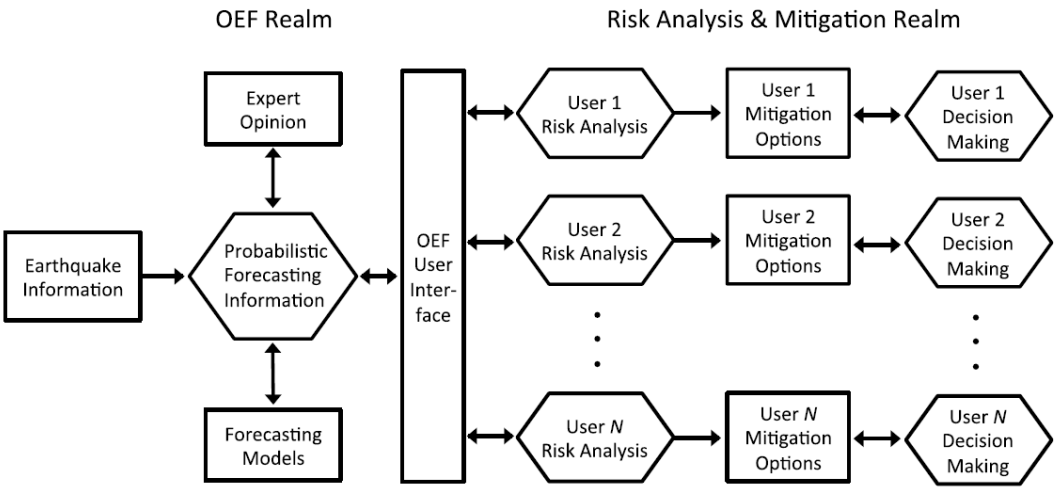

Figure 2.6: Schematic diagram of an operational forecasting system (Jordan et al., 2014).

In this sense, operational earthquake forecasting offers a more cautious approach than the declaration of an alarm or the mass evacuation of an area. Such caution in fact limits the economic damage resulting from a potential false alarm. The

dissemination of short-term seismic hazard estimates allows the individual to interpret and understand the information and thus to undertake the behavior deemed most appropriate in terms of risk mitigation.

2.3.2 Epidemic Type Aftershock Sequence (ETAS) model

Most probabilistic models applied in seismology are based on empirical relationships. The Epidemic Type Aftershock Sequence (ETAS, Ogata, 1988)) is defined as a stochastic point process and is particularly used to model aftershock sequences and to obtain probabilistic estimates of earthquake occurrence. The ETAS model was formulated considering that the decay in time of the aftershock sequence often cannot be described by a single Omori-Utsu law. Guo and Ogata (1997) and Ogata et al., (2003) observed that often the strongest aftershocks are capable of generating a secondary aftershock sequence. Therefore, the ETAS model considers each aftershock as capable of triggering subsequent aftershocks and the occurrence rate for a certain t^{th}instant is given by the superposition, weighted by the magnitude of the parent event, of the decays described by the time-shifted Omori-Utsu decay function (Ogata and Zhuang, 2006) (fig. 2.7). The expected temporal occurrence rate at the time t takes the form:

$$\lambda(t,m) = h(m)\left[\mu + \sum_{t_i<t} k(m_i) f(t,t_i)\right] \tag{2.2}$$

where μ represents the rate of background seismicity (expressed as shocks per unit time) of the analyzed area. In the literature several implementations of the Epidemic Type Aftershock Sequence (ETAS) model are described (e.g., Console et al., 2006, Lombardi and Marzocchi, 2010). In most of them the time dependence $f(t,t_i)$ is formulated as an Omori decay starting at the times of occurrence of each earthquake

$$f(t) = \frac{H(t-t_i)k}{(t-t_i+c)^p} \tag{2.3}$$

where t_i represent the occurrence time of the $i-th$ event, the parameters k, c and p are the typical parameter of the Omori-Utsu law (see section 1.10) that are common

to all $i-th$ event (Ogata, 1998) and $H(t-t_i)$ is the Heaviside step function which is 1 if $t-t_i>0$ and is 0 otherwise. The first term of the summation, $k(m_i)$, is adopted to scale the efficiency of a shock in generating aftershock according to its magnitude m_i and takes the form

$$k(m_i) = e^{\alpha(m_i - m_c)} \tag{2.4}$$

where α is the triggering capability parameter, m_c is the minimum magnitude of completeness. The multiplication factor, $h(m)$, represent the Gutenberg and Richter law for earthquake magnitudes of m_c or larger and takes the form

$$h(m) = \beta e^{-\beta(m-m_c)} \tag{2.5}$$

where $\beta = b\,ln10$ and b is the slope of the frequency-magnitude distribution (eqs. 1.23 and 1.25).

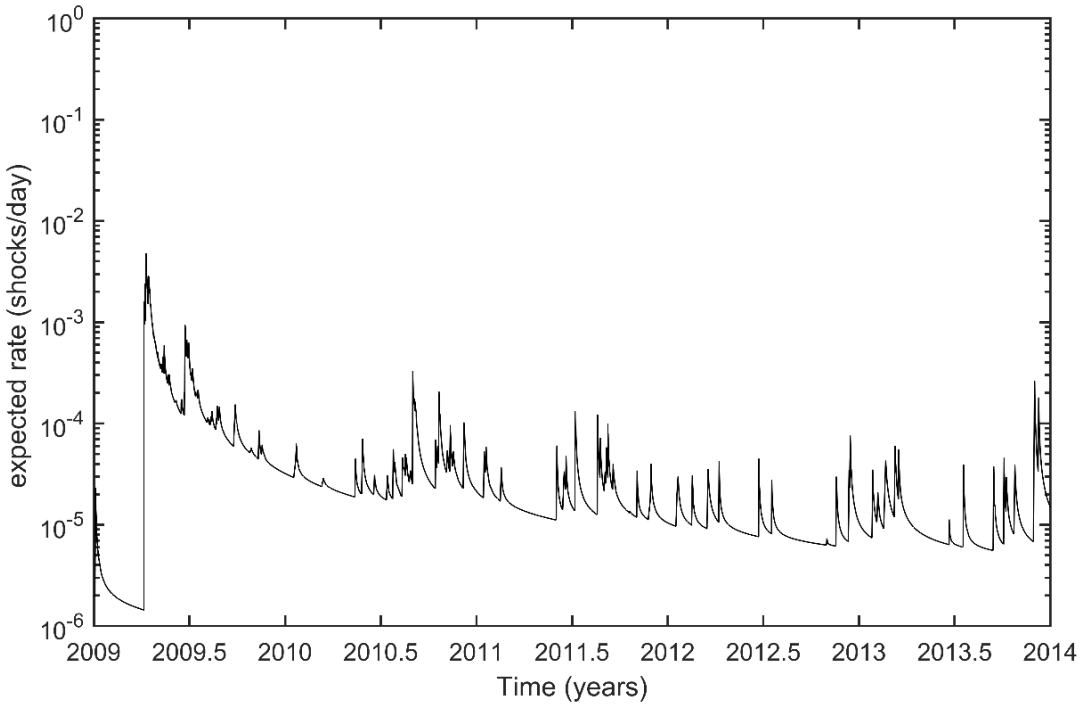

Figure 2.7: Expected daily rate of earthquakes with $M \geq 5.0$ for a squared area of side 43 km surrounding the epicenter of L'Aquila earthquake occurred in Italy on 6 April 2009, estimated using the ETAS model described in section 4.5.

The temporal ETAS model was extended by Ogata (1998) to several space-time models that are defined considering empirical studies of spatial aftershock clustering (Ogata and Zhuang, 2006). The space-time ETAS model is characterized by a conditional intensity function, which is the probability of an earthquake occurring in the infinitesimal volume of space-time conditional on all past seismicity (Ogata and Zhuang, 2006; Lombardi and Marzocchi 2010b) defined with the form

$$\lambda(t_i, x_i, y_i, m_i) = \nu\lambda_0(x, y, m) + \sum_{t_i<t}[f(t - ti)k(m_i)g(x - x_i, y - y_i|m_i)h(m)] \quad (2.6)$$

where $\lambda_0(x, y, m)$ represents the background seismicity, ν represents the ratio between the expected rate of independent events of the background seismicity and the total number of events.

The probability distribution function of the location $g(x - x_i, y - y_i|m_i)$ of triggered events depends on the magnitude m_i and the location (x_i, y_i) of its parent. During the evolution and improvement of the ETAS space-time model through clustering analysis in different regions, several formulations to describe the spatial triggering pdf were proposed (Zhuang et al., 2004, 2011; Ogata and Zhuang, 2006). The most used, summarized in Zhuang et al. (2011), are:

(i) $$g(x - x_i, y - y_i) = \frac{1}{2\pi D^2} e^{-\frac{(x-x_i)^2+(y-y_i)^2}{2D^2}} \quad (2.7)$$

used by Rathbun (1993) and Console et al. (2003) where D is the characteristic triggering distance.

(ii) $$g(x - x_i, y - y_i|m_i) = \frac{1}{2\pi D^2 e^{\alpha(m_i-m_c)}} e^{-\frac{(x-x_i)^2+(y-y_i)^2}{2D^2 e^{\alpha(m_i-m_c)}}} \quad (2.8)$$

used by Ogata (1998) and Console et al. (2003) where the triggering distance from the epicenter (x_i, y_i) is scaled according to the magnitude m_i of the $i - th$ event.

(iii) $$g(x - x_i, y - y_i) = \frac{(q-1)[D^2]^{q-1}}{\pi[(x - x_i)^2 + (y - y_i)^2 + D^2]^q} \quad (2.9)$$

used by (Ogata, 1998; Console et al., 2003; Falcone et al., 2010; A. M. Lombardi and Marzocchi, 2010) where the q parameter is adopted as exponent for the triggering spatial kernel.

(iv)
$$g(x-x_i, y-y_i|m_i) = \frac{(q-1)\left[D^2 e^{\alpha(m_i-m_c)}\right]^{q-1}}{\pi[(x-x_i)^2+(y-y_i)^2+D^2 e^{\alpha(m_i-m_c)}]^q} \tag{2.10}$$

used by (Ogata, 1998; Zhuang et al., 2002, 2004) considering the scaling factor (as in eq. 2.8).

(v)
$$g(x-x_i, y-y_i|m_i) = \frac{(q-1)\left[D^2 e^{\gamma(m_i-m_c)}\right]^{q-1}}{\pi[(x-x_i)^2+(y-y_i)^2+D^2 e^{\gamma(m_i-m_c)}]^q} \tag{2.11}$$

used by (Zhuang, 2005; Ogata and Zhuang, 2006; Marzocchi and Lombardi, 2009) where the scaling factor γ is assumed independent by the scaling factor α used to scaling the productivity of the $i-th$ event.

The estimation of parameters of the ETAS model (e.g., $k, c, p, D, \alpha, \gamma, q$, and ν) can be done through the MLE method (Ogata, 1998). Given the set of times, magnitudes, and space coordinates $\{(t_i, m_i, x_i, y_i)|m_i \geq m_C, i = 1, \dots, n\}$ for events that occurred within an analysis region R during a time range $[T_1, T_2]$ the log likelihood of the space-time ETAS model (eq. 2.6) is given by:

$$\ln L = \sum_{t_i \in (T_1,T_2); m_i \geq m_c; (x_i,y_i) \in R} \ln \lambda(t_i, m_i, x_i, y_i) - \int_{T_1}^{T_2} \int_{m_c}^{m_u} \iint_R \lambda(t, m, x, y)\, dy\, dx\, dm\, dt \tag{2.12}$$

where m_u is the maximum expected magnitude for the region R. The second term of the loglikelihood function (eq. 2.12) represent the expected number N of events during the time windows $[T_1, T_2]$. From N, assuming the occurrence of earthquakes as a generalized Poisson process is possible to estimate the probability of earthquake occurrence with magnitude $m_c \leq m \leq m_u$ within the region R (Fig. 2.8) during the time window $[T_1, T_2]$ as

$$P = 1 - exp\left(-\int_{T_1}^{T_2} \int_{m_c}^{m_u} \iint_R \lambda(t, m, x, y)\, dy\, dx\, dm\, dt\right) \tag{2.13}$$

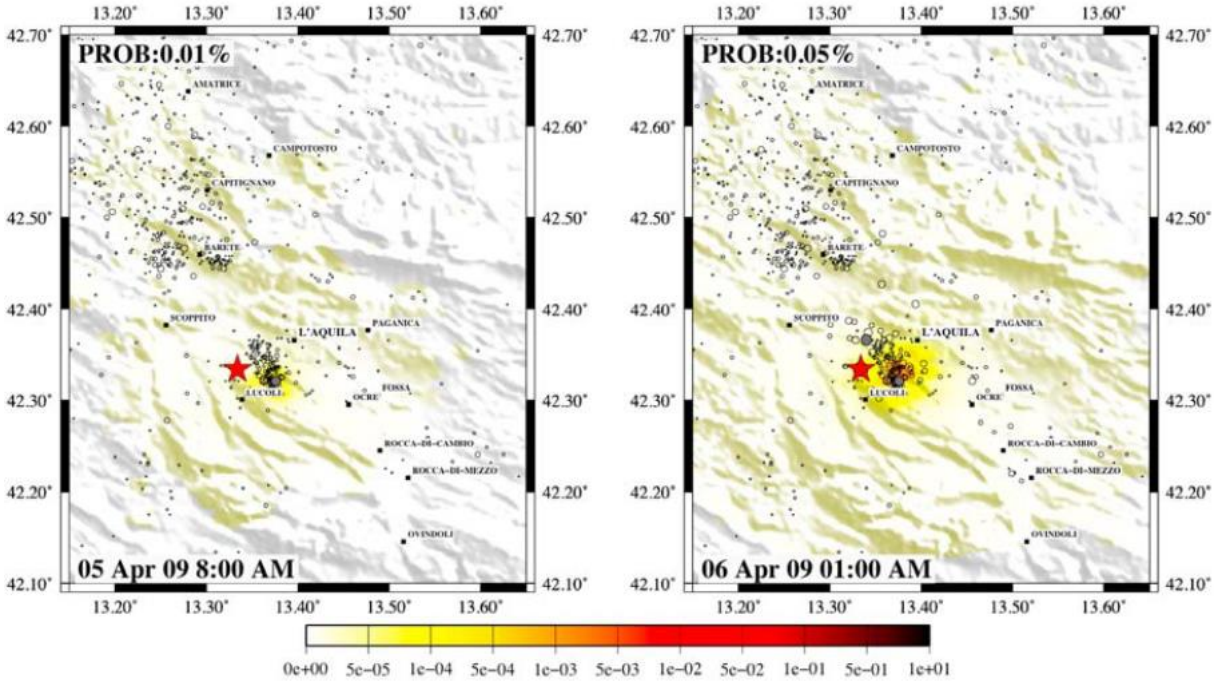

Figure 2.8: Map of expected number of events per square kilometer of magnitude greater than 5.5 for 5 (left) and 6 (right) April 2009 in the L'Aquila earthquake area (Marzocchi and Lombardi, 2009). In the upper left corners are the occurrence probabilities are indicated.

Chapter 3

Retrospective short-term forecasting experiment in Italy based on the occurrence of strong (fore)shocks

P. Gasperini[1,2], E. Biondini[1], B. Lolli[2], A. Petruccelli[1,3], G. Vannucci[2]

[1]Dipartimento di Fisica e Astronomia, Università di Bologna, Italy

[2]Istituto Nazionale di Geofisica e Vulcanologia, Sezione di Bologna, Italy

[3] Swiss Seismological Service, ETH Zurich, Switzerland

From: *Gasperini, P., E. Biondini, B. Lolli, A. Petruccelli, and G. Vannucci, 2021, Retrospective short-term forecasting experiment in Italy based on the occurrence of strong (fore) shocks, Geophys. J. Int., 225, no. 2, 1192–1206, doi: 10.1093/gji/ggaa592.*

**All authors contributed to the work. In particular Gasperini P. and Biondini E., took care of the computational part and interpretation of the results.*

The study and analysis of the frequency with which strong shocks (4.0≤Mw<5.0), widely felt by the population, were followed in the same area by potentially destructive main shocks (Mw≥5.0) have been conducted for various seismic areas around the world. Assuming the stationarity of the seismic release properties, such frequencies can be tentatively used to estimate the probabilities of potentially destructive shocks after the occurrence of future strong shocks. This allows us to set up an alarm-based forecasting hypothesis related to strong foreshocks occurrence. Such hypothesis is tested retrospectively on the data of a homogenized seismic catalogue of the Italian area against a purely random hypothesis that simply forecasts the target main shocks proportionally to the space-time fraction occupied by the alarms. We compute the latter fraction in two ways i) as the ratio between the average time covered by the alarms in each area and the total duration of the forecasting experiment (60 years) and ii) as the same ratio but weighted by the past frequency of occurrence of earthquakes in each area. In

both cases the overall retrospective performance of our forecasting algorithm is definitely better than the random case. Considering an alarm duration of three months, the algorithm retrospectively forecasts more than 70% of all shocks with Mw≥5.5 occurred in Italy from 1960 to 2019 with a total space-time fraction covered by the alarms of the order of 2%. Considering the same space-time coverage, the algorithm is also able to retrospectively forecasts more than 40% of the first main shocks with Mw≥5.5 of the seismic sequences occurred in the same time interval. Given the good reliability of our results, the forecasting algorithm is set and ready to be tested also prospectively, in parallel to other ongoing procedures operating on the Italian territory.

3.1 Introduction

Even if the deterministic prediction of earthquakes is presently not feasible and perhaps it will never be (Geller et al., 1997), several methods of probabilistic operational forecasting have been proposed in the last decades (see Jordan and Jones, 2010 and Jordan et al., 2011 for an overview). Many of such methods take advantage of the well-known property of earthquakes to cluster in space and time (Mulargia and Geller, 2003; Kagan, 2014) and in particular of the possibility that relatively small shocks, occurring in advance (foreshocks) of destructive main shocks, might be used as precursory signal.

Jones and Molnar (1976, 1979) first observed that the property of worldwide strong earthquakes of being preceded by a few days or weeks of smaller shocks could have been used to predict somehow their occurrence. Jones (1984, 1985) noted that in California the occurrence of a weak shock increased of several order of magnitude the probability of occurrence of a main shock in the following hours or days and Agnew and Jones (1991) and Jones (1994) computed the probability of a major earthquake along the San Andreas fault in California, given the occurrence of a potential foreshock nearby the fault. The occurrence of foreshocks was then adopted

as one of possible precursor of large earthquakes by the Southern San Andreas Working Group Southern San Andreas Working Group (1991) and Reasenberg (1999a, 1999b) estimated the prospective frequency of potential foreshock being followed by stronger earthquakes in California and worldwide.

In Italy, Caputo et al. (1977, 1983) analyzed earthquakes' swarms as forerunners of strong earthquakes, Grandori et al. (1988) proposed an alarm system based on the occurrence of a pair of foreshocks, Console et al. (1993) and Console and Murru (1996) studied the foreshock statistics and their possible relationship to earthquake prediction and Di Luccio et al. (1997) and Console et al. (1999) set up a forecasting hypothesis for the occurrence of earthquakes conditioned by prior events.

More recently, Gasperini et al. (2016), by the retrospective analysis of a homogeneous seismic catalogue of the Italian region, computed the relative frequencies with which strong shocks (defined as $4.0 \leq Mw < 5.0$) were followed in the same area by potentially destructive main shocks (defined as $Mw \geq 5.0$, 5.5, 6.0). In particular, they found that just after strong shocks, the relative frequency of potentially destructive main shocks in the same area increases with respect to quiet periods by a factor up to about 100000. Then, as time goes by without any main shock occurring, such factor decreases logarithmically down to less than 10 for time windows of months to years. Within one day after the occurrence of a strong shock, the frequencies of main shocks with $Mw \geq 5.0$ and $Mw \geq 5.5$ range from 5 per cent to 2 per cent while within one month they range from 14 per cent to 6 per cent. Frequencies remain quite stable for about one hour after the strong shock and then start to decrease logarithmically at a rate of about 1 per cent for a doubling of the time elapsed from the strong shock. The frequencies of large main shocks ($Mw \geq 6.0$) are generally lower than 1 per cent except from about one month after a strong shock with $4.5 \leq Mw < 5.0$ when they become of the order of 4 per cent, but they decrease well below 1 per cent about two or three months after the strong shock if the main shock did not actually occur in the meantime. About 30 per cent of main shocks have been preceded by strong shocks in

the day before, about 50 per cent one in the month before and about 60 per cent in the year before.

All such evidence suggests us to formulate an alarm-based forecasting hypothesis related to the simple occurrence of strong shocks in a given area. In this work we first set up such hypothesis and then optimize it by the retrospective analysis of the HOmogenized instRUmental Seismic catalogue (HORUS) of the Italian area from 1960 to 2019 (Lolli et al., 2020) which is an improved and updated version of the seismic catalogue used by Gasperini et al. (2016).

In our knowledge, this is the first alarm-based forecasting experiments applied to the Italian region after the one by Grandori et al. (1988) cited above and after Console et al. (2010) and Murru et al. (2009) who converted to an alarm-based approach previous probabilistic forecasting studies by Console and Murru (2001) and Console et al. (2003, 2006). In fact, the latter studies, as well as others forecasting efforts in Italy (see Schorlemmer et al., 2010 and Marzocchi et al., 2014 for an overview), mostly based on the Epidemic-Type Aftershock Sequence (ETAS) model (Kagan and Knopoff, 1987, Ogata, 1988), were developed to reproduce at best the general behavior of future seismicity, not to issue a warning of a possibly impending damaging earthquake.

The present forecasting hypothesis will be possibly submitted for prospective testing and validation to the testing facilities of the Collaboratory Study of Earthquake Predictability (CSEP, Jordan, 2006, Zechar et al., 2009).

3.2 Setting up the forecasting hypothesis

We issue an alarm of duration Δt within a circular area (CA) of radius R every time a strong shock with $M_{min} \leq M < M_{max}$ occurs inside the CA. As target events to be forecasted we consider all the shock, with magnitude above a threshold $M_m \geq M_{max}$. We must note that after the actual occurrence of a target shock, the forecast of further

target shocks in the same area and in the following weeks or months is somehow favored by the strong aftershocks of the previous target event. Hence, we also verify the ability of our method to forecast only the first target shock of each sequence. We then consider also a declustered set of target shocks obtained by eliminating those target shocks occurred within a distance $D = 50$ km and a time window of a year after another target shock of the sequence, even if they are larger than the first target shock of the sequence. This kind of declustering is somehow different with respect to that adopted for example in seismic hazard assessment (e.g., Gardner and Knopoff, 1974, Reasenberg, 1985) in which each sequence is usually represented by the largest shock, even if it is not the first one in the sequence. We choose the declustering space and time windows based on our experience on past Italian seismic sequences, but we also checked visually that non possible secondary mainshock remains not declustered. Also note that the chosen declustering windows approximately correspond to those determined by the algorithm of Gardner and Knopoff (1974) for M=5.5.

As source areas we consider a regular tessellation of the Italian territory made of partially overlapping CAs with fixed radius R. Starting from an initial CA, centred at latitude 47º and longitude 7º, we compute the centers of the neighbor CAs by moving with steps $D = R\sqrt{2}$ both in longitude (from 7º to 19º) and in latitude (from 47º to 36º) covering then the whole Italian area with partial overlapping (Fig. 3.1). Based on the results of our previous analysis (Gasperini et al., 2016), we choose a radius $R = 30$ km, as a good compromise between the opposing demands of having short spatial resolution and a sufficiently high number of earthquakes within each CA, so obtaining a total of 695 partially overlapping CAs. However, as the completeness of the seismic catalogue is poor in offshore areas, we consider in our analysis only the CAs within which at least one earthquake with Mw≥4.0 occurred inland from 1600 to 1959 (so as to be independent of the seismicity from 1960 to 2019 that will be used for the retrospective testing and optimization of the forecasting method), according to

the CPTI15 catalogue (Rovida et al., 2016, 2020). According to Gasperini et al. (2016), we consider as target shocks the earthquakes with Mw≥5.0, Mw≥5.5 and Mw≥6.0, which, in Italy, usually cause moderate, heavy, and very heavy damage to buildings and none, a few and many victims respectively. Larger thresholds cannot be investigated because only three shocks with Mw ≥6.5 (1976 Friuli with Mw=6.5, 1980 Irpinia with Mw=6.8 and 2016 Norcia with Mw=6.6) occurred during the time interval covered by the HORUS seismic catalogue.

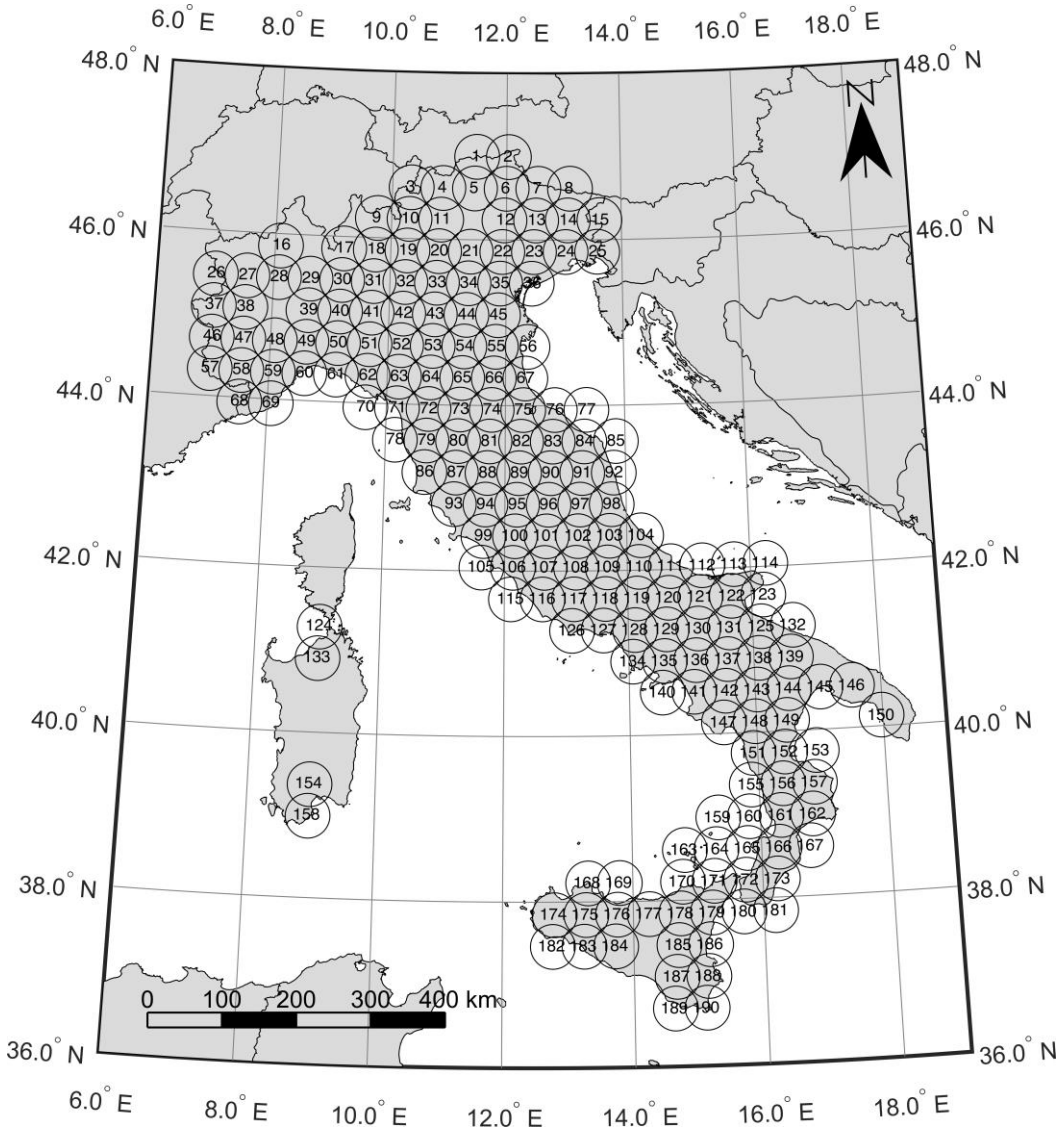

Figure 3.1: Tessellation of the Italian territory used for the retrospective forecast experiment. Circular areas (CA) with R=30 km within which at least one earthquake with Mw≥4.0 occurred inland from 1600 to 1959 according to the CPTI15 catalogue (Rovida et al., 2020).

We count a success if a target shock occurs during one or more alarm time windows Δt and within one or more CA. On the contrary we count a missed forecast if a target shock occurs outside any alarm window of any CA. According to Molchan (1990, 1991) we compute the miss rate as

$$\nu = \frac{N - h}{N} \tag{3.1}$$

where h is the number of target events successfully forecasted and N is the total number of target events.

We also compute the total time duration d_c of alarms as the union of all alarm windows within each CA. This can also be computed by multiplying the window length Δt by the number n of issued alarms and then subtracting the sum of time intersections between alarm windows $\cap\, t_s$

$$d_c = \bigcup \Delta t = n\Delta t - \sum \cap\, t_s \tag{3.2}$$

The fraction of time occupied by alarms within each CA is then computed as

$$\tau_c = \frac{d_c}{T} \tag{3.3}$$

where T is the total duration of the forecasting experiment.

Finally, the overall fraction of space-time occupied by alarms is computed as the average of τ_c over all CAs

$$\tau_u = \frac{1}{M} \sum \tau_c \tag{3.4}$$

where M is the number of CAs. Note that such definition of fraction of space-time occupied by alarms is consistent with strong shocks occurring in the overlapping region of two adjoining CAs because in such case we sum the alarm fraction of time τ_c for both CAs.

Following Shebalin et al. (2011) we also compute the fraction of space-time occupied by alarms by weighting each alarm with the long-term rate of earthquakes within

each CA. We compute such rate based on the data of the CPTI15 catalogue (Rovida et al., 2016, 2020) using different completeness thresholds *Mc* for different time intervals from 1620 to 1959 (Table 3.1). We count the numbers of earthquakes $N(Mc)$ above each magnitude threshold *Mc* occurred within each CA and within the corresponding time interval of completeness $\Delta T(Mc)$. Then we compute for each magnitude threshold the expected rate λ (event/year) of earthquakes with Mw≥4.0, assuming the *b-value* of the frequency-magnitude distribution (Gutenberg & Richter, 1944) equal to 1 (Rovida et al., 2020):

$$\lambda = \frac{N(Mc)}{\Delta T(Mc)} 10^{M_c - 4.0} \tag{3.5}$$

In each CA, we then compute the average λ_{ave} of rates $\lambda > 0$ from different magnitude thresholds. For those CAs for which such average frequency cannot be computed because there are no earthquakes within the completeness time window of any magnitude threshold, we assign the minimum rate computed overall. Finally, the weighted fraction of space-time occupied by alarms is computed from all CAs as

$$\tau_w = \frac{\sum \lambda_{ave} \tau_c}{\sum \lambda_{ave}} \tag{3.6}$$

See the details of such computations for each CA in Table S1 of the supplemental material (Supplementary material 1).

Table 3.1 – Magnitudes of completeness of the CPTI15 catalogue (Rovida et al., 2016, 2020)

Magnitude threshold *Mc*	**Time interval of completeness**	**ΔT (years)**
Mw≥4.5	1880-1959	80
Mw≥5.0	1880-1959	80
Mw≥5.5	1780-1959	180
Mw≥6.0	1620-1959	340

3.3 Dataset used for testing and optimization

To test and optimize our algorithm, we apply it retrospectively to the HOmogenized instRUmental Seismic catalogue (HORUS) of Italian instrumental seismicity from 1960 to 2019 (Lolli et al., 2020). For the time interval from 1960 to 1980, HORUS coincides with the dataset prepared by Lolli et al. (2018). For the period from 1981 to 2019, it is obtained by merging various data sources and homogenizing the magnitudes to Mw as described by Gasperini et al. (2012, 2013). The catalogue used here is updated up to the end of 2019, but an automatic procedure able to continuously update such catalogue in near real-time (with daily to hourly updates) through the downloading of new data from on-line sources and the application of magnitude conversions is implemented by Lolli et al. (2020).

The magnitude completeness threshold for the period 1960-1980 has been assessed by Lolli et al. (2018) to be about 4.0 whereas, according to Gasperini et al. (2013), it is definitely lower for the successive time periods. Such thresholds might be definitely larger in offshore areas owing to the large distances from the closest seismic stations, which are usually located on land (excepting for a few instruments deployed on the sea bottom). This is the reason why we only consider earthquakes with Mw≥4.0 occurred within the 190 CAs containing one inland earthquake at least. As our interest is to forecast earthquakes that potentially threaten lives and goods, we also limit the analysis to shocks shallower than 50 km. We show in Figs. 3.2 and 3.3 the spatial distribution of inland earthquakes from the HORUS catalogue (Lolli et al., 2020) with Mw≥4.0 and depth < 50 km used for testing and optimization, and the time distribution of magnitudes of all inland earthquakes, respectively. The catalogue provides uncertainties for all magnitude estimates, ranging from less than 0.1 (for Mw estimated by moment tensor inversion) to about 0.5 (for Mw proxies from body wave magnitude mb observed by a few stations). In general, magnitude and location errors have the effect to increase the randomness of the catalogue and then to penalize skilled forecasting methods with respect to unskilled ones.

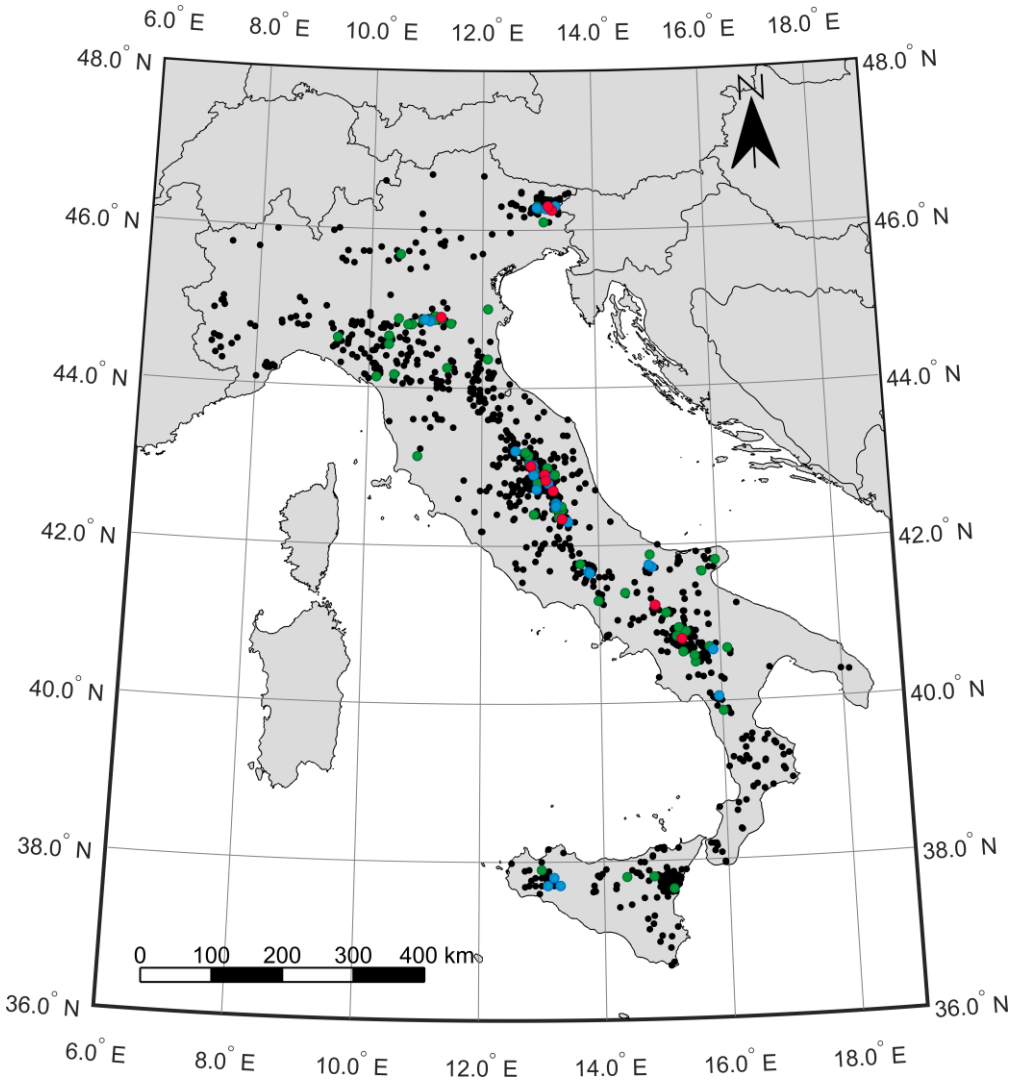

Figure 3.2: Spatial distribution of inland earthquakes from the HORUS catalogue (Lolli et al., 2020) with Mw≥4.0 and depth <50 km used for testing and optimization. Black dots indicate 4.0≤Mw<5.0, green dots 5.0≤Mw<5.5, blue dots 5.5≤Mw<6.0, red dots Mw≥6.0.

Owing to the Gutenberg Richter (1944) law, errors tend on average to overestimate all magnitudes because there are more earthquakes below a given threshold which can be overestimated than earthquakes above the same threshold which can be underestimated. The larger the error the larger the overestimation.

On the other hand, magnitude errors are generally larger for small earthquakes because the latter are observed by less stations and because accurate method of magnitude determination, like moment tensor inversion, cannot be applied to them.

This means that in general small earthquakes are overestimated more than larger ones and then that foreshocks are overestimated more than target shocks.

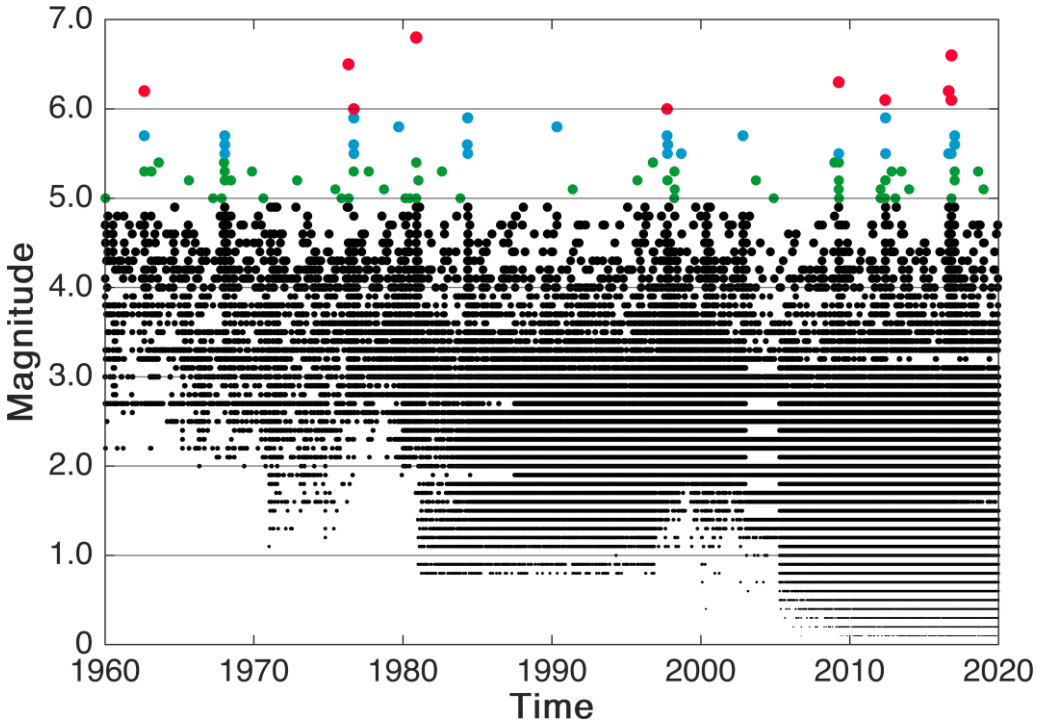

Figure 3.3: Time distribution of magnitudes of inland earthquakes km from the HORUS catalogue (Lolli et al., 2020) with depth <50 km used for testing and optimization. Black dots indicate Mw<5.0, green dots 5.0≤Mw<5.5, blue dots 5.5≤Mw<6.0, red dots Mw≥6.0.

Owing to the Gutenberg Richter (1944) law, errors tend on average to overestimate all magnitudes because there are more earthquakes below a given threshold which can be overestimated than earthquakes above the same threshold which can be underestimated. The larger the error the larger the overestimation.

On the other hand, magnitude errors are generally larger for small earthquakes because the latter are observed by less stations and because accurate method of magnitude determination, like moment tensor inversion, cannot be applied to them. This means that in general small earthquakes are overestimated more than larger ones and then that foreshocks are overestimated more than target shocks.

One possible consequence in the present case is that errors in magnitude might improperly increase the number of alarms and then the space-time fraction occupied by alarms, particularly in earlier times when the coverage of seismic networks was coarser, so that to slightly underestimate the real skill of the method. Conversely the number of target shocks should not be affected much by magnitude errors because in HORUS catalogue the most (about 80%) of Mw≥5.0 are accurately computed by moment tensor inversions.

3.4 Testing and optimizing the forecasting hypothesis

We here follow the approach proposed by Zechar and Jordan (2008, 2010) based on the so called "Molchan error diagram" (Molchan, 1990, 1991; Molchan and Kagan, 1992). The latter consists of a plot (e.g., Fig. 3.4) of the miss rate ν (eq. 3.1) as a function of the fractions of space-time occupied by alarms τ (τ_u of eq. 3.4 or τ_w of eq. 3.6). For a paradoxical forecasting method not issuing any alarm, the space-time occupied by alarms is 0 and no target events can be forecasted (all target events are missed) then it is represented by the point $(\tau, \nu) = (0{,}100\%)$ at the upper left corner of the Molchan diagram. On the other hand, for a forecasting method issuing an alarm at any time and in any place, so occupying the entire space-time volume, no target events are missed and then the forecasting method is represented by the point $(\tau, \nu) = (100\%, 0)$ at the lower right corner of the diagram. The points on the diagonal line connecting such two points (e.g., the black continuous line in Fig. 3.4), with equation

$$\nu = 1 - \tau \tag{3.7}$$

indicate the expected performance of a purely random forecasting method that simply forecasts target events proportionally to the space-time fraction occupied by the alarms.

On the diagonal line, the ratio between the success rate and the space-time fraction

$$G = \frac{1-\nu}{\tau} \tag{3.8}$$

is 1 for any τ, while for a skilled forecasting method, located below the line, $G > 1$ represents the "probability gain" factor with respect to the random case.

Following Zechar and Jordan (2008), τ (τ_u or τ_w) can be assumed as the probability of forecasting a target event by chance and then can be used to measure the performance of a forecasting method under the reasonable assumption that the probability of having exactly h successful forecasts over N targets is given by the binomial probability function

$$B(h|N\tau) = \binom{N}{h}(\tau)^h(1-\tau)^{N-h} \tag{3.9}$$

Then the cumulative probability of having by chance h or more successful forecasts is

$$\alpha = \sum_{n=h}^{N} B(n|N\tau) = 1 - \sum_{n=0}^{h-1} B(n|N\tau) \tag{3.10}$$

Such statistic allows to measure the skill of a forecasting methods, given the miss rate ν and the fraction of space-time occupied by alarms τ. In particular, the lower the statistic the higher the skill. Moreover, by inverting eq. (3.10), we can compute the expected miss rate ν at a given τ, for a hypothetical forecasting method with given probability α, and then to plot confidence limits on the Molchan diagram (e.g., the blue, violet and green lines in Fig. 3.4).

This statistic can be used to validate a forecasting method using a prospective dataset (collected after the final fixing of the forecasting hypothesis) but even to optimize the forecasting hypothesis by searching the values of the parameters of the forecasting algorithm (if any) for which the statistic is minimum, by using a retrospective dataset.

A given forecasting method with fixed parameter values is represented by a single point (τ, ν) on the Molchan diagram. However, one can even consider curves

(Molchan trajectories) connecting different points referred to the same general forecasting approach but obtained by varying one of the free parameters of the forecasting algorithm. In our case we can vary the alarm time window Δt from 0 to the total duration T of the experiment. In this way, we span the total space-time occupied by the alarms and correspondingly the number of successful forecasts, which increase with increasing Δt.

In the light of such definition, the diagonal line in the Molchan diagram can be seen as the Molchan trajectory of a purely random forecasting method. If a forecasting method performs better than the random one, its trajectory mainly lies in the lower left half of the Molchan diagram below the random line.

Zechar & Jordan (2008, 2010) proposed to use as a measure of the performance of an alarm-based forecasting method the integral of the success rate function $1 - \nu_f(\tau)$ normalized to the alarm space-time coverage τ

$$a_f(\tau) = \frac{1}{\tau}\int_0^{\tau} \left[1 - \nu_f(t)\right] dt \tag{3.11}$$

As the integral corresponds to the area above the Molchan random trajectory, the statistic was named Area Skill (AS) score. The AS score is normalized so that its value ranges between 0 and 1: the larger the statistic the better the performance.

The expected value of the AS score for a purely random method can be derived by substituting the equation (3.7) of the random line $\nu_f(t) = 1 - t$ in equation (3.11). This gives

$$\langle a_f(\tau) \rangle = \frac{1}{\tau}\int_0^{\tau} [1 - (1 - t)]\, dt = \frac{1}{\tau}\frac{\tau^2}{2} = \frac{\tau}{2} \tag{3.12}$$

Such expectance function is represented in a plot as a function of τ by a straight line connecting the axes origin (0,0) with the point (100%, 50%) (e.g., the black line in Fig. 3.5). In such plot, the skilled forecasting methods lie above such random line.

Zechar & Jordan (2008, 2010) explored the AS score distribution and found that, for a continuous alarm function, the AS score at $\tau = 1$ is asymptotically Gaussian with a mean of 1/2 and a variance of 1/(12N). They also found that the kurtosis excess is -6/(5*N*) and hence, for *N* of the order of a dozen at least, the Gaussian approximation provides a good estimate of confidence bounds. Finally, they argued that even if the area skill score can be computed for any τ, the power of the test tends to increase with increasing τ and therefore it is the best to use $a_f(\tau = 1)$ for hypothesis testing.

3.5 Results of retrospective testing

In Fig. 3.4 we show the Molchan trajectories for all target shocks (35) with Mw≥5.5 (not declustered) preceded by strong shocks with 4.4≤Mw<4.8, by varying Δt from a width of a few seconds to the total duration *T*=60 years of the catalogue. Red and dark blue lines refer to the unweighted (τ_u) and weighted (τ_w) fractions of space-time occupied by alarms respectively (see in Table 3.2 the numerical values of plotted curves).

The adopted foreshock Mw range (Mw=4.6±0.2) was chosen after a comparative analysis of the relative performance of various ranges with lower and upper magnitude bounds varying from the completeness threshold of the catalogue (Mw=4.0) to the minimum magnitude of target shocks (Mw=5.0). Such analysis was aimed at maximizing the overall AS score and at the same time minimizing the total number of alarms (Fig. 3.6).

Both the red and dark blue lines in Fig. 3.4 lie well below the α =1% confidence curve (green) for all explored Δt. All the target shocks are successfully forecasted (ν =0) for Δt=20 years (corresponding to $\tau_u = 32\%$ and $\tau_w = 51\%$) or larger. For Δt=1 year, about 83% of target shocks (29) are successfully forecasted, with space-time coverages τ_u =3.3% and τ_w =6.3%. 40% of target shocks (14) are forecasted with Δt=1 day for which $\tau_u = 0.01\%$ and $\tau_w = 0.03\%$. The AS diagram in Fig. 3.5 (see Table 3.2

for numerical values) confirms such good performance with the scores of the forecasting method (red and dark blue lines) well above the random expectation (black) and the 1% confidence line (green) for any Δt. The overall AS scores $a_f(\tau = 1)$ =0.96±0.05 and $a_f(\tau_w = 1)$ =0.94±0.05, based on the Student's t-test, are significantly larger than the expectance of a random method (0.5) with significance level (s.l.) ≪0.01.

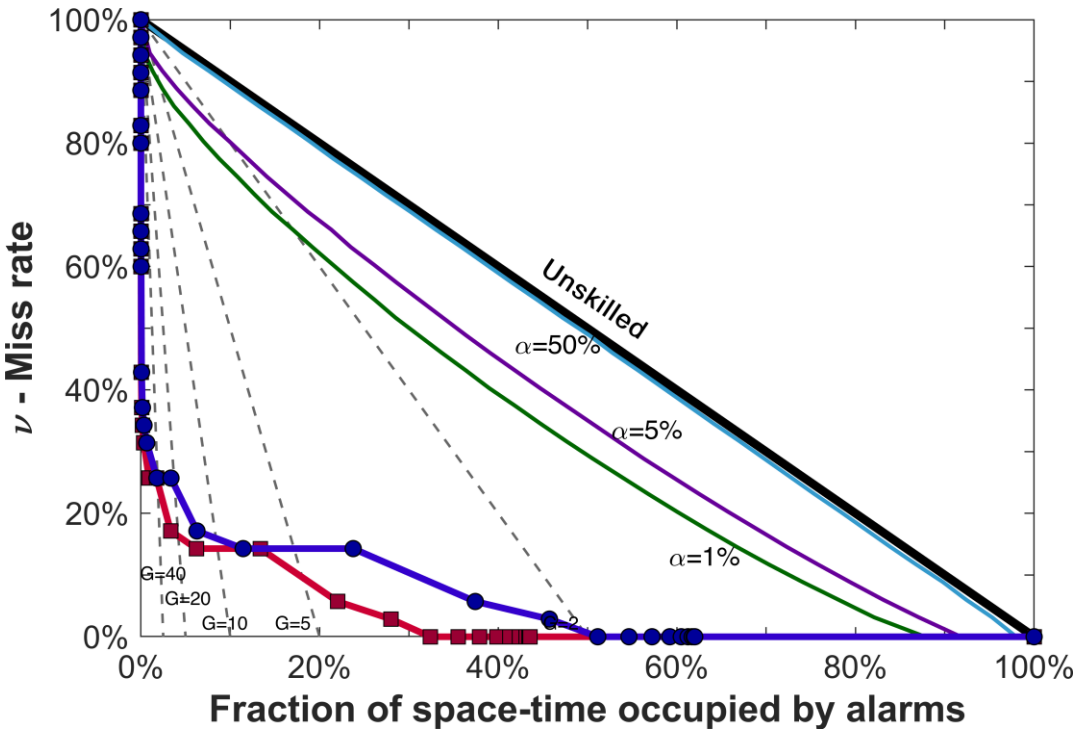

Figure 3.4: Molchan diagram for all target shocks with Mw≥5.5 (not-declustered). Red and dark blue lines indicate the forecasting performance of foreshocks with 4.4≤Mw<4.8 for unweighted (τ_u) and weighted (τ_w) fractions of space-time occupied by alarms respectively (see text). The black continuous line indicates a purely random forecasting method that separates skilled (below the line) from unskilled (above) forecasting methods. The light blue, violet and green lines indicate the confidence limits for α =50%, 5% and 1% respectively. The black dashed lines indicate probability gains G=2, 5, 10, 20 and 50.

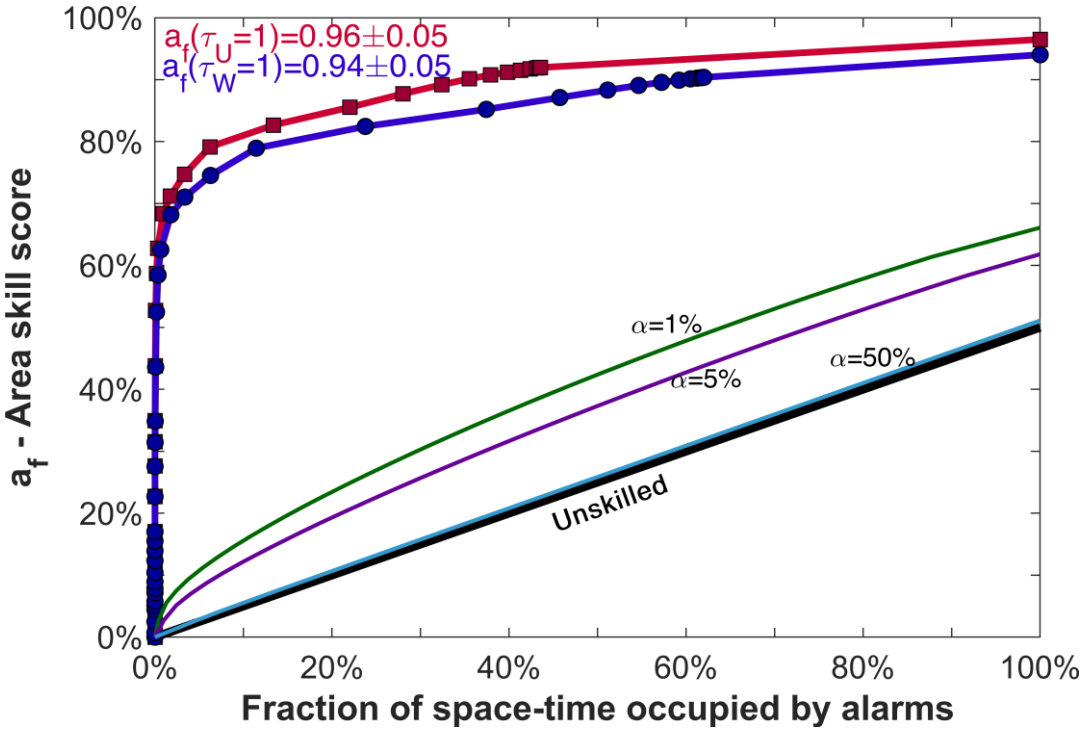

Figure 3.5: Area skill score diagram for all target shocks with Mw≥5.5 (not-declustered). Red and dark blue lines indicate the forecasting performance of foreshocks with 4.4≤Mw<4.8 for unweighted (τ_u) and weighted (τ_w) fractions of space-time occupied by alarms respectively (see text). The black continuous line indicates the performance of a purely random forecasting method that separates skilled (below the line) from unskilled (above) forecasting methods. The light blue, violet and green lines indicate the confidence limits for α =50%, 5% and 1% respectively.

As noted above the aftershocks produced by the first target shocks of seismic sequence may significantly contribute to forecast subsequent target shocks with Mw≥5.5 within the same sequence. We then proceed to analyze in the same way the declustered set of target shocks with Mw≥5.5 obtained by discarding all target shocks occurred within a spatial distance R=50 km and a time window of a year after the first and all subsequent Mw≥5.5 shocks of the sequence. This reduces the number of considered target shocks with Mw≥5.5 from 35 to 14.

In Fig. 3.7 and 3.8 we report the same plots as in Fig. 3.4 and 3.5 but for the (declustered) set of only the first target shocks with Mw≥5.5 of each sequence (see

Table 3.3 for numerical values). The performance is worse than for the not-declustered set but remains well below the random line and the α=1% confidence curve in the Molchan diagram of Fig. 3.7 and also well above the α =1% confidence line of AS diagram of Fig. 3.8. Even in this case all 14 target shocks are successfully forecasted with Δt=20 years or larger. For Δt=1 year, 64% of target shocks (9) are forecasted and 29% (4) for Δt=1 day. The overall AS score $a_f(\tau_u = 1)$ =0.93±0.08 and $a_f(\tau_w = 1)$ =0.87±0.08 are lower than for the not-declustered set but anyhow they are significantly larger than the expectance (0.5) of a random method with s.l. ≪0.01.

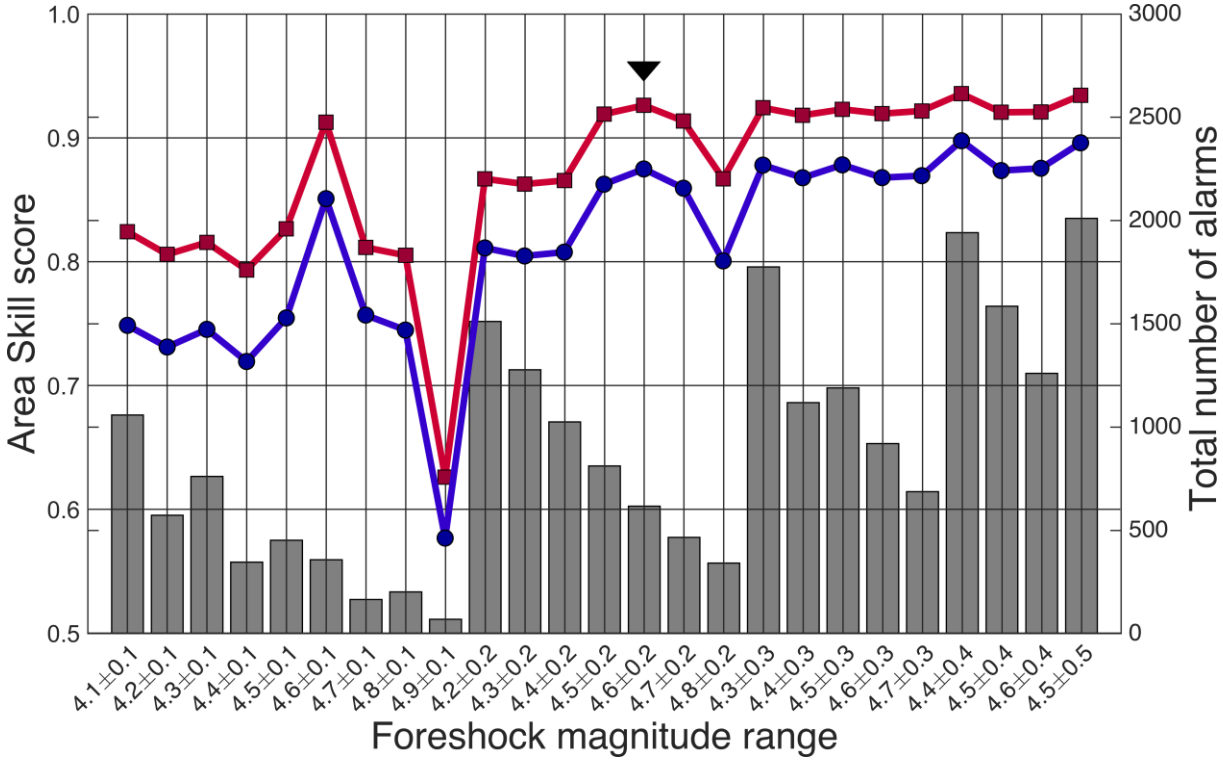

Figure 3.6: Area Skill (AS) score computed for declustered targets with Mw≥5.5, using unweighted (red line) and weighted (blue) fractions of space-time occupied by alarms, and total number of alarms (grey bars) as a function of the foreshock magnitude range. The arrows indicate the range Mw=4.6±0.2, chosen as best compromise between high AS score and low number of alarms.

Table 3.2 – Values of variables in Molchan and Area Skill score plots of Fig. 3.4 and 3.5 for Mw≥5.5 not-declustered targets.

Δt (years)	Δt (days)	τ_u	τ_w	h	ν	$a_f(\tau_u)$	$a_f(\tau_w)$
1.6E-08	5.8E-06	8.6E-10	2.0E-09	0	1.000	0.000	0.000
3.2E-08	1.2E-05	1.7E-09	4.1E-09	1	0.971	0.021	0.022
6.3E-08	2.3E-05	3.4E-09	8.1E-09	2	0.943	0.037	0.038
1.6E-07	5.8E-05	8.6E-09	2.0E-08	2	0.943	0.051	0.051
3.2E-07	1.2E-04	1.7E-08	4.1E-08	2	0.943	0.054	0.054
4.8E-07	1.7E-04	2.6E-08	6.1E-08	3	0.914	0.060	0.060
9.5E-07	3.5E-04	5.1E-08	1.2E-07	3	0.914	0.073	0.073
1.9E-06	6.9E-04	1.0E-07	2.4E-07	3	0.914	0.080	0.080
3.8E-06	1.4E-03	2.0E-07	4.9E-07	4	0.886	0.090	0.090
9.5E-06	3.5E-03	5.1E-07	1.2E-06	4	0.886	0.104	0.104
1.9E-05	6.9E-03	1.0E-06	2.4E-06	6	0.829	0.124	0.124
2.9E-05	1.0E-02	1.5E-06	3.6E-06	6	0.829	0.140	0.139
5.7E-05	2.1E-02	3.0E-06	7.1E-06	6	0.829	0.155	0.155
1.1E-04	4.2E-02	6.0E-06	1.4E-05	7	0.800	0.170	0.170
3.4E-04	0.13	1.7E-05	4.0E-05	11	0.686	0.227	0.227
6.8E-04	0.25	3.4E-05	7.7E-05	12	0.657	0.276	0.276
1.4E-03	0.50	6.5E-05	1.5E-04	13	0.629	0.316	0.314
2.7E-03	1.00	1.3E-04	2.8E-04	14	0.600	0.350	0.349
8.2E-03	3.00	3.6E-04	7.8E-04	20	0.429	0.438	0.436
0.019	7.02	8.1E-04	1.7E-03	22	0.371	0.527	0.525
0.042	15.22	1.7E-03	3.5E-03	23	0.343	0.587	0.585
0.083	30.44	3.2E-03	6.5E-03	24	0.314	0.628	0.625
0.250	91.31	9.1E-03	0.018	26	0.257	0.684	0.682
0.500	182.62	0.017	0.034	26	0.257	0.712	0.710
1.000	365.24	0.033	0.063	29	0.171	0.747	0.745
2.000	730.49	0.062	0.114	30	0.143	0.791	0.789
5.000	1826.21	0.134	0.238	30	0.143	0.827	0.825
10	3652.43	0.220	0.374	33	0.057	0.855	0.852
15	5478.64	0.280	0.457	34	0.029	0.877	0.871
20	7304.85	0.324	0.511	35	0.000	0.892	0.883
25	9131.06	0.355	0.546	35	0.000	0.901	0.891
30	10957.28	0.379	0.572	35	0.000	0.908	0.896
35	12783.49	0.398	0.592	35	0.000	0.912	0.899
40	14609.70	0.413	0.605	35	0.000	0.915	0.901
45	16435.91	0.424	0.613	35	0.000	0.917	0.903
50	18262.13	0.431	0.617	35	0.000	0.919	0.903
55	20088.34	0.434	0.619	35	0.000	0.919	0.904
60	21914.55	0.436	0.620	35	0.000	0.920	0.904
Full occ.	Full occ.	1.000	1.000	35	0.000	0.965	0.940

Δt is the duration of alarms, τ_u and τ_w the unweighted and weighted fraction of space-time occupied by alarms respectively, h the number of successful forecasts, ν the miss rate, $a_f(\tau_u)$ and $a_f(\tau_w)$ the Area Skill scores computed considering the unweighted and weighted fraction of space-time occupied by alarms respectively. The last row (Δt= Full occ.) reports values for a full occupation of the space-time by alarms.

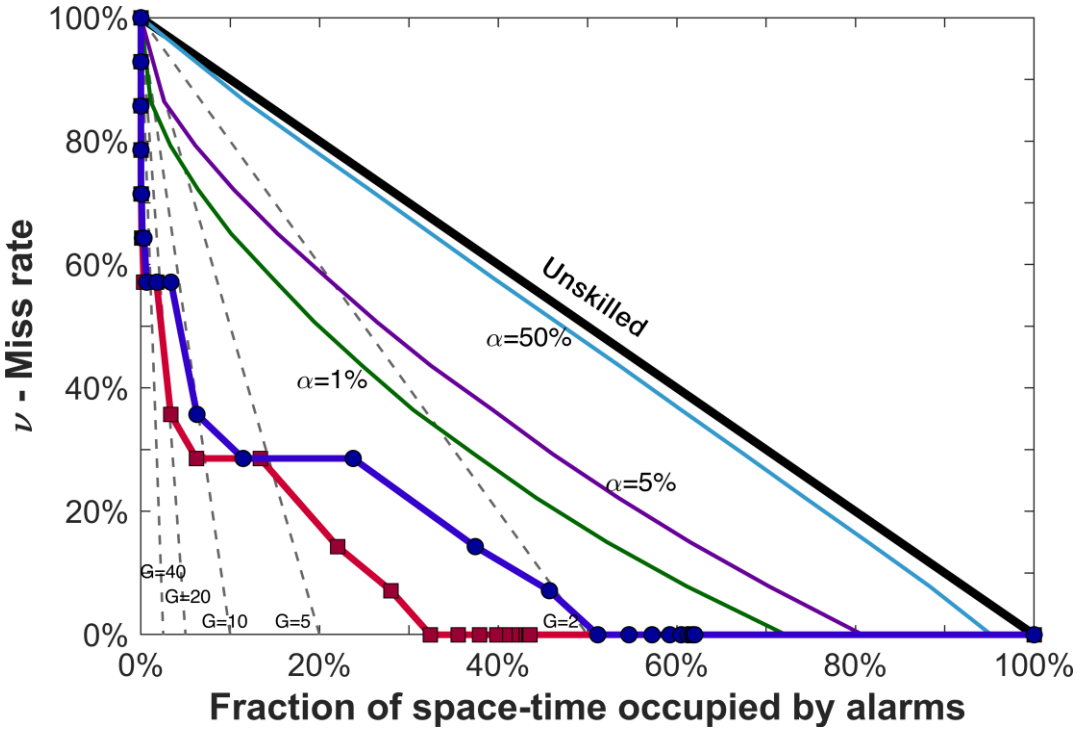

Figure 3.7: Same as Fig. 3.4 for declustered (first) target shocks with Mw≥5.5.

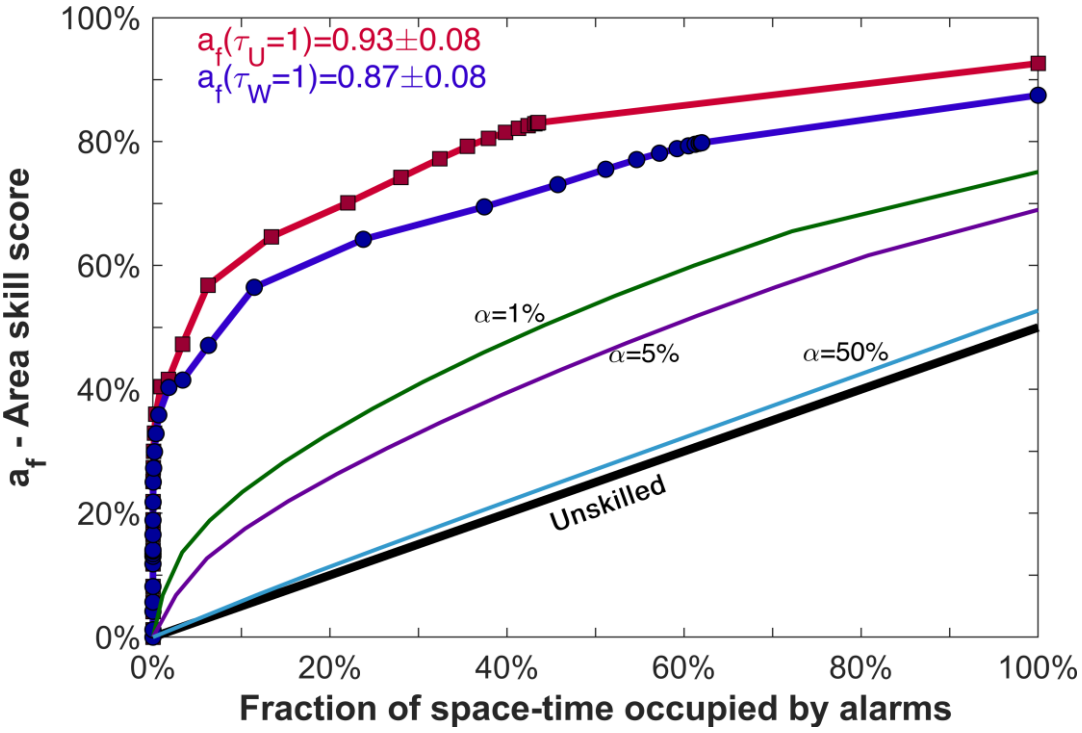

Figure 3.8: Same as Fig. 3.5 for declustered (first) target shocks with Mw≥5.5.

Table 3.3 – Same as Table 3.2 for Mw≥5.5 declustered targets (Fig. 3.7 and 3.8).

Δt (years)	Δt (days)	τ_u	τ_w	h	ν	$a_f(\tau_u)$	$a_f(\tau_w)$
1.6E-08	5.8E-06	8.6E-10	2.0E-09	0	1.000	0.000	0.000
3.2E-08	1.2E-05	1.7E-09	4.1E-09	0	1.000	0.000	0.000
6.3E-08	2.3E-05	3.4E-09	8.1E-09	0	1.000	0.000	0.000
1.6E-07	5.8E-05	8.6E-09	2.0E-08	0	1.000	0.000	0.000
3.2E-07	1.2E-04	1.7E-08	4.1E-08	0	1.000	0.000	0.000
4.8E-07	1.7E-04	2.6E-08	6.1E-08	1	0.929	0.012	0.012
9.5E-07	3.5E-04	5.1E-08	1.2E-07	1	0.929	0.043	0.043
1.9E-06	6.9E-04	1.0E-07	2.4E-07	1	0.929	0.057	0.057
3.8E-06	1.4E-03	2.0E-07	4.9E-07	2	0.857	0.082	0.082
9.5E-06	3.5E-03	5.1E-07	1.2E-06	2	0.857	0.119	0.119
1.9E-05	6.9E-03	1.0E-06	2.4E-06	2	0.857	0.131	0.131
2.9E-05	1.0E-02	1.5E-06	3.6E-06	2	0.857	0.135	0.135
5.7E-05	2.1E-02	3.0E-06	7.1E-06	2	0.857	0.139	0.139
1.1E-04	4.2E-02	6.0E-06	1.4E-05	2	0.857	0.141	0.141
3.4E-04	0.13	1.7E-05	4.0E-05	3	0.786	0.166	0.165
6.8E-04	0.25	3.4E-05	7.7E-05	3	0.786	0.189	0.189
1.4E-03	0.50	6.5E-05	1.5E-04	4	0.714	0.219	0.218
2.7E-03	1.00	1.3E-04	2.8E-04	4	0.714	0.251	0.250
8.2E-03	3.00	3.6E-04	7.8E-04	4	0.714	0.274	0.273
0.019	7.02	8.1E-04	1.7E-03	5	0.643	0.300	0.299
0.042	15.22	1.7E-03	3.5E-03	5	0.643	0.329	0.329
0.083	30.44	3.2E-03	6.5E-03	6	0.571	0.360	0.359
0.250	91.31	9.1E-03	0.018	6	0.571	0.404	0.403
0.500	182.62	0.017	0.034	6	0.571	0.416	0.415
1.000	365.24	0.033	0.063	9	0.357	0.473	0.471
2.000	730.49	0.062	0.114	10	0.286	0.568	0.565
5.000	1826.21	0.134	0.238	10	0.286	0.646	0.642
10	3652.43	0.220	0.374	12	0.143	0.701	0.695
15	5478.64	0.280	0.457	13	0.071	0.742	0.731
20	7304.85	0.324	0.511	14	0.000	0.772	0.755
25	9131.06	0.355	0.546	14	0.000	0.792	0.771
30	10957.28	0.379	0.572	14	0.000	0.805	0.781
35	12783.49	0.398	0.592	14	0.000	0.815	0.789
40	14609.70	0.413	0.605	14	0.000	0.821	0.793
45	16435.91	0.424	0.613	14	0.000	0.826	0.796
50	18262.13	0.431	0.617	14	0.000	0.829	0.797
55	20088.34	0.434	0.619	14	0.000	0.830	0.798
60	21914.55	0.436	0.620	14	0.000	0.831	0.798
Full occ.	Full occ.	1.000	1.000	14	0.000	0.926	0.875

In Figs. 3.9, 3.10, and Figs. S1 and S2 of supplementary material 1, we report the same plots of Fig. 3.4, 3.5, 3.7 and 3.8 for target shocks with Mw≥5.0 (numerical values in Tables S2 and S3). The performance is definitely worse than for Mw≥5.5 but still better than the 1% confidence limit. In particular, even for Δt =60 years, only 89 over

98 (91%) target shocks for the not-declustered set and only 36 over 44 (82%) for the declustered set are successfully forecasted. The reason is that even when Δt is equal to the total duration of the catalogue, in some CAs there remains a fraction of time (before the first strong shock) without any strong shock and then without any alarm. Actually, the maximum fraction of space-time occupied by alarms (τ_u) is only about 44% of the total space-time and 9 target shocks with Mw≥5.0 occurred in the remaining 56%. Here, the last part of the Molchan trajectories, consisting of a linear decrease from the last point defined by the algorithm ($\tau_u = 44\%$ and $\tau_w = 62\%$ with $\nu = 9\%$ for not-declustered and 18% for declustered) to the lower left corner ($\tau = 100\%$, $\nu = 0$), can be interpreted as the application to the remaining earthquakes, not predicted by any foreshock, of a purely random forecasting method with success rate proportional to the fraction of the remaining space-time region not covered by our forecasting algorithm.

The overall AS scores are $a_f(\tau_u = 1)$ =0.89±0.03 and $a_f(\tau_w = 1)$ =0.85±0.03 for the not-declustered set and $a_f(\tau = 1)$ =0.78±0.04 and $a_f(\tau_w = 1)$ =0.70±0.04 for the declustered set. In all cases they are significantly larger than the expectance (0.5) of a random method with s.l. ≪0.01.

In Figs. 3.11, 3.12, and Figs. S3 and S4 of the supplementary material 1, we also report the plots for targets with Mw≥6.0 (see numerical values in Tables S4 and S5). The performance is similar to that for Mw≥5.5 but as the number of target events is smaller (10 not-declustered and 7 declustered), the power of the tests and the reliability of possible inferences are relatively poorer. This is actually reflected by the fact that the confidence limits in this case are relatively close to the Molchan and AS trajectories.

All not-declustered targets are successfully forecasted with $\Delta t = 20$ years, 80% with Δt =1 year and 50% with Δt =1 day. For declustered targets, the corresponding forecasting rates are 100%, 71% and 43% respectively. The overall AS scores are $a_f(\tau_u = 1)$ =0.95±0.09 and $a_f(\tau_w = 1)$ =0.91±0.09 for not-declustered and $a_f(\tau_u =$

1) =0.93±0.11 and $a_f(\tau_w = 1)$ =0.87±0.11 for declustered. In all cases they are significantly larger than the expectance (0.5) of a random method with s.l.≪0.01.

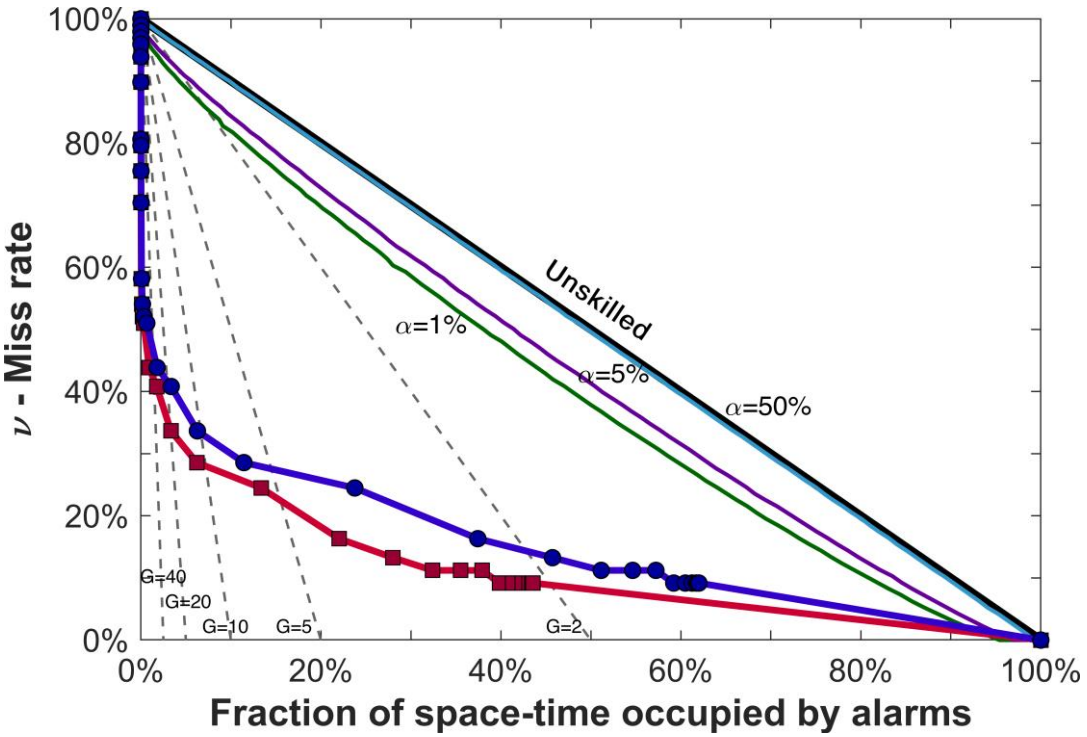

Figure 3.9: Same as Fig. 3.4 for all target shocks with Mw≥5.0 (not-declustered).

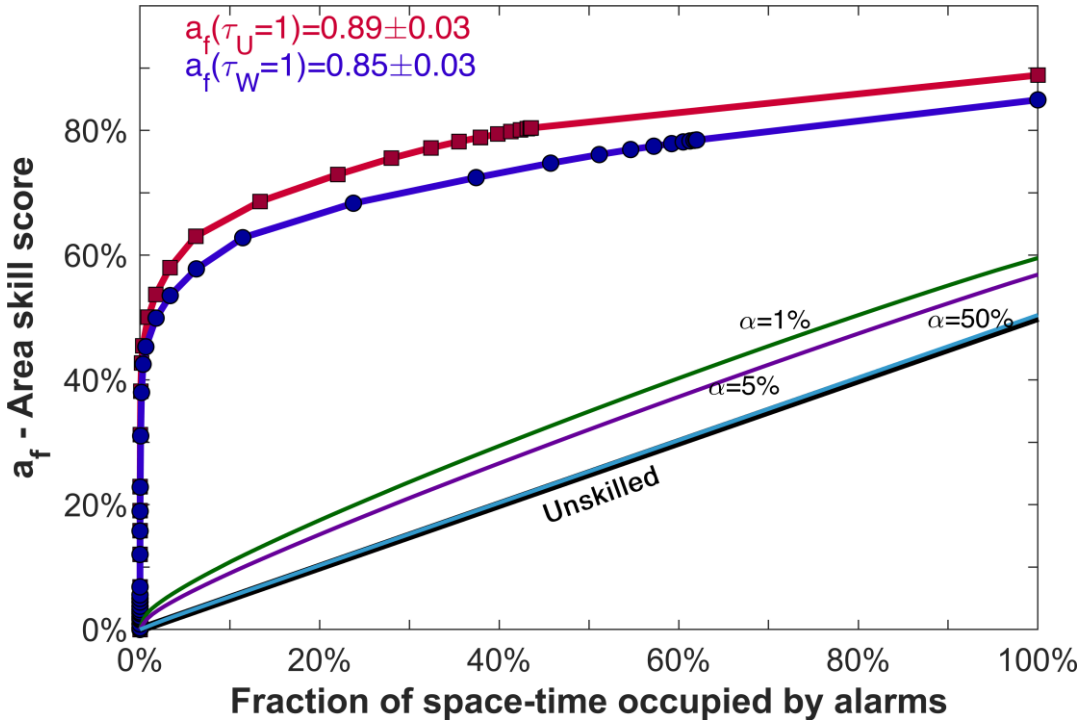

Figure 3.10: Same as Fig. 3.5 for all target shocks with Mw≥5.0 (not-declustered).

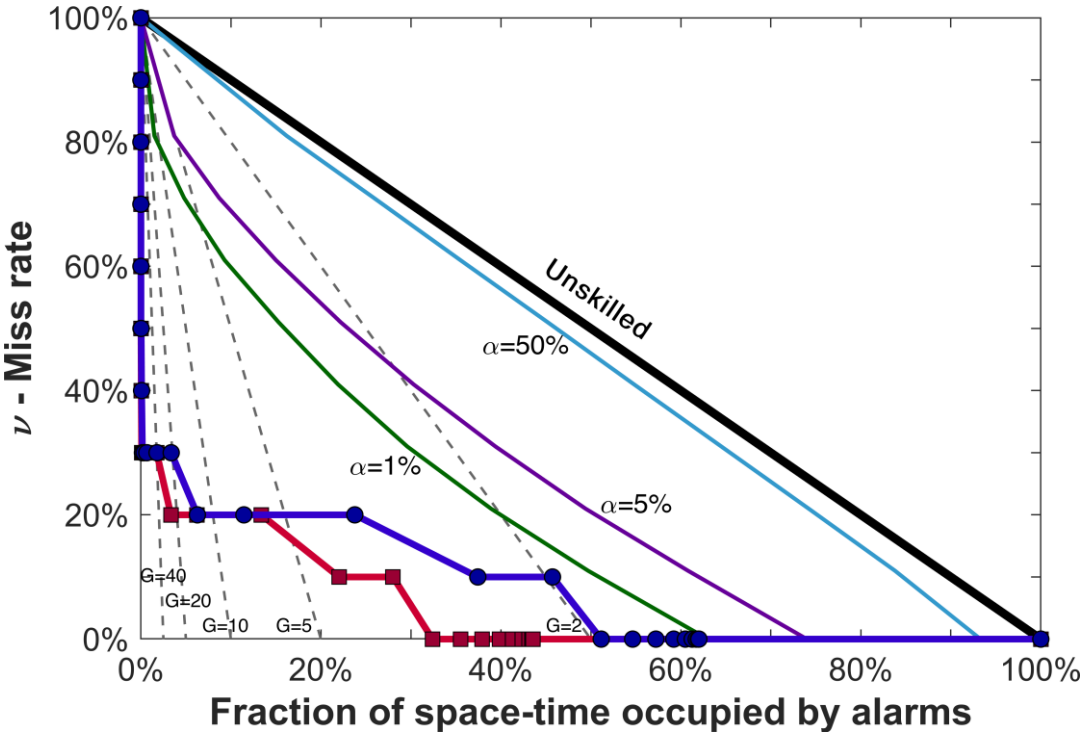

Figure 3.11: Same as Fig. 3.4 for all target shocks with Mw≥6.0 (not-declustered).

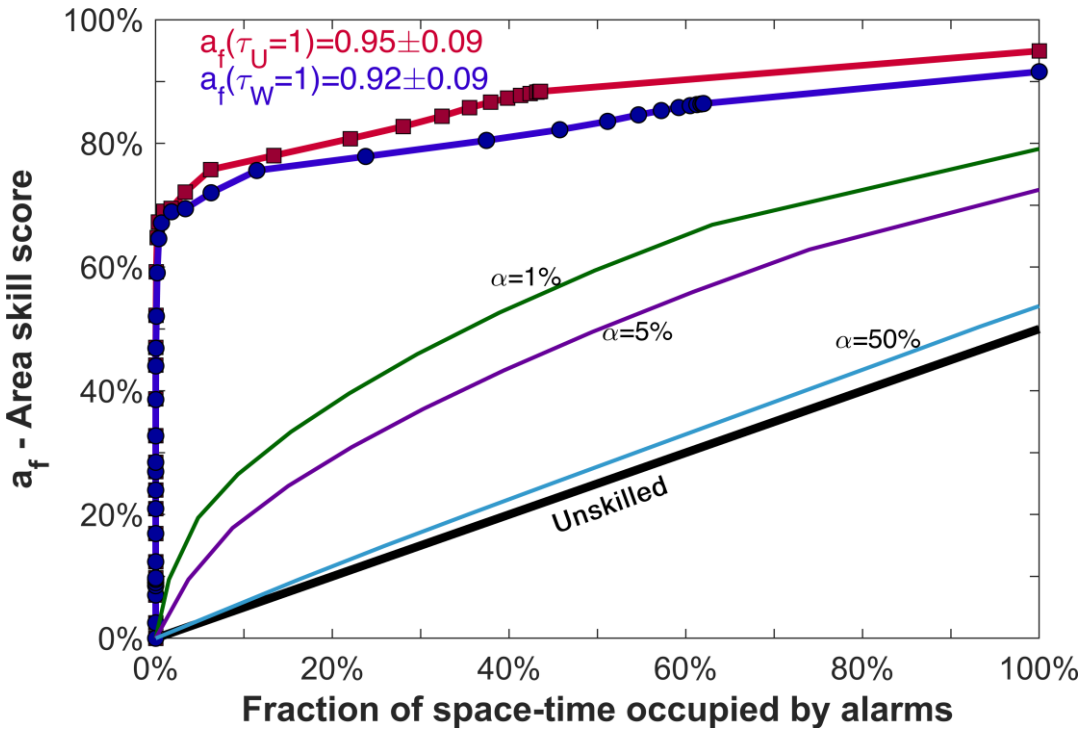

Figure 3.12: Same as Fig. 3.5 for all target shocks with Mw≥6.0 (not-declustered).

One question that may come to mind when looking at the results of such space-time analysis is how much of the observed forecasting performance is due to spatial clustering and how much to time clustering. In order to try to answer such question, we made some further computations in which the time clustering is eliminated by assuming in each CA a permanent alarm for the entire duration of the forecasting experiment (T=60 years). We computed the time independent Molchan and AS score trajectories by adding step by step one CA at a time, starting from the CA with highest weight (highest long-term seismic activity) and then going on, up to add all CAs. At each step, the unweighted and weighted fractions of space occupied by alarms are computed by simply taking $\tau_c = 1$ in eq. (3.4) and (3.6) respectively for the included CAs and $\tau_c = 0$ for the not included CAs.

The results of such time-independent analysis for declustered (first) target shocks with Mw≥5.5 is shown in Figs. 3.13 and 3.14. Even if they are not fully comparable with the time-dependent analysis of Fig. 3.7 and 3.8 because the trajectories depend on the adopted ordering of the CAs, from the most to the least active, we can note that the skill of time-independent analysis appears definitely lower, particularly at small τ and for the weighted trajectories (blue lines). This can be easily explained by the higher time clustering at short times (and then at small τ) and by the fact that the weights based on the long-term seismic activity penalize more the CAs where the target shocks actually occurred in the last 60 years.

The results for declustered (first) target shocks with Mw≥5.0 and Mw≥6.0 are reported in Figs. S5, S6, S7 and S8 of supplementary material 1. For Mw≥5.0, the comparison of Fig. S5 and S6 with the time-dependent analysis of Figs. S1 and S2 is similar to the case for Mw≥5.5 described before. For Mw≥6.0, the comparison of Fig. S13 and S14 with the time-dependent analysis of Figs. S3 and S4, apart for small τ, apparently indicates an overall higher skill for the time-independent analysis with respect to the time-dependent one. This is due to the fact that for Mw≥6.0 all declustered target shocks occurred in CAs with very high long-term seismic activity

and that, as noted above, time-independent and time-dependent statistics are not fully comparable between them.

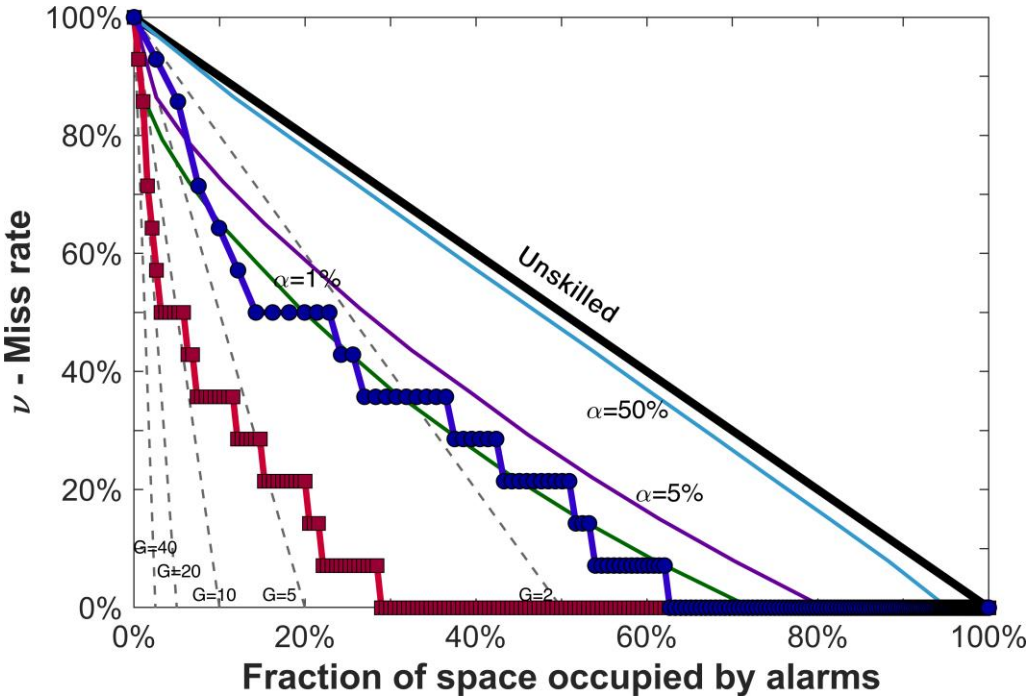

Figure 3.13: Same as Fig. 3.4 for time-independent analysis of declustered (first) target shocks with Mw≥5.5.

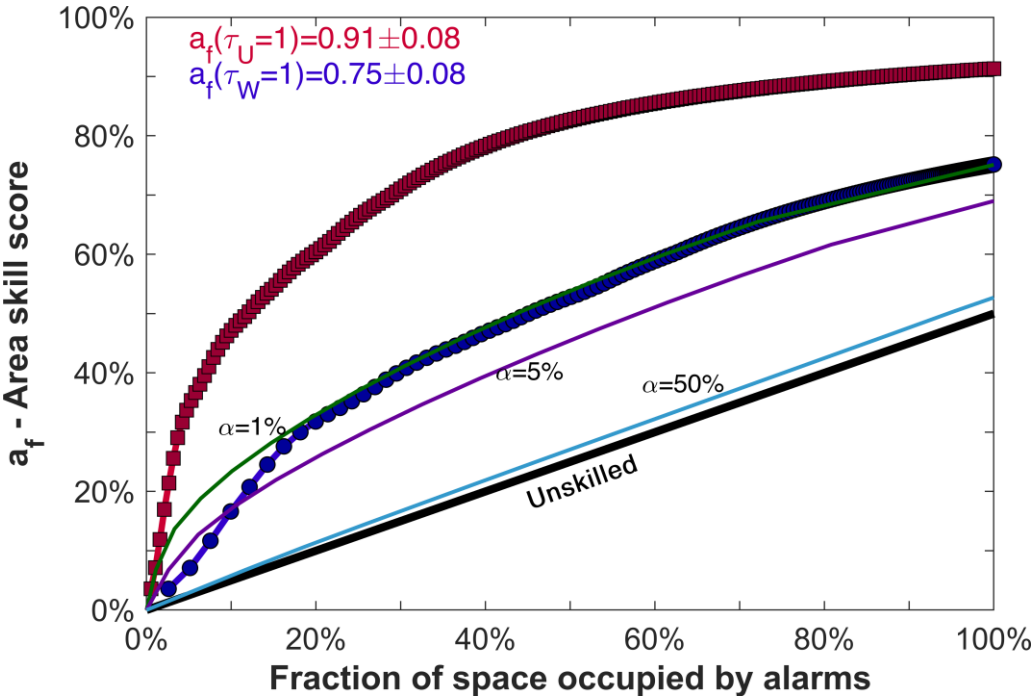

Figure 3.14: Same as Fig. 3.5 for time-independent analysis of declustered (first) target shocks with Mw≥5.5.

3.6 Optimization of the forecasting algorithm

For a practical application of the forecasting method, it might be useful to determine the values of the algorithm parameter Δt for which the forecasting method is more efficient and useful for risk mitigation. To accomplish this purpose, we analyze the behavior of some statistics that depend on the alarm time window Δt.

In Fig. 3.15 we report, for declustered targets and weighted fraction of space-time occupied by alarms (τ_w), the binomial probability (Eq. 3.9), that is the probability that the observed number of successful forecasts is obtained by chance, as a function of Δt. The lower the probability the higher the strength of the forecast. In general, probabilities are relatively low within a wide range going from one day to some years. For Mw≥5.0 (red line), very low probabilities are observed around $\Delta t = 2 \div 10$ days. For Mw≥5.5 (blue line) and Mw≥6.0 (green line) the minimum probabilities are larger than the ones for Mw≥5.0, and they remain relatively low from a few hours to a few months. Within such ranges, the forecasting ability of our method reaches its higher efficiency.

The behavior of the probability gain G (eq. 3.8) as a function Δt (Fig. 3.16) shows, for all the three magnitude thresholds, monotonically descending trends from more than 100000 at very short Δt (less than a minute) to slightly more than 1 at very long Δt (tens of years). Such curves also show relatively milder slopes in correspondence of steep decreases of binomial probabilities in Fig. 3.15 (i.e., around 0.001 day and a few days).

In Fig. 3.17 we show the miss rate ν as a function of Δt. In general, it decreases with increasing Δt. The (negative) trends - with respect to $\log_{10}\Delta t$ - are in between the -5% and -10% per decade, for Δt ranging from a few seconds to about 1 year. Then they start to decrease more rapidly (about -20% per decade) reaching 0 for Mw≥5.5 and Mw≥6.0 and 19% for Mw≥5.0 at very large Δt.

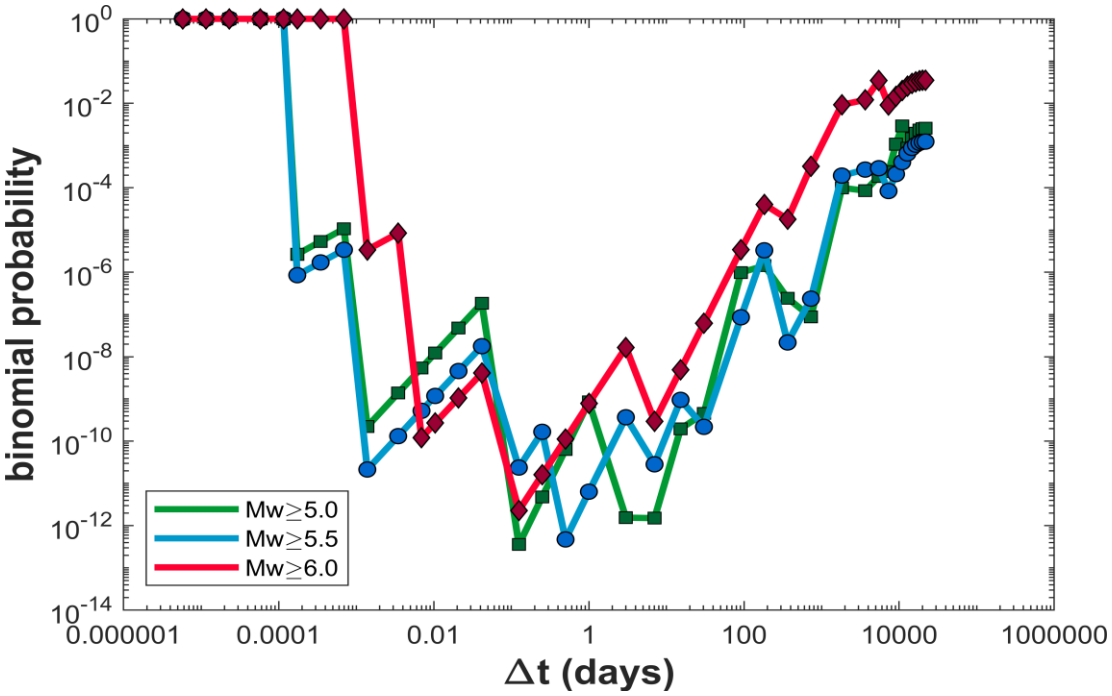

Figure 3.15: Binomial probability density for declustered (first) target shocks and weighted fraction of space-time occupied by alarms for different magnitude thresholds as a function of the alarm duration Δt.

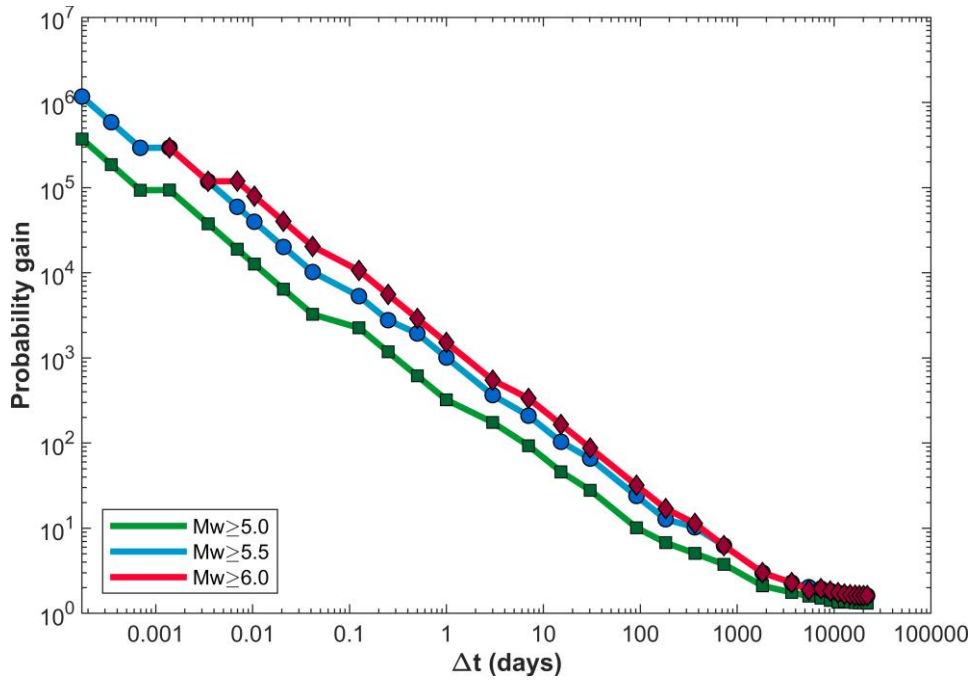

Figure 3.16: Probability gain for declustered (first) target shocks and weighted fraction of space-time occupied by alarms for different magnitude thresholds (see inset) as a function of the alarm duration Δt.

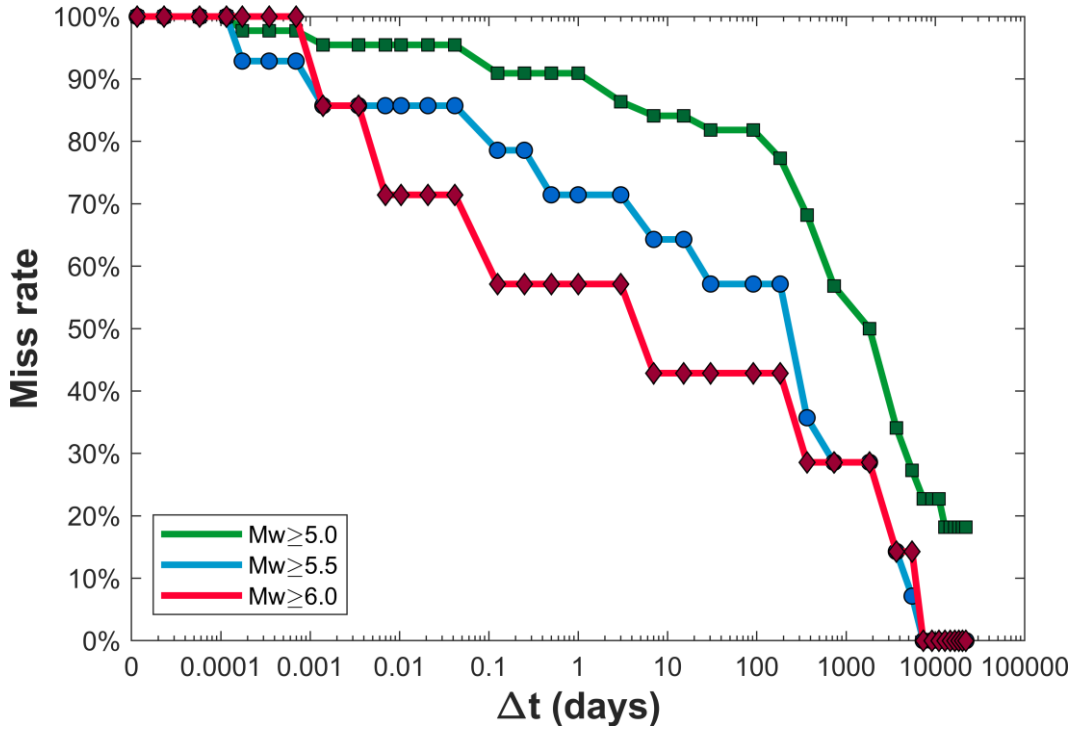

Figure 3.17: Miss rate for declustered (first) target shocks and different magnitude thresholds (see inset) as a function of the alarm duration Δt.

The behavior of the same statistic for the full set of target events (not declustered) is reported in Figs. S9, S10 and S11 of the supplemental material. It is similar to those of the declustered set but the binomial probabilities are lower, the probability gains are higher, and the miss rates decrease more rapidly with Δt.

Another aspect to be considered for the practical application of the forecasting method is the dependence on Δt of the fractions of space-time occupied by alarms τ_u and τ_w (Fig. 3.18). A long alarm interval Δt (with a corresponding long fraction of space-time occupied by alarms τ) allows to forecast more target earthquakes but at the same time it has relatively lower probabilities of occurrence than a shorter Δt. Furthermore, a longer duration of alarms would impact more with life activities of the population in the involved area. Even if any decision on the possible practical application in real situations would eventually require a careful evaluation by decision makers even considering a cost-benefits analysis (e.g., van Stiphout et al., 2010; Herrmann et al., 2016), we examine here as an example the choice of Δt= 3

months (0.25 years). This choice, in most cases, results in a fairly trade-off between a good efficiency and a narrow space-time fraction covered by alarms $\tau \approx 2$.

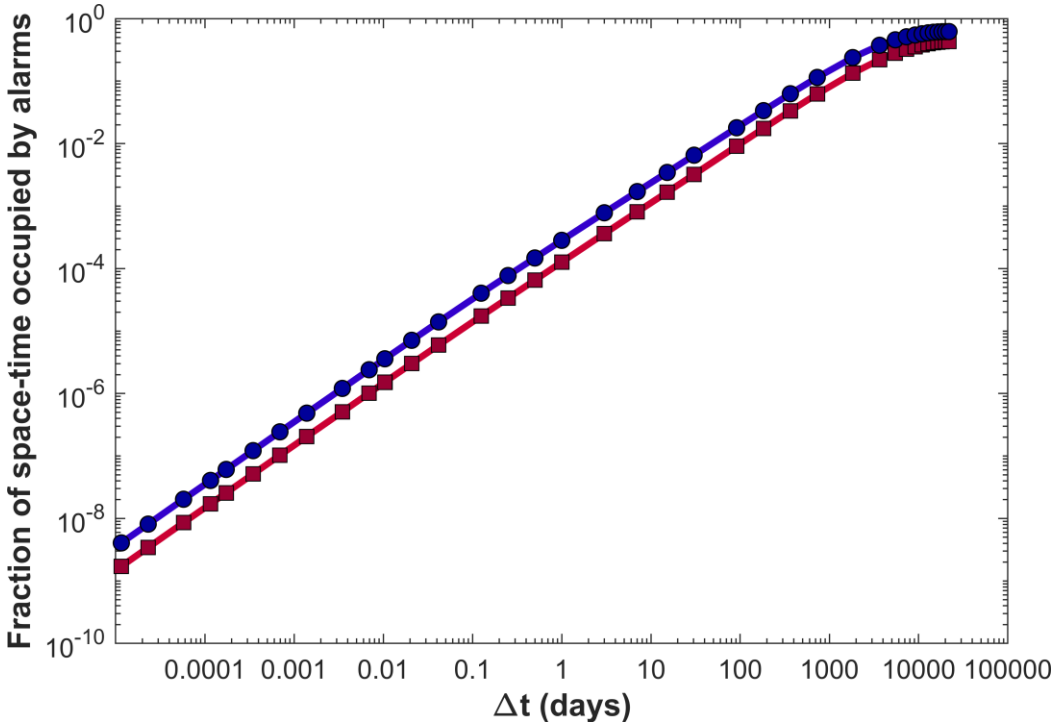

Figure 3.18: Unweighted (red) and weighted (dark blue) fraction of space-time occupied by alarms as a function of the alarm duration Δt.

We can see in Table 3.4 that in this case the method is able to retrospectively forecast more than 50% of not-declustered target shocks with Mw≥5.0 and more than 70% of those with Mw≥5.5 and Mw≥6.0. We also report in Table 3.4 the statistic of the numbers of successful alarms with respect to the total number of alarms indicating higher rates for target with Mw≥5.0. About one fifth of alarms actually forecast an earthquake, while the fraction of successful alarms definitely decreases for larger targets and further decreases for declustered sets down to about 1%. Note that several alarm time windows are actually overlapped and then the total duration of alarms is shorter than the simple sum of alarm windows (Eq. 3.2).

Table 3.4 – Retrospective forecasting performance of the algorithm for Δt= 3 months.

Target Magnitude	≥5.0		≥5.5		≥6.0		τ_u	τ_w
Not declustered								
Forecasted/total shocks	55/98	56%	26/35	74%	7/10	70%	0.9%	1.9%
Successful/total alarms	115/617	18.6%	72/617	11.7%	30/617	4.9%	0.9%	1.9%
Declustered								
Forecasted/total shocks	8/44	18%	6/14	43%	4/7	57%	0.9%	1.9%
Successful /total alarms	13/617	2.1%	9/617	1.5%	8/617	1.3%	0.9%	1.9%

The performance of the method is definitely worse for the first target shocks (declustered set), but it improves by increasing the magnitude of target shocks. Actually, 4 over 7 first target shocks with Mw≥6.0 over the last 60 years in Italy are retrospectively forecasted in this way.

We tested the stability with time of the forecasting performance by subdividing the seismic catalog in two equal parts of 30 years: before and after 1/1/1990. The same computations of Table 3.4 for Δt= 3 months for intervals 1960-1989 and 1990-2019 are reported in Tables 3.5 and 3.6 respectively. The rates of successfully forecasted target shocks (declustered or not) are similar in the two periods whereas the space-time fraction occupied by alarms is definitely lower in the most recent period, consistently with the higher ratios between successful and total alarms. We could argue that smaller magnitude errors in most recent times, owing to the continuous improvement of the Italian seismic network, reduce the number of false alarms and then increase the observed skill of the forecasting method with respect to the previous period.

In Table 3.7 and 3.8 we report the lists of retrospective forecasts of the first (declustered) target shocks with Mw≥5.5 and Mw≥6.0 respectively occurred in Italy from 1960 to 2019 (also see the results for the declustered first shocks with Mw≥5.0 in Table S6 and the results for not-declustered targets with Mw≥5.0, 5.5 and 6.0 in Tables S7, S8 and S9 respectively of the supplemental material 1).

Table 3.5 – Same as Table 3.4 for the time interval 1960-1989.

Target Magnitude	≥5.0		≥5.5		≥6.0		τ_u	τ_w
Not declustered								
Forecasted/total shocks	21/45	47%	11/15	73%	3/4	75%	1.0%	2.1%
Successful/total alarms	45/336	12.9%	22/336	6.6%	9/336	2.7%	1.0%	2.1%
Declustered								
Forecasted/total shocks	3/25	12%	3/7	43%	2/3	67%	1.0%	2.1%
Successful/total alarms	5/336	1.5%	5/336	1.5%	3/336	0.89%	1.0%	2.1%

Table 3.6 – Same as Table 3.4 for the time interval 1990-2019.

Target Magnitude	≥5.0		≥5.5		≥6.0		τ_u	τ_w
Not declustered								
Forecasted/total shocks	34/53	64%	15/20	75%	4/6	67%	0.4%	0.7%
Successful/total alarms	70/281	24.9%	50/281	17.8%	21/281	7.5%	0.4%	0.7%
Declustered								
Forecasted/total shocks	5/19	26%	3/7	43%	2/4	50%	0.4%	0.7%
Successful/total alarms	8/281	3.5%	4/281	1.4%	5/281	1.8%	0.4%	0.7%

Table 3.7 – Results of retrospective forecast of first main shocks (declustered targets) with Mw≥5.5 in Italy from 1960 to 2019, using Δt= 3 months (0.25 years).

Year	Month	Day	Lat	Lon	Mw	t_a (days)		Epicentral area
1962	8	21	41.233	14.933	5.7	0.093	2.22 h	Irpinia
1968	1	15	37.700	13.100	5.7	0.425	10.2 h	Valle del Belice
1976	5	6	46.250	13.250	6.5	7.8×10^{-4}	67 s	Friuli
1979	*9*	*19*	*42.717*	*12.950*	*5.8*	*Missed*		*Valnerina*
1980	*11*	*23*	*40.800*	*15.367*	*6.8*	*Missed*		*Irpinia-Basilicata*
1984	*4*	*29*	*43.204*	*12.585*	*5.6*	*Missed*		*Umbria settentrionale*
1984	*5*	*7*	*41.666*	*13.820*	*5.9*	*Missed*		*Monti della Meta*
1990	5	5	40.650	15.882	5.8	1.5×10^{-4}	13 s	Potentino
1997	9	26	43.023	12.891	5.7	22.1		Appennino umbro-marchigiano
1998	*9*	*9*	*40.060*	*15.949*	*5.5*	*Missed*		*Appennino lucano*
2002	*10*	*31*	*41.717*	*14.893*	*5.7*	*Missed*		*Molise*
2009	4	6	42.342	13.380	6.3	6.5		Aquilano
2012	*5*	*20*	*44.896*	*11.264*	*6.1*	*Missed*		*Pianura Emiliana*
2016	*8*	*24*	*42.698*	*13.234*	*6.2*	*Missed*		*Monti della Laga*

t_a is the maximum time advance of the foreshock with respect to the main shock. "*Missed*" indicates that the target shock was not forecasted. Epicentral area identifiers are taken from the CPTI15 catalogue (Rovida et al., 2016, 2020).

We can note that for two target shocks (1976 Friuli and 1990 Potentino) the forecast could have hardly been used by civil protection services to adopt safety countermeasures because the forecasting strong shocks occurred too shortly before the main shock (67 s and 13 s respectively). In other cases, the time delay between the forecasting shock and the main shock (going from a couple of hours to a few weeks) would have been sufficient to take some countermeasures.

Table 3.8 – Same as Table 3.7 for first main shocks with Mw≥6.0.

Year	Month	Day	Lat	Lon	Mw	t_a (days)		Epicentral area
1962	8	21	41.233	14.933	6.2	0.100	2.40 h	Irpinia
1976	5	6	46.250	13.250	6.5	7.8×10^{-4}	67 s	Friuli
1980	*11*	*23*	*40.800*	*15.367*	*6.8*	*Missed*		*Irpinia-Basilicata*
1997	9	26	43.015	12.854	6.0	22.5		Appennino umbro-marchigiano
2009	4	6	42.342	13.380	6.3	6.5		Aquilano
2012	*5*	*20*	*44.896*	*11.264*	*6.1*	*Missed*		*Pianura Emiliana*
2016	*8*	*24*	*42.698*	*13.234*	*6.2*	*Missed*		*Monti della Laga*

We could note that a foreshock did actually occur a couple of days before the first mainshock of 20 May 2012 (Mw=6.1) in the area of Pianura Emiliana, but its magnitude (Mw=4.2) was only slightly below the lower threshold of Mw=4.4 we adopted. The retrospective ability to predict Mw≥6.0 earthquakes might have been improved then by slightly reducing such lower threshold but at a cost of a general reduction of the performance of the algorithm, because of the increment of the number of alarms and of the fraction of space-time covered by alarms.

3.7 Conclusions of chapter 3

We analyzed a simple algorithm to forecast shallow (depth<50 km) main shocks (Mw≥5.0, 5.5, 6.0) that threaten the life and the goods of the population living on the Italian mainland territory, based on the previous occurrence within circular areas of 30 km of radius of widely felt strong shocks (4.4 ≤Mw<4.8) not particularly harmful in themselves. Based on a retrospective analysis of the HOmogenized instRUmental Seismic catalogue (HORUS) of Italy from 1960 to 2019 (Lolli et al., 2020) this method retrospectively forecast the majority of damaging earthquakes occurred in Italy in the

past 60 years by issuing alarms covering only a small fraction of the space-time coverage.

We estimated such fraction even considering the different levels of seismic activity in different areas of Italy by weighting more the alarm times in circular areas where the average seismicity rate, computed from the CPTI15 seismic catalogue (Rovida et al., 2016, 2020) from 1600 to 1959, is higher.

The retrospective testing using the Molchan diagram (Molchan, 1990, 1991, Molchan & Kagan, 1992) and the Area Skill score (Zechar & Jordan, 2008) methods indicates that such approach clearly overperforms a purely random method with high or very high confidence, depending on the target shock magnitude threshold.

As the secondary main shocks during seismic sequences are definitely easier to be forecasted by this method because the aftershocks of the first main shock usually generate alarms at weakly (if not daily) rate, we also tested the ability of our approach to predict only the first main shock of each sequence. We found that the forecasting ability remains high even if being lower than that considering all main shocks.

Even if the true verification of the efficiency of the method will only be made on a prospective dataset, we believe that such simple forecasting algorithm could be useful, like other operational forecasting approaches presently considered by the Italian Civil Protection Department, for planning preparation measures in the field (e.g., Marzocchi et al., 2014).

The latter approaches are mainly based on the ETAS model (Kagan & Knopoff, 1987, Ogata, 1988) and, as well as that of the present work, showed to retrospectively forecast the evolution of Italian seismicity better than an inhomogeneous random process with spatial rates corresponding to past seismicity. On the other hand, Marzocchi and Zhuang (2011) showed that ETAS models is able to describe quite well even the observed foreshock activity. However, a comparison of the relative

efficiency of our approach with ETAS models and even with other forecasting approaches (like for example the EEPAS method (Rhoades and Evison, 2004) would require that the probabilistic formulation of the latter methods is adapted to the alarm-based one (for example by selecting a particular probability thresholds above which to declare an alarm). However, such adaptation is not trivial and hence, the question on which of the different approaches is better in predicting future damaging earthquakes remains not answered presently and has to be deferred to future papers comparing all methods in an alarm-based context by using, for example, the approach proposed by Shebalin et al. (2014).

One advantage of the present forecasting approach is that it is easy to implement and communicate because it does not require any other scientific analysis than the correct determination of the location and of the magnitude of the precursory shock. In principle every person could be informed very quickly by a notification sent by one of the already available mobile Apps which provide near real-time access to the INGV online earthquake list (http://terremoti.ingv.it/en#).

Chapter 4

Application of EEPAS earthquake forecasting model to Italy

E. Biondini[1*], D.A. Rhoades[2], P. Gasperini[1,3]

[1]Dipartimento di Fisica e Astronomia, Università di Bologna, Italy

[2] GNS Science P.O. Box 30-368, Lower Hutt 5040, New Zealand

[3]Istituto Nazionale di Geofisica e Vulcanologia, Sezione di Bologna, Italy

*Corresponding author

From: *Biondini, E., D. A. Rhoades, and P. Gasperini, 2022, Application of the EEPAS earthquake forecasting model to Italy, Geophys. J. Int., 234, no. 3, 1681–1700, doi: 10.1093/gji/ggad123.*

**This work was conducted by Biondini E., with the supervision of Gasperini P., who also contributed to writing and correcting the article. D.A Rhoades made valuable contribution especially on the clarification of some aspects of the EEPAS model.*

The EEPAS (Every Earthquake a Precursor According to Scale) forecasting model is a space–time point-process model based on the precursory scale increase (ψ) phenomenon and associated predictive scaling relations. It has been previously applied to New Zealand, California and Japan earthquakes with target magnitude thresholds varying from about 5 to 7. In all previous application, computations were done using the computer code implemented in Fortran language by the model authors. In this work we applied it to Italy using a suite of computing codes completely rewritten in Matlab. We first compared the two software codes to ensure the convergence and adequate coincidence between the estimated model parameters for a simple region capable of being analysed by both software codes. Then, using the rewritten codes, we optimised the parameters for a different and more complex polygon of analysis using

the Homogenized instRUmental Seismic catalogue (HORUS) data from 1990 to 2011. We then perform a pseudo-prospective forecasting experiment of Italian earthquakes from 2012 to 2021 with Mw≥5.0 and compare the forecasting skill of EEPAS with those obtained by other time independent (SUP, SVP, and PPE) and time dependent (ETAS) forecasting models using the information gain per active cell (IGPA). The preference goes to the ETAS model for short time intervals (3 months) and to the EEPAS model for longer time intervals (6 months to 10 years).

4.1 Introduction

EEPAS is an earthquake forecasting method based on the statistical analysis of seismicity (Rhoades and Evison, 2004). Its basic assumption is that magnitudes and rates of minor seismicity increase before a strong shock. This phenomenon (called $\psi - phenomenon$) was described by Evison and Rhoades (2004) for some regions of the world in which high quality earthquakes catalogues are available. They analyzed 47 earthquakes with magnitude ranging between 5.8 and 8.2 to derive three empirical scaling relations: for time, magnitude and area. These relate the magnitude of mainshock (M_m) with the precursor magnitude (M_P) the precursor time (T_P) and the precursor area (A_p). Such empirical scaling relations show that in general the magnitude of precursor events is smaller than the magnitude of the mainshock by at least one magnitude unit. The EEPAS model considers each earthquake as an individual precursor according to the scale indicated by its magnitude, rather than as a possible member of a ψ phenomenon.

The details of the EEPAS method are described in several papers (e.g., Rhoades and Evison, 2004; Evison and Rhoades, 2005; Rhoades, 2007, 2011; Rhoades et al., 2020), some of which contain typos that makes the formulation not perfectly identical in all of them. For such reason in this work, we describe again the method as well as some assumptions made without explicit mentions in previous papers.

We implemented such formulations in a suite of MATLAB codes that we first compared with the code EEPSOF (Rhoades, 2021) used in all previous applications of EEPAS methods. Even if the results of this comparison are not identical, they indicate a tight agreement between parameters estimates from the two codes, before the introduction of spatial parameters in the optimization procedure. After that, the differences become a little more pronounced for parameters a_T, σ_A and b_T, where the two codes differ by 12.5%, 10.2% and 24.0%, respectively. These differences can be explained by the different numerical algorithm adopted by the two codes for spatial integration. However, the final maximum log-likelihood scores and the numbers of forecasted earthquakes are very similar. Details on EEPAS software comparison are described in section 4.4.

For comparison purposes we also consider other forecasting models and in particular the Epidemic Type Aftershock Sequence (ETAS) model (Ogata, 1988, 1989, 1998) and two time-independent forecasting models: the Spatially Uniform Poisson (SUP) and the Spatially Variable Poisson (SVP) models (Console et al., 2006). A summary of the characteristics of each model is given in Table 4.1.

The fitting of the free parameters of various models is carried out by maximizing the log-likelihood function of an inhomogeneous Poisson point process, which is given by:

$$\ln L = \sum_{t_i \in (t_a, t_b); m_i \geq m_T; (x_i, y_i) \in R} \ln \lambda(t_i, m_i, x_i, y_i) - \int_{t_a}^{t_b} \int_{m_T}^{m_u} \iint_R \lambda(t, m, x, y)\, dy\, dx\, dm\, dt \quad (4.1)$$

where $\lambda(t, m, x, y)$ is the rate density function for PPE (eq. 4.13), EEPAS (eq. 4.5), ETAS (eq. 4.29), SUP or SVP (eq. 4.30) models; (t_a, t_b) is the time interval of the fitting period; (m_T, m_u) is the magnitude range of target earthquakes; and R is the spatial region of analysis.

Table 4.1- Summary of applied forecasting models.

Model	Main features	Reference
SUP	Stationary uniform Poisson model based on the observed seismicity rate $M \geq m_T$.	Console & Murru (2001)
SVP	Space variable Poisson model based on the smoothed seismicity rate $M \geq m_T$ observed in each cell.	Console & Murru (2001)
PPE	Quasi time-dependent model based on the hypothesis that future earthquakes tend to occur near the place of the recent ones. The rate-density of future earthquakes is modelled as proportional to a smoothed version of past seismicity.	Jackson & Kagan (1999); Rhoades & Evison (2004)
EEPAS-NW	Space/time-dependent model based on the hypothesis that each earthquake ($M \geq m_c$) contributes to the transient increment of the future rate of $M \geq m_T$ in its vicinity according to ψpredictive relations.	Rhoades & Evison (2004)
EEPAS-W	As above but the contribution of aftershocks and triggered events are downweighed.	Rhoades & Evison (2004)
ETAS-SUP	Epidemic-type aftershock model based on the hypothesis that each earthquake can perturb the rate of earthquakes and generate its own Omori-like decay sequence. The SUP is used as background model.	Ogata (1988, 1989), Ogata & Zhuang (2006)
ETAS-SVP	As above but with SVP as background model.	Ogata (1988, 1989), Ogata & Zhuang (2006)

4.2 The EEPAS earthquake forecasting model

The EEPAS model is based on the increase in rate and in magnitude of the minor seismicity observed before the occurrence of major earthquakes (ψ-phenomenon, Rhoades and Evison, 2004). Evison and Rhoades (2004) analyzed the ψ-phenomenon that evolved before 47 major earthquakes in well catalogued regions (such as California, New Zealand, northern Mexico, Japan, and Greece) developing three empirical scaling relations that relate the precursor magnitude (M_p) with the mainshock magnitude (M_m), precursor time (T_p) and precursory area (A_p). Where, as M_p is assumed as the mean of the three largest precursor shocks, as T_p is the time interval between the onset of the ψ-phenomenon and mainshock, and A_p (expressed

in km) is the smallest rectangular spatial box containing the precursory events, mainshock and aftershocks (for details see Evison and Rhoades, 2004). The predictive scale relations are thus defined as

$$M_m = a_m + b_m M_p \,, \tag{4.2}$$

$$\log\left(T_p\right) = a_t + b_t M_p \,, \tag{4.3}$$

and

$$\log\left(A_p\right) = a_a + b_a M_p. \tag{4.4}$$

In the EEPAS model each *i*-th earthquake, occurring at time t_i with magnitude m_i and located at (x_i, y_i), is assumed to contribute to the transient increment of the rate density $\lambda_i(t, m, x, y)$ of future seismicity (defined as the derivative of the expected number of earthquakes with respect to time, magnitude and location coordinates) by the term

$$\lambda_i(t, m, x, y) = w_i f_{1i}(t) g_{1i}(m) h_{1i}(x, y) \tag{4.5}$$

where w_i is a weighting factor which depends on other earthquakes in its proximity (see below). $f_{1i}(t)$, $g_{1i}(m)$ and $h_{1i}(x, y)$ are the probability density functions of time, magnitude and location, respectively. The assumed forms for these distributions are defined consistently with the ψ scaling relations by Rhoades and Evison (2004). The time distribution is assumed to be Lognormal with the form

$$f_{1i}(t) = \frac{H(t - t_i)}{(t - t_i)\ln(10)\,\sigma_T\sqrt{2\pi}} \exp\left[-\frac{1}{2}\left(\frac{\log(t - t_i) - a_T - b_T m_i}{\sigma_T}\right)^2\right] \tag{4.6}$$

where $H(t - t_i)$ is the Heaviside step function, which takes the value 1 if $t - t_i > 0$, and 0 otherwise. This means that at the time *t*, the rate density function is contributed only by earthquakes occurring before *t*. Here a_T, b_T and σ_T are free parameters to be determined.

The magnitude distribution $g_{1i}(m)$ is assumed to be normal with the form:

$$g_{1i}(m) = \frac{1}{\sigma_M\sqrt{2\pi}} \exp\left[-\frac{1}{2}\left(\frac{m - a_M - b_M m_i}{\sigma_M}\right)^2\right] \tag{4.7}$$

where a_M, b_M and σ_M are free parameters.

The space distribution is assumed to be bivariate Normal with circular symmetry with the form

$$h_{1i}(x, y) = \frac{1}{2\pi\sigma_A^2 10^{b_A m_i}} \exp\left[-\frac{(x - x_i)^2 + (y - y_i)^2}{2\sigma_A^2 10^{b_A m_i}}\right] \tag{4.8}$$

where σ_A and b_A are free parameters.

An adjustment is necessary because of the missing contribution of earthquakes below the minimum completeness magnitude m_c which causes the rate density at magnitude m to be underestimated on average by a fraction $\Delta(m)$ of its real value given by

$$\Delta(m) = \phi\left(\frac{m - a_M - b_M m_c - \sigma_M^2\beta}{\sigma_M}\right) \tag{4.9}$$

where ϕ is the Normal distribution integral. Then $\Delta(m)$ can also be written as

$$\Delta(m) = \frac{1}{2}\mathrm{erf}\left[\left(\frac{m - a_M - b_M m_c - \sigma_M^2\beta}{\sigma_M\sqrt{2}}\right) + 1\right] \tag{4.10}$$

where erf is the Error function.

Hence, to compensate for the lack of earthquakes with magnitude lower than the completeness magnitude m_c, $\lambda_i(t, m, x, y)$ is inflated by a factor $\frac{1}{\Delta(m)}$.

The total rate density is obtained by summing the contribution of all past earthquakes and also adding a background term that allows for the possibility that an earthquake can occur without an appreciable scale increase of precursory shocks:

$$\lambda(t, m, x, y) = \mu\lambda_0(t, m, x, y) \quad + \sum_{t_i \geq t_0; m_i \geq m_c}^{t-delay} \eta(m_i)\lambda_i(t, m, x, y) \tag{4.11}$$

where $\lambda_0(t, m, x, y)$ is the background rate density, t_0 is the time of the beginning of the catalogue, μ is the mixing parameter and can be interpreted as the proportion of earthquakes that occur without precursory shocks. The normalizing function η is defined by

$$\eta(m_i) = \frac{b_M(1-\mu)}{E(w)} \exp\left[-\beta\left(a_M + (b_M - 1)m_i + \frac{\sigma_M^2\beta}{2}\right)\right] \tag{4.12}$$

where $E(w)$ is the mean weight of earthquakes in the catalogue; a_M, b_M and σ_M are free parameters; and $\beta = b \ln 10$, with b being the slope of the frequency-magnitude distribution of Gutenberg and Richter (1944). The normalizing function $\eta(m_i)$ ensures that the number of earthquakes expected by the model approximatively matches the actual number of target earthquakes. The *delay* term in equation (4.11) is to prevent the fit of the parameters being influenced by the short-term clustering of earthquakes (such as aftershocks and swarms). The EEPAS model is focused on the long-term clustering detected by the precursory scale increase phenomenon and its associated scaling relations. For this reason, the delay (usually assumed to be 50 days) after the time of occurrence of each earthquake is applied and no earthquake from the input catalogue is considered before such time interval elapsed after its occurrence.

The background rate density $\lambda_0(t, m, x, y)$ depends on the proximity of the location (x, y) with respect to previous seismicity. It is described by a quasi-time-invariant smoothed seismicity model, described by Rhoades and Evison (2004), which is similar to the forecasting model proposed by Jackson and Kagan (1999) and is called PPE (Proximity to Past Earthquakes). It takes the form

$$\lambda_{0i}(t, m, x, y) = f_{0i}(t) g_{0i}(m) h_{0i}(x, y) \tag{4.13}$$

where $f_{0i}(t)$ is the time density function, $g_{0i}(m)$ is the magnitude density function and $h_{0i}(x, y)$ is the spatial density function. The time density function takes the form

$$f_{0i}(t) = \frac{1}{t_i - t_0} \tag{4.14}$$

This ensures that at any time the estimated rate of earthquakes with $m \geq m_T$ within the region R is similar to the past rate.

The magnitude density function is that implied by the frequency magnitude law of Gutenberg and Richter (1944):

$$g_{0i}(m) = \beta \exp[-\beta(m_i - m_c)] \tag{4.15}$$

Finally, $h_{0i}(x, y)$ is the sum over all earthquakes with $m_i \geq m_T$ from time t_0 up to, but not including time t of smoothing kernels with the form

$$h_{0i}(x_i, y_i) = \sum_{t_i > t_0; m_i > m_T}^{t-delay} a(m_i - m_T) \frac{1}{\pi} \left(\frac{1}{d^2 + r_i^2} \right) + s \tag{4.16}$$

where r_i is the distance in km between (x, y) and the epicenter (x_i, y_i); a is a normalizing parameter, d is a smoothing distance and s is a small term that includes the contribution from earthquakes that occur far from past epicenters.

The rate density $\lambda_0(t, m, x, y)$ of the PPE model decreases gradually with time elapsed after an earthquake occurrence and increases when a new earthquake occurs. The function $h_{0i}(x, y)$ considers the earthquake location and the function $f_{0i}(t)$ the passage of time.

The purpose of the weighting factor w_i in eq. (4.5) is to give more weight to earthquakes that are more likely to be part of a long-term clustering, thus giving less weight to events that are aftershocks of previous earthquakes. Two different weighting strategies were applied in the past application of EEPAS. The simplest one is giving the same weight $w_i = 1$ to each earthquake in the catalogue. With this strategy aftershocks triggered by previous earthquakes have the same weight of any other shock. The other strategy is to assign a lower weight to any earthquake which is likely to be an aftershock of a previous earthquake. Therefore, the total rate density is mostly given by earthquakes that are part of long-term clustering.

This latter strategy requires estimating the rate density λ' for aftershock occurrence, incorporating epidemic-type aftershock behavior (Ogata, 1988, 1989; Console and Murru, 2001). The aftershock model adopted for EEPAS takes the form:

$$\lambda'(t,m,x,y) = \nu\lambda_0(t,m,x,u) + k\sum_{t_i \geq t_0} \lambda_i'(t,m,x,y) \tag{4.17}$$

where λ_0 is the rate density given by PPE model, ν is the proportion of earthquake that are not aftershocks, k is a normalization constant and $\lambda'(t,m,x,y)$ describes the aftershocks occurrence with the form:

$$\lambda_i'(t,m,x,y) = f_{2i}(t)g_{2i}(m)h_{2i}(x,y) \tag{4.18}$$

where $f_{2i}(t)$, $g_{2i}(m)$ and $h_{2i}(x,y)$ are respectively the density functions for time, magnitude, and locations of the aftershocks of the i-th earthquake. The time distribution is given by the modified Omori law (Utsu, 1961; Ogata, 1983):

$$f_{2i}(t) = H(t-t_i)\frac{p-1}{(t-t_i+c)^p} \tag{4.19}$$

where t_i is the time of the i-th earthquake, and c and p are the Omori law parameters.

The magnitude distribution follows the Gutenberg and Richter (1944) law, and it is assumed that the magnitude of an aftershock is smaller than its mainshock by at least δ units

$$g_{2i}(m) = H(m_i - \delta - m)\beta\exp[-\beta(m-m_i)] \tag{4.20}$$

The addition of the parameter δ is based on the so-called Bath's law (Båth, 1965), according to which the largest aftershock typically has a magnitude about 1.2 units smaller than the mainshock. Finally, the spatial distribution is assumed to be bivariate Normal with circular symmetry:

$$h_{2i}(x,y) = \frac{1}{2\pi\sigma_U^2 10^{m_i}} exp\left[-\frac{(x-x_i)^2+(y-y_i)^2}{2\sigma_U^2 10^{m_i}}\right] \tag{4.21}$$

where σ_U is a free parameter. The weighting factor is then computed as

$$w_i = \frac{\nu\lambda_0(t_i,m_i,x_i,y_i)}{\lambda'(t_i,m_i,x_i,y_i)} \tag{4.22}$$

In this way, if an earthquake has the characteristics of an aftershock, it will have a weight close to 0; on the contrary, if an earthquake that in no way resembles an aftershock it will have a weight close to 1. Short descriptions of the parameters of the PPE and EEPAS models are listed in Table 4.2.

4.3 Application to Italy

We chose $m_T = 5.0$ as the lower magnitude limit for target shocks, because in Italy such earthquakes potentially cause damage to buildings and threaten the health and life of inhabitants. This choice is also consistent with most of the applications of EEPAS model to other regions of the World (Rhoades and Evison 2004, Evison and Rhoades 2005, Rhoades 2007, 2011).

We chose the learning time interval from 1990 to 2011 for fitting the EEPAS model, because the accuracy and completeness of the Italian catalogue has improved significantly since 1990 (Gasperini et al., 2013), We use the independent ten-year interval from 2012 to 2021 for retrospective testing of the model.

As application region R, we consider a regular tessellation of the Italian territory made of square cells with side $L = 30\sqrt{2}$ km from 7°E to 19°E in longitude and from 36°N to 47°N in latitude. The choice of L is made for compatibility with previous work by Gasperini et al. (2021), so that each square cell is (almost) perfectly inscribed in a circular cell with radius of 30 km. Because the completeness of the earthquake catalogue is poor in offshore areas, according to Gasperini et al. (2021), we consider only the cells within which at least one earthquake with $M \geq 4.0$ occurred inland from 1600 to 1959 according to the CPTI15 catalogue (Rovida et al., 2020) and from 1960 to 2021 according to the Homogenized instrRUmental Seismic (HORUS) catalogue (Lolli et al., 2020). We also excluded the cells that are not contiguous to the main analysis polygon (such as insulated cells on islands). In total, 177 square cells constitute the region of analysis R (Fig. 4.1).

Table 4.2- Summary of PPE and EEPAS parameters.

Model	Parameter	Description	Restriction
PPE	a	Normalizing constant.	≥ 0
	d	Smoothing kernel kilometric distance.	≥ 1
	s	Small value to account for earthquakes far from past epicenters.	≥ 0
EEPAS	a_M	Intercept of scaling relation between precursor magnitude and target magnitude (eq. A1).	$1.0 - 2.0$
	b_M	Slope of scaling relation between precursor magnitude and target magnitude (eq. A1).	$1\ (fixed)$
	σ_M	Standard deviation of scaling relation between precursor magnitude and target magnitude (see Fig.1, Rhoades and Evison, 2011)	$0.2 - 0.65$
	a_T	Intercept of scaling relation between precursor time and target magnitude (eq. A2)	$1 - 3$
	b_T	Slope of scaling relation between precursor time and target magnitude (eq. A2)	$0.3 - 0.65$
	σ_T	Standard deviation of the scaling relation between precursor magnitude and target magnitude (see Fig.1, Rhoades and Evison, 2011).	$0.15 - 0.6$
	b_A	Slope of scaling relation between precursory area and target magnitude (eq. A3).	$0.2 - 0.6$
	σ_A	Related to Aa of scaling relation between precursory area and magnitude (see Fig.1, Rhoades and Evison, 2011).	$1 - 30$
	μ	Proportion of target shocks that occurs without an appreciable sequence of precursory shocks.	$0 - 1$
Aftershocks (EEPAS)	c	c-parameter of Omori-Utsu law	$0 - 0.5$
	p	p-parameter of Omori-Utsu law	$1 - 1.6$
	k	Normalizing constant.	≥ 0
	ν	Proportion of earthquake that are not aftershocks	$0 - 1$
	δ	Average magnitude difference between the mainshock and the largest aftershock	$0.7\ (Fixed)$
	σ_U	Cluster diffusion parameter	$0.006\ (Fixed)$

For fitting of the EEPAS model parameters, an earthquake catalogue with a completeness magnitude (m_c) at least two units lower than the target magnitude (m_T) is desirable (Rhoades and Evison, 2004). For Italy an earthquake catalogue with

homogeneous magnitudes and high resolution is the HORUS catalogue (Lolli et al., 2020) reporting earthquakes from 1960 to the present. According to Lolli et al. (2020), HORUS can be considered complete within the Italian mainland for $m \geq 4.0$ since 1960, for $m \geq 3.0$ since 1981, for $m \geq 2.5$ since 1990, for $m \geq 2.1$ since 2003 and for $m \geq 1.8$ since 2005. In the dataset for this work, we used only shallow earthquakes with depth $Z \leq 40\ km$. To avoid edge effects in the fitting of model parameters, the contribution of earthquakes in the neighborhood of the region R must also be considered (Rhoades and Evison, 2004). We assume as neighborhood region the area included in the CPTI15 polygon (Fig. 4.2) according to Rovida et al. (2020).

To account for the limited accuracy of magnitude data, we binned all magnitudes to the nearest tenth of a unit:

$$m_{binned} = \frac{\text{int}(m_{raw} \times 10 + 0.5)}{10} \tag{4.23}$$

This also means that a magnitude lower threshold rounded to the nearest tenth of a unit (e.g., $m_T = 5.0$) implies an effective threshold 0.05 units smaller (e.g., $m_T = 4.95$).

The HORUS catalogue reports 27 target shocks with Mw≥ 5.0 from 1990 to 2011 and 27 from 2012 to 2021. Thus, the rate of target shocks in the testing period is about twice that in the learning period. Hence, the forecasting of the correct number of earthquakes in the testing period by any forecasting method will be difficult.

After the first target shock ("mainshock") of a seismic sequence, the forecasting of successive target shock ("aftershocks") is easier, owing to the presence of small aftershocks. Hence, we also fit and test the models against a set of target earthquakes only including the first target shock of each sequence. According to Gasperini et al. (2021), we eliminate the target shocks, occurring within a spatial window of 50 km and a time window of one year after any other target shock. In order to prevent various models from trying to forecast removed target earthquakes, we also remove all other (minor) shocks belonging to such spatial and time windows. The numbers

of considered target shocks for the mainshock only set then reduce to 12 and 9 for the learning and testing time intervals, respectively.

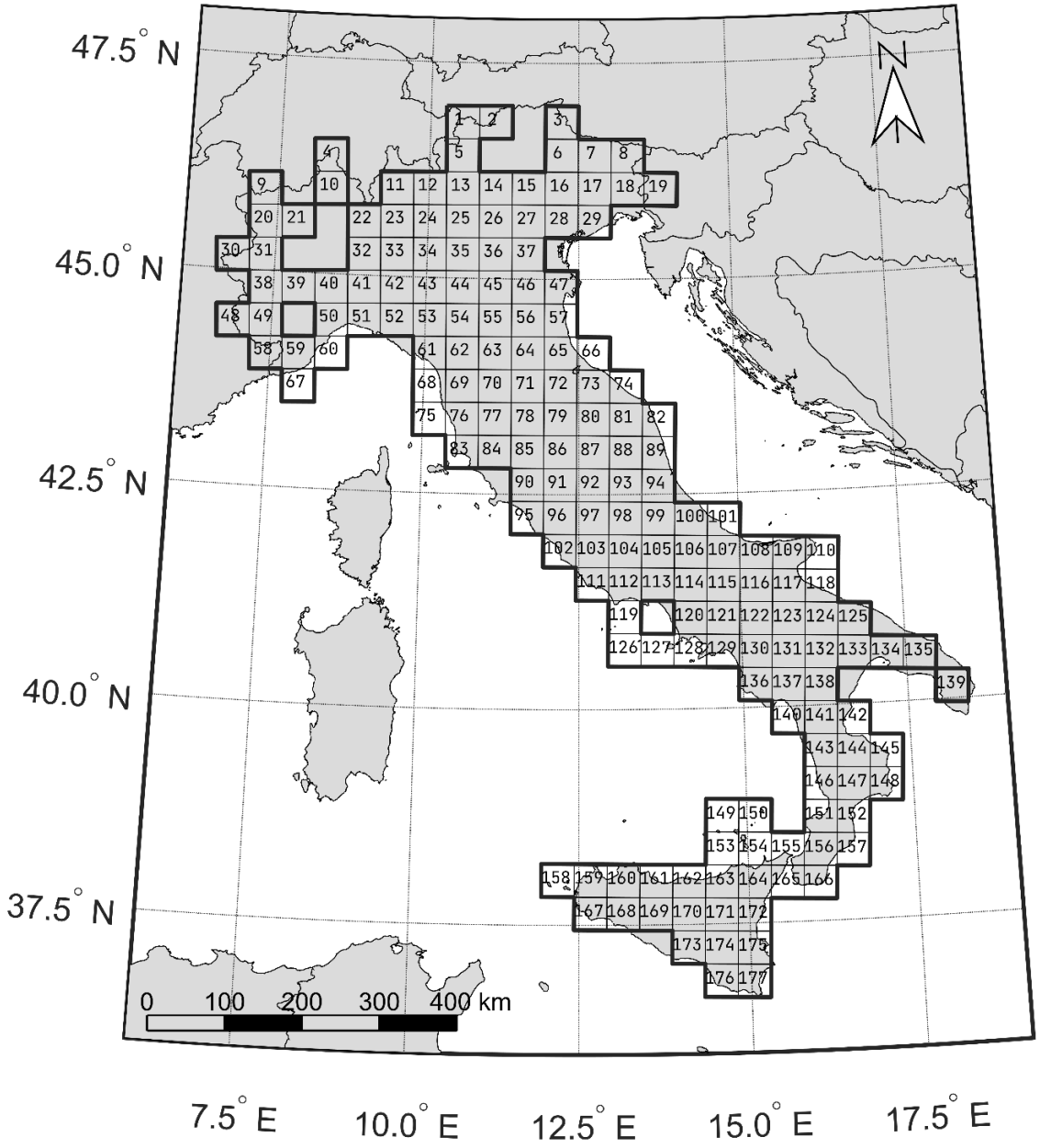

Figure 4.1: Tessellation of the Italian territory region used for the fitting of parameters and for the retrospective experiment. The thick black line delimits the analysis region R. The cells that R comprises are only those within which at least one earthquake with $M \geq 4.0$ from 1600 to 2021 have occurred according to CPTI15 catalogue (Rovida, Locati, Camassi, and Lolli, 2020) and have $30\sqrt{2}$ km of side.

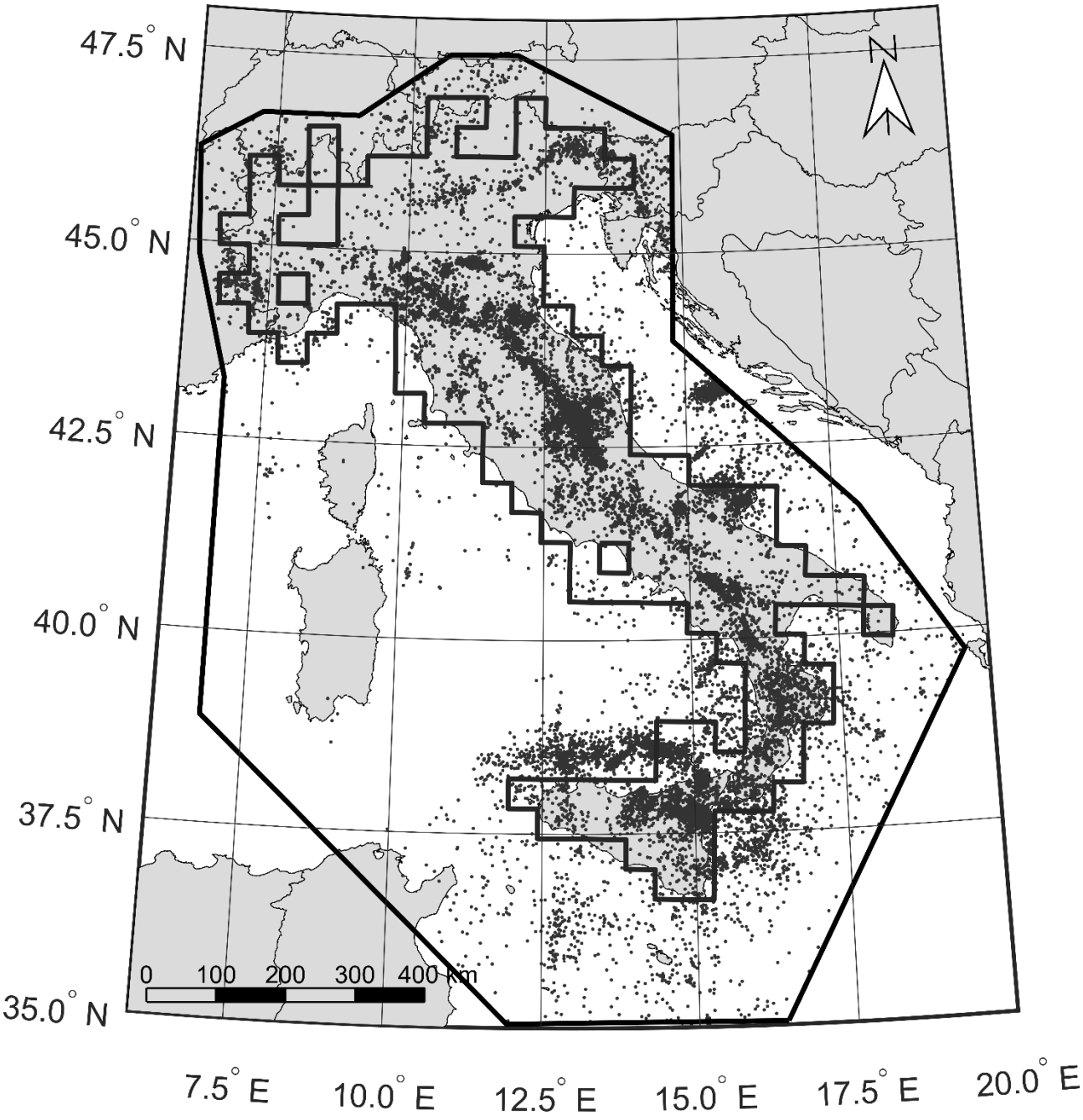

Figure 4.2: Epicenters of earthquakes with magnitude ≥ 2.5 that occurred within the CPTI15 polygon (outer thick polygon) between 1990 and 2021. The inner thick polygon represents the forecasting area *R*.

4.4 Implementation of MATLAB code and comparison with EEPSOF Version 2.3w

We developed a suite of codes in MATLAB language reproducing the formulation of the EEPAS model described in section 4.2. We tested them against the EEPSOF code (Version 2.3w) developed by D. A. Rhoades (Rhoades, 2021) and provided as a binary Linux executable file compiled by Fortran77. To make the comparison, we adopted a simplified spatial geometry of an Italian areas (Fig. 4.3) as EEPSOF hardly manages the complex shape made by or tessellation of the application area (e.g., figure 4.1). The purpose of the comparison is to ensure that the optimized parameter values and the relative maximum log-likelihoods are satisfactorily similar.

One difference between the MATLAB implementation and EEPSOF is the treatment of spatial data. While the EEPSOF code itself computes the kilometric distances directly from geographical coordinates, for the MATLAB implementation we have chosen to firstly convert all coordinates from the WGS84 geographic reference to kilometric coordinates in the RDN2008 Italy Zone (E-N) EPSG: 7794 by the QGIS software.

We applied both codes to the dataset of target earthquakes with magnitude $M \geq 5.0$ that occurred from 1990 to 2020 within the analysis polygon. The latter is a rectangle with sides of 576 km eastward and of 745 km northward (Fig. 4.3). The vertices of the polygon for EEPSOF were converted from kilometric coordinates in the RDN2008 Italy Zone (E-N) system to the WGS84 coordinate reference system. For fitting the EEPAS model, we used the earthquakes from the HORUS seismic catalogue (Lolli et al., 2020) with $M \geq 2.5$ and $Z \leq 50\,km$ occurring inside the polygon from 1960 to 2020. To avoid edge effects in the fitting of model parameters, the contribution of earthquakes in the neighborhood up to 200 km from the polygon were also considered (Fig. 4.3). The used dataset contains 38,086 events, of which 24,816 are within the analysis polygon. For both software codes, the log-likelihood optimization

is carried out using the downhill simplex method (Nelder and Mead, 1965) as described in Rhoades and Evison (2004).

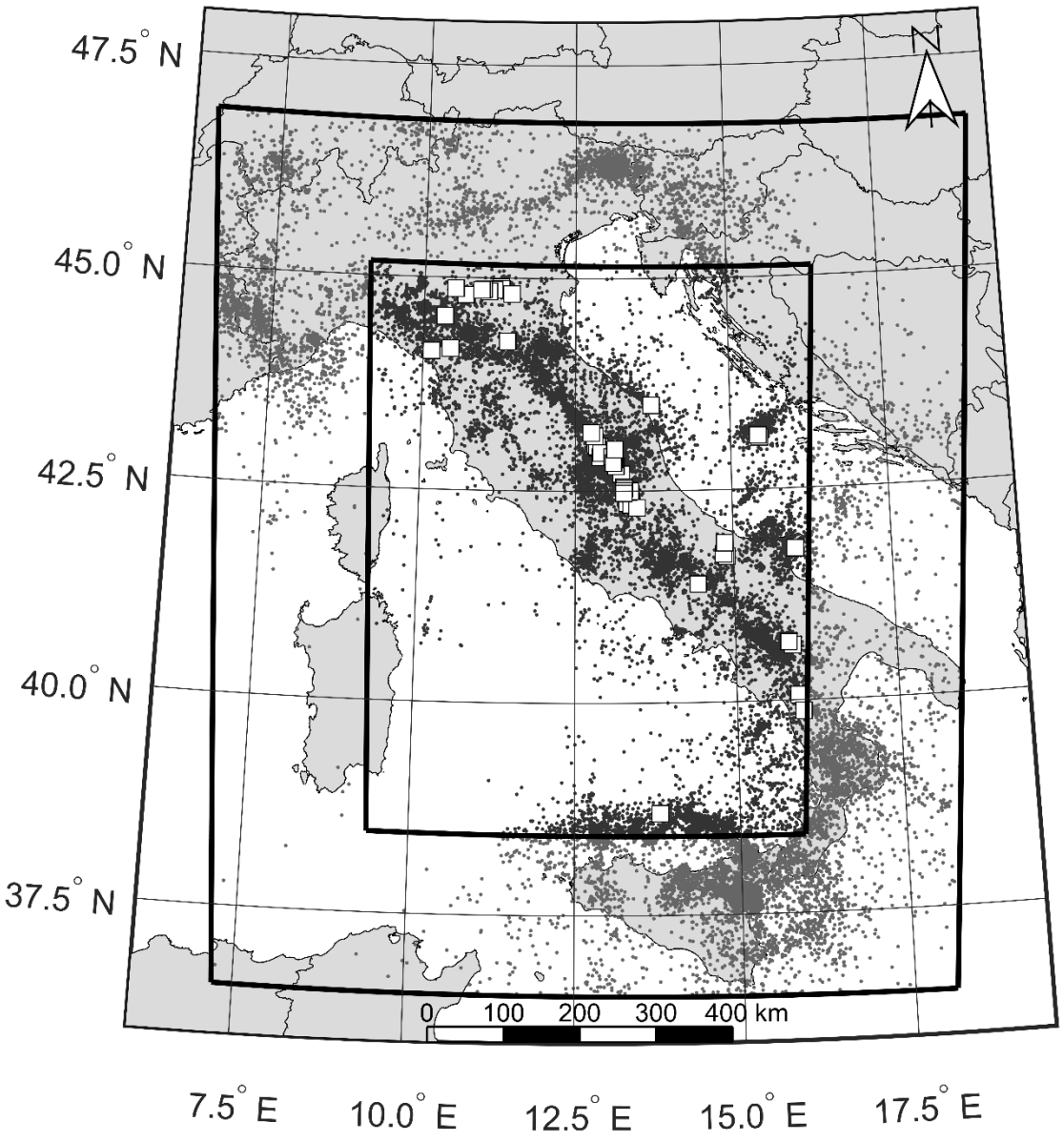

Figure 4.3: Map of epicenters of earthquakes with $M \geq 2.5$ and $Z \leq 50km$ that occurred from 1990 to 2020 within the region adopted for the software codes comparison. The interior rectangular area represents the analysis polygon for which the EEPAS model is applied. The black point represents the epicenters of earthquake occurred within the analysis polygon. The external rectangle represents the influence area for which earthquake indicated by the grey points are also considered for the parameters estimation to avoid edge effects. The white squares represent target earthquakes with $M \geq 5.0$ that occurred within the analysis polygon in the period 1990-2020.

For the comparison, the fit of the EEPAS parameters is made in five iterations, one for the parameters a_T, a_M and ϑ_A and the others adding one at a time the parameters $(\vartheta_T, \vartheta_M, b_A, b_T)$ to notice the onset of possible deviations. In the first iteration the parameters $\vartheta_T, \vartheta_M, b_A, b_T$ were set to 0.23, 0.32, 0.35 and 0.40 respectively, based on analyses conducted on scaling relationships obtained from the analysis of individual earthquakes (Rhoades and Evison, 2004). With these parameters set, a_T, a_M and σ_A were fit by the maximum likelihood estimation using as starting values 1.5, 1.4 and 3.3, respectively. The fit procedure continued by adding one parameter at a time and considering the previously obtained values as initial values. The parameters, log-likelihoods values and the expected numbers of earthquakes are reported in Table 4.3.

Table 4.3: Estimated parameters, expected number of target earthquake and log-likelihood values for each iteration step.

EEPSOF code									
1st step		**2nd step (σ_T)**		**3rd step (σ_M)**		**4th step (b_A)**		**5th step (b_T)**	
a_T	2.2264	a_T	2.2109	a_T	2.2204	a_T	2.2187	a_T	2.2173
a_M	1.2295	a_M	1.2289	a_M	1.0165	a_M	1.0339	a_M	1.0141
σ_A	2.3893	σ_A	2.3739	σ_A	2.3360	σ_A	1.2387	σ_A	1.1125
		σ_T	0.2757	σ_T	0.2696	σ_T	0.2686	σ_T	0.2683
				σ_M	0.4845	σ_M	0.4820	σ_M	0.4918
						b_a	0.4899	b_a	0.5181
								b_T	0.4021
L	-961.64	L	-961.491	L	-960.876	L	-960.632	L	-960.594
$\bar{E}$	40.8569	$\bar{E}$	40.0899	$\bar{E}$	39.7087	$\bar{E}$	39.8445	$\bar{E}$	39.5826
MATLAB code									
1st step		**2nd step (σ_T)**		**3rd step (σ_M)**		**4th step (b_A)**		**5th step (b_T)**	
a_T	2.2190	a_T	2.2074	a_T	2.2118	a_T	2.2075	a_T	2.4950
a_M	1.2188	a_M	1.2208	a_M	1.0477	a_M	1.0049	a_M	1.0025
σ_A	2.3929	σ_A	2.3769	σ_A	2.3456	σ_A	1.0015	σ_A	1.0097
		σ_T	0.2670	σ_T	0.2603	σ_T	0.2607	σ_T	0.2652
				σ_M	0.4493	σ_M	0.4771	σ_M	0.4642
						b_a	0.5413	b_a	0.5399
								b_T	0.3236
L	-961.791	L	-961.719	L	-961.264	L	-960.945	L	-960.755
$\bar{E}$	41.222	$\bar{E}$	40.6459	$\bar{E}$	40.5468	$\bar{E}$	40.6171	$\bar{E}$	40.9646

The optimized parameter values for the first iteration are unequivocally similar for the two codes, because the differences are less than 0.9%. In the second and third step, the estimates of parameters a_M and ϑ_T begin to slightly deviate, with maximum percentage differences up to about 3.0%. With the introduction in the fit of the spatial parameters, the differences of the other parameters also increase. In the fifth and final iteration, the differences are more pronounced, particularly for the parameters a_T, σ_A and b_T, where the codes differ by 12.5%, 10.2% and 24.0%, respectively. However, the differences in log-likelihoods and expected numbers of earthquakes remain small. Such differences mainly concern spatial parameters and may be related to the different way in which distances are handled by the two software codes and to the different method used to integrate over space.

4.5 Implementation of the ETAS, SUP, and SVP models

In the literature we can find several implementations of the Epidemic Type Aftershock Sequence (ETAS) model to earthquake forecasting in Italy (e.g., Console et al., 2006, Lombardi and Marzocchi, 2010, see also section 2.3.2). In all of them the time dependence is formulated as a sum of Omori decays starting at the times of occurrence of each earthquake

$$f(t) = \sum_{i=1}^{n} \frac{H(t-t_i)K}{(t-t_i+c)^p} \tag{4.24}$$

where K, p and c are free parameters and $H(t-t_i)$ is the Heaviside step function which is 1 if $t-t_i > 0$ and is 0 otherwise.

The productivity of each earthquake of magnitude M_i is described by

$$r = e^{\alpha(M_i - M_c)} \tag{4.25}$$

where α is a free parameter and M_c is the minimum magnitude of completeness.

The decay of the productivity with the distance from the epicenter (x_i, y_i) of each earthquake can be described by many probability density functions (e.g., Ogata,

1998; Console et al., 2003; Zhuang et al., 2004; Lombardi and Marzocchi, 2010; Marzocchi and Zhuang, 2011, see also section 2.3.2). In this work we considered the spatial PDF as described in Ogata and Zhuang (2006) where the smoothing term is an exponential function of the magnitude:

$$g(x,y) = \frac{(q-1)\left[D^2 e^{\gamma(m_i - m_c)}\right]^{q-1}}{\pi[(x-x_i)^2 + (y-y_i)^2 + D^2 e^{\gamma(m_i - m_c)}]^q} \tag{4.26}$$

where q, D and γ are free parameters.

Finally, the frequency magnitude distribution of shocks is given by the Gutenberg and Richter (1944) law

$$h(m) = \beta e^{-\beta(m - M_c)} \tag{4.27}$$

where $\beta = b\ ln10$ is a free parameter.

Combining all the previous terms together, and adding a time invariant background seismicity term $\lambda_0(x,y,m)$, the rate density of ETAS models is given by

$$\lambda(t,x,y,m) = f_r \lambda_0(x,y,m) + [f(t) r g(x,y) h(m)] \tag{4.28}$$

That is

$$\lambda(t,x,y,m) = f_r \lambda_0(x,y,m) + \\ + \left\{ \sum_{i=1}^{n} \frac{H(t-t_i)K}{(t-t_i+c)^p} e^{\alpha(M_i - M_c)} \frac{(q-1)\left[D^2 e^{\gamma(m_i - m_c)}\right]^{q-1}}{\pi[(x-x_i)^2 + (y-y_i)^2 + D^2 e^{\gamma(m_i - m_c)}]^q} \beta e^{-\beta(m - M_c)} \right\} \tag{4.29}$$

The parameter ν represents the ratio between the expected number of independent events of the background seismicity $\lambda_0(x,y,m)$ and the total number of events.

The time invariant models of seismicity consist of stationary Poisson processes, in which the average earthquake occurrence rate may be spatially uniform (Spatially Uniform Poisson, SUP) or variable (Spatially Variable Poisson, SVP). SUP and SVP can also be seen as independent models of seismicity occurrence to compare with other forecasting models (Console et al., 2006).

Their rate density is given by:

$$\lambda_0(x,y,m) = \mu_0(x,y)\beta \exp[-\beta(m - M_c)] \tag{4.30}$$

where $\mu_0(x, y)$ is the spatial rate density of earthquakes with magnitudes equal or larger than M_c. In the SUP model the space-density is assumed to be uniform and independent of the location (x, y). μ_0 is obtained by dividing the number of earthquakes with magnitude above M_c over the whole analysis region R by the total surface area considered.

In the SVP model, the spatial density $\mu_0(x, y)$ is considered as a continuous smooth function of the geographical location (x, y). To estimate it as a spatially varying function, it is necessary to divide the polygon into squared cells of suitable size. The number of earthquakes N_k with magnitude equal to or larger than M_c in each cell is estimated. Each N_k value, representative of a single cell is then smoothed by a Gaussian filter with correlation distance d_c and normalized so as to preserve the total number of events as described in Frankel (1995). For each cell, the smoothed N_k is given by

$$\widetilde{N}_k = \frac{\Sigma_l N_k \exp\left(-\Delta_{kl}^2 / {d_c}^2\right)}{\Sigma_l \exp\left(-\Delta_{kl}^2 / {d_c}^2\right)} \tag{4.31}$$

where Δ_{kl} is the distance between the center of the $k_{\text{th}}$and the l_{th} cells. To obtain $\widetilde{N}_k$ in terms of number of events per unit of time and area, it must be divided by the total duration of the earthquake catalogue and by the area of the cell. The value of $\mu_0(x, y)$ in each point of the space is computed by the weighted mean over the distance of the four nearest cells that surround the point. To determine d_c we follow the procedure suggested by Console and Murru, (2001): the learning dataset (from 1990 to 2011) is divided into two sub-catalogues of about the same temporal length and d_c is chosen as the value that maximizes the log-likelihood of a sub-catalogue using the smoothed seismicity obtained from the other sub-catalogue (Fig 4.4). The analysis for the optimal d_c is conducted for both sub-catalogues and the obtained values for d_c are respectively $d_{c1} = 16.0$ and $d_{c2} = 13.0$. The optimal correlation distance $d_c = 14.5$ is given by the mean of these two estimates. Once the value d_c is optimized, the spatial

density of earthquakes $\mu_0(x, y)$ of the SVP background model can be assessed for each cell and for each point in space (Fig. 4.1).

The parameter q of the ETAS model is set to 1.5, according to physical investigation showing that the static stress changes decrease with epicentral distance as r^{-3} (Lombardi and Marzocchi, 2010). The other parameters (k, p, c, α, d, v) are fitted by the maximization of the likelihood function (eq. 4.1) of using the interior point method.

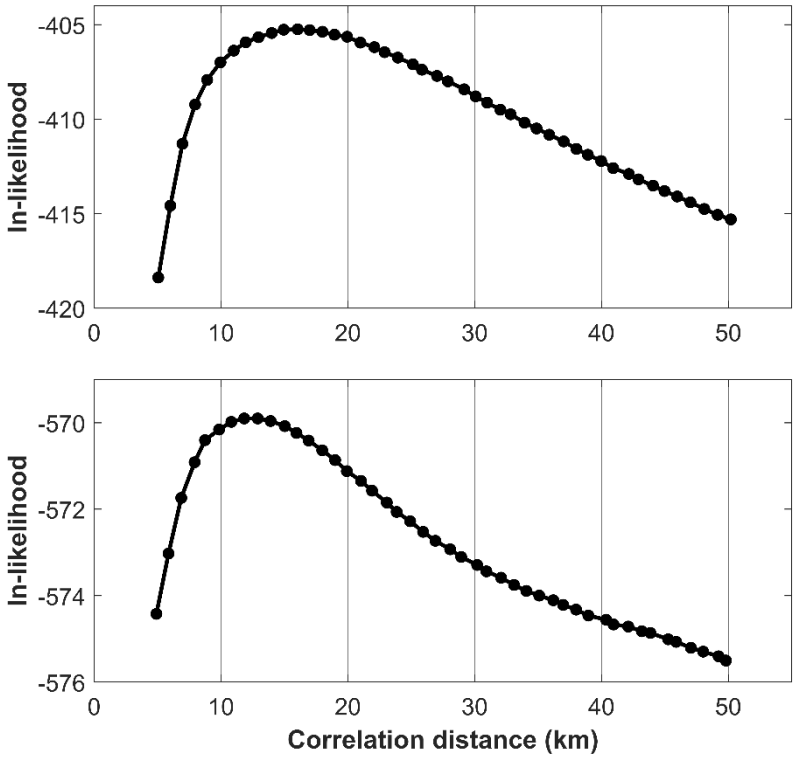

Figure 4.4: (Upper frame) Log-likelihood of the sub-catalogue of earthquakes that occurred in the period 1990 - April 2000 under the time-independent SVP model obtained by the seismicity from April 2000 to 2011. (Lower frame) Log-likelihood of the sub-catalogue of earthquakes that occurred in the period April 2000 to 2011 under the time-independent SVP model obtained by the seismicity from 1990 - April 2000.

4.6 Estimation of parameters of EEPAS and other forecasting models using the learning dataset

Considering the high number of free parameters to be determined for the EEPAS model (in principle about 20), the maximization of the log-likelihood function (eq. 4.1) would be very time consuming and subject to numerical instability. However, according to Rhoades and Evison (2004), simultaneous optimization of all parameters is not necessary because some of them, such as the b-value of the Gutenberg and Richter (1944) relation and the parameters of the aftershock epidemic decay model (p, k, c, ν), can be, in fact, separately fitted or even be simply assigned based on previous works in the same area.

The $b-$value of the Gutenberg and Richter (1944) relation is chosen to be representative of the behavior of the frequency magnitude distribution of target events in the fitting time interval. For the mainshocks + aftershocks and mainshocks only target earthquake sets, the values $b = 1.084$ and $b = 1.176$, respectively, are computed so that the number of predicted target events by the spatial uniform Poisson model (SUP) exactly match the number of observed events (27 and 12 respectively) in the learning set. This also makes the numbers of shocks predicted by the other models implemented for comparison consistent with observed ones. The parameters of the aftershock model are not particularly critical for the EEPAS model; however, they are necessary to determine the weight w (eq. 4.22) of the contribution of each earthquake ($M \geq m_c$), by defining the probability of an earthquake being an aftershock of a previous seismic event. The parameters $p = 1.2$ and $c = 0.03$ of equation (4.19) were chosen as typical parameters of Omori's law (Ogata, 1983). The two parameters ν and k in equation (4.17) were fitted by maximizing the likelihood of earthquakes with $m \geq m_T$ occurring within R in the period 1990-2011.

Finally, the parameter $\sigma_U = 0.006$ of equation (4.21) is chosen to be consistent with the mean value of the cluster diffusion parameter for Italy (Musmeci and Vere-Jones, 1992). The parameter $\delta = 0.7$ of equation (4.20) is taken from previous works for

New Zealand, California and Japan (Evison and Rhoades 2005, Rhoades and Evison, 2004, Rhoades, 2007, 2011). The parameters of the PPE model (eq. 4.16) a, d, and s are fitted simultaneously using the maximum likelihood method.

Regarding EEPAS parameters, the fit is made in three successive iterations. The parameter b_M is fixed to 1 for all three iterations; that means there is perfect scaling between precursor and target magnitudes (Rhoades and Evison, 2004).

In the first iteration, the parameters b_T and b_A are fixed to 0.40 and 0.35, respectively, based on analyses conducted on scaling relationships obtained from the analysis of individual earthquakes. The parameters σ_M and σ_T are also fixed to 0.32 and 0.23, respectively. Such values correspond to the residual standard deviation for the magnitude and time scaling relations (Rhoades and Evison, 2004). Finally, parameters a_T, a_M, σ_A and μ are computed by maximum likelihood estimation.

In the second iteration, the previously fitted parameters a_T, a_M, σ_A are kept fixed at the obtained values and the parameters b_T, b_A, σ_M, σ_T and μ are computed instead by the maximum likelihood.

In the third and last iteration a final computation is made of all parameters (a_T, a_M, σ_A, b_T, b_A, σ_M,σ_T and μ) simultaneously, by providing the optimizer with starting values of the parameters as obtained in previous optimizations. The parameter μ, responsible for mixing the two models PPE and EEPAS, is the only parameter fitted in all three iterations of optimization.

The parameter values obtained by maximizing the likelihood are reported in Tables 4.4 and 4.5 for the mainshocks+aftershocks and the mainshocks only target sets respectively. In the same tables, we also report the parameters of the other forecasting models (SUP, SVP, ETAS-SUP and ETAS-SVP) computed for comparison (see Table 4.1) and the parameter standard errors estimated as the square roots of the diagonal elements of the variance-covariance matrix, computed as the inverse of the Hessian matrix of the log-likelihood function at the maximum (Ogata, 1988).

Table 4.4 - Estimated parameters for various models (mainshock + aftershocks).

SUP		**SVP**		**ETAS-SUP**	
b	$1.08*$	b	$1.08*$	b	$1.08*$
		d_c	$14.5*$	k	0.029 ± 0.001
PPE (parameters shared with EEPAS)				c	0.004 ± 0.001
b	$1.08*$			p	1.042 ± 0.004
a	0.62 ± 0.18			D	1.04 ± 0.03
d	30 ± 12			γ	0.45 ± 0.04
s	$9.0 \times 10^{-13} \pm 1.5 \times 10^{-3}$			α	1.11 ± 0.03
EEPAS-NW		**EEPAS-W**		q	1.5^*
a_M	1.22 ± 0.17	a_M	1.23 ± 0.16	f_r	0.264 ± 0.006
b_M	1^*	b_M	1^*	**ETAS-SVP**	
σ_M	0.25 ± 0.11	σ_M	0.24 ± 0.11	b	1.08
a_T	2.55 ± 0.07	a_T	2.72 ± 0.07	k	$0.0207 \pm 5 \times 10^{-4}$
b_T	0.35 ± 0.02	b_T	0.32 ± 0.02	c	$0.0021 \pm 1 \times 10^{-4}$
σ_T	0.15 ± 0.01	σ_T	0.15 ± 0.01	p	1.084 ± 0.003
b_A	0.52 ± 0.06	b_A	0.51 ± 0.05	D	0.895 ± 0.022
σ_A	1.00 ± 0.03	σ_A	1.00 ± 0.03	γ	0.53 ± 0.04
μ	0.18 ± 0.13	μ	0.16 ± 0.12	α	1.22 ± 0.02
		c	0.03^*	q	1.5^*
		p	1.2^*	f_r	0.416 ± 0.006
		k	0.13^*		
		ν	0.61^*		
		δ	0.7^*		
		σ_U	0.006^*		

*fixed or fitted independently

Table 4.5 - Estimated parameters for various models (mainshocks only).

SUP		SVP		ETAS-SUP	
b	$1.18*$	b	$1.18*$	b	$1.18*$
		d_c	$14.5*$	k	0.028 ± 0.001
PPE (parameters shared with EEPAS)				c	$0.002 \pm 2 \times 10^{-4}$
b	$1.18*$			p	1.002 ± 0.003
a	0.39 ± 0.20			D	1.28 ± 0.04
d	32 ± 15			γ	0.36 ± 0.07
s	$91.58 \times 10^{-7} \pm 1.5 \pm 0.002$			α	0.81 ± 0.03
EEPAS-NW		**EEPAS-W**		q	1.5^*
a_M	1.33 ± 0.13	a_M	1.23 ± 0.16	f_r	0.39 ± 0.01
b_M	1^*	b_M	1^*	**ETAS-SVP**	
σ_M	0.20 ± 0.01	σ_M	0.20 ± 0.01	b	1.18
a_T	1.35 ± 0.11	a_T	1.36 ± 0.11	k	$0.0180 \pm 5 \times 10^{-4}$
b_T	0.60 ± 0.03	b_T	0.60 ± 0.03	c	$0.001 \pm 8 \times 10^{-5}$
σ_T	0.15 ± 0.06	σ_T	0.15 ± 0.07	p	1.065 ± 0.003
b_A	0.45 ± 0.07	b_A	0.48 ± 0.07	D	1.04 ± 0.02
σ_A	1.63 ± 0.55	σ_A	1.00 ± 0.44	γ	0.53 ± 0.04
μ	0.34 ± 0.30	μ	0.36 ± 0.30	α	0.86 ± 0.03
		c	0.03^*	q	1.5^*
		p	1.2^*	f_r	0.55 ± 0.008
		k	0.13^*		
		ν	0.61^*		
		δ	0.7^*		
		σ_U	0.006^*		

*fixed or fitted independently

In Tables 4.6 and 4.7, we report the information gain per event (IGPE) and the Akaike information criterion (AIC, Akaike, 1974) goodness of fit estimators of various models for the mainshocks+aftershocks and the aftershocks only target sets respectively. The IGPE is defined as

$$IGPE = \frac{L - \hat{L}}{N} \tag{4.32}$$

where L and $\hat{L}$ are the likelihoods obtained by a model and reference model, respectively. The Akaike information criterion (AIC) defined as

$$AIC = -2\log(L) + 2k \tag{4.33}$$

where L and k are the maximum likelihood and the number of fitted parameters for the model involved, respectively. The lower the AIC statistic, the better the fit to the

data. We can note how both the ETAS models have better scores (higher loglikelihood, information gain per event and lower AIC) than EEPAS and other models. Both EEPAS models also have lower loglikelihoods than SVP and higher AIC (worse) than SUP for the mainshock only set. Such scores are not particularly significant because they only represent the goodness of the fit of the models to learning dataset and might include some degree of data overfitting.

Table 4.6 – Performance estimators of various models in the learning time interval (1990-2011) (mainshock + aftershocks).

	SUP	**SVP**	**PPE**	**EEPAS-NW**	**EEPAS-W**	**ETAS-SVP**	**ETAS-SUP**
E	27	27.22	27	27.67	27.73	27.49	27.52
lnL	-524.63	-465.47	-514.11	-500.39	-496.06	-363.87	-363.58
IGPE	0.00	2.19	0.39	0.90	1.06	5.95	5.97
AIC	1051.3	934.9	1036.2	1026.8	1018.1	727.7	727.1
ΔAIC	0.00	2.15	0.28	0.45	0.61	5.99	6.00

E: number of predicted events, lnL: loglikelihood score, IGPE: information gain per event with respect to model SUP, AIC: Akaike Information Criteria, ΔAIC Akaike Information Criteria difference with respect to model SUP per event.

Table 4.7 – Performance estimators of various models in the learning time interval (1990-2011) (mainshocks only).

	SUP	SVP	PPE	EEPAS-NW	EEPAS-W	ETAS-SVP	ETAS-SUP
E	12.00	12.19	11.99	14.26	14.75	12.01	11.97
lnL	-246.15	-237.68	-243.52	-239.92	-239.79	-215.57	-212.91
IGPE	0.00	0.75	0.22	0.52	0.54	3.03	3.16
AIC	494.30	479.37	495.04	505.84	505.40	435.49	432.57
DAIC	0.00	0.62	-0.03	-0.48	-0.46	1.88	2.10

E: number of predicted events, lnL: loglikelihood score, IGPE: information gain per event with respect to model SUP, AIC: Akaike Information Criteria, ΔAIC Akaike Information Criteria difference with respect to model SUP.

4.7 Retrospective comparison of forecasting models on the independent testing dataset

We apply the suite of tests defined by the Collaboratory for the Study of Earthquake Predictability (CSEP, Jordan, 2006, Zechar et al., 2010) and particularly the new ones described by Bayona et al., (2022).

Such tests assess the consistency of observed earthquakes with a forecast model by i) the conditional loglikelihood (cL-test) ii) the observed number of earthquakes (N-test), iii) their spatial distribution (S-test) and iv) their magnitude distribution (M-Test). However, we do not report the results for the latter, because all forecasting models assume a Gutenberg–Richter frequency–magnitude distribution and all pass the M-test.

Traditional CSEP tests are based on a likelihood function that regards earthquakes in individual cells or bins as independent and Poisson distributed (Schorlemmer et al., 2007, 2010, Zechar et al., 2010). However, the Poisson distribution insufficiently

captures the spatiotemporal variability of earthquakes, especially in the presence of clusters of seismicity (Werner and Sornette, 2008; Lombardi and Marzocchi, 2010; Nandan et al., 2019). The new CSEP tests are characterized by a lower sensitivity to clustering of target events rather than the traditional ones.

The new CSEP N-test compares the number of predicted earthquakes in all (time–space–magnitude) bins with the number of target earthquakes observed and is based on the negative binomial distribution (NBD)

$$p[(\omega|\tau,\nu)] = \frac{\Gamma(\tau+\omega)}{\Gamma(\tau)\omega!}\nu^{\omega}(1-\nu)^{\omega} \tag{4.34}$$

Where $\omega = 1,2,\ldots$ is the number of events, $\tau > 0$ and $0 \leq \nu \leq 1$ are parameters and Γ is the Gamma function. The mean and the variance of NBD are given by

$$\mu = \tau\frac{1-\nu}{\nu};\ \sigma^2 = \frac{1-\nu}{\nu^2} \tag{4.35}$$

According to Werner et al. (Werner et al., 2010) and Bayona et al. (2022) we used the number of expected earthquakes as the mean value μ of the NBD. The variances are determined considering the numbers of events with Mw ≥5.0 within 10 years non overlapping intervals from 1882 to 2011 (Fig.4.5) from the Italian historical catalogue CPTI15 (Rovida et al., 2020). The computed variances are $\sigma_{ND}^2 = 67.76$ and $\sigma_D^2 = 35.94$ for the mainshocks+aftershocks and the mainshocks only data sets, respectively. The numbers of earthquakes corresponding to 95% (p=0.025÷0.975) and 97.5% (p=0.0125÷0.9875) predictive limits, based on the NBD cumulative distribution function, are computed. If the observed number of earthquakes falls within such limits, the model satisfactorily describe the observed data.

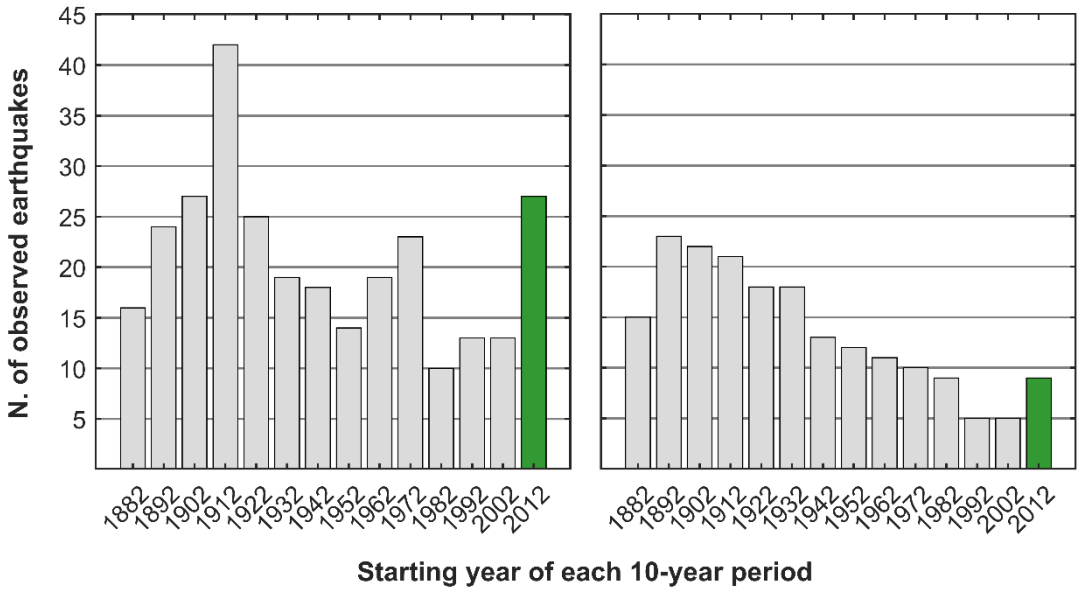

Figure 4.5: Number of target events ($M \geq 5.0$) reported in the CPTI15 earthquake catalogue (from 1880 to 1959) and in the HORUS seismic catalogue (from 1960 to 2021) in non-overlapped 10-year intervals for mainshocks+aftershocks (left) and mainshocks only (right). Green bars indicate the number of target shocks occurred during the test period.

The binary cL-test compares the joint binary log-likelihood (JBLL) of the forecasted events by a model with the observed seismicity, with the distribution of joint binary log-likelihoods obtained by the simulation of random catalogues.

The rates forecasted by the model within each active bin (i.e., time-space-magnitude bins containing observed events) are first normalized to the total number of observed active bins (so that their sum is 1). The active bins are then sorted according to the increasing value of the normalized rate and a vector of cumulated normalized rates is computed (ranging from 0 and 1). The number N_{sim} of target earthquakes to simulate is fixed to the number of observed active bin. For each simulated earthquake (or observed bin), a uniformly distributed random number is extracted in the interval]0,1]. The earthquake is then placed in the first bin for which the cumulated normalized rate exceeds the random sampled value (Zechar et al., 2010).

For each simulated catalogue the JBLL is estimated and, after $N = 10000$ simulated catalogues, the simulated JBLL distribution is obtained. If the JBLL obtained by a

model lies in the lower tail of the simulated JBLL distribution, the forecasting model does not reproduce well the real seismicity pattern and then the test fails.

The binary log-likelihood is obtained by calculating the probability of an earthquake in a forecast bin. Assuming the Poissonian distribution, the probability of observing $\omega = 0$ events, given an expected rate λ, is $P_0 = \exp(-\lambda)$, while the probability of observing more than zero events is $P_1 = 1 - P_0$ (Bayona et al., 2022). The binary log-likelihood for each bin is thus given by

$$BLL = X_i \ln(1 - \exp(-\lambda)) + (1 - X_i) \ln(\exp(-\lambda)) \tag{4.36}$$

where $X_i = 1$ if the $i - th$ bin contains at least one event and $X_i = 0$ otherwise. The observed binomial joint log-likelihood is given by the summation of the BLL over all space-magnitude-time bins:

$$JBLL = \sum_{l=1}^{s} \sum_{j=1}^{m} \sum_{k=1}^{t} X(l,j,k) \ln\left[1 - \exp\left(-\lambda(l,j,k)\right)\right] + [1 - X(l,j,k) \ln(\exp(-\lambda(l,j,k)] \tag{4.37}$$

The S-test evaluates the consistency of the spatial occurrence of target earthquakes regardless of their magnitudes.

For the new S-test the joint binary log-likelihood of the forecasted catalogue is calculated considering only the spatial distribution of forecasted events. To isolate the spatial distribution, the forecasted events are summed over the magnitude and time bins. In addition, to assess the JBLL, the forecasted catalogue is normalized to the number of active spatial cells. The simulation procedure to obtain the spatial simulated JBLL is similar to that described above for the binary cL-test, but N_{sim} is fixed to the number of active spatial cells. For the cL, N and S test, the computed statistic is the quantile score: that is, the fraction of simulated likelihoods that are less than or equal to the likelihood observed by the model. A small value, lower than the usual significance level $\alpha = 0.05$ or than the Bonferroni-adjusted significance level $\alpha_{Bf} = 0.05/2 = 0.025$ means that the model inadequately describes the seismicity pattern.

To evaluate the relative skill of the forecasting models, we use the information gain per active bin (IGPA, Bayona et al., 2022), which is based on the likelihood difference with respect to a reference (baseline) forecasting model divided by the number of earthquakes or by the number of active bins (the bins in which the likelihood contribution is not zero) respectively.The IGPA is thus given by

$$IGPA = \frac{N_{base} - N_{mod}}{M} + \frac{1}{M}\sum_{m=1}^{M}[X_{mod}(m) - X_{base}(m)] \tag{4.38}$$

Where N_{base} and N_{mod} are the total number of earthquakes expected by the baseline and the model respectively, M is the number of active bins, and $X_{mod}(m)$ and $X_{base}(m)$ are the joint log-likelihood score obtained in the bin with the $m-th$ target earthquake by the model and the reference baseline model respectively. According to Rhoades et al. (2011) the variance of $X_{mod}(m) - X_{base}(m)$ is given by

$$s^2 = \frac{1}{M-1}\sum_{m=1}^{M}(X_{mod}(m) - X_{base}(m))^2 - \frac{1}{M^2 - M}\left[\sum_{m=1}^{M} X_{mod}(m) - X_{base}(m)\right]^2. \tag{4.39}$$

The IGPA error is estimated as $\pm ts\sqrt{M}$, where t is the 95th (or 97.5th) percentile of the Student's t distribution with $M-1$ degrees of freedom.

As baseline model we take the SUP, which is the simpler one. We do not need a correction for the number of free parameters, as proposed by Rhoades et al., (2014), because the fitting of models is independent of the testing set targets, being made using the learning set. In addition, we do not use the parimutuel gambling score (PGS) by Zhuang (2010) and Zechar and Zhuang (2014), because Serafini et al. (2022) recently demonstrated that PGS is improper when the number of forecasting methods being tested is greater than two.

4.8 Results

In Fig. 4.6 and Table 4.8, we report the numbers of mainshocks+aftershocks targets predicted by various models using different time intervals (3 months, 6 months, 1 year, 5 years, and 10 years) of prediction. All models definitely underestimate the total number of target earthquakes (27) that actually occurred. The reason is that the

average rate of targets in the testing set (about 2.7 per year) is more than twice than that in learning set (about 1.2 per year). However, according to Werner et al. (2011), the negative binomial N-test is characterized by wider confidence intervals than the traditional Poissonian N-test and then the forecast models are found to be consistent as the observed number earthquakes is within both the 95% and 97.5% confidence intervals (Fig. 4.7 and Table 4.9). The binary cL-tests show that all forecasted models adequately describe the observed seismicity as the quantile scores exceed the 0.025 and 0.05 significance levels (Fig. 4.8 and Table 4.10). The S-test (Fig. 4.9 and Table 4.11) confirm the spatial consistency between the forecasts and the observed dataset. The results of the IGPA (T-test) for mainshocks+aftershocks targets in Fig. 4.10 and Table 4.12 indicate that for the shortest prediction interval of 3 months the best performing models are the ETAS-SVP and ETAS-SUP. For longer prediction intervals, the best performing models are the EEPAS-NW and EEPAS-W, but such superior performance appears to be statistically significant only for time intervals of 5 and 10 years.

In Fig. 4.11 and Table 4.13, we report the numbers of mainshocks only targets predicted by various models using different time intervals of prediction. All models still underestimate the total number of targets (9) that actually occurred, as even in this case the average rate of targets in the testing set (0.9 per year) is greater than in the learning set (0.5 per year). All models pass the negative binary N-test (Fig. 4.12 and Table 4.14), cL-test (Fig. 4.13 and Table 4.15) and S-test (Fig. 4.14 and Table 4.16) for all time intervals of prediction. The results of the IGPA (T-test) mainshock only targets in Fig. 4.15 and Table 4.17 confirm that the best performing models are ETAS-SVP and ETAS-SUP for the shortest prediction interval of 3 months and the EEPAS-NW and EEPAS-W for longer prediction intervals. However, such superior performance is not significant for any time interval.

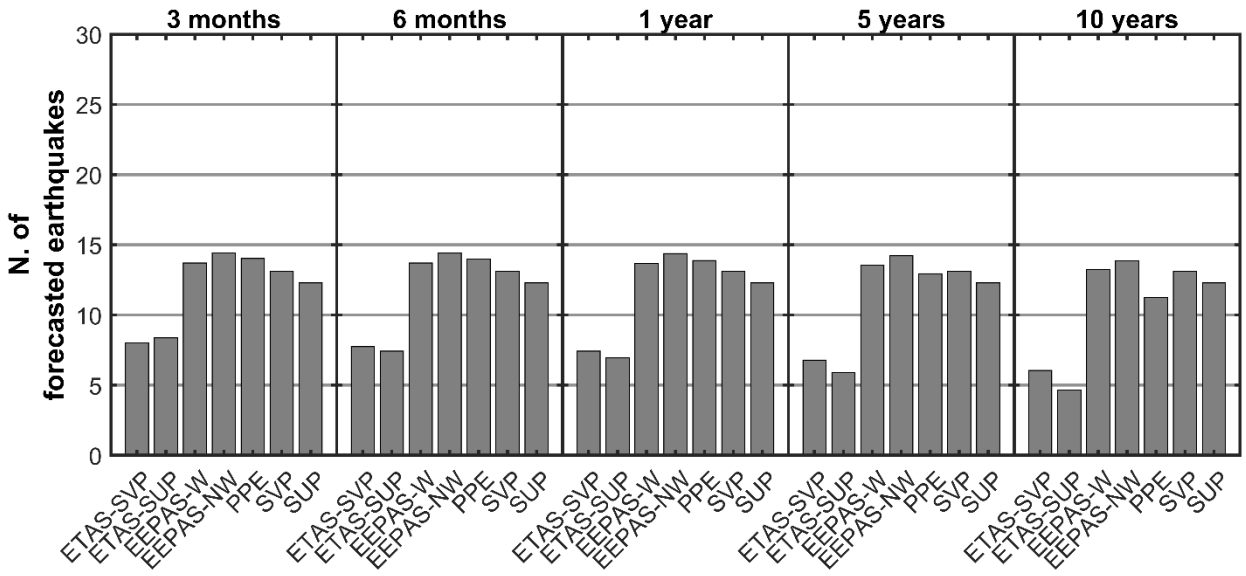

Figure 4.6: Numbers of targets (mainshocks+aftershocks) in the testing set (2012-2021) predicted by various models using different prediction intervals. The effective total number of targets is 27.

Table 4.8 - Numbers of earthquakes predicted by various models in the testing time interval (2012-2021) (mainshocks + aftershocks).

Time interval	SUP	SVP	PPE	EEPAS-NW	EEPAS-W	ETAS-SUP	ETAS-SVP
3 Months	12.27	13.11	14.03	14.41	13.70	8.36	8.00
6 Months	12.27	13.11	13.98	14.40	13.69	7.43	7.73
1 Year	12.27	13.11	13.87	14.38	13.67	6.94	7.42
5 Years	12.27	13.11	12.94	14.21	13.53	5.90	6.79
10 Years	12.27	13.11	11.25	13.86	13.25	4.66	6.05

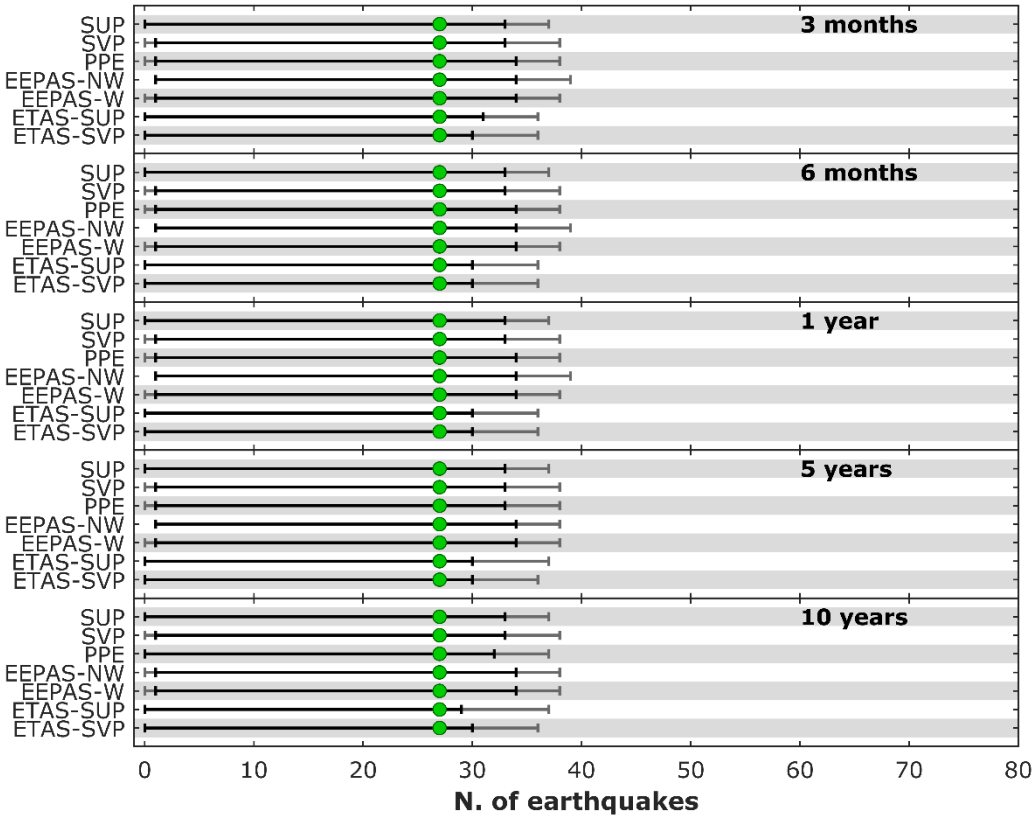

Figure 4.7: Results of number consistency test (N-test) in the testing set (2012-2021) for various models using different prediction intervals (mainshocks+aftershocks). Colored circles indicate the number of observed events in the testing set. Black and grey bars indicate the 95% and 97.5% confidence limits, respectively. Green colored circles indicates that all models passed the test.

Table 4.9 – Binary N test in the testing time interval (2012-2021) (mainshocks + aftershocks).

Time intvl	SUP	SVP	PPE	EEPAS-NW	EEPAS-W	ETAS-SUP	ETAS-SVP
3 Months	0.112	0.125	0.143	0.151	0.136	0.073	0.071
6 Months	0.112	0.125	0.142	0.151	0.136	0.068	0.070
1 Year	0.112	0.125	0.140	0.150	0.136	0.066	0.068
5 Years	0.112	0.125	0.123	0.147	0.133	0.061	0.065
10 Years	0.112	0.125	0.099	0.139	0.128	0.057	0.062

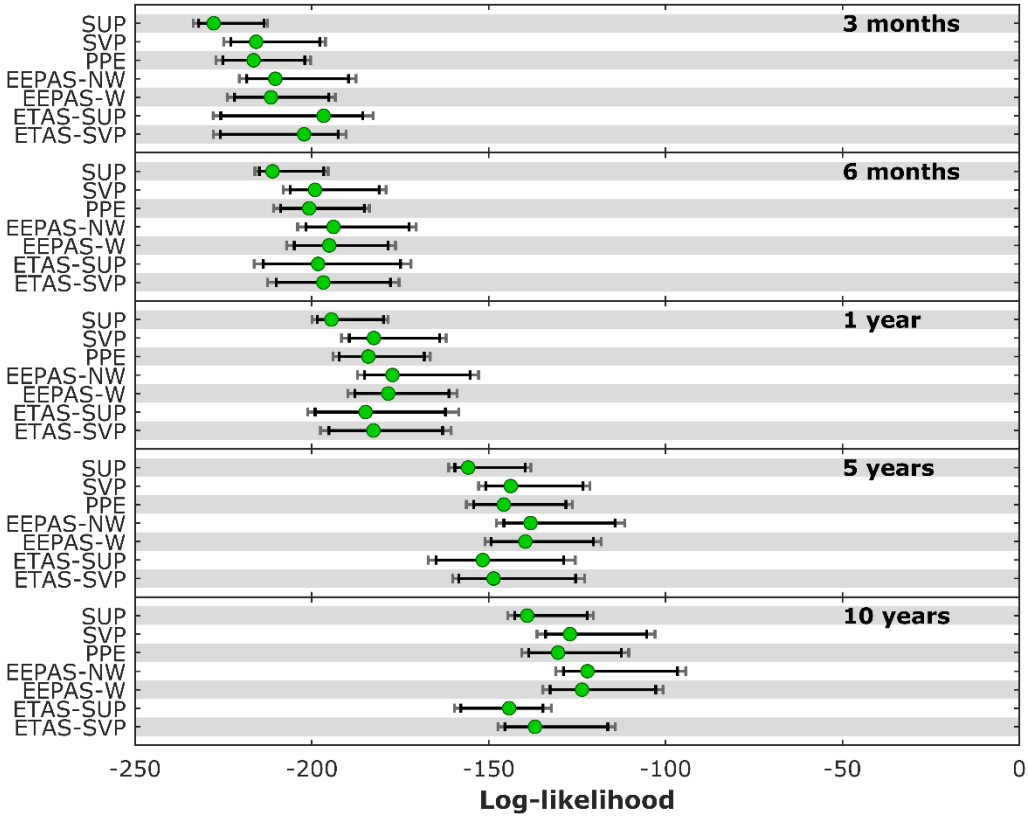

Figure 4.8: Results of conditional likelihood consistency test (cL-test) in the testing set (2012-2021) for various models using different prediction intervals (mainshocks+aftershocks). Black and grey bars indicate the 95% and 97.5% confidence limits, respectively. Green colored circles indicates that all models passed the test.

Table 4.10 – Binary cL test in the testing time interval (2012-2021) (mainshocks + aftershocks).

Time intvl	SUP	SVP	PPE	EEPAS-NW	EEPAS-W	ETAS-SUP	ETAS-SVP
3 Months	0.109	0.180	0.287	0.186	0.321	0.826	0.815
6 Months	0.106	0.177	0.241	0.182	0.305	0.391	0.387
1 Year	0.109	0.171	0.247	0.171	0.292	0.390	0.346
5 Years	0.105	0.167	0.241	0.165	0.275	0.366	0.228
10 Years	0.096	0.151	0.240	0.131	0.231	0.650	0.214

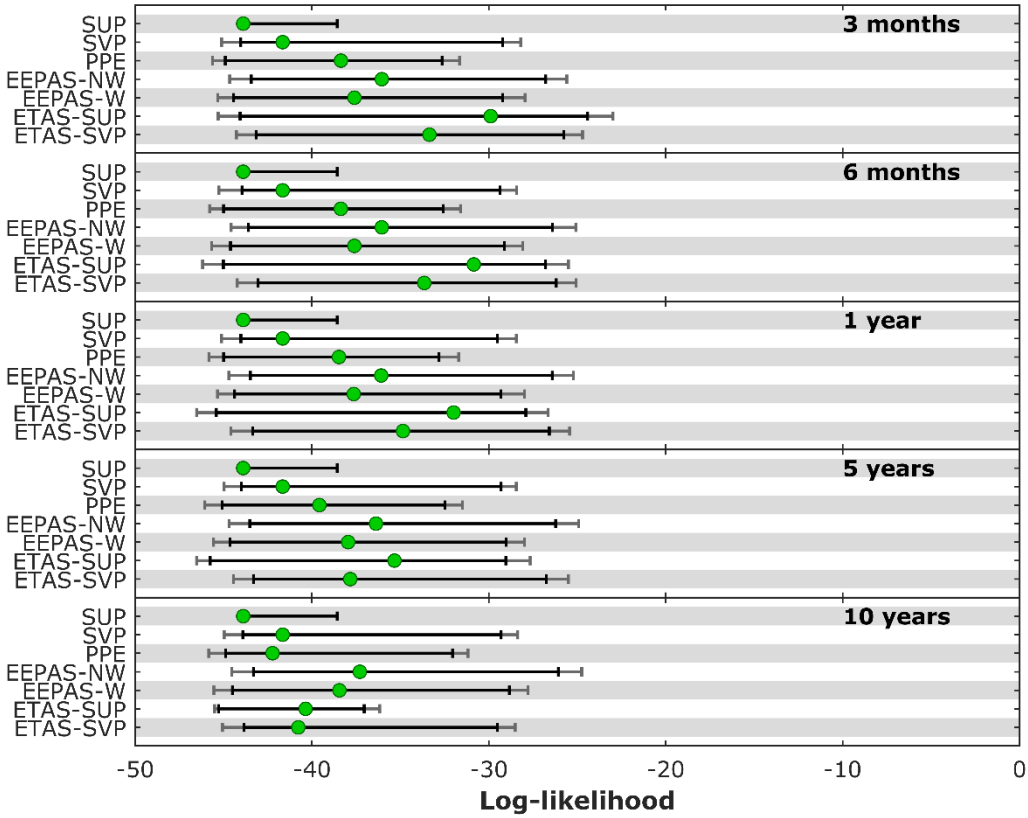

Figure 4.9: Results of spatial consistency test (S-test) in the testing set (2012-2021) for various models using different prediction intervals (mainshocks+aftershocks). Black and grey bars indicate the 95% and 97.5% confidence limits, respectively. Green colored circles indicates that all models passed the test.

Table 4.11 – Binary S test in the testing time interval (2012-2021) (mainshocks + aftershocks).

Time intvl	SUP	SVP	PPE	EEPAS-NW	EEPAS-W	ETAS-SUP	ETAS-SVP
3 Months	0.095	0.084	0.598	0.415	0.443	0.820	0.581
6 Months	0.613	0.090	0.589	0.416	0.452	0.865	0.589
1 Year	0.277	0.091	0.581	0.415	0.441	0.856	0.496
5 Years	0.083	0.085	0.434	0.358	0.393	0.720	0.250
10 Years	0.092	0.009	0.148	0.283	0.344	0.798	0.131

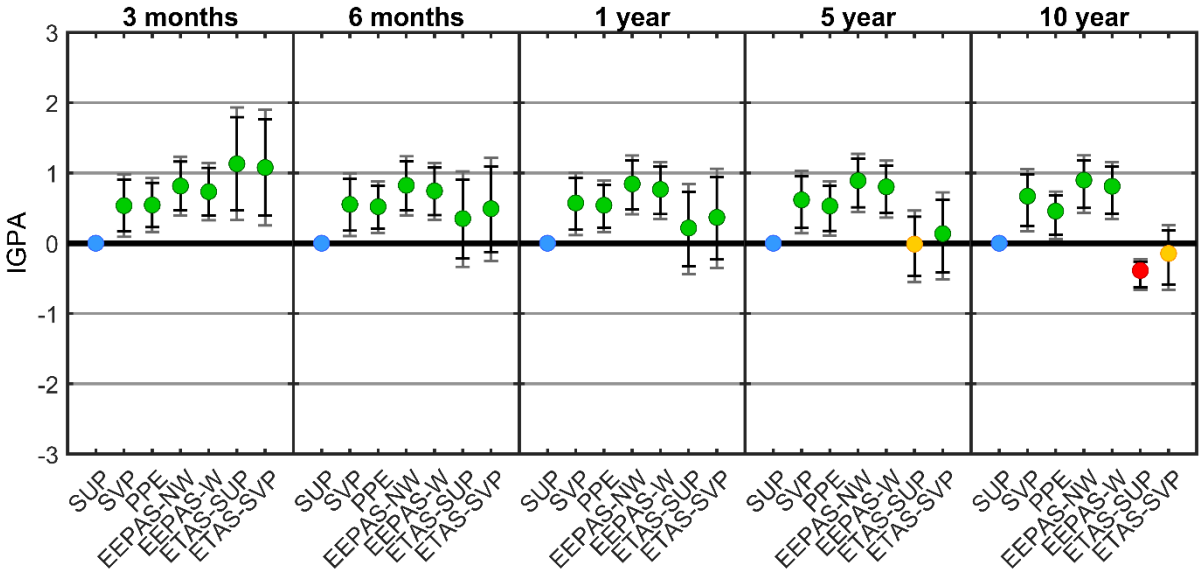

Figure 4.10: Comparison between various models in different time intervals (mainshocks+aftershocks) in the testing set (2012-2021) by the IGPA (T-test). Black and grey bars indicate the 95% and 97.5% confidence limits, respectively. Colored circles are green if the IGPA of a model is larger than the reference value 0 corresponding to the SUP model, yellow if IGPA of a model is lower than the reference model, but not significantly and red if a model IGPA is significantly lower than the reference model.

Table 4.12 – Information Gain per active bin in the testing time interval (2012-2021) (mainshocks + aftershocks).

Time intvl	SUP	SVP	PPE	EEPAS-NW	EEPAS-W	ETAS-SUP	ETAS-SVP
3 Months	0.00(7)	0.53(6)	0.54(5)	0.81(3)	0.73(4)	1.13(1)	1.08(2)
6 Months	0.00(7)	0.55(3)	0.52(4)	0.82(1)	0.74(2)	0.35(6)	0.49(5)
1 Year	0.00(7)	0.57(3)	0.54(4)	0.84(1)	0.76(2)	0.22(6)	0.37(5)
5 Years	0.00(7)	0.62(3)	0.53(4)	0.89(1)	0.80(2)	-0.01(6)	0.14(5)
10 Years	0.00(7)	0.67(3)	0.46(4)	0.90(1)	0.81(2)	-0.38(6)	-0.15(5)

Numbers within brackets indicate the ranking of models from 1 (best) to 7 (worst).

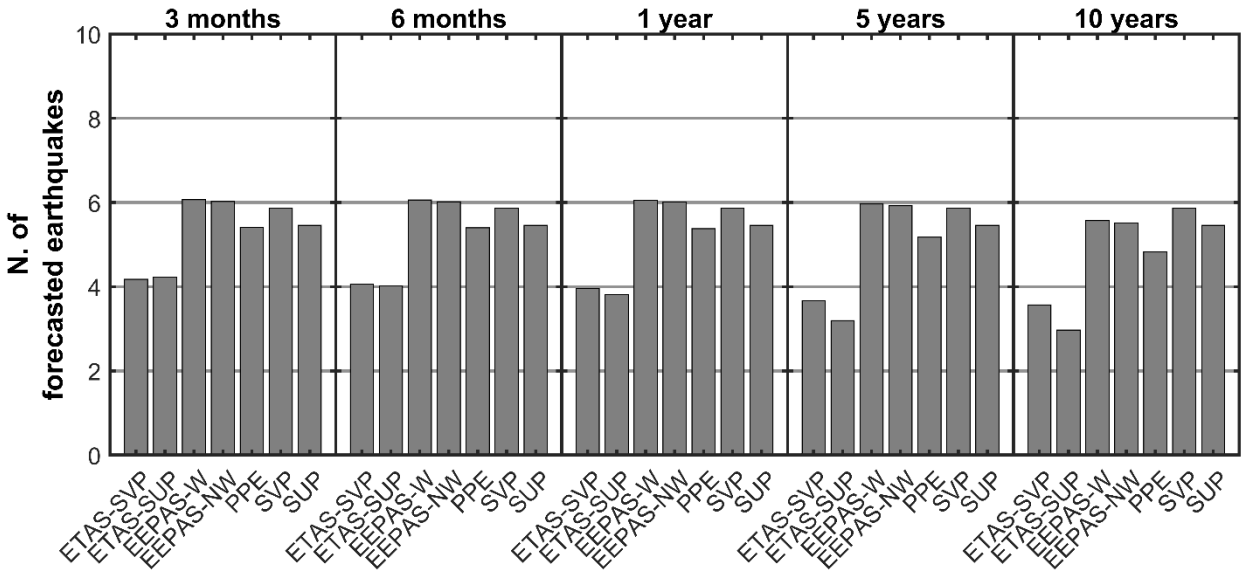

Figure 4.11: Numbers of targets (mainshocks only) in the testing set (2012-2021) predicted by various models and prediction intervals. The effective total number of targets is 9.

Table 4.13 - Numbers of earthquakes predicted by various models in the testing time interval (2012-2021) (mainshocks only).

Time interval	SUP	SVP	PPE	EEPAS-NW	EEPAS-W	ETAS-SUP	ETAS-SVP
3 Months	5.46	5.86	5.41	6.02	6.06	4.23	4.17
6 Months	5.46	5.86	5.40	6.02	6.06	4.02	4.06
1 Year	5.46	5.86	5.38	6.01	6.05	3.82	3.96
5 Years	5.46	5.86	5.18	5.92	5.96	3.19	3.67
10 Years	5.46	5.86	4.82	5.51	5.57	2.97	2.57

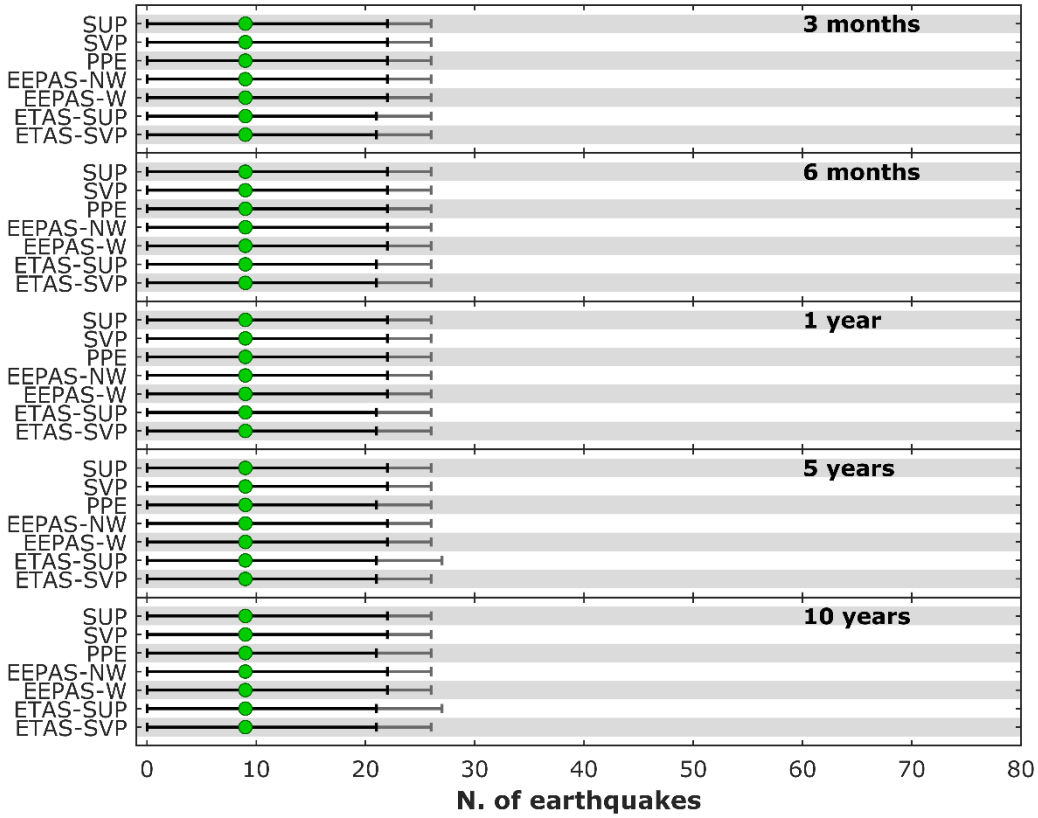

Figure 4.12: Results of number consistency test (N-test) in the testing set (2012-2021) for various models using different prediction intervals (mainshocks only). Black and grey bars indicate the 95% and 97.5% confidence limits, respectively. Colored circles indicate the number of observed events in the testing set. Green colored circles indicates that all model passed the test.

Table 4.14 – Binary N test in the testing time interval (2012-2021) (mainshocks).

Time intvl	SUP	SVP	PPE	EEPAS-NW	EEPAS-W	ETAS-SUP	ETAS-SVP
3 Months	0.373	0.410	0.369	0.424	0.428	0.275	0.271
6 Months	0.373	0.410	0.368	0.424	0.428	0.260	0.263
1 Year	0.373	0.410	0.366	0.423	0.427	0.246	0.256
5 Years	0.373	0.410	0.349	0.415	0.419	0.205	0.236
10 Years	0.373	0.410	0.320	0.378	0.383	0.190	0.229

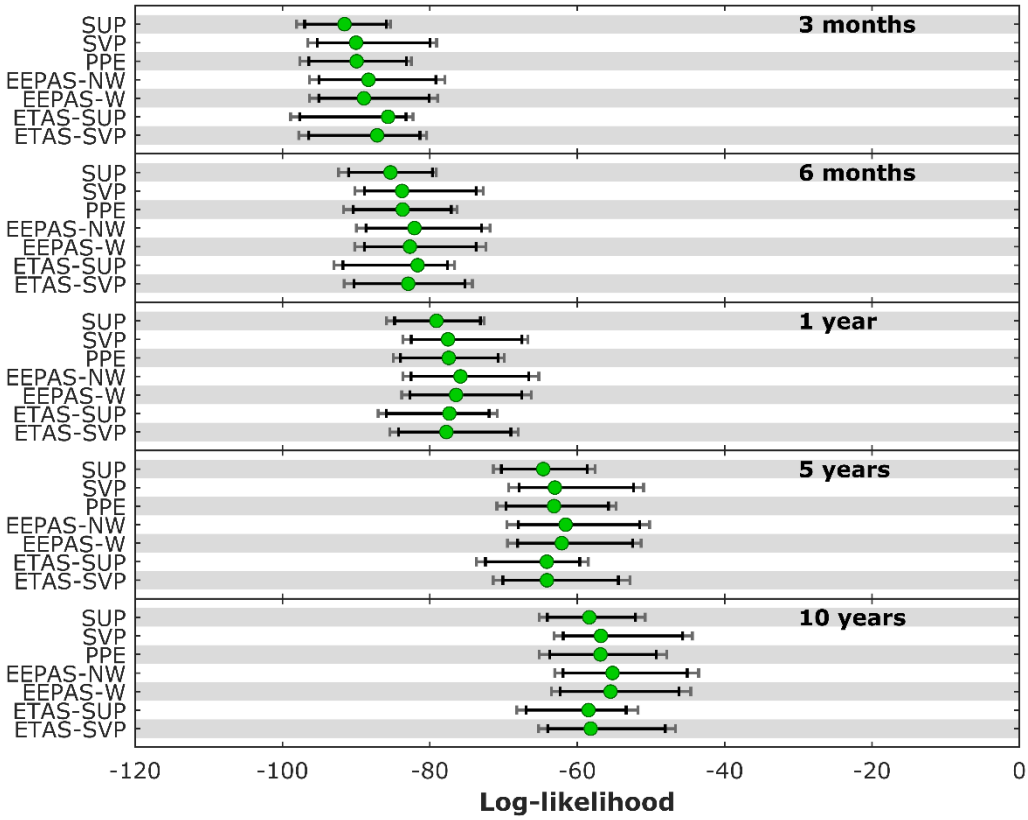

Figure 4.13: Results of conditional likelihood consistency test (cL-test) in the testing set (2012-2021) for various models using different time intervals (mainshocks only). Black and grey bars indicate the 95% and 97.5% confidence limits, respectively. Green colored circles indicates that all model passed the test.

Table 4.15 – Binary cL test in the testing time interval (2012-2021) (mainshocks).

Time intvl	SUP	SVP	PPE	EEPAS-NW	EEPAS-W	ETAS-SUP	ETAS-SVP
3 Months	0.362	0.211	0.3945	0.349	0.337	0.890	0.620
6 Months	0.355	0.209	0.3833	0.354	0.341	0.773	0.414
1 Year	0.356	0.209	0.3946	0.350	0.343	0.624	0.328
5 Years	0.346	0.210	0.3748	0.342	0.319	0.668	0.292
10 Years	0.349	0.202	0.4079	0.383	0.391	0.671	0.279

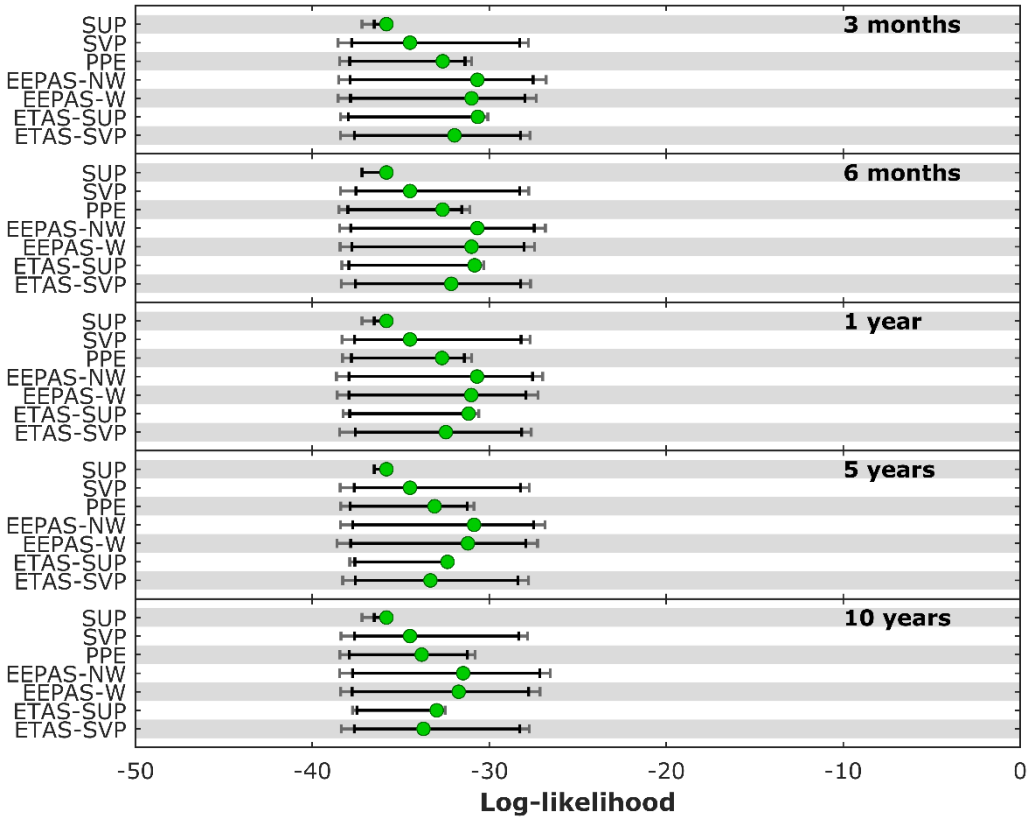

Figure 4.14: Results of spatial consistency test (S-test) in the testing set (2012-2021) for various models using different prediction intervals (mainshocks only). Black and grey bars indicate the 95% and 97.5% confidence limits, respectively. Green colored circles indicates that all model passed the test.

Table 4.16– Binary S test in the testing time interval (2012-2021) (mainshocks).

Time intvl	SUP	SVP	PPE	EEPAS-NW	EEPAS-W	ETAS-SUP	ETAS-SVP
3 Months	0.457	0.159	0.710	0.631	0.641	0.887	0.427
6 Months	0.439	0.160	0.711	0.632	0.641	0.881	0.439
1 Year	0.397	0.158	0.695	0.628	0.640	0.866	0.397
5 Years	0.290	0.161	0.623	0.605	0.611	0.865	0.290
10 Years	0.241	0.162	0.484	0.509	0.536	0.834	0.241

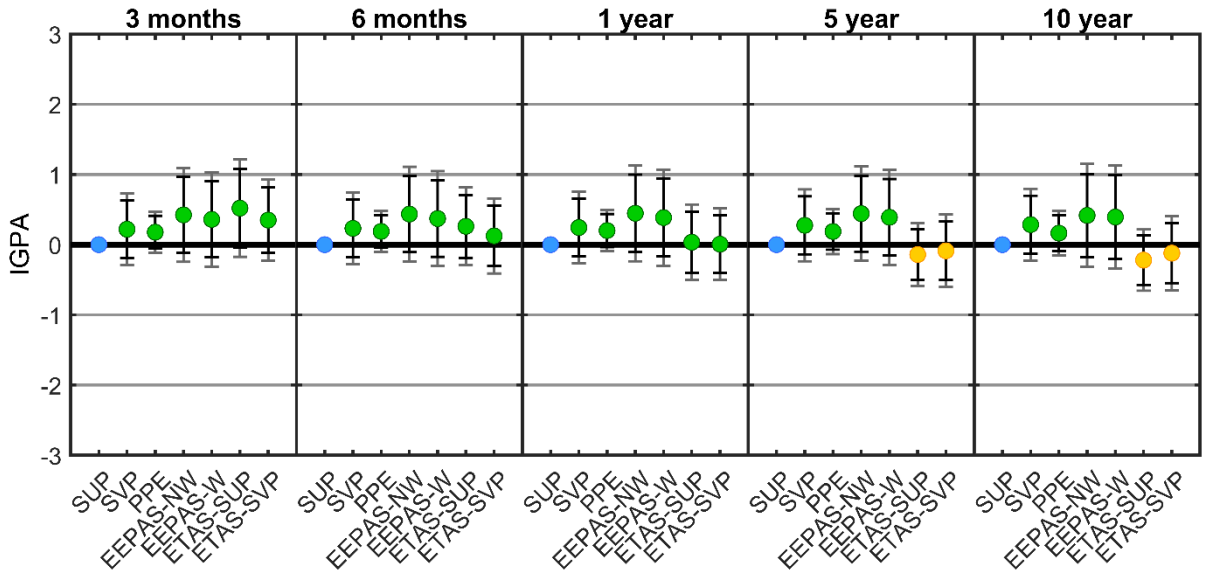

Figure 4.15: Comparison between various models in different time intervals (mainshocks only) in the testing set (2012-2021) by the IGPA (T-test). Black and grey bars indicate the 95% and 97.5% confidence limits, respectively. Colored circles are green if the IGPA of a model is larger than the reference value 0 corresponding to the SUP model, yellow if IGPA of a model is lower than the reference model, but not significantly and red if a model IGPA is significantly lower than the reference model.

Table 4.17 – Information Gain per active bin in the testing time interval (2012-2021) (mainshocks).

Time intvl	SUP	SVP	PPE	EEPAS-NW	EEPAS-W	ETAS-SUP	ETAS-SVP
3 Months	0.00(7)	0.22(5)	0.18(6)	0.42(2)	0.36(3)	0.52(1)	0.35(4)
6 Months	0.00(7)	0.25(4)	0.20(5)	0.45(1)	0.39(2)	0.26(3)	0.12(3)
1 Year	0.00(7)	0.28(3)	0.23(4)	0.75(1)	0.42(2)	0.03(5)	0.01(6)
5 Years	0.00(7)	0.36(3)	0.27(4)	0.52(1)	0.47(2)	-0.14(6)	-0.09(5)
10 Years	0.00(7)	0.39(3)	0.27(4)	0.52(1)	0.50(2)	-0.22(6)	-0.12(5)

Numbers within brackets indicate the ranking of models from 1 (best) to 7 (worst).

4.9 Conclusions of Chapter 4

We applied the EEPAS earthquake forecasting model to Italy, similarly to previous application in other seismic regions of the world (e.g., Rhoades and Evison, 2004, Evison and Rhoades, 2005, Rhoades, 2007, 2011, Rhoades et al., 2020), using a suite of computing codes completely rewritten in MATLAB and implementing both EEPAS formulations with the input earthquakes not weighted (EEPAS-NW) and weighted (EEPAS-W). We calibrated and fitted the model parameters using earthquakes of the HORUS seismic catalogue of Italy (Lolli et al., 2020) for the learning period 1990-2011. The EEPAS model was then applied to forecast all earthquakes (mainshocks + aftershocks) of the same seismic catalogue with $M \geq 5.0$ and only the mainshocks that occurred within the polygon of analysis for the test period 2012-2021. We compared the forecasting skill of EEPAS with the ones obtained by other time dependent (ETAS-SUP and ETAS-SVP) and time independent (SUP, SVP and PPE) models implemented on the same dataset. We used a set of new CSEP consistency tests based on a negative binary likelihood function as described in Bayona et al., (2022). This latter likelihood function reduces the sensitivity of spatial log-likelihood scores to the occurrence of seismic events (Bayona et al., 2022) compared to previous versions of the tests based on a Poisson distribution assumption. The number of expected target earthquakes forecasted by each model tends to decrease as the forecasting interval increases. The highest expected number of earthquakes is for a window of 3 months. However, all models tend to underestimate the total numbers of expected events that actually occurred, 27 and 9 for the mainshocks + aftershocks and mainshocks only datasets, respectively. This is due to the different average rate of target events in the learning and testing period. This difference does not affect the performance of consistency tests, which are passed by all models. In particular, the cL and S-test showed an adequate consistency between the forecasted and the observed events distribution as the quantile scores exceed the significance values of 0.025 and 0.05. The difference in the seismicity rate between the learning and the testing period is less pronounced for the mainshocks only dataset and the

consistency tests show similar results. We also assess the relative forecasting skill of various models using the IGPA (Rhoades et al., 2011, Bayona et al., 2022) considering as baseline reference model the SUP. For both mainshocks+aftershocks and mainshocks only datasets, the best performing model is the ETAS-SUP and ETAS-SVP for the shortest prediction interval of 3 months and the EEPAS-NW and EEPAS-W for the longer prediction intervals. These results confirm the different characteristics of the models ETAS and EEPAS. The latter model seems more appropriate than the ETAS model for making forecasts of the long-term seismicity, even if the small number of target shocks suggest some caution. In particular, the weighted version of EEPAS is designed so that to weigh less earthquakes that are likely to be aftershocks of a previous one. These results also suggests that EEPAS could be a valid candidate for hybrid forecasting models in combination to ETAS.

Chapter 5

Analysis and comparisons of FORE, EEPAS, and ETAS models using the alarm-based approach

From this chapter it was taken the following article: Biondini, E., and P. Gasperini, 2023, Comparison between alarm-based and probability-based earthquake forecasting methods Geophys. J. Int. (submitted)

In chapter 4, the Every Earthquake a Precursor According to Scale (EEPAS) probabilistic model has been applied to the pseudo-prospective forecasting of shallow earthquakes with magnitude $M \geq 5.0$ in the Italian region. The forecasting performance of EEPAS with that of the Epidemic Type Aftershock Sequences (ETAS) forecasting model, have been compared using the most recent tests developed within the Collaboratory Study for Earthquake Predictability (CSEP). In this chapter, the performance of EEPAS and ETAS models are compared with that obtained by a deterministic model based on the occurrence of strong foreshocks (FORE model) using an alarm-based approach. The model parameters and probability thresholds for issuing the alarms are calibrated on a learning dataset from 1990 to 2011 while the pseudo-prospective forecasting performance is assessed on a validation dataset from 2012 to 2022.

Such tests demonstrate that, even if all models outperform a purely random method, the EEPAS model exhibits lower forecasting performance than ETAS model and the latter a slightly lower performance than the FORE model. However, truly prospective tests are necessary to validate such results, ideally using new testing procedures allowing the analysis of alarm-based models, not yet developed within the CSEP.

5.1 Introduction

Estimates of earthquake occurrence probabilities provided by empirical probabilistic models based on short-term (e.g., ETAS) or medium- to long-term (e.g., EEPAS) earthquake clustering can provide relevant information in terms of probability increases of several orders of magnitude prior to the occurrence of a strong earthquake or during an earthquake sequence (Marzocchi et al., 2015). However, these probabilities hardly exceed a few percent. Although the main purpose of Operational Earthquake Forecasting (OEF) is the near-real-time or daily dissemination of information on seismic risk and thus the probability of occurrence of a certain target earthquake $M \geq M_{min}$, predictions intended as the definition in advance of the location, time, and magnitude range of an impending or future earthquake require much higher probability estimates than those currently provided by forecast models. From a decision-making perspective, to set up generalized immediate seismic risk mitigation operations, such low probability values are difficult to employ even if they provide relevant information.

In this chapter we follow Jordan et al. (2011) to distinguish between a probabilistic forecast and a deterministic prediction using strict definitions: the former is the indication of the probability that one or more target event will occur in a given space-time domain, whereas the latter is the binary assertion that target events will occur or not in a given space-time alarm window.

To evaluate the forecasting performance of probabilistic models, a suite of statistical test has been developed, within the ambit of the Collaboratory Study for Earthquake Predictability (Schorlemmer et al., 2007; Werner et al., 2010; Bayona et al., 2022), while tests appropriate for deterministic models were developed by Molchan (1990, 1991), Zechar and Jordan (2008, 2010) and Shebalin et al. (2011). The two approaches are not directly compatible and hence a problem arises for comparing the performance of probabilistic versus deterministic models.

The implementation of the probabilistic approach, to assess the forecasting performance of deterministic models (for example using the CSEP tests) is not trivial because it can be difficult to associate a rate of occurrence of target earthquakes with some kind of potentially precursory phenomenon. A similar approach has been implemented by Murru et al. (2009) and Console et al. (2010) to evaluate probabilistic models applied to Italian and New Zealand seismicity respectively. Thus, to compare the forecasting performance of probabilistic and deterministic methods, the use of tests and procedure developed for deterministic methods is usually preferable.

In this chapter, the probabilistic forecasting models described in chapter 4 (see also Biondini et al., 2023) are compared with a deterministic forecasting method based on the occurrence of strong (fore) shocks (hereafter FORE method) described in chapter 3 (see also Gasperini et al., 2021).

In this chapter, the probabilistic EEPAS-NW and ETAS-SVP models (see Table 4.1) described in Chapter 4 are examined and applied to the retrospective forecast of target earthquakes with $M \geq 5.0$ occurred in Italy using the deterministic alarm-based approach (see Chapter 3). The forecasting capabilities are then compared with the forecasting method based on the occurrence of strong (fore)shocks (hereafter FORE method) described in Chapter 3.

5.2 Setting up the deterministic experiment

The probabilistic models discussed in Chapter 4 were fitted to forecast earthquakes of magnitude $M \geq 5.0$. For this experiment, such magnitude is chosen as lower limit of target earthquakes to be forecasted. Similarly, the grid consisting of 177 non-overlapped square cells of side $L = 30\sqrt{2}$ km described in section 4.3 and showed in Fig. 4.1 was considered as application region R.

To implement the alarm-based approach, the analysis and optimization of both the threshold rate for the probabilistic models and the magnitude range required by the FORE method was conducted for the period 1990-2011. This period corresponds to the learning period in which the parameters of the EEPAS and ETAS probabilistic models applied to Italian seismicity (described in Chapter 4) were fitted and optimized. The retrospective alarm-based forecasting experiment is conducted for the period 2012-2022. This period corresponds to the test set used for the retrospective application of the EEPAS and ETAS models described in Chapter 4. Both the optimization and the retrospective forecasting experiment are conducted using the HORUS seismic catalogue (Lolli et al., 2020). The two formulations of EEPAS (EEPAS-NW and EEPAS-W) and ETAS (ETAS-SUP and ETAS-SVP) produced quite similar retrospective forecasting results and performance, respectively (see sections 4.7 and 4.8). Therefore, for this experiment, only the EEPAS-NW and ETAS-SVP models are considered. These latter are characterized by a slightly better forecasting performance than EEPAS-W and ETAS-SUP, respectively. The FORE method, based on the occurrence of potential foreshocks, (described in Chapter 3) was adapted for application to the region of analysis and dataset defined above.

5.3 Setting forecast assumptions and testing procedures

The expected daily rate for the probabilistic EEPAS-NW and ETAS-SVP models is re-estimated for each cell, every time an earthquake of magnitude $m \geq 2.5$ (depth <40 km) occurs within the analysis polygon R (Fig. 4.1) according to the HORUS seismic catalogue.

An alarm with duration Δt, is issued in a given cell, every time the expected rate estimated by such models exceeds some threshold value. Similarly, for the FORE method, an alarm is issued whenever a strong shocks of magnitude within $M \pm$

ΔM occurs. A target earthquake ($M \geq 5.0$) is considered successfully predicted if occurs within an alarm window. On the contrary, it is considered as a failure to predict if occurs outside any alarm windows.

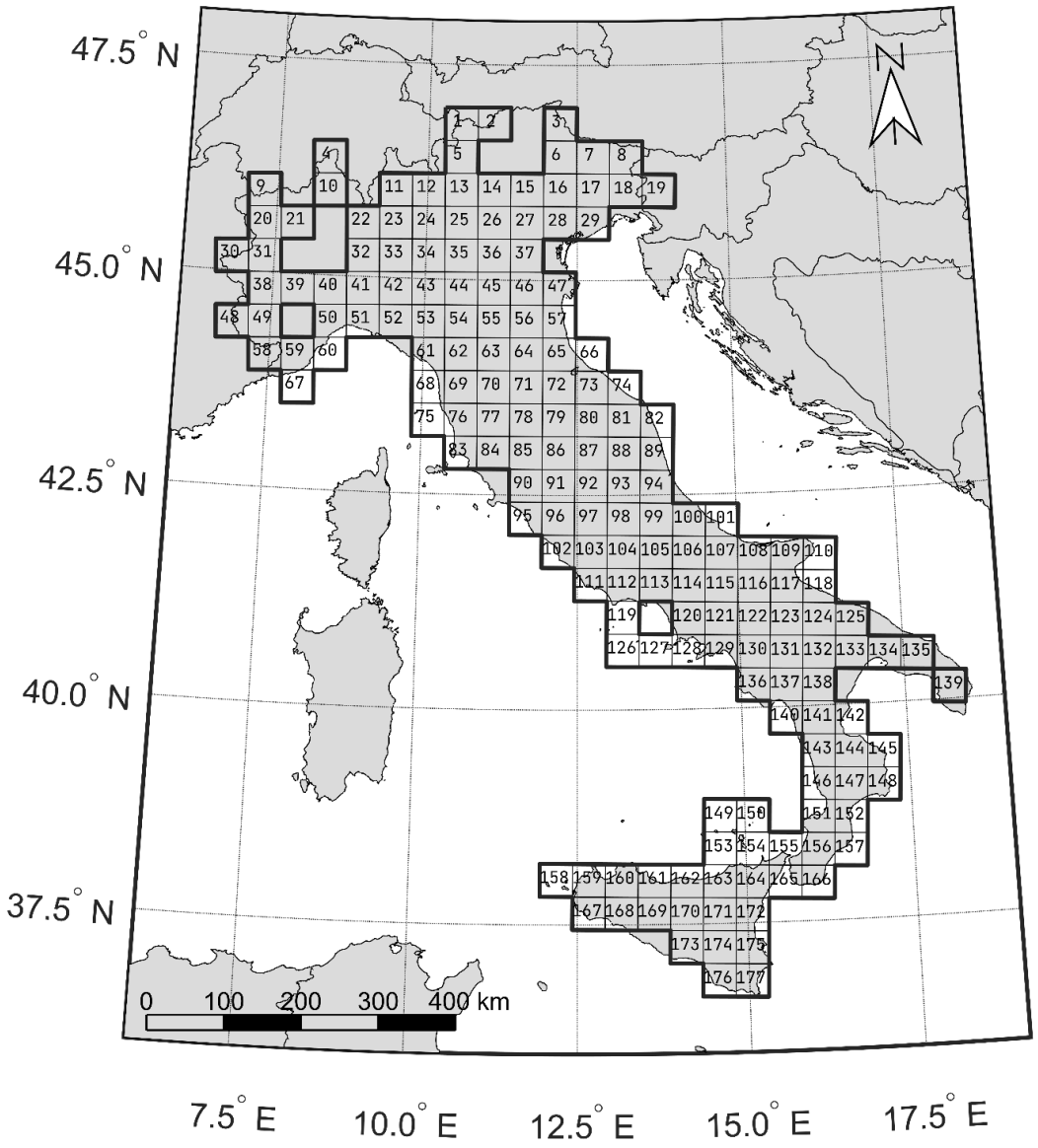

Figure 5.1: Tessellation of the Italian territory region used for the fitting of parameters and for the pseudo prospective experiment. The thick black line delimits the analysis region R. The cells that R comprises are only those within which at least one earthquake with $M \geq 4.0$ from 1600 to 2021 have occurred according to CPTI15 catalogue (Rovida, et al. 2020) and have $30\sqrt{2}$ km of side.

The experiment is then repeated several times, expanding the alarm time window from a few second to the total duration of the experiment (10 years). Similarly to what was described in Chapter 3, according to Molchan (1990, 1991), the miss rate ν, i.e. the fraction of unexpected earthquakes (eq. 3.1) and the space-time duration of the alarms τ given by the union of all alarm windows for each cell (eqs. 3.2 and 3.3) are computed. Following Shebalin et al. (2011) the fraction of the space-time τ_w occupied by the alarms is also calculated by weighting each alarm with the long-term earthquake rate of each cell (eqs. 3.5 and 3.6) as described in section 3.2. See the details of such computations for each cell in Table S1 of the supplemental material 2. Following the approach of Zechar and Jordan (2008, 2010), based on the Molchan error diagram (Molchan, 1990, 1991) the miss rate ν and the fraction of space-time occupied by alarms τ are used to represent the so-called Molchan diagram (Figs. 5.5, 5.6, 5.7). This diagram compares the prediction skills of a given forecasting method with those of a random model that simply predicts target earthquakes proportional to the fraction of space-time occupied by alarms (see section 3.4 for more details). To assess how much better (or worse) the performance of the forecasting models compared to the random model is, the Ares Skill (AS) score (eq. 3.11) is computed according to Zechar and Jordan (2008, 2010).

5.4 Optimization of alarm thresholds

To identify the optimal expected daily rate threshold for the probabilistic models, an optimization procedure has been conducted by varying the threshold value logarithmically from 10^{-6} to 0.5. For the FORE method the optimal range of potential foreshocks has been chosen by considering various increasing magnitude ranges with central values varying from 4.1 to 4.5 and ranges with respect to the central values varying from 0.1 to 0.5. Using the different thresholds, each model was thus applied to retrospectively forecast target events (27) occurred during the learning period (1990-2011). Using the AS score, the forecasting performance for the tested

threshold have been evaluated. In the previous work (see Chapter 3), the maximum AS score and the minimum number of alarms are considered as criteria for selecting the optimal threshold value. However, in this comparison experiment since the expected daily rate was estimated for all cells at each earthquake occurrence time, the alarms, in periods of high seismicity, are mostly overlapped. For this reason, the number of alarms may not be representative of the fraction of space-time occupied by the alarms. As second criterion to identify the best alarm threshold, the fraction of space-time occupied by alarms (τ_{1yr}) was used considering the alarm window extension equal to one year. In addition, as further restriction, only threshold values with τ_{1yr} lower than 20% are considered.

In Figs. 5.2, 5.3 and 5.4 are showed the variations of the AS scores of the EEPAS-NW, ETAS-SUP and FORE models as a function of the analyzed alarm thresholds, respectively. Red and dark blue lines refer to the unweighted (τ_u) and weighted (τ_w) fractions of space-time occupied by alarms respectively (see in Tables S2 and S3 in Supplementary material 2 for the numerical values of plotted curves). The bars of the histogram represent the unweighted fraction of space-time occupied by alarms (τ_{1yr}), considering one year as the alarm time (Δt). In the same figures, the black arrowheads indicate our choices of the best probability thresholds or ranges: $p = 3 \times 10^{-5}$ for EEPAS, $p = 3 \times 10^{-4}$ for ETAS and 4.5 ± 0.3 for FORE.

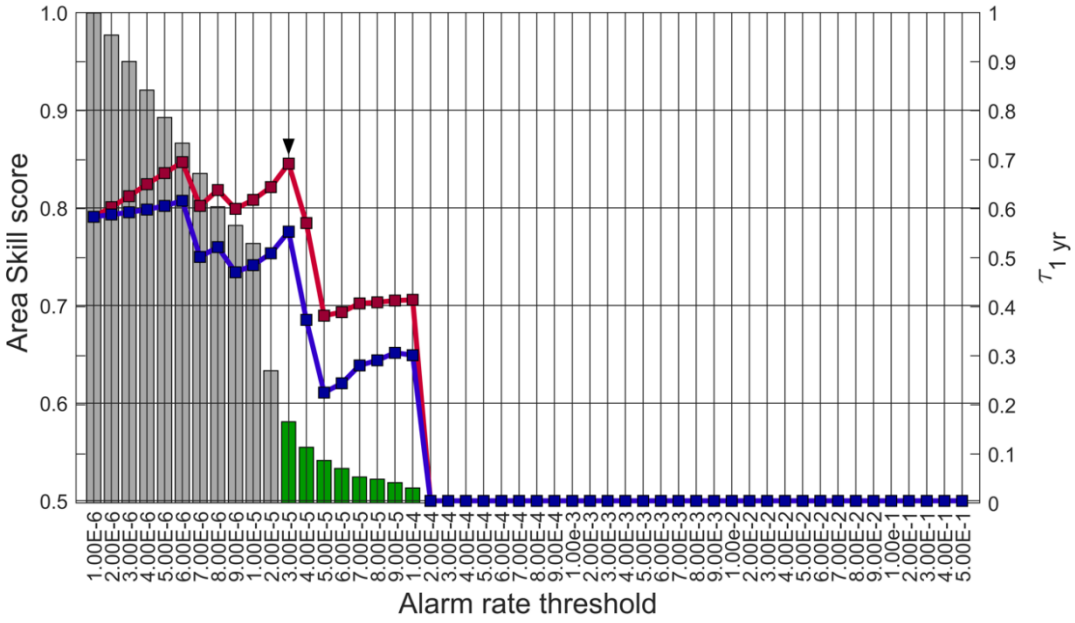

Figure 5.2: For EEPAS forecasting model, Area Skill (AS) score computed for targets with Mw≥5.0, using unweighted (red) and weighted (dark blue) fractions of space-time occupied by alarms, and fractions of space-time occupied by of alarms considering Δt=1 year (bars), as a function of the expected daily rate threshold. The chosen threshold is indicated by the black arrowhead (3×10^{-5}).

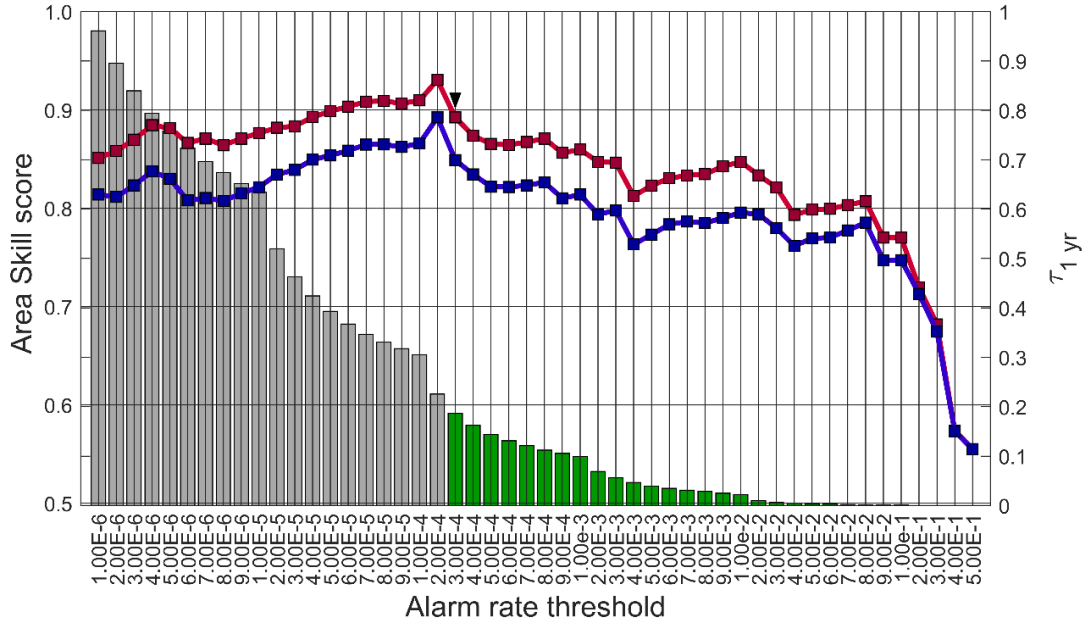

Figure 5.3: Same as Fig. 5.2 for ETAS-SVP. With the criteria adopted the chosen expected daily rate threshold indicated by the black arrow is 3×10^{-4}.

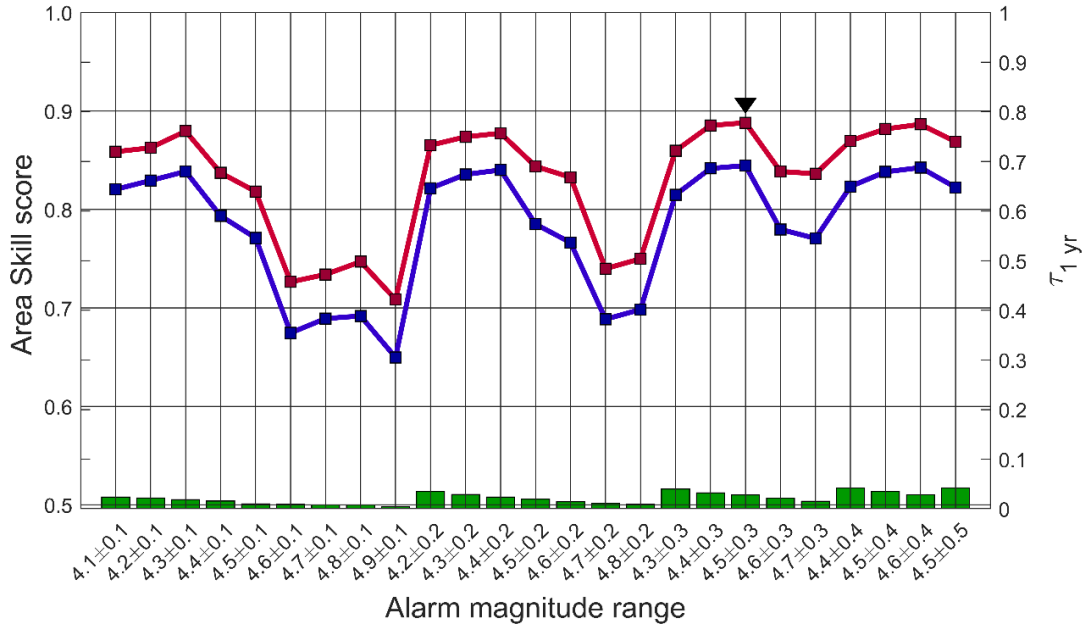

Figure 5.4: Same as Fig. 5.2 for the FORE model. The AS score and the fraction of space-time occupied by alarms are computed as a function of the foreshock magnitude range. The arrows indicate the range Mw=4.5±0.3, chosen as best compromise between high AS score and low fraction of space-time occupied by 1-year alarms (τ_{1yr}).

5.5 Results of pseudo-prospective testing

Using the thresholds optimized for the learning interval 1990-2011, the models were applied pseudo-prospectively to forecast the 27 target events with Mw≥5.0 that occurred in the test period 2012-2021. In Fig. 5.5 the Molchan trajectories obtained by the EEPAS-NW for target shocks preceded by an increase of the expected daily rate larger than the threshold 3×10^{-5} are reported, by varying Δt from a width of a few seconds to the total duration T=11 years of the test period. Red and dark blue lines refer to the unweighted (τ_u) and weighted (τ_w) fractions of space-time occupied by alarms respectively (see in Table 5.1 the numerical values of plotted curves). Both the red and dark blue lines in Fig. 5.5 lie below the diagonal line representing the Molchan trajectory of the purely random model, indicating a better forecasting performance than this latter for all explored Δt. The model fails to predict the total

number of target earthquakes even for Δt=11 years, for which only 14 over 27 (51.9%) target events are predicted with a corresponding $\tau_u \approx 21\%$ and $\tau_w \approx 48\%$. The 51.9% of forecasted target events is reached starting form Δt=0.25 days (6 hours) with a corresponding $\tau_u \approx 7.8\%$ and $\tau_w \approx 19\%$. The overall AS scores $a_f(\tau = 1)$ =0.71±0.06 and $a_f(\tau_w = 1)$ =0.63±0.06, based on the Student's t-test, are larger than the expectance of a random method (0.5).

In Fig. 5.6 the same plot as in Fig. 5.5 is showed but for the ETAS-SVP model using 3.00E-4 as daily rate threshold (see Table 5.2 for numerical values). The performance is definitely better than EEPAS-NW. In particular, the Molchan trajectory remains well below the diagonal line and for τ_u and τ_w less than 65% is also below the α=1% confidence curve (green). As for the EEPAS-NW, ETAS-SUP fails to predict the total number of target earthquakes even for Δt=11 years, for which only 23 over 27 (85.2%) target events are predicted with a corresponding $\tau_u \approx 44\%$ and $\tau_w \approx 66\%$. Such percentage of forecasted events is reached starting from Δt=2 years with the corresponding $\tau_u \approx 28\%$ and $\tau_w \approx 47\%$. The overall AS scores $a_f(\tau = 1)$ =0.88±0.06 and $a_f(\tau_w = 1)$ =0.85±0.06, are higher than those obtained by EEPAS-NW.

In Fig. 5.7 it is showed the Molchan trajectory obtained by the FORE model using $4.2 \leq Mw \leq 4.8$ as magnitude range for the foreshock events (see Table 5.3 for numerical values). The forecasting performance is better than EEPAS-NW and ETAS-SVP, respectively. In particular, the Molchan trajectory remains well below the diagonal line and for τ_u and τ_w less than 80% is also below the α=1% confidence curve (green). As for the two previous models, FORE fails to predict the total number of target earthquakes even for Δt=11 years, for which the 25 over 27 (92.3%) target events are predicted with a corresponding $\tau_u \approx 34\%$ and $\tau_w \approx 49\%$. For all Δt analysed, the FORE model is characterised by lower τ_u and τ_w than those reported by the other models (see Tables 5.1 and 5.2). The overall AS scores $a_f(\tau_u = 1)$ =0.92±0.06 and $a_f(\tau_w = 1)$ =0.90±0.06, are higher than those obtained by EEPAS-NW and ETAS-SUP.

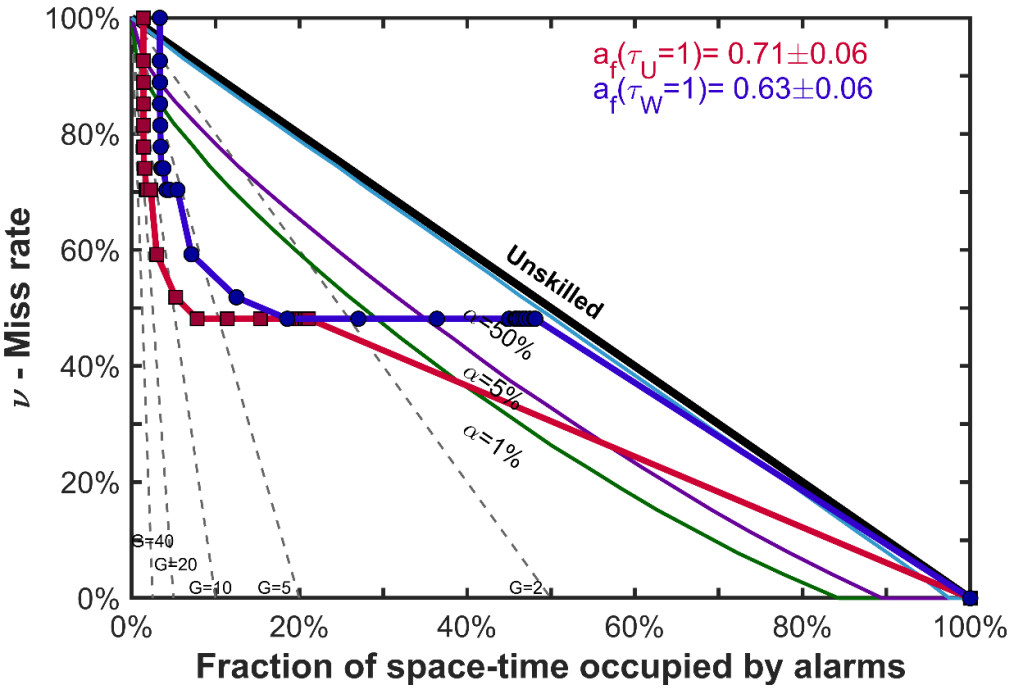

Figure 5.5: Molchan diagram and AS score of the EEPAS-NW model for target shocks with Mw≥5.0. Red and dark blue lines indicate the forecasting performance of expected daily rate threshold $3 \times 10^{-5}$for unweighted (τ_u) and weighted (τ_w) fractions of space-time occupied by alarms respectively (see text). The black continuous line indicates a purely random forecasting method that separates skilled (below the line) from unskilled (above) forecasting methods. The light blue, violet and green lines indicate the confidence limits for α =50%, 5% and 1% respectively. The black dashed lines indicate probability gains G=2, 5, 10, 20 and 50.

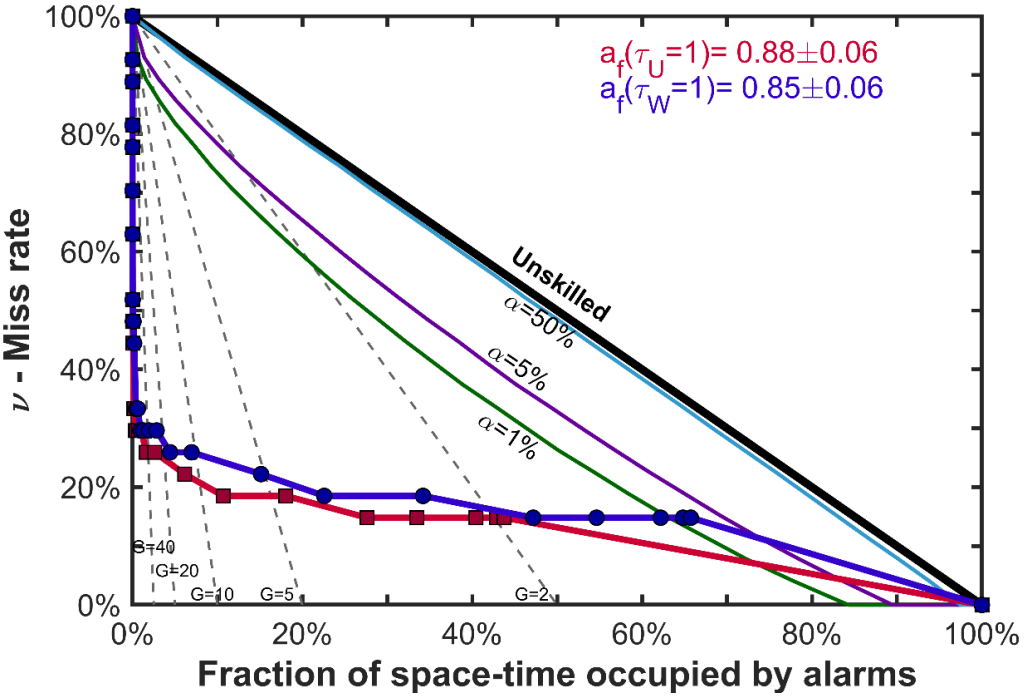

Figure 5.6: Same as Fig. 5.5 for the ETAS-SVP model.

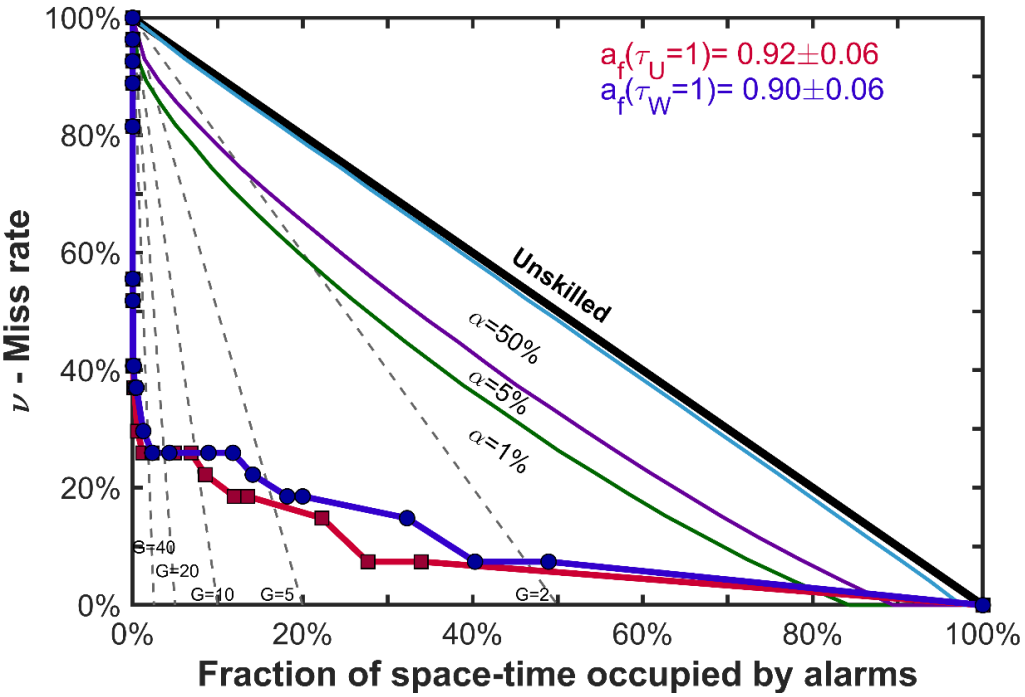

Figure 5.7: Same as Fig. 5.5 for the FORE model.

Table 5.1. Values of variables in Molchan plot of Fig. 5.5 for the EEPAS-NW model.

Δt (years)	Δt (days)	τ_u	τ_w	h	ν	$a_f(\tau_u)$	$a_f(\tau_w)$
1.6E-08	5.8E-06	1.4E-02	3.4E-02	0	1.000	0.037	0.037
3.2E-08	1.2E-05	1.4E-02	3.4E-02	2	0.926	0.074	0.074
6.3E-08	2.3E-05	1.4E-02	3.4E-02	3	0.889	0.099	0.099
1.6E-07	5.8E-05	1.4E-02	3.4E-02	3	0.889	0.105	0.105
3.2E-07	1.2E-04	1.4E-02	3.4E-02	3	0.889	0.114	0.114
4.8E-07	1.7E-04	1.4E-02	3.4E-02	4	0.852	0.140	0.140
9.5E-07	3.5E-04	1.4E-02	3.4E-02	5	0.815	0.172	0.172
1.9E-06	6.9E-04	1.4E-02	3.5E-02	6	0.778	0.205	0.205
3.8E-06	1.4E-03	1.5E-02	3.5E-02	7	0.741	0.236	0.236
9.5E-06	3.5E-03	1.6E-02	3.8E-02	7	0.741	0.255	0.255
1.9E-05	6.9E-03	1.7E-02	4.2E-02	8	0.704	0.268	0.268
2.9E-05	1.0E-02	1.9E-02	4.5E-02	8	0.704	0.281	0.281
5.7E-05	2.1E-02	2.3E-02	5.5E-02	8	0.704	0.312	0.312
1.1E-04	4.2E-02	3.0E-02	7.1E-02	11	0.593	0.390	0.390
3.4E-04	0.13	5.3E-02	1.2E-01	13	0.519	0.434	0.434
6.8E-04	0.25	7.8E-02	1.9E-01	14	0.481	0.464	0.464
1.4E-03	0.50	1.1E-01	2.7E-01	14	0.481	0.480	0.480
2.7E-03	1.00	1.5E-01	3.6E-01	14	0.481	0.488	0.488
8.2E-03	3.00	1.9E-01	4.5E-01	14	0.481	0.488	0.488
0.019	7.02	1.9E-01	4.6E-01	14	0.481	0.488	0.488
0.042	15.22	1.9E-01	4.6E-01	14	0.481	0.488	0.488
0.083	30.44	1.9E-01	4.6E-01	14	0.481	0.488	0.488
0.250	91.31	1.9E-01	4.6E-01	14	0.481	0.489	0.488
0.500	182.62	0.195	0.459	14	0.481	0.489	0.488
1.000	365.24	0.197	0.462	14	0.481	0.489	0.489
2.000	730.49	0.201	0.466	14	0.481	0.490	0.489
3.000	1095.73	0.203	0.470	14	0.481	0.490	0.489
5.000	1826.21	0.207	0.475	14	0.481	0.491	0.490
7.000	2556.70	0.210	0.480	14	0.481	0.491	0.490
10	3652.43	0.211	0.481	14	0.481	0.491	0.490
11	4017.66	0.211	0.481	14	0.481	0.491	0.490
Full occ.	Full occ.	1.000	1.000	27	0.000	0.706	0.634

Δt is the duration of alarms, τ_u and τ_w the unweighted and weighted fraction of space-time occupied by alarms respectively, h the number of successful forecasts, ν the miss rate, $a_f(\tau_u)$ and $a_f(\tau_w)$ the Area Skill scores computed considering the unweighted and weighted fraction of space-time occupied by alarms respectively. The last row (Δt= Full occ.) reports values for a full occupation of the space-time by alarms.

Table 5.2. Same of Table 5.1 for the ETAS-SVP model.

Δt (years)	Δt (days)	τ_u	τ_w	h	ν	$a_f(\tau_u)$	$a_f(\tau_w)$
1.6E-08	5.8E-06	2.5E-07	6.6E-07	0	1.000	0.000	0.000
3.2E-08	1.2E-05	5.1E-07	1.3E-06	2	0.926	0.037	0.037
6.3E-08	2.3E-05	1.0E-06	2.6E-06	3	0.889	0.074	0.074
1.6E-07	5.8E-05	2.5E-06	6.6E-06	3	0.889	0.099	0.099
3.2E-07	1.2E-04	5.1E-06	1.3E-05	3	0.889	0.105	0.105
4.8E-07	1.7E-04	7.6E-06	2.0E-05	5	0.815	0.120	0.120
9.5E-07	3.5E-04	1.5E-05	3.9E-05	6	0.778	0.162	0.162
1.9E-06	6.9E-04	2.8E-05	7.4E-05	8	0.704	0.209	0.209
3.8E-06	1.4E-03	5.2E-05	1.4E-04	10	0.630	0.266	0.266
9.5E-06	3.5E-03	1.1E-04	2.9E-04	13	0.519	0.350	0.351
1.9E-05	6.9E-03	1.9E-04	5.1E-04	14	0.481	0.413	0.415
2.9E-05	1.0E-02	2.6E-04	7.0E-04	14	0.481	0.441	0.443
5.7E-05	2.1E-02	4.3E-04	1.2E-03	14	0.481	0.473	0.474
1.1E-04	4.2E-02	7.1E-04	2.0E-03	15	0.444	0.498	0.499
3.4E-04	0.13	1.5E-03	4.1E-03	18	0.333	0.558	0.558
6.8E-04	0.25	2.3E-03	6.3E-03	18	0.333	0.595	0.596
1.4E-03	0.50	3.4E-03	9.3E-03	19	0.296	0.624	0.624
2.7E-03	1.00	4.6E-03	1.3E-02	19	0.296	0.646	0.646
8.2E-03	3.00	7.0E-03	1.9E-02	19	0.296	0.665	0.666
0.019	7.02	1.0E-02	2.8E-02	19	0.296	0.677	0.678
0.042	15.22	1.6E-02	4.4E-02	20	0.259	0.694	0.694
0.083	30.44	2.6E-02	7.0E-02	20	0.259	0.712	0.711
0.250	91.31	6.2E-02	1.5E-01	21	0.222	0.739	0.737
0.500	182.62	0.107	0.226	22	0.185	0.763	0.757
1.000	365.24	0.181	0.342	22	0.185	0.784	0.776
2.000	730.49	0.276	0.472	23	0.148	0.801	0.792
3.000	1095.73	0.335	0.546	23	0.148	0.810	0.800
5.000	1826.21	0.404	0.622	23	0.148	0.817	0.806
7.000	2556.70	0.429	0.648	23	0.148	0.819	0.808
10	3652.43	0.438	0.657	23	0.148	0.820	0.809
11	4017.66	0.438	0.657	23	0.148	0.820	0.809
Full occ.	Full occ.	1.000	1.000	27	0.000	0.880	0.849

Table 5.3. Same of Table 5.1 for the FORE model.

Δt (years)	Δt (days)	τ_u	τ_w	h	v	$a_f(\tau_u)$	$a_f(\tau_w)$
1.6E-08	5.8E-06	8.9E-10	2.2E-09	0	1.000	0.009	0.009
3.2E-08	1.2E-05	1.8E-09	4.4E-09	1	0.963	0.032	0.032
6.3E-08	2.3E-05	3.5E-09	8.7E-09	2	0.926	0.057	0.057
1.6E-07	5.8E-05	8.9E-09	2.2E-08	2	0.926	0.066	0.066
3.2E-07	1.2E-04	1.8E-08	4.4E-08	2	0.926	0.069	0.069
4.8E-07	1.7E-04	2.7E-08	6.5E-08	2	0.926	0.071	0.071
9.5E-07	3.5E-04	5.3E-08	1.3E-07	2	0.926	0.073	0.073
1.9E-06	6.9E-04	1.1E-07	2.6E-07	2	0.926	0.073	0.073
3.8E-06	1.4E-03	2.2E-07	5.2E-07	2	0.926	0.074	0.074
9.5E-06	3.5E-03	5.3E-07	1.3E-06	2	0.926	0.083	0.083
1.9E-05	6.9E-03	1.0E-06	2.5E-06	3	0.889	0.092	0.092
2.9E-05	1.0E-02	1.5E-06	3.7E-06	3	0.889	0.101	0.101
5.7E-05	2.1E-02	2.9E-06	7.0E-06	3	0.889	0.123	0.123
1.1E-04	4.2E-02	5.5E-06	1.3E-05	5	0.815	0.246	0.245
3.4E-04	0.13	1.5E-05	3.6E-05	12	0.556	0.338	0.337
6.8E-04	0.25	2.8E-05	6.7E-05	12	0.556	0.386	0.386
1.4E-03	0.50	5.2E-05	1.2E-04	12	0.556	0.421	0.420
2.7E-03	1.00	9.6E-05	2.2E-04	13	0.519	0.495	0.493
8.2E-03	3.00	2.7E-04	5.8E-04	16	0.407	0.550	0.548
0.019	7.02	6.1E-04	1.3E-03	16	0.407	0.580	0.578
0.042	15.22	1.2E-03	2.5E-03	17	0.370	0.602	0.600
0.083	30.44	2.2E-03	4.4E-03	17	0.370	0.642	0.643
0.250	91.31	5.7E-03	1.3E-02	19	0.296	0.684	0.680
0.500	182.62	0.012	0.023	20	0.259	0.711	0.708
1.000	365.24	0.023	0.043	20	0.259	0.727	0.725
2.000	730.49	0.049	0.089	20	0.259	0.731	0.729
3.000	1095.73	0.069	0.118	20	0.259	0.736	0.734
5.000	1826.21	0.086	0.141	21	0.222	0.753	0.748
7.000	2556.70	0.119	0.182	22	0.185	0.761	0.754
10	3652.43	0.135	0.200	22	0.185	0.789	0.784
11	5478.64	0.339	0.489	25	0.074	0.789	0.784
Full occ.	Full occ.	1.000	1.000	27	0.000	0.918	0.896

Following Shebalin et al. (2011), the miss rates (ν) of the analyzed models can also be compared to another skilled reference model, characterized by its space-time fractions occupied by alarms (τ_{ref}) and miss rates (ν_{ref}), instead of the purely random model.

In such comparison, the miss rates ν_{ref}'s of the reference model are plotted on the diagonal line of the Molchan diagram were $\tau = 1 - \nu_{ref}$. Even for the other compared models, the expected miss rates (ν) must be plotted versus $\tau = 1 - \nu_{ref}$, but as they are computed at different values of τ than the τ_{ref}'s of the reference model, a linear interpolation is required. Hence for each τ_{ref} of the reference ETAS-SVP model, we compute the interpolated miss-rates, for both EEPAS and FORE models, as

$$\nu_{int} = \frac{\nu_a - \nu_b}{\tau_a - \tau_b}\left(\tau_{ref} - \tau_b\right) + \nu_b \qquad (5.1)$$

Where τ_a and τ_b are the fractions occupied by alarms, of the compared models, immediately larger and smaller than τ_{ref} respectively, and ν_a and ν_b the corresponding miss rates respectively.

As for the Molchan diagrams showed above (Figs. 5.5, 5.6, and 5.7), if the miss rates of a compared model (ν_{int}) for the corresponding $\tau = 1 - \nu_{ref}$, are lower than ν_{ref}, it has a better predictive ability than the reference model. The predictive ability is compared considering both the unweighted (τ_u) and weighted (τ_w) fractions of space-time occupied by alarms (reported in Tables 5.4 and 5.5).

In Figs. 5.8 and 5.9 the Molchan (or better Molchan-Shebalin) diagrams and the AS scores for unweighted (τ_u) and weighted (τ_w) fractions of space-time occupied by alarms are reported, respectively (see Tables 5.4 and 5.5 for numerical values). Where the ETAS model is reported as the diagonal line (orange) joining the coordinate points $(1 - \nu_{ref}, \nu_{ref})$. The Molchan trajectory for the EEPAS-NW (blue) and FORE models (red) join the points $(1 - \nu_{ref},\ \nu_{int})$.The predictive power is compared considering both the unweighted (τ_u) and weighted (τ_w) fractions of space-time

occupied by alarms. For this comparison the ETAS-SVP is used as reference model using as τ_{ref} the τ values (τ_u and τ_w) reported in Table 5.2. The miss rates (ν_{int}) of EEPAS-NW and FORE models associated to the τ_{ref} are obtained by the linear interpolation of the coordinate points (τ, ν) reported in Tables 5.1 and 5.3, respectively.

In Figs. 5.8 and 5.9 the Molchan diagrams and the AS scores for unweighted (τ_u) and weighted (τ_w) fractions of space-time occupied by alarms are reported, respectively (see Tables 5.4 and 5.5 for numerical values). The ETAS-SVP model is reported as the diagonal line (orange) joining the coordinate points $(1 - \nu_{ref}, \nu_{ref})$. The Molchan trajectory for the EEPAS-NW (blue) and FORE models (red) join the coordinates points $(1 - \nu_{ref}, \nu_{int})$. In both Figs. 5.8 and 5.9 the EEPAS-NW model is characterized by a Molchan trajectory well above the reference diagonal line showing a worse predictive performance than ETAS-SVP since for the same $\tau = 1 - \nu_{ref}$, the ν_{int} of the EEPAS-NW is always greater than that of ETAS-SVP. Such worst forecasting performance is also confirmed by the AS scores $a_f(\tau_u = 1)$ and $a_f(\tau_w = 1)$, which both equal to 0.18, that is smaller than that (0.5) of the reference ETAS model. On the contrary, the FORE model is characterized by Molchan trajectories lower or close to the reference model for $\tau < 60\%$. For $\tau > 60\%$ the FORE Molchan trajectory lies for short stretches slightly above the diagonal line. However, overall, the predictive performance is (slightly) better than the reference model because the AS scores for the unweighted and weighted trajectories, $a_f(\tau_u = 1) = 0.54$ and $a_f(\tau_w = 1) = 0.55$ respectively, confirm such better forecasting skills.

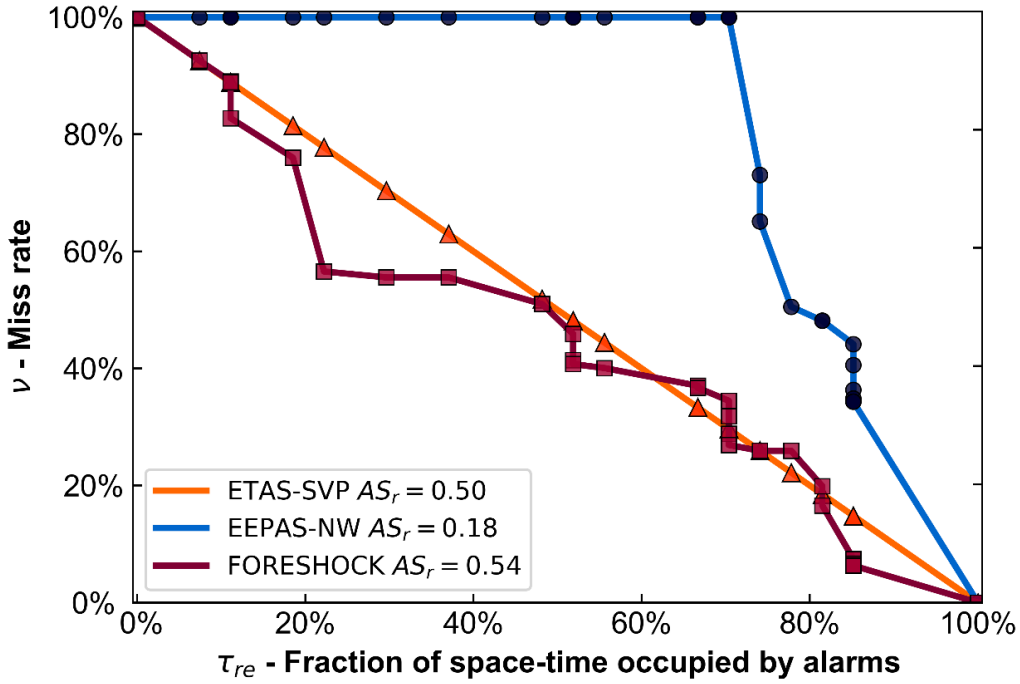

Figure 5.8: Molchan diagram and AS score of the EEPAS-NW and FORE models considering the ETAS-SVP model as reference and unweighted fraction of space-time occupied by alarms (τ_u). The Molchan trajectory of EEPAS-NW and FORE models are indicated by the blue and red curves, respectively. The diagonal continuous line (orange) indicates the miss rates of the ETAS-SVP model and separates models with higher performance (below the line) from worst (above) forecasting methods compared to the reference.

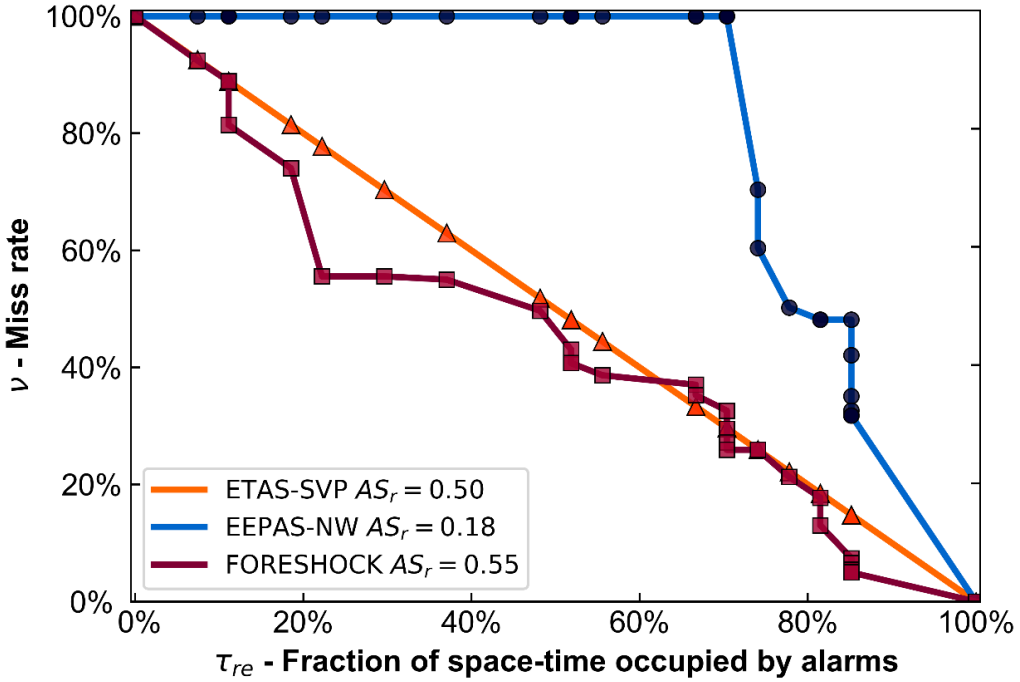

Figure 5.9: Same as Fig. 5.8 for weighted fraction of space-time occupied by alarms (τ_w).

Table 5.4. Values of variables in Molchan plot of Fig. 5.8 for unweighted fractions of space-time occupied by alarms (τ_u).

τ_{re}	ν_{ref}	$a_f(\tau_{re})$	$\nu_{int_{EEPAS}}$	$a_{EEPAS}(\tau_{re})$	$\nu_{int_{FORE}}$	$a_{FORE}(\tau_{re})$
0.000	1.000	0.000	1.000	0.000	1.000	0.000
0.074	0.926	0.037	1.000	0.000	0.926	0.037
0.111	0.889	0.056	1.000	0.000	0.890	0.055
0.111	0.889	0.056	1.000	0.000	0.889	0.055
0.111	0.889	0.056	1.000	0.000	0.828	0.055
0.185	0.815	0.093	1.000	0.000	0.760	0.116
0.222	0.778	0.111	1.000	0.000	0.566	0.153
0.296	0.704	0.148	1.000	0.000	0.556	0.224
0.370	0.630	0.185	1.000	0.000	0.556	0.268
0.481	0.519	0.241	1.000	0.000	0.510	0.314
0.519	0.481	0.259	1.000	0.000	0.459	0.329
0.519	0.481	0.259	1.000	0.000	0.414	0.329
0.519	0.481	0.259	1.000	0.000	0.407	0.329
0.556	0.444	0.278	1.000	0.000	0.401	0.346
0.667	0.333	0.333	1.000	0.000	0.370	0.391
0.667	0.333	0.333	1.000	0.000	0.367	0.391
0.704	0.296	0.352	1.000	0.000	0.345	0.404
0.704	0.296	0.352	1.000	0.000	0.318	0.404
0.704	0.296	0.352	1.000	0.000	0.288	0.404
0.704	0.296	0.352	1.000	0.000	0.269	0.404
0.741	0.259	0.370	0.731	0.007	0.259	0.421
0.741	0.259	0.370	0.651	0.007	0.259	0.421
0.778	0.222	0.389	0.506	0.026	0.259	0.436
0.815	0.185	0.407	0.481	0.048	0.199	0.451
0.815	0.185	0.407	0.481	0.048	0.166	0.451
0.852	0.148	0.426	0.442	0.070	0.075	0.470
0.852	0.148	0.426	0.406	0.070	0.074	0.470
0.852	0.148	0.426	0.363	0.070	0.067	0.470
0.852	0.148	0.426	0.349	0.070	0.064	0.470
0.852	0.148	0.426	0.343	0.070	0.063	0.470
0.852	0.148	0.426	0.343	0.070	0.063	0.470
0.852	0.148	0.426	0.343	0.070	0.063	0.470
0.852	0.148	0.426	0.343	0.070	0.063	0.470
1.000	0.000	0.500	0.000	0.182	0.000	0.544

$\boldsymbol{\nu_{ref}}$ is the miss rate of the ETAS-SVP model (reference), τ_{re} the fractions of space time occupied by alarms used to plot the Molchan diagram and given by $1-\nu_{ref}$, ν_{ref} the reference miss rate, ν_{ref} the interpolated miss rate, $a_f(\tau_{re})$, $a_{EEPAS}(\tau_{re})$ and $a_{FORE}(\tau_{re})$ the Area Skill scores computed for the reference, EEPAS and FORE models, respectively.

Table 5.5. Values of variables in Molchan plot of Fig. 5.9 for weighted fractions of space-time occupied by alarms (τ_w).

τ_{re}	ν_{ref}	$a_f(\tau_{re})$	$\nu_{int_{EEPAS}}$	$a_{EEPAS}(\tau_{re})$	$\nu_{int_{FORE}}$	$a_{FORE}(\tau_{re})$
0.000	1.000	0.000	1.000	0.000	1.000	0.000
0.074	0.926	0.037	1.000	0.000	0.924	0.038
0.111	0.889	0.056	1.000	0.000	0.889	0.056
0.111	0.889	0.056	1.000	0.000	0.889	0.056
0.111	0.889	0.056	1.000	0.000	0.814	0.056
0.185	0.815	0.093	1.000	0.000	0.740	0.123
0.222	0.778	0.111	1.000	0.000	0.556	0.161
0.296	0.704	0.148	1.000	0.000	0.556	0.232
0.370	0.630	0.185	1.000	0.000	0.550	0.275
0.481	0.519	0.241	1.000	0.000	0.497	0.321
0.519	0.481	0.259	1.000	0.000	0.430	0.337
0.519	0.481	0.259	1.000	0.000	0.407	0.337
0.519	0.481	0.259	1.000	0.000	0.407	0.337
0.556	0.444	0.278	1.000	0.000	0.387	0.355
0.667	0.333	0.333	1.000	0.000	0.370	0.399
0.667	0.333	0.333	1.000	0.000	0.353	0.399
0.704	0.296	0.352	1.000	0.000	0.326	0.413
0.704	0.296	0.352	1.000	0.000	0.295	0.413
0.704	0.296	0.352	1.000	0.000	0.272	0.413
0.704	0.296	0.352	1.000	0.000	0.259	0.413
0.741	0.259	0.370	0.704	0.007	0.259	0.429
0.741	0.259	0.370	0.604	0.007	0.259	0.429
0.778	0.222	0.389	0.502	0.028	0.213	0.445
0.815	0.185	0.407	0.481	0.050	0.177	0.461
0.815	0.185	0.407	0.481	0.050	0.130	0.461
0.852	0.148	0.426	0.481	0.071	0.074	0.480
0.852	0.148	0.426	0.421	0.071	0.066	0.480
0.852	0.148	0.426	0.351	0.071	0.055	0.480
0.852	0.148	0.426	0.327	0.071	0.051	0.480
0.852	0.148	0.426	0.318	0.071	0.050	0.480
0.852	0.148	0.426	0.318	0.071	0.050	0.480
0.852	0.148	0.426	0.318	0.071	0.050	0.480
0.852	0.148	0.426	0.318	0.071	0.050	0.480
1.000	0.000	0.500	0.000	0.185	0.000	0.554

5.6 Conclusion of chapter 5

In this chapter, the deterministic forecasting method based on the occurrence of strong foreshocks described in Chapter 3 (called FORE) was compared with the probabilistic EPAS-NW and ETAS-SVP models described in Chapter 4 using the deterministic alarm-based approach. The forecasting models were applied to retrospectively forecast shallow earthquakes (depth<40 km) of magnitude $M \geq 5.0$ occurred in Italy from 2012 to 2022. All models were calibrated through a learning dataset from 1990 to 2011 using earthquakes reported in the HORUS seismic catalogue (Lolli et al., 2020). Based on the learning dataset, various expected daily rate thresholds for the EEPAS-NW and ETAS-SVP models and various magnitude ranges of foreshocks for the FORE model were considered to identify the optimal alarm threshold required to implement the deterministic approach. For each threshold analyzed the miss rates and the fractions of space-time occupied by the alarms were estimated by varying the temporal extension of the alarm window Δt from a fraction of a second to the total duration of the learning dataset (10 years). Following the method described in section 3.2, such fractions were also estimated by considering the different levels of seismic activity in the various areas of Italy, by weighting more the alarm times in cells where the average seismicity rate, calculated from the CPTI15 seismic catalogue (Rovida et al., 2016, 2020) from 1600 to 1990, is higher. The choice of the optimal alarm thresholds was made by considering both the Area Skill Score (Zechar and Jordan, 2008) and the fraction of space-time occupied by the alarms. Such thresholds were then used for pseudo-prospective tests and comparisons to assess the forecasting performance in the period 2012-2021.

Retrospective tests conducted using the Molchan diagram (Molchan, 1990, 1991, Molchan & Kagan, 1992) and the Area Skill score indicate that all the three models overperform a purely random method. In addition, following the approach suggested by Shebalin et al. (2011), the forecasting performances of the models were compared taking the ETAS-SVP as reference model. These tests show that for the

same fractions of space-time occupied by the alarms, the EEPAS-NW model presents a worse forecasting performance compared to the ETAS-SVP model. In contrast, the FORE model presented a slightly better forecast performance. However, a more careful analysis should be done prospectively, maybe using new method developed within the CSEP.

Overall, this study highlights the potential of deterministic forecasting approaches in improving earthquake forecasting in Italy. Our findings contribute to ongoing efforts to develop more accurate and reliable earthquake forecasting methods, which can ultimately help mitigate the impact of seismic events on communities and infrastructure.

Chapter 6

Overall conclusions

6.1 Discussion and main results

Deterministic earthquake prediction, understood as the definition in advance within narrow limits of the location, time and magnitude, of an impending earthquake has proven to be a complex problem for scientists and progress in this area has been much slower than in other natural phenomena. Although the search for "silver bullets", i.e. precursor signals capable of giving information about the occurrence of an imminent strong earthquake, conducted during the last two decades of the 20th century and supervised by the IASPEI commission was unsuccessful, it made a great contribution to the understanding of seismic phenomena (Jordan et al., 2011). Such research has identified some candidate signals that may be more useful than others in earthquake prediction, such as changes in strain rate, seismic wave velocity, crustal electrical conductivity, anomalous concentrations of Radon or other geochemical gases in groundwater, increased clustering of seismicity near the future epicenters of a stronger earthquakes, and other seismicity-based precursors (Wyss, 1991). However, although the analysis of precursor signals has not led to significant results from a forecasting perspective, it is nevertheless important that these phenomena continue to be analyzed and studied (Wyss, 2001). This is motivated by the fact that, compared to previous decades, analysis techniques and earthquake datasets have improved significantly (Jordan, 2006). The failure in the search for the silver bullet has also led to a changing approach. Currently, seismologists prefer to speak about "Earthquake forecasting" instead of "Earthquake prediction". This difference is not only linguistic but requires a probabilistic rather than deterministic approach. Currently, the probability of occurrence of earthquakes in a given area over time is estimated using empirical models generally based on seismicity.

However, improving earthquake forecasting remains one of the greatest goals for seismology and a key objective for the future. Reliable forecasting plays a fundamental role in protecting the lives of people and mitigating the economic and material damage caused by a strong earthquake.

This thesis presented the development, analysis, evaluation and comparison of the retrospective forecasting performance of models applied to the prediction of Italian earthquakes using both alarm-based deterministic and probabilistic approaches. Regarding the deterministic approach, the capabilities of a simple algorithm (FORE) based on the occurrence of strong (fore)shocks of magnitude $4.4 \leq M_w \leq 4.8$, described in Chapter 3, were examined. This method was applied for the retrospective forecast of shallow earthquakes with magnitude Mw≥5.0,5.5,6.0 occurred in the period 1960-2020 within an analysis grid consisting of partially overlapping circles of radius 30 km. According to this model, an alarm of duration Δt is issued within a circle, every time an earthquake of magnitude within the range of potential foreshocks occurs. The method was applied to retrospectively forecast earthquakes occurred between 1960 and 2020 reported in the HORUS catalogue. In particular, the forecasting performance of the method was evaluated on the entire set of target earthquakes (non declustered), and on a subset of them in which only the first shocks of the earthquake sequences (declustered) are considered. Following Shebalin et al. (2011), we also computed the performance of the model by weighting each circle with the long-term earthquake rate in order to penalize the model where medium to strong earthquakes are more likely to occur making easier to predict target earthquakes with this forecasting method. The results of the retrospective evaluation tests provided significant results, showing a clear superiority to a hypothetical purely random prediction model. In particular, the Molchan diagrams (Molchan 1990,1991) and the related area skill diagrams (Zechar and Jordan, 2008) score showed that the highest performance was obtained for target earthquakes of Mw≥5.5. In fact, they show that using an optimized alarm Δt of 3 months (0.25 years)

26 of the 35 (74.3%) not declustered target earthquakes that occurred in the region of analysis were predicted with an unweighted $\tau_u = 0.9\%$ and weighted $\tau_w = 1.9\%$ fraction of space-time occupied by alarms.

Such excellent forecasting performance is also confirmed for declustered target earthquakes with Mw≥5.5 where retrospective application of the model revealed that 6 of the 14 target earthquakes (42.9%) that occurred in the test period were forecast with the same spatiotemporal coverage of alarms of the not declustered analysis ($\tau_u = 0.9\%$ and $\tau_w = 1.9\%$).

Regarding probabilistic models, the focus of this thesis has been the application and comparison of the EEPAS (Every Earthquake a Precursor According to Scale) forecasting model with other models used in the literature in the context of earthquake forecastability (Chapter 4). The EEPAS model is a space-time point process model based on the scale increase of the precursor phenomenon (Ψ). This phenomenon was observed and analyzed by Evison and Rhoades (2004) for various regions of the world and consists of an increase in the rate and magnitude of minor seismicity before a strong earthquake. The EEPAS model developed by Rhoades and Evison (2004), described in Chapter 4, considers each i-th earthquake to contribute to the variation in expected future rate density according to its magnitude, time of occurrence and geographical location. However, as the model is designed, the expected future rate density should only be defined by the long-term clustering of earthquakes. To prevent the model from being affected by short-term clustering, according to Rhoades and Evison (2004), the weighting factor was also used to reduce the contribution of aftershocks to the definition of the expected rate density. The EEPAS-NW and EEPAS-W nomenclature was adopted to distinguish the two different formulations with unweighted (NW) and weighted (W) seismicity, respectively. Although the EEPAS model has been applied in many seismic regions, such as New Zealand, California and Japan (Rhoades and Evison, 2004; Evison and Rhoades, 2005; Rhoades, 2007, 2011; Rhoades et al., 2020), no application has ever

been made on Italian seismicity. In this thesis, the EEPAS model was therefore applied to Italy and its retrospective forecasting performance was compared with those obtained by other time-independent and time-dependent models using the new CSEP consistency methods based on the negative binomial distribution (cL-test, N-test and S-test) the IGPA (Information Gain per Active cell/bin) statistic as described in Bayona et al. (2022). In particular, the EEPAS model was compared with the time independent SUP (Space Uniform Poisson), SVP (Space Variable Poisson) and the time dependent PPE (Proximity to Past Earthquakes) and ETAS (Epidemic Type Aftershock Sequence) models. For the latter, two variants were implemented with SUP and SVP as background models, respectively. $m_T = 5.0$ was chosen as the lower magnitude limit of the target earthquakes, also in agreement with previous work on EEPAS.

Using the HORUS seismic catalogue, the analyzed probabilistic models were calibrated using the period 1990-2012 as the learning dataset. A grid consisting of 177 cells of side $L = 30\sqrt{2}$ km was considered as the application region. Using the fitted parameters on the seismicity of the learning period, the models were applied to retrospectively forecast 27 target earthquakes ("mainshocks+aftershocks") that occurred in the period 2012-2022, reported in the HORUS seismic catalogue, using different forecast windows from 3 months to 10 years. Since forecasting of target earthquakes occurring after the first shock of a sequence may sometimes be easier, the forecasting performance of only the first shocks of sequences ("mainshocks") was also examined. For the test period, all analyzed models, in particular ETAS-SUP and ETAS-SVP underestimated the number of target earthquakes for both target datasets of mainshocks+aftershocks and mainshocks only. This probably was due to the different rate of target earthquakes that characterized this learning and the test periods. The consistency of the spatial distribution, the spatial-magnitude distribution and the number of expected earthquakes with those observed were examined using the new CSEP S-test, cL-test and N-test, respectively, as described in

Bayona et al., 2022. These tests, based on the negative binomial distribution, are characterized by lower sensitivity than the traditional CSEP tests. Although the number of earthquakes forecasted by each model is lower than the number of earthquakes observed, all CSEP consistency tests gave positive results, showing adequate consistency between forecasted and observed earthquakes for both the "mainshocks + aftershocks" and the "mainshocks only" target datasets. However, these results may depend on a too low cell resolution, as usually such consistency tests are conducted considering a grid of cells having sides 0.1°x0.1°. Relative forecasting skills were examined used the IGPA statistic (Information Gain for Active bin, Bayona et al., 2022) which is based on the difference in likelihood of a model from that of a reference model. The SUP model was considered as the reference model. IGPA results for both mainshocks+aftershocks and mainshocks target earthquakes showed that for forecast intervals shorter than 3 months, the best performing models are ETAS-SVP and ETAS-SUP. For longer forecast intervals, the best performing models are EEPAS-NW and EEPAS-W, respectively. Such superior performance, however, is found to be significant only for forecast intervals greater than 5 years.

The EEPAS-NW and ETAS-SVP probabilistic models, which showed slightly better retrospective forecasting performance, were compared with the FORE model using the deterministic alarm-based approach as described in chapter 3. For this purpose, the FORE model was applied on the same analysis region of ETAS and EEPAS using the same dataset. To implement the alarm-based analysis, an optimization procedure was conducted to identify the optimal alarm threshold consisting of a certain expected daily rate value for the ETAS and EEPAS models and a range of potential foreshocks for the FORE model, respectively.

The optimization procedure was conducted using the learning dataset 1990-2012. The Area Skill score and the fraction of space-time occupied by alarms considering the duration of an alarm window equal to one year were considered as criteria for

choosing the optimal alarm threshold. Using the chosen thresholds, the models were applied and to the evaluation of retrospective forecasts of earthquakes that occurred in the 2012-2022 test dataset using the Molchan diagram and Area Skill score. The retrospective evaluation methods showed that all three models considered overperform a purely random forecast model, in particular the ETAS-SVP and FORE models. Using the approach suggested by Shebalin et al. (2011), the relative performance of the models was also evaluated using the ETAS-SVP model as a reference model. The latter test showed that for the same fractions of space-time occupied by alarms, using the alarm-based approach, ETAS-SVP and FORE models presented better forecasting performance than EEPAS-NW.

For a real performance evaluation and comparison of the forecast performance of the EEPAS, ETAS, and FORE models, however, it would be appropriate to conduct prospective forecast tests possibly within CSEP.

6.2 A new EEPAS software

The implementation of all the models examined in this thesis was done by developing original software and codes. In particular, for the EEPAS model, this implementation represents an important step in terms of replicability and applicability of the model. In fact, the model's authors developed proprietary, license-protected software that permits the application of the model under predefined conditions and, under certain aspects, limiting the model's reproducibility. In fact, such software (EEPSOF), is available only for the Fortran language in the form of an executable file for Linux operating systems. During the doctoral activities, a careful analysis of the EEPAS model was conducted to understand, reproduce and apply the model. Through numerous attempts to reproduce the several published works (Rhoades and Evison, 2004; Evison and Rhoades, 2005; Rhoades, 2007, 2011) concerning EEPAS, it was possible to develop a

new, more flexible code in MATLAB. Before reaching an adequate consistency between the two codes, many experiments were conducted by submitting the same input datasets to both software and examining the outputs. Although the two codes operate differently, particularly in terms of the treatment of distances and the method by which the integral of the expected rate density is calculated over space, they showed fairly consistent results in estimating optimal model parameters and in earthquake forecasting. To extend the possibility of understanding and applying the method the new code will be developed later in Python.

6.3 Future perspectives and final remarks

The analysis conducted for the FORE model and the results obtained highlight how the deterministic approach can also make an active and potentially significant contribution to improving earthquake forecasting capability. Although the analysis of precursor phenomena has not yielded great results in previous decades, it cannot be abandoned. In fact, the progress of technology provides now improved analysis tools and better data sets that could reveal new information for studying earthquakes and improving their predictability. Although an increase in the research of deterministic methods has been observed in recent years, there are still no standard prospective testing methodologies available in the CSEP field.

To improve the ability to forecast earthquakes, it is important that the models developed are reproducible. In this regard, for the analyses in this thesis, the EEPAS model was applied independently by its developers for retrospective forecast of Italian earthquakes. For this purpose, new software has been developed in MATLAB, although, to increase usability it will later be implemented in Python as well. Although the characteristics of the model found by the analyses conducted using the new software are consistent with what has been observed in previous applications, this model should nevertheless be studied further and analyzed prospectively using CSEP testing methods. Comparison of deterministic models based on precursor signals with probabilistic models such as ETAS or EEPAS using objective standard

procedures could provide interesting results in terms of performance and potential applicability for earthquake risk mitigation. Therefore, the possibility of being able to include to the CSEP prospective tests also evaluation tests for deterministic models that possibly allow comparison with probabilistic models should be explored.

Supplementary material 1

Retrospective short-term forecasting experiment in Italy based on the occurrence of strong (fore) shocks

P. Gasperini[1,2], E. Biondini[1], B. Lolli[2], A. Petruccelli[1,3], G. Vannucci[2]

[1]Dipartimento di Fisica e Astronomia, Università di Bologna, Italy

[2]Istituto Nazionale di Geofisica e Vulcanologia, Sezione di Bologna, Italy

[3] Swiss Seismological Service, ETH Zurich, Switzerland

From: Gasperini, P., E. Biondini, B. Lolli, A. Petruccelli, and G. Vannucci, 2021, Retrospective short-term forecasting experiment in Italy based on the occurrence of strong (fore) shocks, Geophys. J. Int., 225, no. 2, 1192–1206, doi: 10.1093/gji/ggaa592.

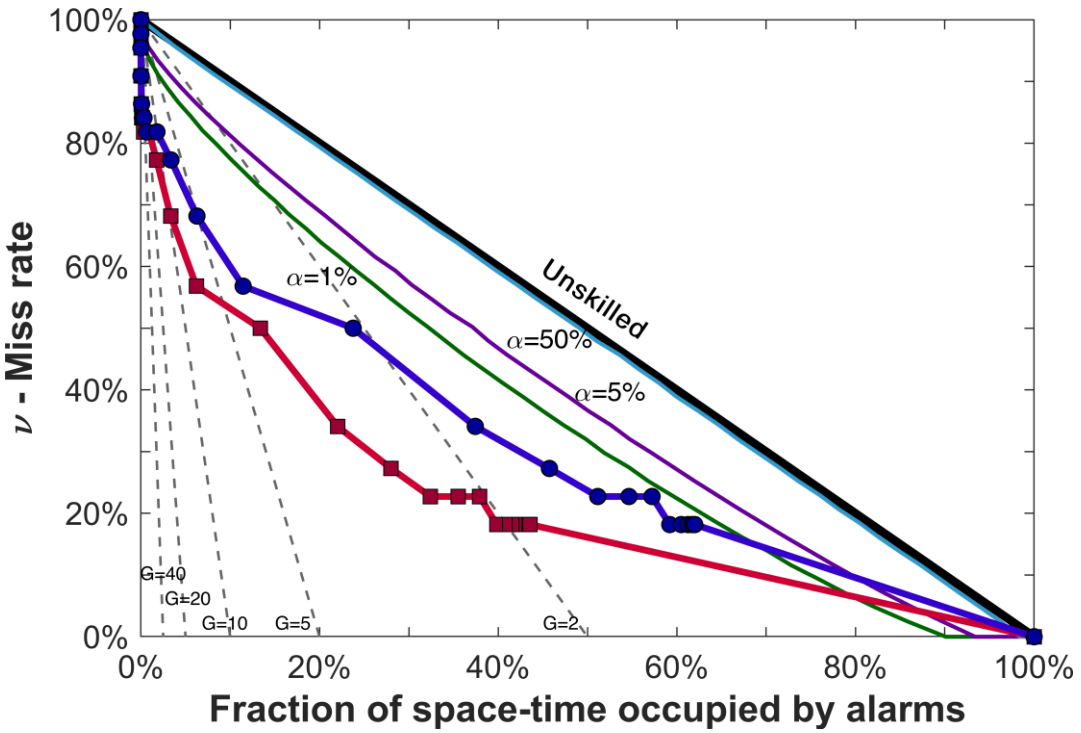

Figure S1: Molchan diagram declustered (first) target shocks with Mw≥5.0. Red and dark blue lines indicate the forecasting performance of foreshocks with 4.4≤Mw<4.8 for unweighted (τ_u) and weighted (τ_w) fractions of space-time occupied by alarms respectively (see main text). The black continuous line indicates the performance of a purely random forecasting method that separates skilled (below the line) from unskilled (above) forecasting methods. The light blue, violet and green lines indicate the confidence limits for α =50%, 5% and 1% respectively. The black dashed lines indicate probability gains G=2, 5, 10, 20 and 50.

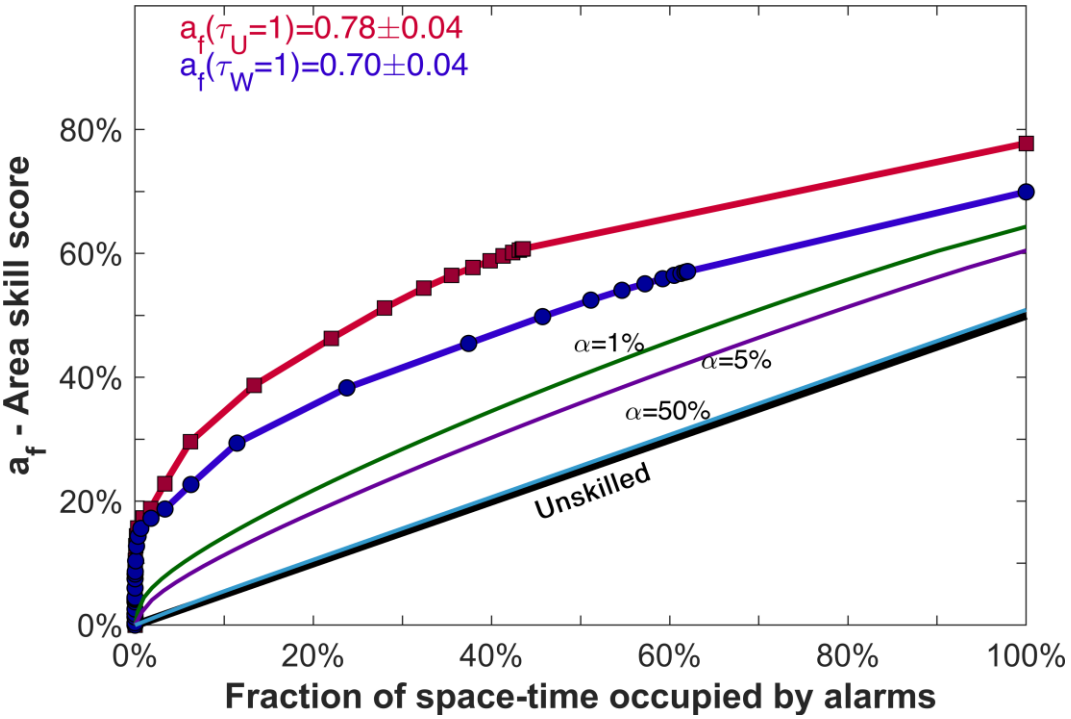

Figure S2: Area skill score diagram declustered (first) shocks with Mw≥5.0. Red and dark blue lines indicate the forecasting performance of foreshocks with 4.4≤Mw<4.8 for unweighted (τ_u) and weighted (τ_w) fractions of space-time occupied by alarms respectively (see main text). The black continuous line indicates the performance of a purely random forecasting method that separates skilled (below the line) from unskilled (above) forecasting methods. The light blue, violet and green lines indicate the confidence limits for α =50%, 5% and 1% respectively.

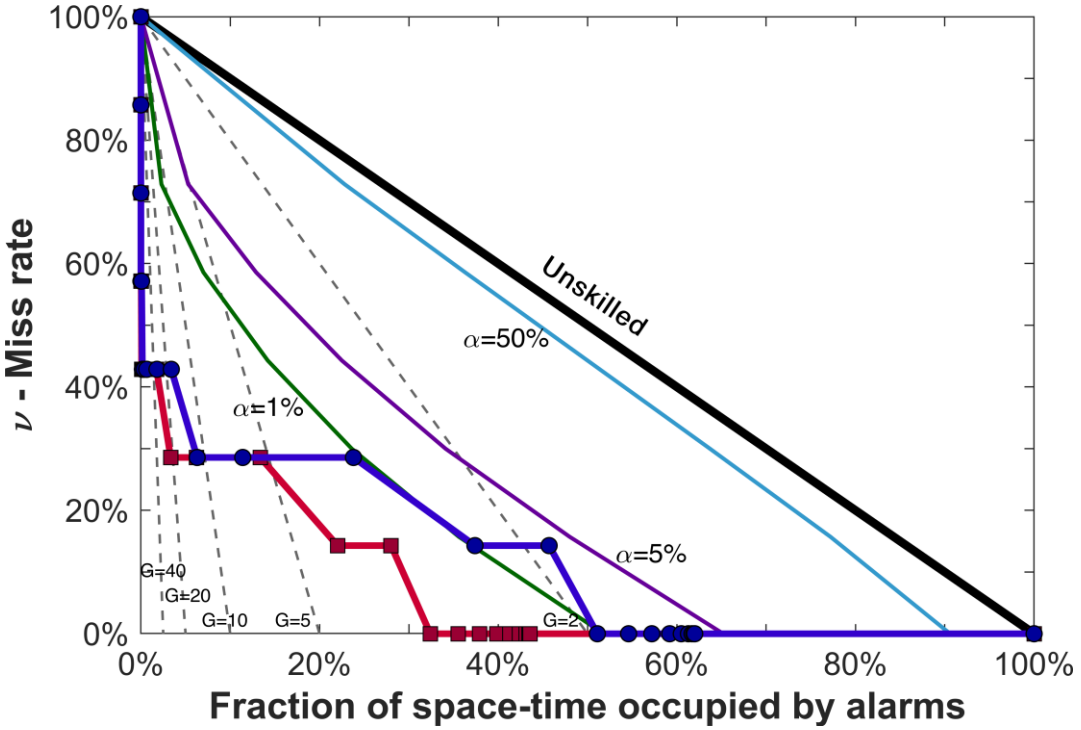

Figure S3: Same as Fig. S1 for declustered (first) target shocks with Mw≥6.0.

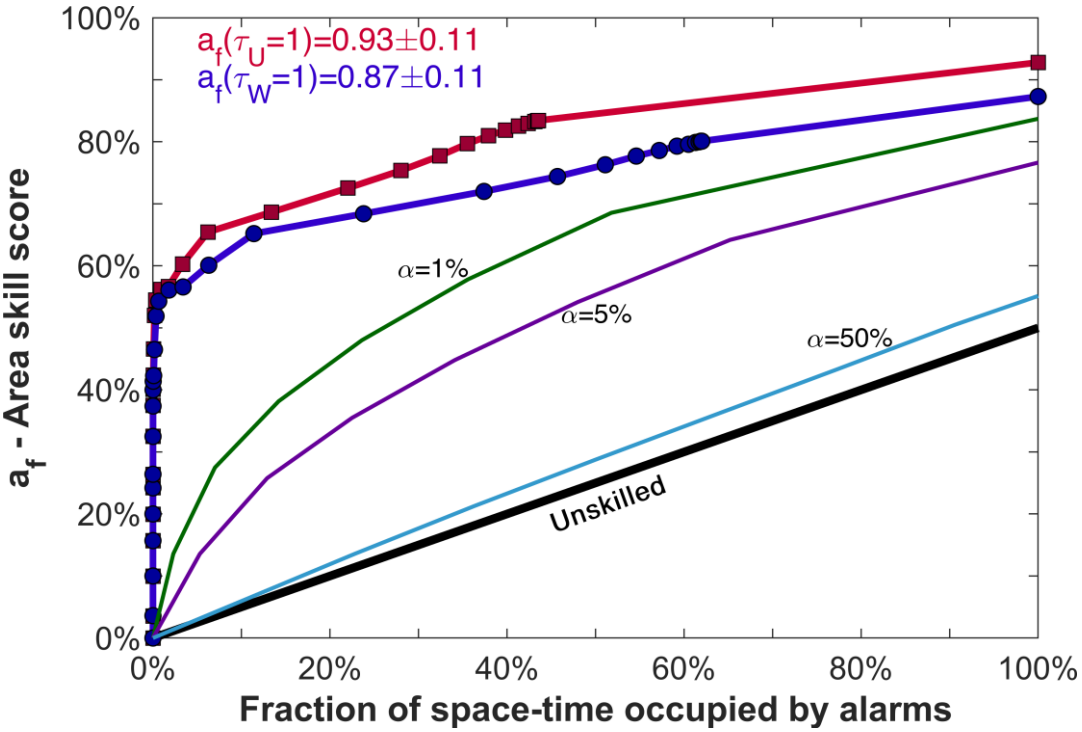

Figure S4: Same as Fig. S2 for declustered (first) target shocks with Mw≥6.0.

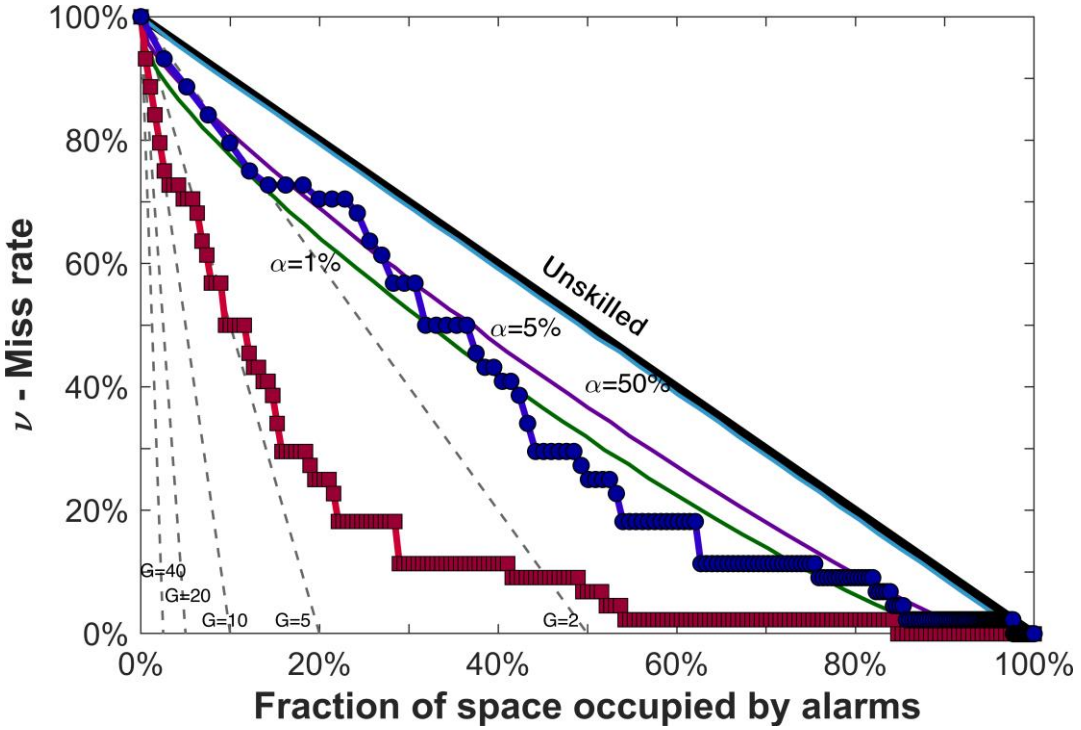

Figure S5: Same as Fig. S1 for time-independent analysis of declustered (first) target shocks with Mw≥5.0.

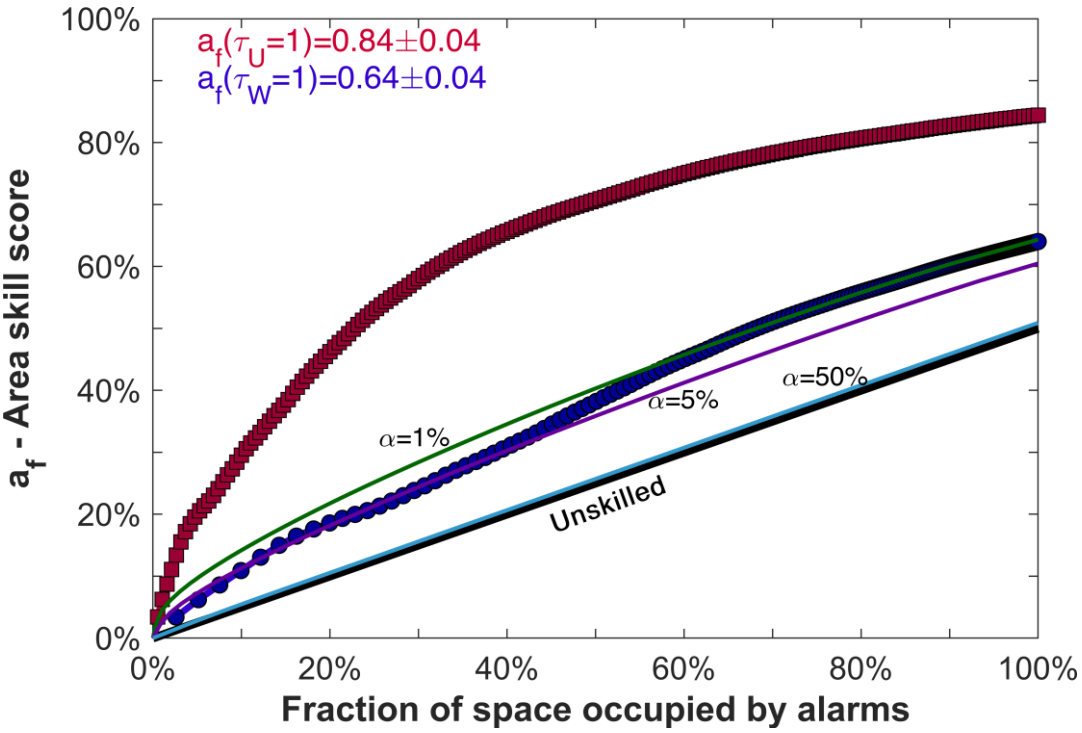

Figure S6: Same as Fig. S2 for time-independent analysis of declustered (first) target shocks with Mw≥5.0.

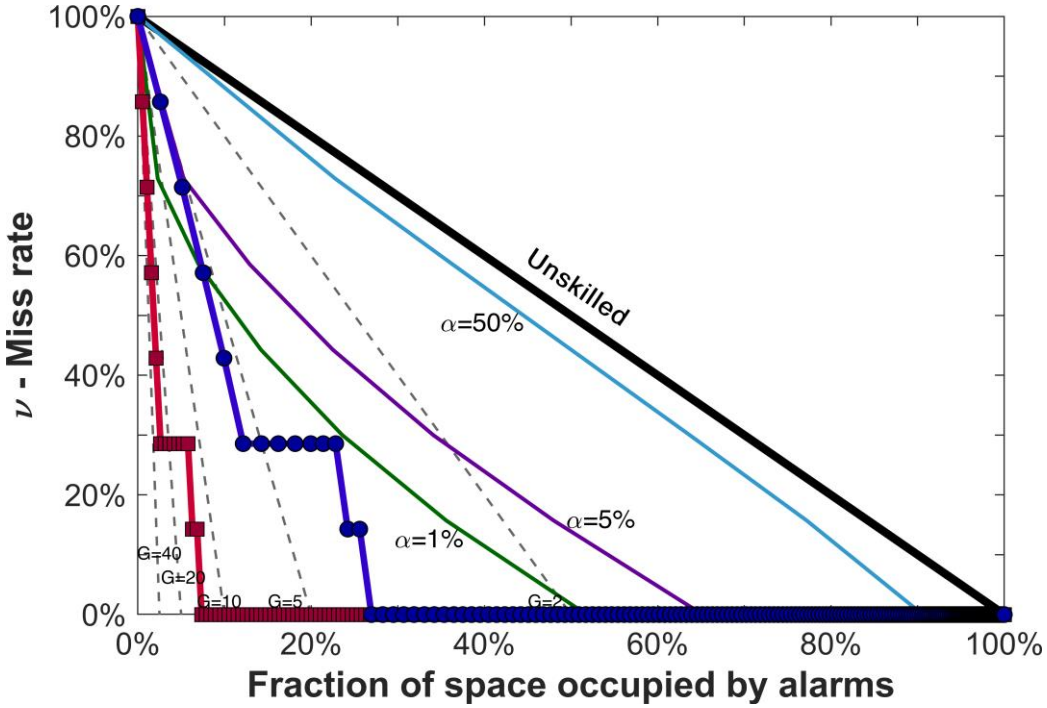

Figure S7: Same as Fig. S1 for time-independent analysis of declustered (first) target shocks with Mw≥6.0.

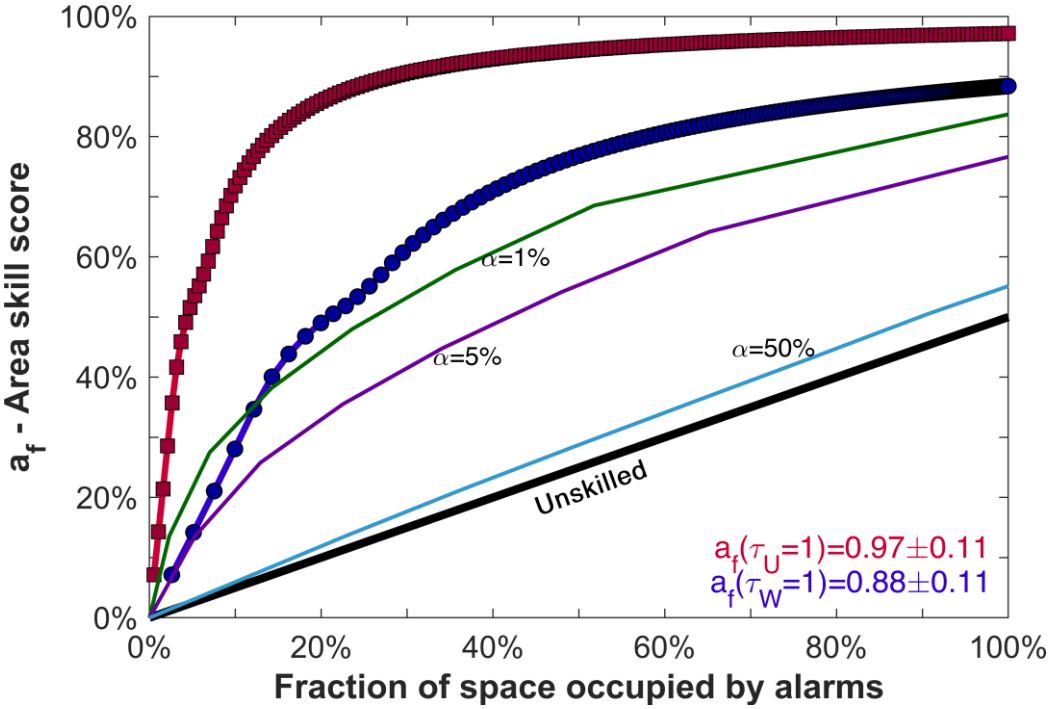

Figure S8: Same as Fig. S2 for time-independent analysis of declustered (first) target shocks with Mw≥6.0.

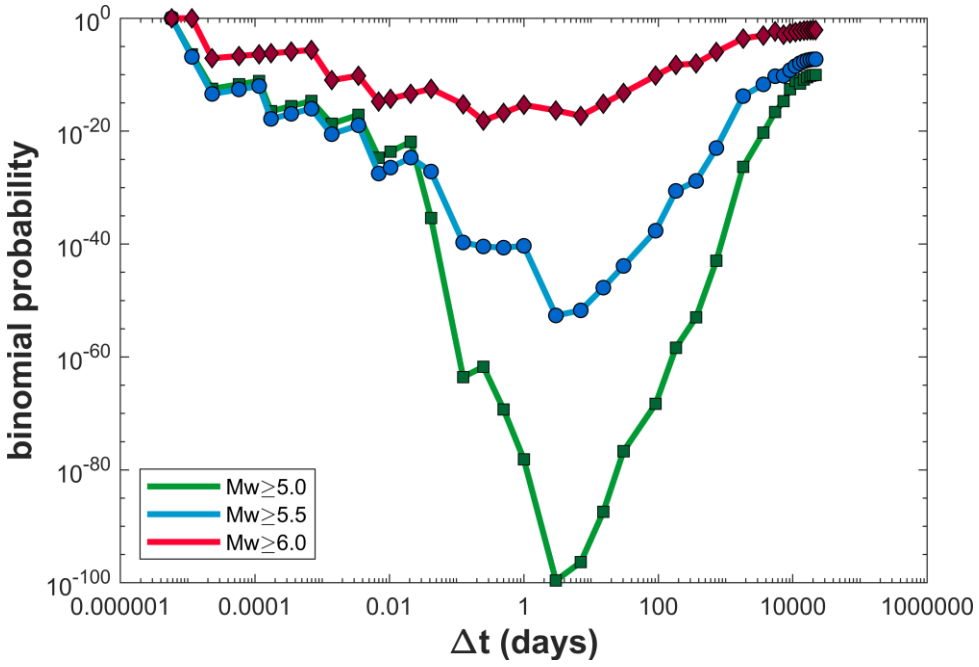

Figure S9: Binomial probability density for all target shocks (not-declustered) and weighted fraction of space-time occupied by alarms for different magnitude thresholds (see inset) as a function of the alarm duration Δt.

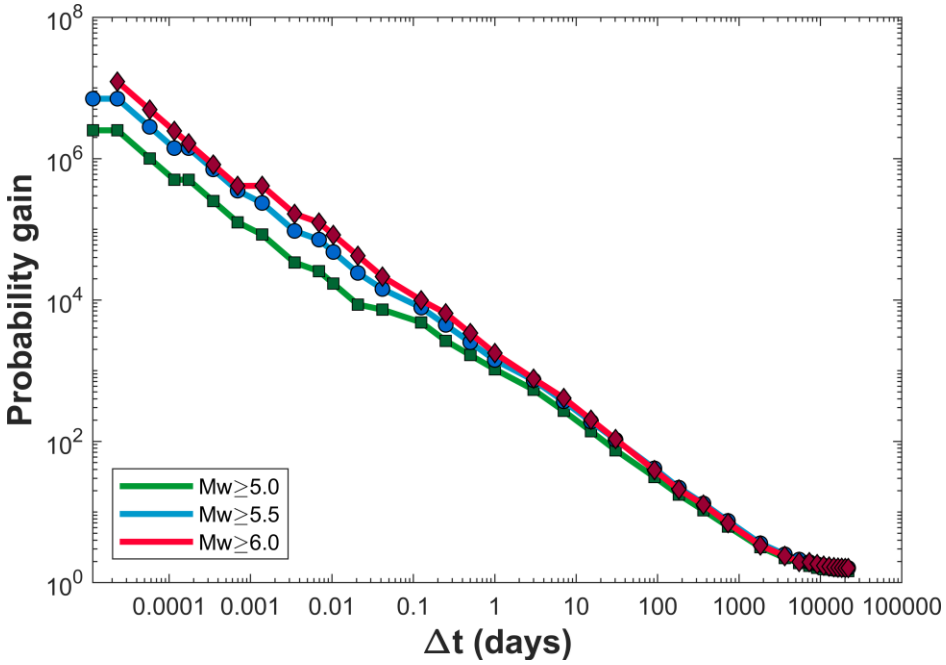

Figure S10: Probability gain for all target shocks (not-declustered) and weighted fraction of space-time occupied by alarms for different magnitude thresholds (see inset) as a function of the alarm duration Δt.

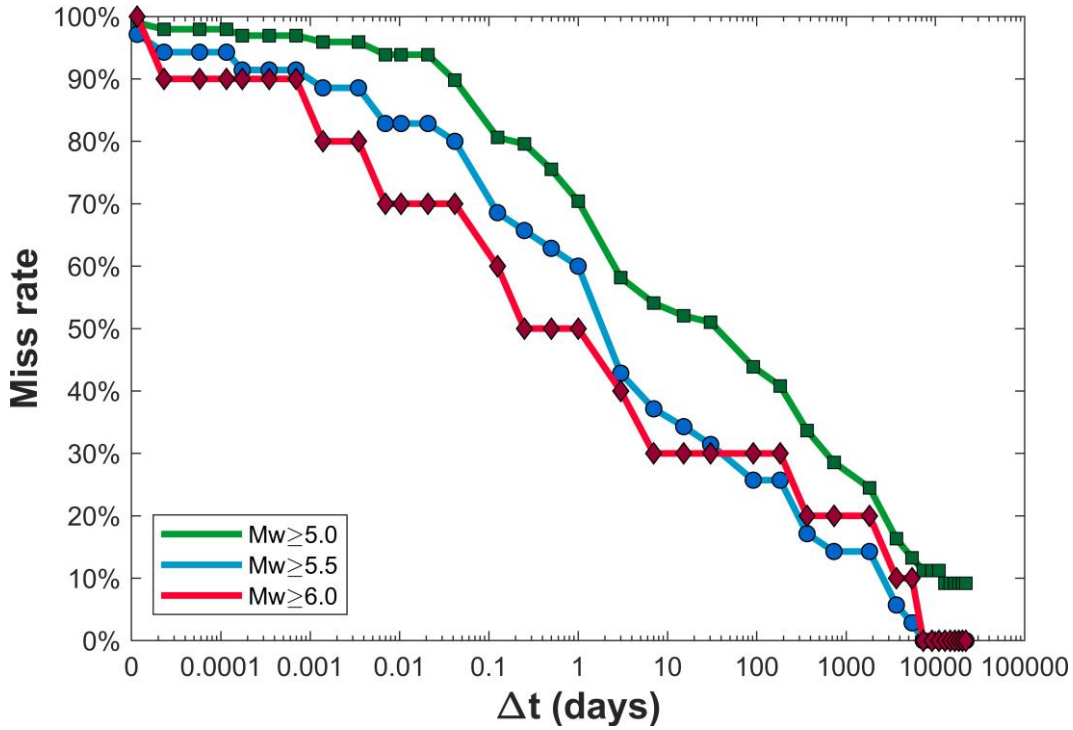

Figure S11: Miss rate for all target shocks (not-declustered) for different magnitude thresholds (see inset) as a function of the alarm duration Δt.

Table S1 – List of center coordinates of circular areas (CA) with radius of 30 km. $N_{4.5}$, $N_{5.0}$, $N_{5.5}$, $N_{6.0}$: numbers of earthquakes occurred within each CA, according to the CPTI15 catalogue up to year 1959, with Mw≥4.5, 5.0, 5.5 and 6.0 respectively in respective time intervals of completeness. $\lambda_{4.5}$, $\lambda_{5.0}$, $\lambda_{5.5}$, $\lambda_{6.0}$: average rates (events/y) of earthquakes with Mw≥4.0 within each CA computed from observed earthquakes with Mw≥4.5, 5.0, 5.5 and 6.0 respectively and assuming a b-value=1 (see text). λ_{ave}: average of non-null rates $\lambda_{4.5}$, $\lambda_{5.0}$, $\lambda_{5.5}$, $\lambda_{6.0}$. $w = \lambda_{ave} / \sum \lambda_{ave}$: overall weight of each CA ($\sum w = 1$).

Nc	Latitude	Longitude	$N_{4.5}$	$N_{5.0}$	$N_{5.5}$	$N_{6.0}$	$\lambda_{4.5}$	$\lambda_{5.0}$	$\lambda_{5.5}$	$\lambda_{6.0}$	λ_{ave}	w
1	47.0000	11.4757	4	2	0	0	0.1581	0.2500	-	-	0.2041	0.004107
2	47.0000	12.0351	1	1	0	0	0.0395	0.1250	-	-	0.0823	0.001656
3	46.6185	10.3330	4	0	0	0	0.1581	-	-	-	0.1581	0.003182
4	46.6185	10.8885	2	0	0	0	0.0791	-	-	-	0.0791	0.001591
5	46.6185	11.4440	2	0	0	0	0.0791	-	-	-	0.0791	0.001591
6	46.6185	11.9995	1	0	0	0	0.0395	-	-	-	0.0395	0.000796
7	46.6185	12.5550	5	1	0	0	0.1976	0.1250	-	-	0.1613	0.003247
8	46.6185	13.1105	15	8	2	1	0.5929	1.0000	0.3514	0.2941	0.5596	0.011263

Nc	Latitude	Longitude	$N_{4.5}$	$N_{5.0}$	$N_{5.5}$	$N_{6.0}$	$\lambda_{4.5}$	$\lambda_{5.0}$	$\lambda_{5.5}$	$\lambda_{6.0}$	λ_{ave}	w
9	46.2369	9.7581	1	0	0	0	0.0395	-	-	-	0.0395	0.000796
10	46.2369	10.3098	1	0	0	0	0.0395	-	-	-	0.0395	0.000796
11	46.2369	10.8614	1	0	0	0	0.0395	-	-	-	0.0395	0.000796
12	46.2369	11.9647	1	1	0	0	0.0395	0.1250	-	-	0.0823	0.001656
13	46.2369	12.5163	9	1	4	2	0.3558	0.1250	0.7027	0.5882	0.4429	0.008915
14	46.2369	13.0679	34	16	7	2	1.3440	2.0000	1.2298	0.5882	1.2905	0.025974
15	46.2369	13.6195	11	5	2	0	0.4348	0.6250	0.3514	-	0.4704	0.009468
16	45.8554	8.0957	0	0	0	0	-	-	-	-	0.0395	0.000796
17	45.8554	9.1913	1	0	0	0	0.0395	-	-	-	0.0395	0.000796
18	45.8554	9.7392	4	0	0	0	0.1581	-	-	-	0.1581	0.003182
19	45.8554	10.2870	5	0	0	0	0.1976	-	-	-	0.1976	0.003978
20	45.8554	10.8348	8	2	0	0	0.3162	0.2500	-	-	0.2831	0.005698
21	45.8554	11.3827	2	0	0	0	0.0791	-	-	-	0.0791	0.001591
22	45.8554	11.9305	6	3	1	1	0.2372	0.3750	0.1757	0.2941	0.2705	0.005444
23	45.8554	12.4783	6	1	2	1	0.2372	0.1250	0.3514	0.2941	0.2519	0.005070
24	45.8554	13.0262	0	0	0	0	-	-	-	-	0.0395	0.000796
25	45.8554	13.5740	1	1	0	0	0.0395	0.1250	-	-	0.0823	0.001656
26	45.4738	7.0000	0	0	0	0	-	-	-	-	0.0395	0.000796
27	45.4738	7.5441	3	0	0	0	0.1186	-	-	-	0.1186	0.002387
28	45.4738	8.0882	3	0	0	0	0.1186	-	-	-	0.1186	0.002387
29	45.4738	8.6323	1	0	0	0	0.0395	-	-	-	0.0395	0.000796
30	45.4738	9.1764	1	0	0	0	0.0395	-	-	-	0.0395	0.000796
31	45.4738	9.7206	3	1	1	0	0.1186	0.1250	0.1757	-	0.1398	0.002813
32	45.4738	10.2647	6	1	0	0	0.2372	0.1250	-	-	0.1811	0.003645
33	45.4738	10.8088	9	4	1	0	0.3558	0.5000	0.1757	-	0.3438	0.006920
34	45.4738	11.3529	5	1	1	0	0.1976	0.1250	0.1757	-	0.1661	0.003343
35	45.4738	11.8970	0	0	0	0	-	-	-	-	0.0395	0.000796
36	45.4738	12.4411	0	0	0	0	-	-	-	-	0.0395	0.000796
37	45.0923	7.0000	4	2	0	0	0.1581	0.2500	-	-	0.2041	0.004107
38	45.0923	7.5405	7	2	0	0	0.2767	0.2500	-	-	0.2633	0.005300
39	45.0923	8.6214	3	0	0	0	0.1186	-	-	-	0.1186	0.002387
40	45.0923	9.1619	2	1	0	0	0.0791	0.1250	-	-	0.1020	0.002054
41	45.0923	9.7023	1	1	0	0	0.0395	0.1250	-	-	0.0823	0.001656
42	45.0923	10.2428	1	1	0	0	0.0395	0.1250	-	-	0.0823	0.001656
43	45.0923	10.7832	6	1	1	0	0.2372	0.1250	0.1757	-	0.1793	0.003608
44	45.0923	11.3237	8	3	1	1	0.3162	0.3750	0.1757	0.2941	0.2903	0.005842
45	45.0923	11.8642	0	0	0	0	-	-	-	-	0.0395	0.000796

Nc	Latitude	Longitude	$N_{4.5}$	$N_{5.0}$	$N_{5.5}$	$N_{6.0}$	$\lambda_{4.5}$	$\lambda_{5.0}$	$\lambda_{5.5}$	$\lambda_{6.0}$	λ_{ave}	w
46	44.7107	7.0000	3	1	1	0	0.1186	0.1250	0.1757	-	0.1398	0.002813
47	44.7107	7.5369	2	0	1	0	0.0791	-	0.1757	-	0.1274	0.002564
48	44.7107	8.0738	0	0	0	0	-	-	-	-	0.0395	0.000796
49	44.7107	8.6107	4	0	0	0	0.1581	-	-	-	0.1581	0.003182
50	44.7107	9.1476	7	1	1	0	0.2767	0.1250	0.1757	-	0.1925	0.003874
51	44.7107	9.6844	6	0	0	0	0.2372	-	-	-	0.2372	0.004774
52	44.7107	10.2213	11	5	2	0	0.4348	0.6250	0.3514	-	0.4704	0.009468
53	44.7107	10.7582	19	4	3	0	0.7510	0.5000	0.5270	-	0.5927	0.011929
54	44.7107	11.2951	20	10	2	1	0.7906	1.2500	0.3514	0.2941	0.6715	0.013515
55	44.7107	11.8320	7	2	0	0	0.2767	0.2500	-	-	0.2633	0.005300
56	44.7107	12.3689	2	0	0	0	0.0791	-	-	-	0.0791	0.001591
57	44.3292	7.0000	5	1	0	0	0.1976	0.1250	-	-	0.1613	0.003247
58	44.3292	7.5334	5	0	0	0	0.1976	-	-	-	0.1976	0.003978
59	44.3292	8.0668	3	0	0	0	0.1186	-	-	-	0.1186	0.002387
60	44.3292	8.6002	0	0	0	0	-	-	-	-	0.0395	0.000796
61	44.3292	9.1335	0	0	0	0	-	-	-	-	0.0395	0.000796
62	44.3292	9.6669	5	2	1	0	0.1976	0.2500	0.1757	-	0.2078	0.004182
63	44.3292	10.2003	19	8	4	1	0.7510	1.0000	0.7027	0.2941	0.6870	0.013827
64	44.3292	10.7337	9	2	0	0	0.3558	0.2500	-	-	0.3029	0.006096
65	44.3292	11.2671	20	8	0	0	0.7906	1.0000	-	-	0.8953	0.018019
66	44.3292	11.8005	15	3	2	1	0.5929	0.3750	0.3514	0.2941	0.4034	0.008118
67	44.3292	12.3338	6	2	2	0	0.2372	0.2500	0.3514	-	0.2795	0.005626
68	43.9476	7.5299	0	0	1	0	-	-	0.1757	-	0.1757	0.003536
69	43.9476	8.0599	4	1	2	1	0.1581	0.1250	0.3514	0.2941	0.2321	0.004672
70	43.9476	9.6497	0	0	0	0	-	-	-	-	0.0395	0.000796
71	43.9476	10.1797	13	2	2	1	0.5139	0.2500	0.3514	0.2941	0.3523	0.007091
72	43.9476	10.7096	12	2	1	0	0.4743	0.2500	0.1757	-	0.3000	0.006038
73	43.9476	11.2396	14	4	2	1	0.5534	0.5000	0.3514	0.2941	0.4247	0.008548
74	43.9476	11.7695	25	4	2	2	0.9882	0.5000	0.3514	0.5882	0.6070	0.012216
75	43.9476	12.2995	11	4	3	0	0.4348	0.5000	0.5270	-	0.4873	0.009808
76	43.9476	12.8294	22	12	3	0	0.8696	1.5000	0.5270	-	0.9656	0.019434
77	43.9476	13.3594	5	3	1	0	0.1976	0.3750	0.1757	-	0.2494	0.005020
78	43.5661	10.1595	2	0	0	0	0.0791	-	-	-	0.0791	0.001591
79	43.5661	10.6861	4	0	1	1	0.1581	-	0.1757	0.2941	0.2093	0.004213
80	43.5661	11.2126	9	2	1	0	0.3558	0.2500	0.1757	-	0.2605	0.005243
81	43.5661	11.7392	2	0	0	0	0.0791	-	-	-	0.0791	0.001591
82	43.5661	12.2658	8	4	3	1	0.3162	0.5000	0.5270	0.2941	0.4093	0.008239

Nc	Latitude	Longitude	$N_{4.5}$	$N_{5.0}$	$N_{5.5}$	$N_{6.0}$	$\lambda_{4.5}$	$\lambda_{5.0}$	$\lambda_{5.5}$	$\lambda_{6.0}$	λ_{ave}	w
83	43.5661	12.7924	3	1	1	2	0.1186	0.1250	0.1757	0.5882	0.2519	0.005069
84	43.5661	13.3190	7	3	1	1	0.2767	0.3750	0.1757	0.2941	0.2804	0.005643
85	43.5661	13.8455	3	2	0	0	0.1186	0.2500	-	-	0.1843	0.003709
86	43.1845	10.6629	3	0	0	0	0.1186	-	-	-	0.1186	0.002387
87	43.1845	11.1862	3	2	0	0	0.1186	0.2500	-	-	0.1843	0.003709
88	43.1845	11.7095	1	1	0	0	0.0395	0.1250	-	-	0.0823	0.001656
89	43.1845	12.2328	9	2	2	0	0.3558	0.2500	0.3514	-	0.3190	0.006421
90	43.1845	12.7561	25	10	6	3	0.9882	1.2500	1.0541	0.8824	1.0437	0.021006
91	43.1845	13.2793	9	2	2	1	0.3558	0.2500	0.3514	0.2941	0.3128	0.006296
92	43.1845	13.8026	4	2	0	0	0.1581	0.2500	-	-	0.2041	0.004107
93	42.8030	11.1603	0	0	0	0	-	-	-	-	0.0395	0.000796
94	42.8030	11.6803	10	2	0	0	0.3953	0.2500	-	-	0.3226	0.006494
95	42.8030	12.2004	6	1	0	0	0.2372	0.1250	-	-	0.1811	0.003645
96	42.8030	12.7204	37	13	8	1	1.4626	1.6250	1.4055	0.2941	1.1968	0.024088
97	42.8030	13.2405	34	12	6	3	1.3440	1.5000	1.0541	0.8824	1.1951	0.024054
98	42.8030	13.7605	3	2	1	0	0.1186	0.2500	0.1757	-	0.1814	0.003651
99	42.4214	11.6518	3	0	0	0	0.1186	-	-	-	0.1186	0.002387
100	42.4214	12.1686	1	0	0	0	0.0395	-	-	-	0.0395	0.000796
101	42.4214	12.6855	12	3	2	0	0.4743	0.3750	0.3514	-	0.4002	0.008056
102	42.4214	13.2024	29	17	5	3	1.1463	2.1250	0.8784	0.8824	1.2580	0.025320
103	42.4214	13.7192	11	8	3	1	0.4348	1.0000	0.5270	0.2941	0.5640	0.011351
104	42.4214	14.2361	2	2	0	0	0.0791	0.2500	-	-	0.1645	0.003311
105	42.0399	11.6237	0	0	0	0	-	-	-	-	0.0395	0.000796
106	42.0399	12.1375	1	0	0	0	0.0395	-	-	-	0.0395	0.000796
107	42.0399	12.6512	6	3	0	0	0.2372	0.3750	-	-	0.3061	0.006161
108	42.0399	13.1650	12	1	1	0	0.4743	0.1250	0.1757	-	0.2583	0.005200
109	42.0399	13.6787	15	5	1	1	0.5929	0.6250	0.1757	0.2941	0.4219	0.008492
110	42.0399	14.1925	5	4	1	1	0.1976	0.5000	0.1757	0.2941	0.2919	0.005874
111	42.0399	14.7062	0	0	0	0	-	-	-	-	0.0395	0.000796
112	42.0399	15.2200	4	0	1	0	0.1581	-	0.1757	-	0.1669	0.003359
113	42.0399	15.7337	4	2	0	1	0.1581	0.2500	-	0.2941	0.2341	0.004711
114	42.0399	16.2475	1	0	0	1	0.0395	-	-	0.2941	0.1668	0.003358
115	41.6583	12.1069	1	0	0	0	0.0395	-	-	-	0.0395	0.000796
116	41.6583	12.6176	10	4	1	0	0.3953	0.5000	0.1757	-	0.3570	0.007185
117	41.6583	13.1283	3	0	0	0	0.1186	-	-	-	0.1186	0.002387
118	41.6583	13.6390	19	4	0	1	0.7510	0.5000	-	0.2941	0.5151	0.010366
119	41.6583	14.1497	12	4	1	0	0.4743	0.5000	0.1757	-	0.3833	0.007715

Nc	Latitude	Longitude	$N_{4.5}$	$N_{5.0}$	$N_{5.5}$	$N_{6.0}$	$\lambda_{4.5}$	$\lambda_{5.0}$	$\lambda_{5.5}$	$\lambda_{6.0}$	λ_{ave}	w
120	41.6583	14.6604	7	3	3	1	0.2767	0.3750	0.5270	0.2941	0.3682	0.007411
121	41.6583	15.1711	7	2	2	2	0.2767	0.2500	0.3514	0.5882	0.3666	0.007378
122	41.6583	15.6818	18	10	2	1	0.7115	1.2500	0.3514	0.2941	0.6517	0.013118
123	41.6583	16.1925	11	6	0	0	0.4348	0.7500	-	-	0.5924	0.011923
124	41.2768	9.0308	1	0	0	0	0.0395	-	-	-	0.0395	0.000796
125	41.2768	16.1385	1	0	0	0	0.0395	-	-	-	0.0395	0.000796
126	41.2768	13.0924	0	0	0	0	-	-	-	-	0.0395	0.000796
127	41.2768	13.6001	0	0	0	0	-	-	-	-	0.0395	0.000796
128	41.2768	14.1077	6	1	0	0	0.2372	0.1250	-	-	0.1811	0.003645
129	41.2768	14.6154	8	3	2	3	0.3162	0.3750	0.3514	0.8824	0.4812	0.009686
130	41.2768	15.1231	11	5	3	4	0.4348	0.6250	0.5270	1.1765	0.6908	0.013904
131	41.2768	15.6308	3	0	0	1	0.1186	-	-	0.2941	0.2064	0.004153
132	41.2768	16.6462	0	0	0	0	-	-	-	-	0.0395	0.000796
133	40.8952	9.0190	1	0	0	0	0.0395	-	-	-	0.0395	0.000796
134	40.8952	14.0666	0	0	0	0	-	-	-	-	0.0395	0.000796
135	40.8952	14.5714	6	0	0	0	0.2372	-	-	-	0.2372	0.004774
136	40.8952	15.0761	21	7	4	5	0.8301	0.8750	0.7027	1.4706	0.9696	0.019515
137	40.8952	15.5809	31	9	5	4	1.2254	1.1250	0.8784	1.1765	1.1013	0.022166
138	40.8952	16.0856	2	1	0	0	0.0791	0.1250	-	-	0.1020	0.002054
139	40.8952	16.5904	1	0	0	0	0.0395	-	-	-	0.0395	0.000796
140	40.5137	14.5281	0	0	0	0	-	-	-	-	0.0395	0.000796
141	40.5137	15.0300	1	1	0	0	0.0395	0.1250	-	-	0.0823	0.001656
142	40.5137	15.5318	20	3	1	0	0.7906	0.3750	0.1757	-	0.4471	0.008998
143	40.5137	16.0337	9	2	2	1	0.3558	0.2500	0.3514	0.2941	0.3128	0.006296
144	40.5137	16.5356	4	1	0	0	0.1581	0.1250	-	-	0.1416	0.002849
145	40.5137	17.0375	1	0	0	0	0.0395	-	-	-	0.0395	0.000796
146	40.5137	17.5393	0	0	0	0	-	-	-	-	0.0395	0.000796
147	40.1321	15.4838	2	0	2	0	0.0791	-	0.3514	-	0.2152	0.004332
148	40.1321	15.9828	9	4	4	1	0.3558	0.5000	0.7027	0.2941	0.4632	0.009322
149	40.1321	16.4819	1	0	0	0	0.0395	-	-	-	0.0395	0.000796
150	40.1321	17.9790	1	0	0	0	0.0395	-	-	-	0.0395	0.000796
151	39.7506	15.9329	4	3	0	0	0.1581	0.3750	-	-	0.2666	0.005365
152	39.7506	16.4291	6	3	2	0	0.2372	0.3750	0.3514	-	0.3212	0.006464
153	39.7506	16.9254	5	1	1	1	0.1976	0.1250	0.1757	0.2941	0.1981	0.003987
154	39.3690	8.9742	0	0	0	0	-	-	-	-	0.0395	0.000796
155	39.3690	15.8838	1	1	1	0	0.0395	0.1250	0.1757	-	0.1134	0.002282
156	39.3690	16.3774	9	3	6	2	0.3558	0.3750	1.0541	0.5882	0.5933	0.011941

Nc	Latitude	Longitude	$N_{4.5}$	$N_{5.0}$	$N_{5.5}$	$N_{6.0}$	$\lambda_{4.5}$	$\lambda_{5.0}$	$\lambda_{5.5}$	$\lambda_{6.0}$	λ_{ave}	w
157	39.3690	16.8709	1	0	1	2	0.0395	-	0.1757	0.5882	0.2678	0.005390
158	38.9875	8.9635	0	0	0	0	-	-	-	-	0.0395	0.000796
159	38.9875	15.3449	6	3	0	0	0.2372	0.3750	-	-	0.3061	0.006161
160	38.9875	15.8358	1	1	1	1	0.0395	0.1250	0.1757	0.2941	0.1586	0.003192
161	38.9875	16.3266	4	0	3	5	0.1581	-	0.5270	1.4706	0.7186	0.014463
162	38.9875	16.8175	3	0	1	1	0.1186	-	0.1757	0.2941	0.1961	0.003947
163	38.6059	14.8121	8	3	0	0	0.3162	0.3750	-	-	0.3456	0.006956
164	38.6059	15.3003	7	3	0	0	0.2767	0.3750	-	-	0.3258	0.006558
165	38.6059	15.7886	5	2	2	1	0.1976	0.2500	0.3514	0.2941	0.2733	0.005500
166	38.6059	16.2768	7	1	4	4	0.2767	0.1250	0.7027	1.1765	0.5702	0.011477
167	38.6059	16.7651	1	1	1	0	0.0395	0.1250	0.1757	-	0.1134	0.002282
168	38.2244	13.3139	4	1	0	0	0.1581	0.1250	-	-	0.1416	0.002849
169	38.2244	13.7996	7	3	1	0	0.2767	0.3750	0.1757	-	0.2758	0.005551
170	38.2244	14.7709	6	1	1	1	0.2372	0.1250	0.1757	0.2941	0.2080	0.004186
171	38.2244	15.2566	13	2	2	2	0.5139	0.2500	0.3514	0.5882	0.4259	0.008571
172	38.2244	15.7423	13	6	4	3	0.5139	0.7500	0.7027	0.8824	0.7122	0.014335
173	38.2244	16.2280	3	2	2	1	0.1186	0.2500	0.3514	0.2941	0.2535	0.005103
174	37.8428	12.7979	15	6	2	1	0.5929	0.7500	0.3514	0.2941	0.4971	0.010005
175	37.8428	13.2811	9	6	1	1	0.3558	0.7500	0.1757	0.2941	0.3939	0.007928
176	37.8428	13.7642	2	1	0	0	0.0791	0.1250	-	-	0.1020	0.002054
177	37.8428	14.2474	11	3	0	0	0.4348	0.3750	-	-	0.4049	0.008150
178	37.8428	14.7306	8	2	0	0	0.3162	0.2500	-	-	0.2831	0.005698
179	37.8428	15.2137	12	2	2	1	0.4743	0.2500	0.3514	0.2941	0.3425	0.006893
180	37.8428	15.6969	0	0	0	0	-	-	-	-	0.0395	0.000796
181	37.8428	16.1800	3	1	0	0	0.1186	0.1250	-	-	0.1218	0.002451
182	37.4613	12.7682	4	0	0	0	0.1581	-	-	-	0.1581	0.003182
183	37.4613	13.2489	1	0	0	0	0.0395	-	-	-	0.0395	0.000796
184	37.4613	13.7296	0	0	0	0	-	-	-	-	0.0395	0.000796
185	37.4613	14.6909	6	2	1	0	0.2372	0.2500	0.1757	-	0.2210	0.004447
186	37.4613	15.1716	8	3	3	1	0.3162	0.3750	0.5270	0.2941	0.3781	0.007610
187	37.0797	14.6521	5	2	1	0	0.1976	0.2500	0.1757	-	0.2078	0.004182
188	37.0797	15.1303	1	0	0	2	0.0395	-	-	0.5882	0.3139	0.006317
189	36.6982	14.6139	1	1	0	0	0.0395	0.1250	-	-	0.0823	0.001656
190	36.6982	15.0898	0	0	0	0	-	-	-	-	0.0395	0.000796

Table S2 – Values of variables in Molchan and Area Skill score plots of Fig. 3.9 and 3.10 (section 3.5) for Mw≥5.5 not-declustered targets.

Δt (years)	Δt (days)	τ_u	τ_w	h	ν	$a_f(\tau_u)$	$a_f(\tau_w)$
1.6E-08	5.8E-06	8.6E-10	2.0E-09	0	1.000	0.000	0.000
3.2E-08	1.2E-05	1.7E-09	4.1E-09	1	0.990	0.003	0.003
6.3E-08	2.3E-05	3.4E-09	8.1E-09	2	0.980	0.009	0.009
1.6E-07	5.8E-05	8.6E-09	2.0E-08	2	0.980	0.016	0.016
3.2E-07	1.2E-04	1.7E-08	4.1E-08	2	0.980	0.018	0.018
4.8E-07	1.7E-04	2.6E-08	6.1E-08	3	0.969	0.021	0.021
9.5E-07	3.5E-04	5.1E-08	1.2E-07	3	0.969	0.026	0.026
1.9E-06	6.9E-04	1.0E-07	2.4E-07	3	0.969	0.028	0.028
3.8E-06	1.4E-03	2.0E-07	4.9E-07	4	0.959	0.032	0.032
9.5E-06	3.5E-03	5.1E-07	1.2E-06	4	0.959	0.037	0.037
1.9E-05	6.9E-03	1.0E-06	2.4E-06	6	0.939	0.044	0.044
2.9E-05	1.0E-02	1.5E-06	3.6E-06	6	0.939	0.050	0.050
5.7E-05	2.1E-02	3.0E-06	7.1E-06	6	0.939	0.055	0.055
1.1E-04	4.2E-02	6.0E-06	1.4E-05	10	0.898	0.068	0.068
3.4E-04	0.13	1.7E-05	4.0E-05	19	0.806	0.121	0.120
6.8E-04	0.25	3.4E-05	7.7E-05	20	0.796	0.159	0.158
1.4E-03	0.50	6.5E-05	1.5E-04	24	0.755	0.191	0.190
2.7E-03	1.00	1.3E-04	2.8E-04	29	0.704	0.229	0.228
8.2E-03	3.00	3.6E-04	7.8E-04	41	0.582	0.312	0.310
0.019	7.02	8.1E-04	1.7E-03	45	0.541	0.382	0.380
0.042	15.22	1.7E-03	3.5E-03	47	0.520	0.427	0.425
0.083	30.44	3.2E-03	6.5E-03	48	0.510	0.455	0.453
0.250	91.31	9.1E-03	0.018	55	0.439	0.501	0.499
0.500	182.62	0.017	0.034	58	0.408	0.537	0.535
1.000	365.24	0.033	0.063	65	0.337	0.580	0.578
2.000	730.49	0.062	0.114	70	0.286	0.630	0.628
5.000	1826.21	0.134	0.238	74	0.245	0.686	0.683
10	3652.43	0.220	0.374	82	0.163	0.729	0.724
15	5478.64	0.280	0.457	85	0.133	0.756	0.748
20	7304.85	0.324	0.511	87	0.112	0.772	0.761
25	9131.06	0.355	0.546	87	0.112	0.782	0.769
30	10957.28	0.379	0.572	87	0.112	0.789	0.775
35	12783.49	0.398	0.592	89	0.092	0.794	0.779
40	14609.70	0.413	0.605	89	0.092	0.798	0.782
45	16435.91	0.424	0.613	89	0.092	0.801	0.783
50	18262.13	0.431	0.617	89	0.092	0.803	0.784
55	20088.34	0.434	0.619	89	0.092	0.804	0.785
60	21914.55	0.436	0.620	89	0.092	0.804	0.785
Full occ.	Full occ.	1.000	1.000	98	0.000	0.889	0.849

Δt is the duration of alarms, τ_u and τ_w the unweighted and weighted fraction of space-time occupied by alarms respectively, h the number of successful forecasts, ν the miss rate, $a_f(\tau_u)$ and $a_f(\tau_w)$ the Area Skill scores computed considering the unweighted and weighted fraction of space-time occupied by alarms respectively. The last row (Δt= Full occ.) reports values for a full occupation of the space-time by alarms.

Table S3 – Same as Table S2 for Mw≥5.0 declustered targets (Fig. S1 and S2).

Δt (years)	Δt (days)	τ_u	τ_w	h	ν	$a_f(\tau_u)$	$a_f(\tau_w)$
1.6E-08	5.8E-06	8.6E-10	2.0E-09	0	1.000	0.000	0.000
3.2E-08	1.2E-05	1.7E-09	4.1E-09	0	1.000	0.000	0.000
6.3E-08	2.3E-05	3.4E-09	8.1E-09	0	1.000	0.000	0.000
1.6E-07	5.8E-05	8.6E-09	2.0E-08	0	1.000	0.000	0.000
3.2E-07	1.2E-04	1.7E-08	4.1E-08	0	1.000	0.000	0.000
4.8E-07	1.7E-04	2.6E-08	6.1E-08	1	0.977	0.004	0.004
9.5E-07	3.5E-04	5.1E-08	1.2E-07	1	0.977	0.013	0.013
1.9E-06	6.9E-04	1.0E-07	2.4E-07	1	0.977	0.018	0.018
3.8E-06	1.4E-03	2.0E-07	4.9E-07	2	0.955	0.026	0.026
9.5E-06	3.5E-03	5.1E-07	1.2E-06	2	0.955	0.038	0.038
1.9E-05	6.9E-03	1.0E-06	2.4E-06	2	0.955	0.042	0.042
2.9E-05	1.0E-02	1.5E-06	3.6E-06	2	0.955	0.043	0.043
5.7E-05	2.1E-02	3.0E-06	7.1E-06	2	0.955	0.044	0.044
1.1E-04	4.2E-02	6.0E-06	1.4E-05	2	0.955	0.045	0.045
3.4E-04	0.13	1.7E-05	4.0E-05	4	0.909	0.060	0.060
6.8E-04	0.25	3.4E-05	7.7E-05	4	0.909	0.075	0.075
1.4E-03	0.50	6.5E-05	1.5E-04	4	0.909	0.083	0.082
2.7E-03	1.00	1.3E-04	2.8E-04	4	0.909	0.087	0.087
8.2E-03	3.00	3.6E-04	7.8E-04	6	0.864	0.104	0.104
0.019	7.02	8.1E-04	1.7E-03	7	0.841	0.128	0.128
0.042	15.22	1.7E-03	3.5E-03	7	0.841	0.144	0.144
0.083	30.44	3.2E-03	6.5E-03	8	0.818	0.157	0.156
0.250	91.31	9.1E-03	0.018	8	0.818	0.173	0.172
0.500	182.62	0.017	0.034	10	0.773	0.188	0.187
1.000	365.24	0.033	0.063	14	0.682	0.228	0.227
2.000	730.49	0.062	0.114	19	0.568	0.296	0.294
5.000	1826.21	0.134	0.238	22	0.500	0.387	0.383
10	3652.43	0.220	0.374	29	0.341	0.463	0.455
15	5478.64	0.280	0.457	32	0.273	0.512	0.498
20	7304.85	0.324	0.511	34	0.227	0.544	0.525
25	9131.06	0.355	0.546	34	0.227	0.564	0.541
30	10957.28	0.379	0.572	34	0.227	0.578	0.551
35	12783.49	0.398	0.592	36	0.182	0.588	0.559
40	14609.70	0.413	0.605	36	0.182	0.596	0.565
45	16435.91	0.424	0.613	36	0.182	0.602	0.568
50	18262.13	0.431	0.617	36	0.182	0.606	0.570
55	20088.34	0.434	0.619	36	0.182	0.607	0.571
60	21914.55	0.436	0.620	36	0.182	0.608	0.571
Full occ.	Full occ.	1.000	1.000	44	0.000	0.778	0.699

Table S4 – Same as Table S2 for Mw≥6.0 not-declustered targets (Fig. 3.11 and 3.12 of section 3.5).

Δt (years)	Δt (days)	τ_u	τ_w	h	ν	$a_f(\tau_u)$	$a_f(\tau_w)$
1.6E-08	5.8E-06	8.6E-10	2.0E-09	0	1.000	0.000	0.000
3.2E-08	1.2E-05	1.7E-09	4.1E-09	0	1.000	0.000	0.000
6.3E-08	2.3E-05	3.4E-09	8.1E-09	1	0.900	0.025	0.025
1.6E-07	5.8E-05	8.6E-09	2.0E-08	1	0.900	0.070	0.070
3.2E-07	1.2E-04	1.7E-08	4.1E-08	1	0.900	0.085	0.085
4.8E-07	1.7E-04	2.6E-08	6.1E-08	1	0.900	0.090	0.090
9.5E-07	3.5E-04	5.1E-08	1.2E-07	1	0.900	0.095	0.095
1.9E-06	6.9E-04	1.0E-07	2.4E-07	1	0.900	0.097	0.097
3.8E-06	1.4E-03	2.0E-07	4.9E-07	2	0.800	0.124	0.124
9.5E-06	3.5E-03	5.1E-07	1.2E-06	2	0.800	0.169	0.169
1.9E-05	6.9E-03	1.0E-06	2.4E-06	3	0.700	0.209	0.209
2.9E-05	1.0E-02	1.5E-06	3.6E-06	3	0.700	0.240	0.239
5.7E-05	2.1E-02	3.0E-06	7.1E-06	3	0.700	0.270	0.269
1.1E-04	4.2E-02	6.0E-06	1.4E-05	3	0.700	0.285	0.284
3.4E-04	0.13	1.7E-05	4.0E-05	4	0.600	0.328	0.327
6.8E-04	0.25	3.4E-05	7.7E-05	5	0.500	0.387	0.386
1.4E-03	0.50	6.5E-05	1.5E-04	5	0.500	0.442	0.440
2.7E-03	1.00	1.3E-04	2.8E-04	5	0.500	0.470	0.469
8.2E-03	3.00	3.6E-04	7.8E-04	6	0.400	0.522	0.521
0.019	7.02	8.1E-04	1.7E-03	7	0.300	0.593	0.591
0.042	15.22	1.7E-03	3.5E-03	7	0.300	0.648	0.646
0.083	30.44	3.2E-03	6.5E-03	7	0.300	0.673	0.671
0.250	91.31	9.1E-03	0.018	7	0.300	0.690	0.690
0.500	182.62	0.017	0.034	7	0.300	0.695	0.694
1.000	365.24	0.033	0.063	8	0.200	0.721	0.720
2.000	730.49	0.062	0.114	8	0.200	0.758	0.756
5.000	1826.21	0.134	0.238	8	0.200	0.780	0.778
10	3652.43	0.220	0.374	9	0.100	0.808	0.804
15	5478.64	0.280	0.457	9	0.100	0.827	0.821
20	7304.85	0.324	0.511	10	0.000	0.844	0.834
25	9131.06	0.355	0.546	10	0.000	0.858	0.844
30	10957.28	0.379	0.572	10	0.000	0.867	0.850
35	12783.49	0.398	0.592	10	0.000	0.873	0.855
40	14609.70	0.413	0.605	10	0.000	0.878	0.857
45	16435.91	0.424	0.613	10	0.000	0.881	0.859
50	18262.13	0.431	0.617	10	0.000	0.883	0.860
55	20088.34	0.434	0.619	10	0.000	0.884	0.860
60	21914.55	0.436	0.620	10	0.000	0.884	0.861
Full occ.	Full occ.	1.000	1.000	10	0.000	0.949	0.911

Table S5 – Same as Table S2 for Mw≥6.0 declustered targets (Fig. S3 and S4).

Δt (years)	Δt (days)	τ_u	τ_w	h	v	$a_f(\tau_u)$	$a_f(\tau_w)$
1.6E-08	5.8E-06	8.6E-10	2.0E-09	0	1.000	0.000	0.000
3.2E-08	1.2E-05	1.7E-09	4.1E-09	0	1.000	0.000	0.000
6.3E-08	2.3E-05	3.4E-09	8.1E-09	0	1.000	0.000	0.000
1.6E-07	5.8E-05	8.6E-09	2.0E-08	0	1.000	0.000	0.000
3.2E-07	1.2E-04	1.7E-08	4.1E-08	0	1.000	0.000	0.000
4.8E-07	1.7E-04	2.6E-08	6.1E-08	0	1.000	0.000	0.000
9.5E-07	3.5E-04	5.1E-08	1.2E-07	0	1.000	0.000	0.000
1.9E-06	6.9E-04	1.0E-07	2.4E-07	0	1.000	0.000	0.000
3.8E-06	1.4E-03	2.0E-07	4.9E-07	1	0.857	0.036	0.036
9.5E-06	3.5E-03	5.1E-07	1.2E-06	1	0.857	0.100	0.100
1.9E-05	6.9E-03	1.0E-06	2.4E-06	2	0.714	0.157	0.157
2.9E-05	1.0E-02	1.5E-06	3.6E-06	2	0.714	0.200	0.200
5.7E-05	2.1E-02	3.0E-06	7.1E-06	2	0.714	0.242	0.242
1.1E-04	4.2E-02	6.0E-06	1.4E-05	2	0.714	0.264	0.264
3.4E-04	0.13	1.7E-05	4.0E-05	3	0.571	0.325	0.325
6.8E-04	0.25	3.4E-05	7.7E-05	3	0.571	0.375	0.374
1.4E-03	0.50	6.5E-05	1.5E-04	3	0.571	0.401	0.400
2.7E-03	1.00	1.3E-04	2.8E-04	3	0.571	0.414	0.414
8.2E-03	3.00	3.6E-04	7.8E-04	3	0.571	0.424	0.423
0.019	7.02	8.1E-04	1.7E-03	4	0.429	0.466	0.465
0.042	15.22	1.7E-03	3.5E-03	4	0.429	0.520	0.519
0.083	30.44	3.2E-03	6.5E-03	4	0.429	0.545	0.543
0.250	91.31	9.1E-03	0.018	4	0.429	0.562	0.561
0.500	182.62	0.017	0.034	4	0.429	0.567	0.566
1.000	365.24	0.033	0.063	5	0.286	0.603	0.601
2.000	730.49	0.062	0.114	5	0.286	0.654	0.652
5.000	1826.21	0.134	0.238	5	0.286	0.686	0.684
10	3652.43	0.220	0.374	6	0.143	0.725	0.720
15	5478.64	0.280	0.457	6	0.143	0.754	0.744
20	7304.85	0.324	0.511	7	0.000	0.777	0.763
25	9131.06	0.355	0.546	7	0.000	0.797	0.777
30	10957.28	0.379	0.572	7	0.000	0.810	0.786
35	12783.49	0.398	0.592	7	0.000	0.819	0.793
40	14609.70	0.413	0.605	7	0.000	0.825	0.796
45	16435.91	0.424	0.613	7	0.000	0.830	0.799
50	18262.13	0.431	0.617	7	0.000	0.833	0.800
55	20088.34	0.434	0.619	7	0.000	0.834	0.801
60	21914.55	0.436	0.620	7	0.000	0.834	0.801
Full occ.	Full occ..	1.000	1.000	7	0.000	0.928	0.873

Table S6 - Results of retrospective forecast of first main shocks (declustered targets) with Mw≥5.0 in Italy from 1960 to 2019, using Δt= 3 months (0.25 years).

Year	Month	Day	Lat	Lon	Mw	t_a (days)		Epicentral area
1960	*1*	*11*	*41.300*	*13.983*	*5.0*	*Missed*		*Roccamonfina*
1962	8	21	41.233	14.933	5.7	0.093	2.22 h	Irpinia
1963	2	2	42.400	12.900	5.3	0.046	1.10 h	Reatino
1963	*2*	*13*	*40.500*	*15.583*	*5.3*	*Missed*		*Potentino*
1963	*8*	*9*	*44.367*	*12.100*	*5.4*	*Missed*		*Romagna*
1965	*8*	*19*	*46.100*	*13.100*	*5.2*	*Missed*		*Prealpi friulane*
1967	*4*	*3*	*44.800*	*10.750*	*5.0*	*Missed*		*Reggiano*
1967	*10*	*31*	*37.800*	*14.367*	*5.0*	*Missed*		*Monti Nebrodi*
1967	*12*	*30*	*45.000*	*12.100*	*5.4*	*Missed*		*Emilia Romagna orientale*
1968	*1*	*14*	*37.900*	*13.000*	*5.2*	*Missed*		*Valle del Belice*
1969	*11*	*14*	*40.583*	*15.567*	*5.3*	*Missed*		*Potentino*
1970	*8*	*19*	*43.133*	*10.883*	*5.0*	*Missed*		*Colline Metallifere*
1972	*11*	*26*	*42.900*	*13.267*	*5.2*	*Missed*		*Marche meridionali*
1975	*6*	*19*	*41.650*	*15.733*	*5.1*	*Missed*		*Gargano*
1975	*11*	*16*	*44.617*	*9.433*	*5.0*	*Missed*		*Appennino piacentino*
1976	5	6	46.250	13.250	6.5	7.8×10^{-4}	67 s	Friuli
1977	*9*	*16*	*46.300*	*12.983*	*5.3*	*Missed*		*Friuli*
1978	*9*	*24*	*40.667*	*16.117*	*5.1*	*Missed*		*Materano*
1979	*9*	*19*	*42.717*	*12.950*	*5.8*	*Missed*		*Valnerina*
1980	*6*	*14*	*41.767*	*13.683*	*5.0*	*Missed*		*Marsica*
1980	*11*	*23*	*40.800*	*15.367*	*6.8*	*Missed*		*Irpinia-Basilicata*
1982	*8*	*15*	*40.943*	*15.320*	*5.3*	*Missed*		*Irpinia*
1983	*11*	*9*	*44.653*	*10.342*	*5.0*	*Missed*		*Parmense*
1984	*4*	*29*	*43.204*	*12.585*	*5.6*	*Missed*		*Umbria settentrionale*
1984	*5*	*7*	*41.666*	*13.820*	*5.9*	*Missed*		*Monti della Laga*
1990	5	5	40.650	15.882	5.8	1.5×10^{-4}	13 s	Potentino
1991	*5*	*26*	*40.689*	*15.822*	*5.1*	*Missed*		*Potentino*
1995	*9*	*30*	*41.790*	*15.971*	*5.2*	*Missed*		*Gargano*
1996	*10*	*15*	*44.799*	*10.679*	*5.4*	*Missed*		*Pianura emiliana*
1997	9	26	43.023	12.891	5.7	22.1		*Appennino umbro-marchigiano*
1998	*9*	*9*	*40.060*	*15.949*	*5.5*	*Missed*		*Appennino lucano*
2002	*10*	*31*	*41.717*	*14.893*	*5.7*	*Missed*		*Molise*
2003	*9*	*14*	*44.255*	*11.380*	*5.2*	*Missed*		*Costa croata settentrionale*
2004	*11*	*24*	*45.685*	*10.521*	*5.0*	*Missed*		*Garda occidentale*
2008	*12*	*23*	*44.544*	*10.345*	*5.4*	*Missed*		*Parmense*
2009	4	6	42.342	13.380	6.3	6.5		Aquilano
2012	*1*	*25*	*44.871*	*10.510*	*5.0*	*Missed*		*Pianura emiliana*
2012	*5*	*20*	*44.896*	*11.264*	*6.1*	*Missed*		*Pianura emiliana*
2012	*10*	*25*	*39.875*	*16.016*	*5.3*	*Missed*		*Pollino*
2013	*1*	*25*	*44.164*	*10.446*	*5.0*	*Missed*		*Garfagnana*

Year	Month	Day	Lat	Lon	Mw	t_a (days)	Epicentral area
2013	*12*	*29*	*41.395*	*14.434*	*5.1*	*Missed*	*Matese*
2016	*8*	*24*	*42.698*	*13.234*	*6.2*	*Missed*	*Monti della Laga*
2018	8	16	41.874	14.865	5.3	1.9	Molise
2018	12	26	37.644	15.116	5.2	81.1	Etna sud-orientale

t_a is the maximum time advance of the foreshock with respect to the mainshock. "*Missed*" indicates that the target shock was not forecasted. Epicentral area identifiers are taken from the CPTI15 catalog (Rovida et al., 2016, 2020).

Table S7 – Results of retrospective forecast of not-declustered targets with Mw≥5.0 in Italy from 1960 to 2019, using Δt= 3 months (0.25 years).

Year	Month	Day	Latitude	Longitude	Mw	t_a(days)
1960	*1*	*11*	*41.3000*	*13.9833*	*5.0*	*Missed*
1962	8	21	41.2333	14.9333	5.7	9.26E-02
1962	8	21	41.2333	14.9333	6.2	9.99E-02
1962	8	21	41.1333	15.1167	5.3	1.17E-01
1963	2	2	42.4000	12.9000	5.3	4.59E-02
1963	*2*	*13*	*40.5000*	*15.5833*	*5.3*	*Missed*
1963	*8*	*9*	*44.3667*	*12.1000*	*5.4*	*Missed*
1965	*8*	*19*	*46.1000*	*13.1000*	*5.2*	*Missed*
1967	*4*	*3*	*44.8000*	*10.7500*	*5.0*	*Missed*
1967	*10*	*31*	*37.8000*	*14.3667*	*5.0*	*Missed*
1967	*12*	*30*	*45.0000*	*12.1000*	*5.4*	*Missed*
1968	*1*	*14*	*37.9000*	*13.0000*	*5.2*	*Missed*
1968	1	15	37.8000	13.2000	5.3	4.05E-01
1968	1	15	37.7000	13.1000	5.7	4.25E-01
1968	1	15	37.8000	13.2000	5.5	9.10E-01
1968	1	16	37.7000	13.3000	5.6	2.03E+00
1968	1	25	37.7000	13.1000	5.2	1.07E+01
1968	*6*	*16*	*37.8000*	*14.8000*	*5.2*	*Missed*
1969	*11*	*14*	*40.5833*	*15.5667*	*5.3*	*Missed*
1970	*8*	*19*	*43.1333*	*10.8833*	*5.0*	*Missed*
1972	*11*	*26*	*42.9000*	*13.2667*	*5.2*	*Missed*
1975	*6*	*19*	*41.6500*	*15.7333*	*5.1*	*Missed*
1975	*11*	*16*	*44.6167*	*9.4333*	*5.0*	*Missed*

Year	Month	Day	Latitude	Longitude	Mw	t_a(days)
1976	5	6	46.2500	13.2500	6.5	7.74E-04
1976	5	11	46.2667	13.0167	5.0	5.10E+00
1976	9	11	46.2667	13.1667	5.3	7.71E+01
1976	9	11	46.3000	13.3167	5.6	8.59E+01
1976	9	15	46.2667	13.1500	5.9	8.05E+01
1976	9	15	46.3000	13.1833	6.0	8.08E+01
1976	9	16	46.2800	12.9800	5.5	8.24E+01
1977	*9*	*16*	*46.3000*	*12.9833*	*5.3*	*Missed*
1978	*9*	*24*	*40.6667*	*16.1167*	*5.1*	*Missed*
1979	*9*	*19*	*42.7167*	*12.9500*	*5.8*	*Missed*
1980	*2*	*28*	*42.8000*	*12.9667*	*5.0*	*Missed*
1980	*6*	*14*	*41.7667*	*13.6833*	*5.0*	*Missed*
1980	*11*	*23*	*40.8000*	*15.3667*	*6.8*	*Missed*
1980	11	24	40.8333	15.2833	5.0	2.30E-01
1980	11	24	40.8667	15.3333	5.0	3.41E-01
1980	11	25	40.6333	15.3833	5.4	1.97E+00
1981	1	16	40.8903	15.4398	5.2	5.32E+01
1982	*8*	*15*	*40.9433*	*15.3202*	*5.3*	*Missed*
1983	*11*	*9*	*44.6525*	*10.3423*	*5.0*	*Missed*
1984	*4*	*29*	*43.2040*	*12.5853*	*5.6*	*Missed*
1984	*5*	*7*	*41.6657*	*13.8202*	*5.9*	*Missed*
1984	5	11	41.6502	13.8437	5.5	3.68E+00
1990	5	5	40.6495	15.8818	5.8	1.46E-04
1991	*5*	*26*	*40.6890*	*15.8217*	*5.1*	*Missed*
1995	*9*	*30*	*41.7903*	*15.9712*	*5.2*	*Missed*
1996	*10*	*15*	*44.7988*	*10.6787*	*5.4*	*Missed*
1997	9	26	43.0228	12.8910	5.7	2.21E+01
1997	9	26	43.0147	12.8538	6.0	2.25E+01
1997	10	3	43.0427	12.8245	5.2	2.95E+01
1997	10	6	43.0275	12.8467	5.5	3.31E+01
1997	10	12	42.9062	12.9203	5.2	3.86E+01
1997	10	14	42.8982	12.8987	5.6	4.07E+01
1998	3	21	42.9485	12.9143	5.0	4.27E+01
1998	3	26	43.1458	12.8090	5.3	4.77E+01
1998	4	3	43.1853	12.7568	5.1	5.53E+01
1998	*9*	*9*	*40.0600*	*15.9490*	*5.5*	*Missed*

Year	Month	Day	Latitude	Longitude	Mw	t_a(days)
2002	*10*	*31*	*41.7167*	*14.8932*	*5.7*	*Missed*
2002	*11*	*1*	*41.7415*	*14.8432*	*5.7*	*Missed*
2003	*9*	*14*	*44.2550*	*11.3800*	*5.2*	*Missed*
2004	*11*	*24*	*45.6850*	*10.5210*	*5.0*	*Missed*
2008	*12*	*23*	*44.5440*	*10.3450*	*5.4*	*Missed*
2009	4	6	42.3420	13.3800	6.3	6.50E+00
2009	4	6	42.3600	13.3280	5.1	6.54E+00
2009	4	6	42.4630	13.3850	5.1	7.41E+00
2009	4	7	42.3360	13.3870	5.1	7.83E+00
2009	4	7	42.3030	13.4860	5.5	8.18E+00
2009	4	9	42.4890	13.3510	5.4	9.47E+00
2009	4	9	42.5040	13.3500	5.2	1.03E+01
2009	4	13	42.4980	13.3770	5.0	1.43E+01
2012	*1*	*25*	*44.8710*	*10.5100*	*5.0*	*Missed*
2012	*5*	*20*	*44.8955*	*11.2635*	*6.1*	*Missed*
2012	*5*	*20*	*44.8787*	*11.1202*	*5.0*	*Missed*
2012	*5*	*20*	*44.9052*	*11.1650*	*5.0*	*Missed*
2012	*5*	*20*	*44.8737*	*11.2703*	*5.2*	*Missed*
2012	5	20	44.8597	11.1520	5.0	3.54E-02
2012	5	20	44.8135	11.4407	5.2	4.62E-01
2012	5	29	44.8417	11.0657	5.9	9.18E+00
2012	5	29	44.8652	10.9795	5.5	1.04E-01
2012	5	29	44.8558	10.9410	5.2	1.07E-01
2012	*10*	*25*	*39.8747*	*16.0158*	*5.3*	*Missed*
2013	*1*	*25*	*44.1643*	*10.4458*	*5.0*	*Missed*
2013	*6*	*21*	*44.1308*	*10.1357*	*5.3*	*Missed*
2013	*12*	*29*	*41.3952*	*14.4342*	*5.1*	*Missed*
2016	*8*	*24*	*42.6983*	*13.2335*	*6.2*	*Missed*
2016	8	24	42.7922	13.1507	5.5	2.60E-02
2016	10	26	42.8747	13.1243	5.5	6.35E+01
2016	10	26	42.9048	13.0902	6.1	6.36E+01
2016	10	30	42.8303	13.1092	6.6	6.71E+01
2016	11	1	42.9902	13.1345	5.0	6.91E+01
2017	1	18	42.5450	13.2768	5.3	8.36E+01
2017	1	18	42.5310	13.2838	5.7	4.97E+01
2017	1	18	42.5033	13.2770	5.6	4.97E+01

Year	Month	Day	Latitude	Longitude	Mw	t_a(days)
2017	1	18	42.4733	13.2747	5.2	4.98E+01
2018	8	16	41.8742	14.8648	5.3	1.86E+00
2018	12	26	37.6440	15.1160	5.1	8.11E+01

t_a is the maximum time advance of the foreshock with respect to the mainshock. "*Missed*" indicates that the target shock was not forecasted.

Table S8– Same as Table S6 for not-declustered targets with Mw≥5.5.

Year	Month	Day	Latitude	Longitude	Mw	t_a(days)
1962	8	21	41.2333	14.9333	5.7	9.26E-02
1962	8	21	41.2333	14.9333	6.2	9.99E-02
1968	1	15	37.7000	13.1000	5.7	4.25E-01
1968	1	15	37.8000	13.2000	5.5	9.10E-01
1968	1	16	37.7000	13.3000	5.6	2.03E+00
1976	5	6	46.2500	13.2500	6.5	7.74E-04
1976	9	11	46.3000	13.3167	5.6	8.59E+01
1976	9	15	46.2667	13.1500	5.9	8.05E+01
1976	9	15	46.3000	13.1833	6.0	8.08E+01
1976	9	16	46.2800	12.9800	5.5	8.24E+01
1979	*9*	*19*	*42.7167*	*12.9500*	*5.8*	*Missed*
1980	*11*	*23*	*40.8000*	*15.3667*	*6.8*	*Missed*
1984	*4*	*29*	*43.2040*	*12.5853*	*5.6*	*Missed*
1984	*5*	*7*	*41.6657*	*13.8202*	*5.9*	*Missed*
1984	5	11	41.6502	13.8437	5.5	3.68E+00
1990	5	5	40.6495	15.8818	5.8	1.46E-04
1997	9	26	43.0228	12.8910	5.7	2.21E+01
1997	9	26	43.0147	12.8538	6.0	2.25E+01
1997	10	6	43.0275	12.8467	5.5	3.31E+01
1997	10	14	42.8982	12.8987	5.6	4.07E+01
1998	*9*	*9*	*40.0600*	*15.9490*	*5.5*	*Missed*
2002	*10*	*31*	*41.7167*	*14.8932*	*5.7*	*Missed*
2002	*11*	*1*	*41.7415*	*14.8432*	*5.7*	*Missed*
2009	4	6	42.3420	13.3800	6.3	6.50E+00
2009	4	7	42.3030	13.4860	5.5	8.18E+00
2012	*5*	*20*	*44.8955*	*11.2635*	*6.1*	*Missed*
2012	5	29	44.8417	11.0657	5.9	9.18E+00
2012	5	29	44.8652	10.9795	5.5	1.04E-01
2016	*8*	*24*	*42.6983*	*13.2335*	*6.2*	*Missed*
2016	8	24	42.7922	13.1507	5.5	2.60E-02
2016	10	26	42.8747	13.1243	5.5	6.35E+01
2016	10	26	42.9048	13.0902	6.1	6.36E+01
2016	10	30	42.8303	13.1092	6.6	6.71E+01
2017	1	18	42.5310	13.2838	5.7	4.97E+01
2017	1	18	42.5033	13.2770	5.6	4.97E+01

Table S9 – Same as Table S6 for not-declustered targets with Mw≥6.0.

Year	Month	Day	Latitude	Longitude	Mw	t_a (days)
1962	8	21	41.2333	14.9333	6.2	9.99E-02
1976	5	6	46.2500	13.2500	6.5	7.74E-04
1976	9	15	46.3000	13.1833	6.0	8.08E+01
1980	*11*	*23*	*40.8000*	*15.3667*	*6.8*	*Missed*
1997	9	26	43.0147	12.8538	6.0	2.25E+01
2009	4	6	42.3420	13.3800	6.3	6.50E+00
2012	*5*	*20*	*44.8955*	*11.2635*	*6.1*	*Missed*
2016	*8*	*24*	*42.6983*	*13.2335*	*6.2*	*Missed*
2016	10	26	42.9048	13.0902	6.1	6.36E+01
2016	10	30	42.8303	13.1092	6.6	6.71E+01

Supplementary material 2

Analysis and comparisons of FORE, EEPAS, and ETAS models using the alarm-based approach

Table S1 – List of center coordinates of cells with side $30\sqrt{2}$ km. $N_{4.5}$, $N_{5.0}$, $N_{5.5}$, $N_{6.0}$: numbers of earthquakes occurred within cell, according to the CPTI15 catalogue up to year 1959, with Mw≥4.5, 5.0, 5.5 and 6.0 respectively in respective time intervals of completeness. $\lambda_{4.5}$, $\lambda_{5.0}$, $\lambda_{5.5}$, $\lambda_{6.0}$: average rates (events/y) of earthquakes with Mw≥4.0 within each cell computed from observed earthquakes with Mw≥4.5, 5.0, 5.5 and 6.0 respectively and assuming a b-value=1 (see text). λ_{ave}: average of non-null rates $\lambda_{4.5}$, $\lambda_{5.0}$, $\lambda_{5.5}$, $\lambda_{6.0}$. $w = \lambda_{ave} / \sum \lambda_{ave}$: overall weight of each cell ($\sum w = 1$).

Nc	Latitude	Longitude	$N_{4.5}$	$N_{5.0}$	$N_{5.5}$	$N_{6.0}$	$\lambda_{4.5}$	$\lambda_{5.0}$	$\lambda_{5.5}$	$\lambda_{6.0}$	λ_{ave}	w
1	46.8073	10.5448	1	-	0	0	0.0395	-	-	-	0.0395	0.001490
2	46.8130	11.1014	2	1	0	0	0.0791	0.1250	-	-	0.1020	0.003845
3	46.8163	12.2148	0	0	0	0	-	-	-	-	0.0395	0.001490
4	46.3759	8.3471	0	0	0	0	-	-	-	-	0.0395	0.001490
5	46.4252	10.5550	2	0	0	0	0.0791	-	-	-	0.0791	0.002979
6	46.4341	12.2133	1	0	0	0	0.0395	-	-	-	0.0395	0.001490
7	46.4317	12.7662	10	6	2	1	0.3953	0.7500	0.3514	0.2941	0.4477	0.016871
8	46.4267	13.3189	10	4	1	0	0.3953	0.5000	0.1757	-	0.3570	0.013453
9	45.9544	7.2787	2	1	0	0	0.0791	0.1250	-	-	0.1020	0.003845
10	45.9944	8.3723	0	0	0	0	-	-	-	-	0.0395	0.001490
11	46.0240	9.4679	0	0	0	0	-	-	-	-	0.0395	0.001490
12	46.0348	10.0163	1	0	0	0	0.0395	-	-	-	0.0395	0.001490
13	46.0430	10.5650	1	0	0	0	0.0395	-	-	-	0.0395	0.001490
14	46.0486	11.1138	0	0	0	0	-	-	-	-	0.0395	0.001490
15	46.0515	11.6628	1	1	0	1	0.0395	0.1250	-	0.2941	0.1529	0.005761
16	46.0518	12.2118	6	1	2	2	0.2372	0.1250	0.3514	0.5882	0.3254	0.012264
17	46.0495	12.7608	2	0	1	0	0.0791	-	0.1757	-	0.1274	0.004800
18	46.0445	13.3097	2	1	0	0	0.0791	0.1250	-	-	0.1020	0.003845
19	46.0369	13.8585	1	0	0	0	0.0395	-	-	-	0.0395	0.001490
20	45.5734	7.3108	0	0	0	0	-	-	-	-	0.0395	0.001490
21	45.5944	7.8536	3	0	0	0	0.1186	-	-	-	0.1186	0.004469
22	45.6288	8.9409	1	0	0	0	0.0395	-	-	-	0.0395	0.001490
23	45.6421	9.4852	1	0	0	0	0.0395	-	-	-	0.0395	0.001490
24	45.6528	10.0298	3	0	0	0	0.1186	-	-	-	0.1186	0.004469
25	45.6609	10.5748	7	3	0	0	0.2767	0.3750	-	-	0.3258	0.012279
26	45.6664	11.1199	4	1	1	0	0.1581	0.1250	0.1757	-	0.1529	0.005763
27	45.6693	11.6651	3	1	1	0	0.1186	0.1250	0.1757	-	0.1398	0.005267
28	45.6696	12.2104	1	1	0	0	0.0395	0.1250	-	-	0.0823	0.003100
29	45.6673	12.7557	0	0	0	0	-	-	-	-	0.0395	0.001490
30	45.1691	6.8036	0	0	0	0	-	-	-	-	0.0395	0.001490
31	45.1924	7.3422	3	2	0	0	0.1186	0.2500	-	-	0.1843	0.006945

Nc	Latitude	Longitude	$N_{4.5}$	$N_{5.0}$	$N_{5.5}$	$N_{6.0}$	$\lambda_{4.5}$	$\lambda_{5.0}$	$\lambda_{5.5}$	$\lambda_{6.0}$	λ_{ave}	w
32	45.2470	8.9615	0	0	0	0	-	-	-	-	0.0395	0.001490
33	45.2601	9.5021	1	1	0	0	0.0395	0.1250	-	-	0.0823	0.003100
34	45.2707	10.0431	1	1	1	0	0.0395	0.1250	0.1757	-	0.1134	0.004274
35	45.2787	10.5844	1	0	0	0	0.0395	-	-	-	0.0395	0.001490
36	45.2841	11.1258	1	0	0	0	0.0395	-	-	-	0.0395	0.001490
37	45.2870	11.6674	0	0	0	0	-	-	-	-	0.0395	0.001490
38	44.8113	7.3731	1	0	1	0	0.0395	-	0.1757	-	0.1076	0.004055
39	44.8318	7.9088	0	0	0	0	-	-	-	-	0.0395	0.001490
40	44.8497	8.4450	0	0	0	0	-	-	-	-	0.0395	0.001490
41	44.8652	8.9816	4	1	1	0	0.1581	0.1250	0.1757	-	0.1529	0.005763
42	44.8782	9.5187	0	0	0	0	-	-	-	-	0.0395	0.001490
43	44.8886	10.0561	2	1	0	0	0.0791	0.1250	-	-	0.1020	0.003845
44	44.8965	10.5938	3	0	1	0	0.1186	-	0.1757	-	0.1471	0.005545
45	44.9018	11.1316	1	0	0	0	0.0395	-	-	-	0.0395	0.001490
46	44.9046	11.6696	1	0	0	0	0.0395	-	-	-	0.0395	0.001490
47	44.9049	12.2076	1	0	0	0	0.0395	-	-	-	0.0395	0.001490
48	44.4075	6.8717	2	1	0	0	0.0791	0.1250	-	-	0.1020	0.003845
49	44.4302	7.4033	5	0	0	0	0.1976	-	-	-	0.1976	0.007448
50	44.4681	8.4682	0	0	0	0	-	-	-	-	0.0395	0.001490
51	44.4834	9.0014	1	0	0	0	0.0395	-	-	-	0.0395	0.001490
52	44.4961	9.5350	2	1	0	0	0.0791	0.1250	-	-	0.1020	0.003845
53	44.5064	10.0689	4	2	1	0	0.1581	0.2500	0.1757	-	0.1946	0.007333
54	44.5142	10.6030	3	2	0	0	0.1186	0.2500	-	-	0.1843	0.006945
55	44.5195	11.1373	13	7	0	0	0.5139	0.8750	-	-	0.6944	0.026169
56	44.5223	11.6718	7	1	0	0	0.2767	0.1250	-	-	0.2008	0.007569
57	44.5226	12.2062	2	0	0	0	0.0791	-	-	-	0.0791	0.002979
58	44.0490	7.4330	0	0	0	0	-	-	-	-	0.0395	0.001490
59	44.0689	7.9618	2	1	1	1	0.0791	0.1250	0.1757	0.2941	0.1685	0.006348
60	44.0865	8.4911	0	0	0	0	-	-	-	-	0.0395	0.001490
61	44.1243	10.0814	9	4	3	1	0.3558	0.5000	0.5270	0.2941	0.4192	0.015798
62	44.1319	10.6121	8	1	0	0	0.3162	0.1250	-	-	0.2206	0.008314
63	44.1372	11.1429	4	1	0	0	0.1581	0.1250	-	-	0.1416	0.005334
64	44.1399	11.6739	16	4	2	3	0.6325	0.5000	0.3514	0.8824	0.5915	0.022292
65	44.1402	12.2049	5	2	2	0	0.1976	0.2500	0.3514	-	0.2663	0.010037
66	44.1380	12.7359	18	11	4	0	0.7115	1.3750	0.7027	-	0.9297	0.035037
67	43.6875	7.9875	0	0	1	0	-	-	0.1757	-	0.1757	0.006620
68	43.7421	10.0936	0	0	0	0	-	-	-	-	0.0395	0.001490
69	43.7496	10.6209	2	1	1	0	0.0791	0.1250	0.1757	-	0.1266	0.004770
70	43.7548	11.1484	5	1	1	0	0.1976	0.1250	0.1757	-	0.1661	0.006260
71	43.7575	11.6760	5	1	1	0	0.1976	0.1250	0.1757	-	0.1661	0.006260
72	43.7578	12.2036	3	2	0	0	0.1186	0.2500	-	-	0.1843	0.006945
73	43.7556	12.7312	3	1	1	1	0.1186	0.1250	0.1757	0.2941	0.1783	0.006721
74	43.7510	13.2587	3	3	1	0	0.1186	0.3750	0.1757	-	0.2231	0.008407
75	43.3598	10.1056	1	0	0	0	0.0395	-	-	-	0.0395	0.001490
76	43.3673	10.6296	2	0	1	1	0.0791	-	0.1757	0.2941	0.1830	0.006894
77	43.3724	11.1538	2	1	0	0	0.0791	0.1250	-	-	0.1020	0.003845
78	43.3751	11.6780	0	0	0	0	-	-	-	-	0.0395	0.001490
79	43.3753	12.2023	3	2	2	0	0.1186	0.2500	0.3514	-	0.2400	0.009044
80	43.3732	12.7266	0	0	0	2	-	-	-	0.5882	0.5882	0.022167
81	43.3687	13.2507	0	0	1	2	-	-	0.1757	0.5882	0.3820	0.014394
82	43.3618	13.7748	1	0	0	0	0.0395	-	-	-	0.0395	0.001490
83	42.9850	10.6381	0	0	0	0	-	-	-	-	0.0395	0.001490
84	42.9900	11.1590	2	2	0	0	0.0791	0.2500	-	-	0.1645	0.006200

Nc	Latitude	Longitude	$N_{4.5}$	$N_{5.0}$	$N_{5.5}$	$N_{6.0}$	$\lambda_{4.5}$	$\lambda_{5.0}$	$\lambda_{5.5}$	$\lambda_{6.0}$	λ_{ave}	w
85	42.9926	11.6800	6	1	0	0	0.2372	0.1250	-	-	0.1811	0.006824
86	42.9929	12.2010	1	0	0	0	0.0395	-	-	-	0.0395	0.001490
87	42.9908	12.7220	5	1	3	1	0.1976	0.1250	0.5270	0.2941	0.2860	0.010776
88	42.9863	13.2430	12	3	3	0	0.4743	0.3750	0.5270	-	0.4588	0.017289
89	42.9795	13.7637	2	2	1	0	0.0791	0.2500	0.1757	-	0.1682	0.006340
90	42.6101	11.6820	3	1	0	0	0.1186	0.1250	-	-	0.1218	0.004590
91	42.6104	12.1998	1	0	0	0	0.0395	-	-	-	0.0395	0.001490
92	42.6083	12.7176	13	2	1	0	0.5139	0.2500	0.1757	-	0.3132	0.011802
93	42.6039	13.2353	12	6	3	4	0.4743	0.7500	0.5270	1.1765	0.7320	0.027584
94	42.5972	13.7529	1	0	0	0	0.0395	-	-	-	0.0395	0.001490
95	42.2276	11.6839	0	0	0	0	-	-	-	-	0.0395	0.001490
96	42.2279	12.1986	0	0	0	0	-	-	-	-	0.0395	0.001490
97	42.2258	12.7133	4	2	1	0	0.1581	0.2500	0.1757	-	0.1946	0.007333
98	42.2215	13.2278	7	2	1	0	0.2767	0.2500	0.1757	-	0.2341	0.008823
99	42.2148	13.7423	1	1	0	0	0.0395	0.1250	-	-	0.0823	0.003100
100	42.2059	14.2565	5	5	1	1	0.1976	0.6250	0.1757	0.2941	0.3231	0.012176
101	42.1946	14.7705	0	0	0	0	-	-	-	-	0.0395	0.001490
102	41.8454	12.1974	1	0	0	0	0.0395	-	-	-	0.0395	0.001490
103	41.8433	12.7090	8	3	1	0	0.3162	0.3750	0.1757	-	0.2890	0.010890
104	41.8390	13.2205	5	1	0	0	0.1976	0.1250	-	-	0.1613	0.006079
105	41.8325	13.7319	12	4	1	1	0.4743	0.5000	0.1757	0.2941	0.3610	0.013605
106	41.8236	14.2430	1	1	0	0	0.0395	0.1250	-	-	0.0823	0.003100
107	41.8125	14.7540	0	0	0	0	-	-	-	-	0.0395	0.001490
108	41.7991	15.2645	4	0	1	2	0.1581	-	0.1757	0.5882	0.3073	0.011582
109	41.7835	15.7748	9	6	1	1	0.3558	0.7500	0.1757	0.2941	0.3939	0.014843
110	41.7655	16.2846	3	2	0	0	0.1186	0.2500	-	-	0.1843	0.006945
111	41.4608	12.7048	1	1	0	0	0.0395	0.1250	-	-	0.0823	0.003100
112	41.4566	13.2133	0	0	0	0	-	-	-	-	0.0395	0.001490
113	41.4501	13.7217	3	0	0	1	0.1186	-	-	0.2941	0.2064	0.007776
114	41.4413	14.2298	4	2	1	1	0.1581	0.2500	0.1757	0.2941	0.2195	0.008271
115	41.4304	14.7377	3	1	0	1	0.1186	0.1250	-	0.2941	0.1792	0.006754
116	41.4172	15.2453	0	0	0	0	-	-	-	-	0.0395	0.001490
117	41.4017	15.7526	6	2	1	1	0.2372	0.2500	0.1757	0.2941	0.2392	0.009016
118	41.3840	16.2594	0	0	0	0	-	-	-	-	0.0395	0.001490
119	41.0741	13.2062	0	0	0	0	-	-	-	-	0.0395	0.001490
120	41.0590	14.2169	0	0	0	0	-	-	-	-	0.0395	0.001490
121	41.0482	14.7218	4	0	0	0	0.1581	-	-	-	0.1581	0.005958
122	41.0352	15.2265	6	3	2	4	0.2372	0.3750	0.3514	1.1765	0.5350	0.020161
123	41.0199	15.7308	1	0	1	1	0.0395	-	0.1757	0.2941	0.1698	0.006398
124	41.0025	16.2347	0	0	0	0	-	-	-	-	0.0395	0.001490
125	40.9829	16.7381	0	0	0	0	-	-	-	-	0.0395	0.001490
126	40.6915	13.1993	1	0	0	0	0.0395	-	-	-	0.0395	0.001490
127	40.6852	13.7018	0	0	0	0	-	-	-	-	0.0395	0.001490
128	40.6767	14.2041	0	0	0	0	-	-	-	-	0.0395	0.001490
129	40.6660	14.7062	2	0	0	0	0.0791	-	-	-	0.0791	0.002979
130	40.6532	15.2080	2	1	1	0	0.0791	0.1250	0.1757	-	0.1266	0.004770
131	40.6381	15.7094	2	1	1	0	0.0791	0.1250	0.1757	-	0.1266	0.004770
132	40.6209	16.2104	2	1	0	0	0.0791	0.1250	-	-	0.1020	0.003845
133	40.6015	16.7110	1	0	0	0	0.0395	-	-	-	0.0395	0.001490
134	40.5800	17.2110	0	0	0	0	-	-	-	-	0.0395	0.001490
135	40.5563	17.7105	0	0	0	0	-	-	-	-	0.0395	0.001490
136	40.2711	15.1898	0	0	0	0	-	-	-	-	0.0395	0.001490
137	40.2563	15.6884	0	0	3	1	-	-	0.5270	0.2941	0.4106	0.015473

Nc	Latitude	Longitude	$N_{4.5}$	$N_{5.0}$	$N_{5.5}$	$N_{6.0}$	$\lambda_{4.5}$	$\lambda_{5.0}$	$\lambda_{5.5}$	$\lambda_{6.0}$	λ_{ave}	w
138	40.2393	16.1867	3	1	0	0	0.1186	0.1250	-	-	0.1218	0.004590
139	40.1501	18.1745	1	0	0	0	0.0395	-	-	-	0.0395	0.001490
140	39.8744	15.6679	0	0	0	0	-	-	-	-	0.0395	0.001490
141	39.8576	16.1633	1	1	0	0	0.0395	0.1250	-	-	0.0823	0.003100
142	39.8388	16.6583	1	1	0	0	0.0395	0.1250	-	-	0.0823	0.003100
143	39.4760	16.1404	4	3	4	0	0.1581	0.3750	0.7027	-	0.4119	0.015524
144	39.4574	16.6328	1	0	1	2	0.0395	-	0.1757	0.5882	0.2678	0.010092
145	39.4367	17.1246	0	0	0	0	-	-	-	-	0.0395	0.001490
146	39.0942	16.1180	1	0	2	3	0.0395	-	0.3514	0.8824	0.4244	0.015994
147	39.0759	16.6076	2	0	0	0	0.0791	-	-	-	0.0791	0.002979
148	39.0555	17.0968	0	0	1	1	-	-	0.1757	0.2941	0.2349	0.008852
149	38.7546	14.6325	2	2	0	0	0.0791	0.2500	-	-	0.1645	0.006200
150	38.7426	15.1206	5	2	0	0	0.1976	0.2500	-	-	0.2238	0.008435
151	38.7125	16.0960	6	2	4	4	0.2372	0.2500	0.7027	1.1765	0.5916	0.022294
152	38.6944	16.5830	1	1	2	2	0.0395	0.1250	0.3514	0.5882	0.2760	0.010402
153	38.3723	14.6186	3	1	0	0	0.1186	0.1250	-	-	0.1218	0.004590
154	38.3604	15.1041	0	0	0	0	-	-	-	-	0.0395	0.001490
155	38.3465	15.5894	5	1	0	0	0.1976	0.1250	-	-	0.1613	0.006079
156	38.3307	16.0743	3	1	2	2	0.1186	0.1250	0.3514	0.5882	0.2958	0.011147
157	38.3128	16.5589	0	0	0	0	-	-	-	-	0.0395	0.001490
158	38.0186	12.1867	0	0	0	0	-	-	-	-	0.0395	0.001490
159	38.0168	12.6706	0	0	0	0	-	-	-	-	0.0395	0.001490
160	38.0131	13.1544	0	0	0	0	-	-	-	-	0.0395	0.001490
161	38.0073	13.6381	2	2	0	0	0.0791	0.2500	-	-	0.1645	0.006200
162	37.9996	14.1216	1	1	1	0	0.0395	0.1250	0.1757	-	0.1134	0.004274
163	37.9899	14.6049	1	0	0	0	0.0395	-	-	-	0.0395	0.001490
164	37.9782	15.0880	3	1	2	1	0.1186	0.1250	0.3514	0.2941	0.2223	0.008376
165	37.9645	15.5707	4	2	1	1	0.1581	0.2500	0.1757	0.2941	0.2195	0.008271
166	37.9488	16.0531	2	1	1	0	0.0791	0.1250	0.1757	-	0.1266	0.004770
167	37.6340	12.6671	0	0	0	0	-	-	-	-	0.0395	0.001490
168	37.6303	13.1484	0	0	0	0	-	-	-	-	0.0395	0.001490
169	37.6247	13.6296	0	0	0	0	-	-	-	-	0.0395	0.001490
170	37.6170	14.1107	1	0	0	0	0.0395	-	-	-	0.0395	0.001490
171	37.6074	14.5915	3	1	0	0	0.1186	0.1250	-	-	0.1218	0.004590
172	37.5959	15.0721	4	1	2	1	0.1581	0.1250	0.3514	0.2941	0.2321	0.008748
173	37.2344	14.0999	0	0	0	0	-	-	-	-	0.0395	0.001490
174	37.2250	14.5783	3	1	1	0	0.1186	0.1250	0.1757	-	0.1398	0.005267
175	37.2136	15.0565	2	1	0	2	0.0791	0.1250	-	0.5882	0.2641	0.009952
176	36.8425	14.5654	1	1	0	0	0.0395	0.1250	-	-	0.0823	0.003100
177	36.8313	15.0412	0	0	0	0	-	-	-	-	0.0395	0.001490

Table S2 – Values Area Skill score and unweighted $(\tau_{u\ 1yr})$ and weighted $(\tau_{w\ 1yr})$ fractions of space-time occupied by alarms considering the duration of each alarm equal to 1 year obtained for each analyzed threshold soil for the EEPAS-NW and ETAS-SVP models plotted in Figs. 5.2 and 5.3 (section 5.4).

	EEPAS-NW			ETAS-SVP		
Threshold soil	**AS score**	$\tau_{u\ 1yr}$	$\tau_{w\ 1yr}$	**AS score**	τ_u	$\tau_{w\ 1yr}$
1.00E-06	0.791	0.999	0.999	0.851	0.961	0.988
2.00E-06	0.801	0.954	0.989	0.858	0.896	0.959
3.00E-06	0.812	0.900	0.978	0.870	0.840	0.931
4.00E-06	0.824	0.842	0.964	0.884	0.794	0.903
5.00E-06	0.836	0.786	0.946	0.881	0.758	0.879
6.00E-06	0.847	0.734	0.921	0.866	0.724	0.854
7.00E-06	0.803	0.672	0.891	0.871	0.696	0.835
8.00E-06	0.819	0.604	0.847	0.864	0.674	0.817
9.00E-06	0.800	0.566	0.819	0.871	0.652	0.799
1.00E-05	0.810	0.529	0.792	0.877	0.634	0.786
2.00E-05	0.824	0.270	0.550	0.882	0.520	0.689
3.00E-05	0.846	0.166	0.434	0.883	0.463	0.636
4.00E-05	0.786	0.114	0.350	0.893	0.424	0.597
5.00E-05	0.692	0.087	0.307	0.899	0.393	0.567
6.00E-05	0.698	0.070	0.270	0.903	0.367	0.542
7.00E-05	0.704	0.053	0.227	0.908	0.347	0.519
8.00E-05	0.705	0.049	0.209	0.909	0.331	0.501
9.00E-05	0.708	0.042	0.181	0.907	0.318	0.485
0.0001	0.708	0.031	0.140	0.910	0.305	0.470
0.0002	0.500	0.000	0.000	0.930	0.225	0.365
0.0003	0.500	0.000	0.000	0.892	0.187	0.316
0.0004	0.500	0.000	0.000	0.874	0.162	0.281
0.0005	0.500	0.000	0.000	0.865	0.144	0.256
0.0006	0.500	0.000	0.000	0.864	0.131	0.238
0.0007	0.500	0.000	0.000	0.867	0.121	0.223
0.0008	0.500	0.000	0.000	0.871	0.112	0.210
0.0009	0.500	0.000	0.000	0.856	0.105	0.199
0.001	0.500	0.000	0.000	0.860	0.100	0.190
0.002	0.500	0.000	0.000	0.847	0.069	0.145
0.003	0.500	0.000	0.000	0.846	0.056	0.125
0.004	0.500	0.000	0.000	0.813	0.047	0.110
0.005	0.500	0.000	0.000	0.823	0.039	0.097
0.006	0.500	0.000	0.000	0.830	0.035	0.089
0.007	0.500	0.000	0.000	0.833	0.031	0.081
0.008	0.500	0.000	0.000	0.835	0.028	0.077
0.009	0.500	0.000	0.000	0.843	0.025	0.072

	EEPAS-NW			ETAS-SVP		
Threshold soil	**AS score**	$\tau_{u\ 1yr}$	$\tau_{w\ 1yr}$	**AS score**	τ_u	$\tau_{w\ 1yr}$
0.01	0.500	0.000	0.000	0.847	0.022	0.066
0.02	0.500	0.000	0.000	0.834	0.010	0.038
0.03	0.500	0.000	0.000	0.821	0.006	0.027
0.04	0.500	0.000	0.000	0.793	0.004	0.018
0.05	0.500	0.000	0.000	0.799	0.003	0.014
0.06	0.500	0.000	0.000	0.799	0.003	0.013
0.07	0.500	0.000	0.000	0.803	0.002	0.010
0.08	0.500	0.000	0.000	0.807	0.001	0.008
0.09	0.500	0.000	0.000	0.770	0.001	0.007
0.1	0.500	0.000	0.000	0.770	0.001	0.005
0.2	0.500	0.000	0.000	0.719	0.000	0.001
0.3	0.500	0.000	0.000	0.682	0.000	0.001
0.4	0.500	0.000	0.000	0.574	0.000	0.000
0.5	0.500	0.000	0.000	0.555	0.000	0.000

Table S3 – Same of Table S2 for the FORE model (Fig. 5.4 of section 5.4)

FORE			
Magnitude range	**AS score**	$\tau_{u\ 1yr}$	$\tau_{w\ 1yr}$
4.1±0.1	0.859	0.024	0.066
4.2±0.1	0.863	0.022	0.061
4.3±0.1	0.880	0.019	0.059
4.4±0.1	0.837	0.016	0.044
4.5±0.1	0.818	0.010	0.026
4.6±0.1	0.726	0.010	0.027
4.7±0.1	0.734	0.008	0.020
4.8±0.1	0.747	0.008	0.020
4.9±0.1	0.709	0.004	0.012
4.2±0.2	0.865	0.035	0.093
4.3±0.2	0.874	0.029	0.074
4.4±0.2	0.877	0.024	0.065
4.5±0.2	0.844	0.019	0.054
4.6±0.2	0.833	0.014	0.037
4.7±0.2	0.740	0.011	0.028
4.8±0.2	0.750	0.009	0.022
4.3±0.3	0.860	0.040	0.099
4.4±0.3	0.885	0.032	0.083
4.5±0.3	0.888	0.028	0.076
4.6±0.3	0.839	0.022	0.059
4.7±0.3	0.836	0.015	0.039
4.4±0.4	0.870	0.042	0.104
4.5±0.4	0.882	0.035	0.087
4.6±0.4	0.886	0.028	0.077
4.5±0.5	0.869	0.043	0.105

List of main figures and tables

Chapter 1:

Chapter 2:

Chapter 3:

Chapter 4:

Figure 4.4: *(Upper frame) Log-likelihood of the sub-catalogue of earthquakes that occurred in the period 1990 - April 2000 under the time-independent SVP model obtained by the seismicity from April 2000 to 2011. (Lower frame) Log-likelihood of the sub-catalogue of earthquakes that occurred in the period April 2000 to 2011 under the time-independent SVP model obtained by the seismicity from 1990 - April 2000.*

Figure 4.5*: Number of target events* $(M \geq 5.0)$ *reported in the CPTI15 earthquake catalogue (from 1880 to 1959) and in the HORUS seismic catalogue (from 1960 to 2021) in non-overlapped 10-year intervals for mainshocks+aftershocks and mainshocks only.*

Figure 4.6*: Numbers of targets (mainshocks+aftershocks) in the testing set (2012-2021) predicted by various models using different prediction intervals.*

Figure 4.7*: Results of number consistency test (N-test) in the testing set (2012-2021) for various models using different prediction intervals (mainshocks+aftershocks).*

Figure 4.8*: Results of conditional likelihood consistency test (cL-test) in the testing set (2012-2021) for various models using different prediction intervals (mainshocks+aftershocks).*

Figure 4.9*: Results of spatial consistency test (S-test) in the testing set (2012-2021) for various models using different prediction intervals (mainshocks+aftershocks).*

Figure 4.10*: Comparison between various models in different time intervals (mainshocks+aftershocks) in the testing set (2012-2021) by the IGPA (T-test).*

Figure 4.11: *Numbers of targets (mainshocks only) in the testing set (2012-2021) predicted by various models and prediction intervals.*

Figure 4.12*: Results of number consistency test (N-test) in the testing set (2012-2021) for various models using different prediction intervals (mainshocks only).*

Figure 4.13*: Results of conditional likelihood consistency test (cL-test) in the testing set (2012-2021) for various models using different time intervals (mainshocks only).*

Chapter 5:

Acknowledgements

The doctoral years represent a unique and challenging, but at the same time very rewarding experience. I would like to express my deep gratitude to all the people who supported me during this journey and allowed me to reach this important milestone.

First, I would like to thank my supervisor, Prof. Paolo Gasperini, for his guidance, support and great expertise in the field of statistical seismology. Thanks to his expertise and constant encouragement, I have been able to learn a great deal and face the challenges of my PhD with more confidence.

I would also like to thank Barbara Lolli, Laura Gulia, and Gianfranco Vannucci for their valuable contributions, motivation, and valuable advice. Their support was crucial to the success of my research.

Special thanks go to Danijel Schorlemmer, with whom I had the privilege of working and sharing moments of study and fun in Potsdam. His expertise and passion for the work enabled us to achieve important results.

I would also like to express my gratitude to Professor David A. Rhoades for his contribution, advice, and valuable guidance in understanding and applying the EEPAS model in Italy, which I worked on extensively during my PhD.

I also want to thank the European H2020 RISE project, which funded my PhD fellowship, and especially the coordinator Professor Stefan Wiemer for his trust and support.

I cannot forget to thank the people I love and who have supported me during this life journey: my family, my mother Barbara and father Maurizio, and my brother Mirko, who have always encouraged and supported me at every stage of my life.

Finally, I want to express my gratitude to Patrick, the special person who has always supported and encouraged me during my doctorate, thanks to his constant presence and support.

References

Agnew, D. C., and L. M. Jones, 1991, Prediction probabilities from foreshocks, J. Geophys. Res., 96, no. B7, 11959, doi: 10.1029/91JB00191.

Akaike, H., 1974, A new look at the statistical model identification, IEEE Trans. Autom. Control, 19, no. 6, 716–723, doi: 10.1109/TAC.1974.1100705.

Akaike, H., 1998, Information Theory and an Extension of the Maximum Likelihood Principle, in *Selected Papers of Hirotugu Akaike* E. Parzen, K. Tanabe, and G. Kitagawa (Editors), Springer, New York, NY, Springer Series in Statistics, 199–213.

Aki, K., 1965, Maximum likelihood estimate of b in the formula log N = a−bM and its confidence limits, Bullettin Earthq. Res. Inst., 43, 237–239.

Aki, K., 1956, Some Problems in Statistical Seismology, Zisin J. Seismol. Soc. Jpn. 2nd Ser, 8, no. 4, 205–228, doi: 10.4294/zisin1948.8.4_205.

Allen, C. R., 1976, Responsibilities in earthquake prediction, Bull. Seismol. Soc. Am., 66, no. 6, 2069–2074.

Amorese, D., 2007, Applying a Change-Point Detection Method on Frequency-Magnitude Distributions, Bull. Seismol. Soc. Am., 97, no. 5, 1742–1749, doi: 10.1785/0120060181.

Antonioli, A., M. E. Belardinelli, and M. Cocco, 2004, Modelling dynamic stress changes caused by an extended rupture in an elastic stratified half-space, Geophys. J. Int., 157, no. 1, 229–244, doi: 10.1111/j.1365-246X.2004.02170.x.

Armstrong, J. S., 2001, Evaluating Forecasting Methods, in *Principles of Forecasting* J. S. Armstrong (Editor), Springer US, Boston, MA, International Series in Operations Research & Management Science, 443–472.

Azarbakht, A., A. Rudman, and J. Douglas, 2021, A decision-making approach for operational earthquake forecasting, Int. J. Disaster Risk Reduct., 66, 102591, doi: 10.1016/j.ijdrr.2021.102591.

Båth, M., 1965, Lateral inhomogeneities of the upper mantle, Tectonophysics, 2, no. 6, 483–514, doi: https://doi.org/10.1016/0040-1951(65)90003-X.

Bayona, J. A., W. H. Savran, D. A. Rhoades, and M. J. Werner, 2022, Prospective evaluation of multiplicative hybrid earthquake forecasting models in California, Geophys. J. Int., 229, no. 3, 1736–1753, doi: 10.1093/gji/ggac018.

Bayona, J A, W. H. Savran, D. A. Rhoades, and M. J. Werner, 2022, Prospective evaluation of multiplicative hybrid earthquake forecasting models in California, Geophys. J. Int., 229, no. 3, 1736–1753, doi: 10.1093/gji/ggac018.

Bender, B., 1983, Maximum likelihood estimation of b values for magnitude grouped data, Bull. Seismol. Soc. Am., 73, no. 3, 831–851, doi: 10.1785/BSSA0730030831.

Byrd, R. H., M. E. Hribar, and J. Nocedal, 1999, An Interior Point Algorithm for Large-Scale Nonlinear Programming, SIAM J. Optim., 9, no. 4, 877–900.

Cao, A., and S. S. Gao, 2002, Temporal variation of seismic *b* -values beneath northeastern Japan island arc: TEMPORAL VARIATIONS IN B-VALUES, Geophys. Res. Lett., 29, no. 9, 48-1-48–3, doi: 10.1029/2001GL013775.

Caputo, M., R. Console, A. M. Gabrielov, V. I. Keilis-Borok, and T. V. Sidorenko, 1983, Long-term premonitory seismicity patterns in Italy, Geophys. J. Int., 75, no. 1, 71–75, doi: 10.1111/j.1365-246X.1983.tb01913.x.

Caputo, M., P. Gasperini, V. Keilis-Borok, L. Marcelli, and I. Rotwain, 1977, Earthquake's swarms as forerunners of strong earthquakes in Italy, Ann. Geophys., 30, nos. 3–4, doi: 10.4401/ag-4823.

Cicerone, R. D., J. E. Ebel, and J. Britton, 2009, A systematic compilation of earthquake precursors, Tectonophysics, 476, nos. 3–4, 371–396, doi: 10.1016/j.tecto.2009.06.008.

Console, R., F. D. Luccio, M. Murru, M. Imoto, and G. Stavrakakis, 1999, Short Term and Short Range Seismicity Patterns in Different Seismic Areas of the World, Nat. Hazard, 19, 107–121.

Console, R., and M. Murru, 2001, A simple and testable model for earthquake clustering, J. Geophys. Res. Solid Earth, 106, no. B5, 8699–8711, doi: 10.1029/2000JB900269.

Console, R., and M. Murru, 1996, Probability Gain due to Foreshocks following Quiescence Tested by Synthetic Catalogs, Bull. Seismol. Soc. Am., 86, no. 3, 911–913, doi: 10.1785/BSSA0860030911.

Console, R., M. Murru, and B. Alessandrini, 1993, Foreshock statistics and their possible relationship to earthquake prediction in the italian region, Bull. Seismol. Soc. Am., 83, no. 4, 1248–1263.

Console, R., M. Murru, and F. Catalli, 2006, Physical and stochastic models of earthquake clustering, Tectonophysics, 417, nos. 1–2, 141–153, doi: 10.1016/j.tecto.2005.05.052.

Console, R., M. Murru, and G. Falcone, 2010, Retrospective Forecasting of M ≥ 4.0 Earthquakes in New Zealand, Pure Appl. Geophys., 167, nos. 6–7, 693–707, doi: 10.1007/s00024-010-0068-2.

Console, R., M. Murru, and A. M. Lombardi, 2003, Refining earthquake clustering models, J. Geophys. Res. Solid Earth, 108, no. B10, doi: 10.1029/2002JB002130.

Cornell, C. A., 1968, Engineering seismic risk analysis, Bull. Seismol. Soc. Am., 58, no. 5, 1583–1606.

Daley, D. J., and D. Vere-Jones (eds.), 2008, Basic Theory of Random Measures and Point Processes, in *An Introduction to the Theory of Point Processes: Volume II: General Theory and Structure*, Springer, New York, NY, Probability and Its Applications, 1–75.

Di Luccio, F., R. Console, M. Imotof, and M. Murru, 1997, Analysis of short time-space range seismicity patterns in Italy, Ann. Geophys., 40, no. 4, 2, doi: 10.4401/ag-3880.

Di Stanza, A., and R. Console, 2002, Revision of the amplitude-distance relation for local magnitude estimation in Italy, Juornal Seismol., 6, 87–97.

Eaton, J. P., 1992, Determination of amplitude and duration magnitudes and site residuals from short-period seismographs in northern California, Bull. Seismol. Soc. Am., 82, no. 2, 533–579, doi: 10.1785/BSSA0820020533.

van der Elst, N. J., 2021, B-Positive : A Robust Estimator of Aftershock Magnitude Distribution in Transiently Incomplete Catalogs, J. Geophys. Res. Solid Earth, 126, no. 2, doi: 10.1029/2020JB021027.

Evison, F., and D. Rhoades, 2004, Long-term seismogenesis and self-organized criticality, Earth Planets Space, 56, no. 8, 749–760, doi: 10.1186/BF03353083.

Evison, F., and D. Rhoades, 2005, Multiple - mainshock events and long - term seismogenesis in Italy and New Zealand, N. Z. J. Geol. Geophys., 48, 523–536, doi: 0028-8306/05/4803-0523.

Falcone, G., R. Console, and M. Murru, 2010, Short-term and long-term earthquake occurrence models for Italy: ETES, ERS and LTST, Ann. Geophys., 53, no. 3, doi: 10.4401/ag-4760.

Frankel, A., 1995, Mapping Seismic Hazard in the Central and Eastern United States, 66, no. 4.

Gardner, J. K., and L. Knopoff, 1974, Is the sequence of earthquakes in Southern California, with aftershocks removed, Poissonian?, Bull. Seismol. Soc. Am., 64, no. 5, 1363–1367, doi: 10.1785/BSSA0640051363.

Gasperini, P., 2002, Local magnitude revaluation for recent Italian earthquakes (1981–1996), Juornal Seismol., 6, 503–524.

Gasperini, P., F. Bernardini, G. Valensise, and E. Boschi, 1999, Defining Seismogenic Sources from Historical Earthquake Felt Reports, Bull. Seismol. Soc. Am., 89, no. 1, 94–110.

Gasperini, P., E. Biondini, B. Lolli, A. Petruccelli, and G. Vannucci, 2021, Retrospective short-term forecasting experiment in Italy based on the occurrence of strong (fore) shocks, Geophys. J. Int., 225, no. 2, 1192–1206, doi: 10.1093/gji/ggaa592.

Gasperini, P., B. Lolli, and G. Vannucci, 2013, Empirical Calibration of Local Magnitude Data Sets Versus Moment Magnitude in Italy, Bull. Seismol. Soc. Am., 103, no. 4, 2227–2246, doi: 10.1785/0120120356.

Gasperini, P., B. Lolli, and G. Vannucci, 2016, Relative frequencies of seismic main shocks after strong shocks in Italy, Geophys. J. Int., 207, no. 1, 150–159, doi: 10.1093/gji/ggw263.

Gasperini, P., B. Lolli, G. Vannucci, and E. Boschi, 2012, A comparison of moment magnitude estimates for the European-Mediterranean and Italian regions: Comparison of moment magnitude estimates, Geophys. J. Int., 190, no. 3, 1733–1745, doi: 10.1111/j.1365-246X.2012.05575.x.

Geller, R. J., D. D. Jackson, Y. Y. Kagan, and F. Mulargia, 1997, Earthquakes Cannot Be Predicted, Science, 275, no. 5306, 1616–1616, doi: 10.1126/science.275.5306.1616.

Grandori, G., E. Guagenti, and F. Perotti, 1988, Alarm systems based on a pair of short-term earthquake precursors, Bull. Seismol. Soc. Am., 78, no. 4, 1538–1549, doi: 10.1785/BSSA0780041538.

Gulia, L., and P. Gasperini, 2021, Contamination of Frequency–Magnitude Slope (b-Value) by Quarry Blasts: An Example for Italy, Seismol. Res. Lett., 92, no. 6, 3538–3551, doi: 10.1785/0220210080.

Gulia, L., and S. Wiemer, 2019, Real-time discrimination of earthquake foreshocks and aftershocks, Nature, 574, no. 7777, 193–199, doi: 10.1038/s41586-019-1606-4.

Guo, Z., and Y. Ogata, 1997, Statistical relations between the parameters of aftershocks in time, space, and magnitude, J. Geophys. Res. Solid Earth, 102, no. B2, 2857–2873, doi: 10.1029/96JB02946.

Gutenberg, B., and C. F. Richter, 1942, Earthquake magnitude, intensity, energy, and acceleration*, Bull. Seismol. Soc. Am., 32, no. 3, 163–191, doi: 10.1785/BSSA0320030163.

Gutenberg, B., and C. F. Richter, 1956, Earthquake magnitude, intensity, energy, and acceleration (Second paper), Bull. Seismol. Soc. Am., 46, no. 2, 105–145.

Gutenberg, B., and C. F. Richter, 1944, Frequency of earthquakes in California*, Bull. Seismol. Soc. Am., 34, no. 4, 185–188, doi: 10.1785/BSSA0340040185.

Habermann, R. E., 1987, Man-made changes of seismicity rates, Bull. Seismol. Soc. Am., 77, no. 1, 141–159, doi: 10.1785/BSSA0770010141.

Habermann, R. E., 1982, Seismicity rates in the Kuriles Island arc, 1963-1979., Earthq. Predict. Res., 1, no. 1, 73–94.

Hainzl, S., 2004, Seismicity patterns of earthquake swarms due to fluid intrusion and stress triggering, Geophys. J. Int., 159, no. 3, 1090–1096, doi: 10.1111/j.1365-246X.2004.02463.x.

Hanks, T. C., and H. Kanamori, 1979, A moment magnitude scale, J. Geophys. Res. Solid Earth, 84, no. B5, 2348–2350, doi: 10.1029/JB084iB05p02348.

Herrmann, M., J. Douglas Zechar, and S. Wiemer, 2016, Communicating Time-Varying Seismic Risk during an Earthquake Sequence, Seismol. Res. Lett., 87, no. 2A, 301–312, doi: 10.1785/0220150168.

Hirano, R., 1924, An investigation in aftershocks felt at Kumagai accompanying the great Kwanto earthquake of September 1st, 1923, J. Meteorol. Soc. Jpn., 2, no. 2, 77–83.

Hutton, L. K., and D. M. Boore, 1987, The *ML* scale in Southern California, Bull. Seismol. Soc. Am., 77, no. 6, 2074–2094, doi: 10.1785/BSSA0770062074.

Hutton, K., J. Woessner, and E. Hauksson, 2010, Earthquake Monitoring in Southern California for Seventy-Seven Years (1932-2008), Bull. Seismol. Soc. Am., 100, no. 2, 423–446, doi: 10.1785/0120090130.

Jackson, D. D., and Y. Y. Kagan, 1999, Testable Earthquake Forecasts for 1999, Seismol. Res. Lett., 70, no. 4, 393–403, doi: 10.1785/gssrl.70.4.393.

Jennings, P. C., and H. Kanamori, 1983, Effect of distance on local magnitudes found from strong-motion records, Bull. Seismol. Soc. Am., 73, no. 1, 265–280, doi: 10.1785/BSSA0730010265.

Jones, L. M., 1984, Foreshocks (1966-1980) in the San Andreas system, California, Bull. Seismol. Soc. Am., 74, no. 4, 1361–1380.

Jones, L. M., 1994, Foreshocks, Aftershocks, and Earthquake Probabilities: Accounting for the Landers Earthquake, Bull. Seismol. Soc. Am., 84, no. 3, 892–899, doi: 10.1785/BSSA0840030892.

Jones, L. M., 1985, Foreshocks and time-dependent earthquake hazard assessment in southern california, Bull. Seismol. Soc. Am., 75, no. 6, 1669–1679, doi: 10.1785/BSSA0750061669.

Jones, L., and P. Molnar, 1976, Frequency of foreshocks, Nature, 262, no. 5570, 677–679, doi: 10.1038/262677a0.

Jones, L. M., and P. Molnar, 1979, Some characteristics of foreshocks and their possible relationship to earthquake prediction and premonitory slip on faults, J. Geophys. Res. Solid Earth, 84, no. B7, 3596–3608, doi: 10.1029/JB084iB07p03596.

Jordan, T. H., 2006, Earthquake Predictability, Brick by Brick, Seismol. Res. Lett., 77, no. 1, 3–6, doi: 10.1785/gssrl.77.1.3.

Jordan, T. H., 2009, Earthquake System Science: Potential for Seismic Risk Reduction, Sci. Iran., 16, no. 5, 351–366.

Jordan, T. H., Y.-T. Chen, P. Gasparini, R. Madariaga, I. Main, W. Marzocchi, G. Papadopoulos, G. Sobolev, K. Yamaoka, and J. Zschau, 2011, OPERATIONAL EARTHQUAKE FORECASTING. State of Knowledge and Guidelines for Utilization, Ann. Geophys., 54, no. 4, doi: 10.4401/ag-5350.

Jordan, T. H., and L. M. Jones, 2010, Operational Earthquake Forecasting: Some Thoughts on Why and How, Seismol. Res. Lett., 81, no. 4, 571–574, doi: 10.1785/gssrl.81.4.571.

Jordan, T. H., W. Marzocchi, A. J. Michael, and M. C. Gerstenberger, 2014, Operational Earthquake Forecasting Can Enhance Earthquake Preparedness, Seismol. Res. Lett., 85, no. 5, 955–959, doi: 10.1785/0220140143.

Kagan, Y. Y., 1997, Are earthquakes predictable?, Geophys. J. Int., 131, no. 3, 505–525, doi: 10.1111/j.1365-246X.1997.tb06595.x.

Kagan, Y. Y., 2014, Earthquakes: models, statistics, testable forecasts, John Wiley & Sons Inc, Hoboken, NJ, Statistical physics of fracture and breakdown.

Kagan, Y. Y., and L. Knopoff, 1987, Statistical Short-Term Earthquake Prediction, Science, 236, no. 4808, 1563–1567, doi: 10.1126/science.236.4808.1563.

Keilis-Borok, V., 2002, Earthquake Prediction: State-of-the-Art and Emerging Possibilities, Annu. Rev. Earth Planet. Sci., 30, no. 1, 1–33, doi: 10.1146/annurev.earth.30.100301.083856.

Knopoff, L., 1964, The statistics of earthquakes in Southern California, Bull. Seismol. Soc. Am., 54, no. 6A, 1871–1873, doi: 10.1785/BSSA05406A1871.

Lay, T., and T. Wallace, 1995, Modern global seismology, in *International Geophysics Series*, Accademic Press, San Diego, ii–iii.

Lolli, B., E. Boschi, and P. Gasperini, 2009, A comparative analysis of different models of aftershock rate decay by maximum likelihood estimation of simulated sequences, J. Geophys. Res. Solid Earth, 114, no. B1, doi: 10.1029/2008JB005614.

Lolli, B., and P. Gasperini, 2003, Aftershocks hazard in Italy Part I: Estimation of time-magnitude distribution model parameters and computation of probabilities of occurrence, J. Seismol., 7, no. 2, 235–257, doi: 10.1023/A:1023588007122.

Lolli, B., P. Gasperini, F. M. Mele, and G. Vannucci, 2015, Recalibration of the Distance Correction Term for Local Magnitude (ML) Computations in Italy, Seismol. Res. Lett., 86, no. 5, 1383–1392, doi: 10.1785/0220150020.

Lolli, B., P. Gasperini, and A. Rebez, 2018, Homogenization in Terms of Mw of Local Magnitudes of Italian Earthquakes That Occurred before 1981, Bull. Seismol. Soc. Am., 108, no. 1, 481–492, doi: 10.1785/0120170114.

Lolli, B., D. Randazzo, G. Vannucci, and P. Gasperini, 2020a, The Homogenized Instrumental Seismic Catalog (HORUS) of Italy from 1960 to Present, Seismol. Res. Lett., 91, no. 6, 3208–3222, doi: 10.1785/0220200148.

Lolli, B., D. Randazzo, G. Vannucci, and P. Gasperini, 2020b, The Homogenized Instrumental Seismic Catalog (HORUS) of Italy from 1960 to Present, Seismol. Res. Lett., 91, no. 6, 3208–3222, doi: 10.1785/0220200148.

Lombardi, A. M., and W. Marzocchi, 2010, A double-branching model applied to long-term forecasting of Italian seismicity (ML≥5.0) within the CSEP project, Ann. Geophys., 53, no. 3, doi: 10.4401/ag-4762.

Lombardi, Anna Maria, and W. Marzocchi, 2010, The ETAS model for daily forecasting of italian seismicity in the CSEP experiment, Ann. Geophys., 53, no. 3, 155–164, doi: 10.4401/ag-4848.

Marzocchi, W., I. Iervolino, M. Giorgio, and G. Falcone, 2015, When Is the Probability of a Large Earthquake Too Small?, Seismol. Res. Lett., 86, no. 6, 1674–1678, doi: 10.1785/0220150129.

Marzocchi, W., and A. M. Lombardi, 2009, Real-time forecasting following a damaging earthquake, Geophys. Res. Lett., 36, no. 21, doi: 10.1029/2009GL040233.

Marzocchi, W., A. M. Lombardi, and E. Casarotti, 2014, The Establishment of an Operational Earthquake Forecasting System in Italy, Seismol. Res. Lett., 85, no. 5, 961–969, doi: 10.1785/0220130219.

Marzocchi, W., and J. Zhuang, 2011, Statistics between mainshocks and foreshocks in Italy and Southern California, Geophys. Res. Lett., 38, no. 9, 2011GL047165, doi: 10.1029/2011GL047165.

Matthews, M. V., and P. A. Reasenberg, 1988, Statistical methods for investigating quiescence and other temporal seismicity patterns, Pure Appl. Geophys. PAGEOPH, 126, nos. 2–4, 357–372, doi: 10.1007/BF00879003.

Mogi, K., 1962, On the time distribution of aftershocks accompanying the recent major earthquakes in and near Japan, Bull Earthq Res Inst, 40, 107–124.

Mogi, K., 1989, The mechanism of the occurrence of the Matsushiro earthquake swarm in central Japan and its relation to the 1964 Niigata earthquake, Tectonophysics, 159, no. 1, 109–119, doi: 10.1016/0040-1951(89)90173-X.

Molchan, G. M., 1990, Strategies in strong earthquake prediction, Phys. Earth Planet. Inter., 61, no. 1, 84–98, doi: 10.1016/0031-9201(90)90097-H.

Molchan, G. M., 1991, Structure of optimal strategies in earthquake prediction, Tectonophysics, 193, no. 4, 267–276, doi: 10.1016/0040-1951(91)90336-Q.

Molchan, G. M., and Y. Y. Kagan, 1992, Earthquake prediction and its optimization, J. Geophys. Res., 97, no. B4, 4823, doi: 10.1029/91JB03095.

Mulargia, F., and R. Geller, 2003, Earthquake science and seismic risk reduction: proceedings of the NATO Advanced Research Workshop on ... Arbus, Sardinia, Italy, 14 - 19 October 2000, Kluwer Acad. Publ, Dordrecht, NATO science series Sub-series 4, Earth and environmental sciences 32.

Murru, M., R. Console, and G. Falcone, 2009, Real time earthquake forecasting in Italy, Tectonophysics, 470, nos. 3–4, 214–223, doi: 10.1016/j.tecto.2008.09.010.

Musmeci, F., and D. Vere-Jones, 1992, A space-time clustering model for historical earthquakes, Ann. Inst. Stat. Math., 44, no. 1, 1–11, doi: 10.1007/BF00048666.

Myung, I. J., 2003, Tutorial on maximum likelihood estimation, J. Math. Psychol., 47, no. 1, 90–100, doi: 10.1016/S0022-2496(02)00028-7.

Nandan, S., G. Ouillon, and D. Sornette, 2019, Magnitude of Earthquakes Controls the Size Distribution of Their Triggered Events, J. Geophys. Res. Solid Earth, 124, no. 3, 2762–2780, doi: 10.1029/2018JB017118.

Nelder, J. A., and R. Mead, 1965, A Simplex Method for Function Minimization, Comput. J., 7, no. 4, 308–313, doi: 10.1093/comjnl/7.4.308.

Ogata, Y., 1983a, Estimation of the parameters in the modified omori formula for aftershock frequencies by the maximum likelihood procedure., J. Phys. Earth, 31, no. 2, 115–124, doi: 10.4294/jpe1952.31.115.

Ogata, Y., 1983b, Estimation of the parameters in the modified omori formula for aftershock frequencies by the maximum likelihood procedure, J. Phys. Earth, 31, no. 2, 115–124, doi: 10.4294/jpe1952.31.115.

Ogata, Y., 1998, Space-Time Point-Process Models for Earthquake Occurrences, Ann. Inst. Stat. Math., 50, no. 2, 379–402, doi: 10.1023/A:1003403601725.

Ogata, Y., 1989, Statistical model for standard seismicity and detection of anomalies by residual analysis, Tectonophysics, 169, nos. 1–3, 159–174, doi: 10.1016/0040-1951(89)90191-1.

Ogata, Y., 1988, Statistical Models for Earthquake Occurrences and Residual Analysis for Point Processes, J. Am. Stat. Assoc., 83, no. 401, 9–27, doi: 10.1080/01621459.1988.10478560.

Ogata, Y., 1978, The asymptotic behaviour of maximum likelihood estimators for stationary point processes, Ann. Inst. Stat. Math., 30, no. 2, 243–261, doi: 10.1007/BF02480216.

Ogata, Y., L. M. Jones, and S. Toda, 2003, When and where the aftershock activity was depressed: Contrasting decay patterns of the proximate large earthquakes in southern California, J. Geophys. Res. B Solid Earth, 108, no. 6.

Ogata, Y., and J. Zhuang, 2006, Space–time ETAS models and an improved extension, Tectonophysics, 413, nos. 1–2, 13–23, doi: 10.1016/j.tecto.2005.10.016.

Omori, F., 1894, On the After-shocks of Earthquakes, Juornal Coll. Sci., 7, no. 2, 111–219.

Perry, S. et al., 2008, The ShakeOut Earthquake Scenario— A story that southern Californians are writing, Report 1324, Circular.

Rathbun, S. L., 1993, Modeling marked spatio-temporal point patterns, Bull. Int. Stat. Inst., 2, no. 55, 379–396.

Reasenberg, Paul A., 1999, Foreshock occurrence before large earthquakes, J. Geophys. Res. Solid Earth, 104, no. B3, 4755–4768, doi: 10.1029/1998JB900089.

Reasenberg, Paul A, 1999, Foreshock Occurrence Rates before Large Earthquakes Worldwide, Pure Appl Geophys, 155.

Reasenberg, P., 1985, Second-order moment of central California seismicity, 1969-1982, J. Geophys. Res. Solid Earth, 90, no. B7, 5479–5495, doi: 10.1029/JB090iB07p05479.

Reid, H. F., 1910, Reid_1910.pdf, The California Earthquake of April 18, 1906: Volume II (The Mechanics of the Earthquake), State Earthquake Investigation Comission, 192 p.

Rhoades, D. A., 2011, Application of a long-range forecasting model to earthquakes in the Japan mainland testing region, Earth Planets Space, 63, no. 3, 197–206, doi: 10.5047/eps.2010.08.002.

Rhoades, D. A., 2007, Application of the EEPAS Model to forecasting Earthquakes of moderate magnitude in Southern California, Seismol. Res. Lett., 78, no. 1, 110–115.

Rhoades, D. A., 2021, Manual for EEPAS software (EEPSOF) version 2.3w, GNS Science Internal Report, 49pp. p.

Rhoades, D. A., and F. F. Evison, 2004a, Long-range Earthquake Forecasting with Every Earthquake a Precursor According to Scale, Pure Appl. Geophys., 161, no. 1, 47–72, doi: 10.1007/s00024-003-2434-9.

Rhoades, D. A., and F. F. Evison, 2004b, Long-range earthquake forecasting with every earthquake a precursor according to scale, Pure Appl. Geophys., 161, no. 1, 47–72, doi: 10.1007/s00024-003-2434-9.

Rhoades, D. A., S. J. Rastin, and A. Christophersen, 2020, The effect of catalogue lead time on medium-term earthquake forecasting with application to New Zealand data, Entropy, 22, no. 11, 1–15, doi: 10.3390/e22111264.

Richter, C. F., 1935, An instrumental earthquake magnitude scale, Bull. Seismol. Soc. Am., 25, no. 1, 1–32, doi: 10.1785/BSSA0250010001.

Roberts, N. S., A. F. Bell, and I. G. Main, 2015, Are volcanic seismic b -values high, and if so when?, J. Volcanol. Geotherm. Res., 308, 127–141, doi: 10.1016/j.jvolgeores.2015.10.021.

Rovida, A., M. Locati, R. Camassi, and B. Lolli, 2020, The Italian earthquake catalogue CPTI15, Springer Netherlands.

Rovida, A., M. Locati, R. Camassi, B. Lolli, and P. Gasperini, 2016, Catalogo Parametrico dei Terremoti Italiani (CPTI15), versione 1.5, Istituto Nazionale di Geofisica e Vulcanologia (INGV), 4584 earthquakes p.

Rovida, A., M. Locati, R. Camassi, B. Lolli, and P. Gasperini, 2020, The Italian earthquake catalogue CPTI15, Bull. Earthq. Eng., 18, no. 7, 2953–2984, doi: 10.1007/s10518-020-00818-y.

Rovida, A., M. Locati, R. Camassi, B. Lolli, P. Gasperini, and A. Antonucci, 2022, Italian Parametric Earthquake Catalogue CPTI15, version 4.0, Ist. Naz. Geofis. E Vulcanol. INGV, doi: https://doi.org/10.13127/cpti/cpti15.4.

Rydelek, P. A., and I. S. Sacks, 1989, Testing the completeness of earthquake catalogues and the hypothesis of self-similarity, 6204, Nature, 337, no. 6204, 251–253, doi: 10.1038/337251a0.

Schorlemmer, D., A. Christophersen, A. Rovida, F. Mele, M. Stucchi, and W. Marzocchi, 2010, Setting up an earthquake forecast experiment in Italy, Ann. Geophys., 53, no. 3, doi: 10.4401/ag-4844.

Serafini, F., M. Naylor, F. Lindgren, M. J. Werner, and I. Main, 2022, Ranking earthquake forecasts using proper scoring rules: binary events in a low probability environment, Geophys. J. Int., 230, no. 2, 1419–1440, doi: 10.1093/gji/ggac124.

Shebalin, P., C. Narteau, M. Holschneider, and D. Schorlemmer, 2011, Short-Term Earthquake Forecasting Using Early Aftershock Statistics, Bull. Seismol. Soc. Am., 101, no. 1, 297–312, doi: 10.1785/0120100119.

Shebalin, P. N., C. Narteau, J. D. Zechar, and M. Holschneider, 2014, Combining earthquake forecasts using differential probability gains, Earth Planets Space, 66, no. 1, 37, doi: 10.1186/1880-5981-66-37.

Shi, Y., and B. A. Bolt, 1982, The standard error of the magnitude-frequency *b* value, Bull. Seismol. Soc. Am., 72, no. 5, 1677–1687, doi: 10.1785/BSSA0720051677.

Southern San Andreas Working Group, 1991, Short-Term Earthquake Hazard Assessment for the San Andreas Fault in Southern California, Open-File Report 91–32, U.S. Geological Survey.

Stephan Marshak, 2004, La terra, ritratto di un pianeta, Zanichelli editore S.p.A, Bologna.

van Stiphout, T., S. Wiemer, and W. Marzocchi, 2010, Are short-term evacuations warranted? Case of the 2009 L'Aquila earthquake:, Geophys. Res. Lett., 37, no. 6, 1–5, doi: 10.1029/2009GL042352.

Utsu, T., 1966, A Statistical Significance Test of the Difference in b-value between Two Earthquake Groups, J. Phys. Earth, 14, no. 2, 37–40, doi: 10.4294/jpe1952.14.37.

Utsu, T., 1961, A Statistical Study on the Occurrence of Aftershocks, Geophys. Mag., 30, 521–605.

Wang, K., C. Qi-Fu, S. Shihong, and W. Andong, 2006, Predicting the 1975 Haicheng Earthquake, Bull. Seismol. Soc. Am., 96, no. 3, 757–795, doi: 10.1785/0120050191.

Wei, W., Z. Jiang, and Y. Wu, 2015, Cognitions and questions regarding crustal deformation and location forecasts of strong earthquakes, Geod. Geodyn., 6, no. 3, 210–219, doi: 10.1016/j.geog.2015.03.006.

Wells, D. L., and K. J. Coppersmith, 1994, New Empirical Relationships among Magnitude, Rupture Length, Rupture Width, Rupture Area, and Surface Displacement, Bull. Seismol. Soc. Am., 84, no. 4, 974–1002.

Werner, M. J., and D. Sornette, 2008, Magnitude Uncertainties Impact Seismic Rate Estimates, Forecasts and Predictability Experiments, J. Geophys. Res. Solid Earth, 113, no. B8, doi: 10.1029/2007JB005427.

Werner, M. J., J. D. Zechar, W. Marzocchi, and S. Wiemer, 2010, Retrospective evaluation of the five-year and ten-year CSEP-Italy earthquake forecasts, Ann. Geophys., 53, no. 3, doi: 10.4401/ag-4840.

Wiemer, S., 2000, Minimum Magnitude of Completeness in Earthquake Catalogs: Examples from Alaska, the Western United States, and Japan, Bull. Seismol. Soc. Am., 90, no. 4, 859–869, doi: 10.1785/0119990114.

Wiemer, S., D. Giardini, D. Fäh, N. Deichmann, and S. Sellami, 2009, Probabilistic seismic hazard assessment of Switzerland: best estimates and uncertainties, J. Seismol., 13, no. 4, 449–478, doi: 10.1007/s10950-008-9138-7.

Wiemer, S., and D. Schorlemmer, 2007, ALM: An Asperity-based Likelihood Model for California, Seismol. Res. Lett., 78, no. 1, 134–140, doi: 10.1785/gssrl.78.1.134.

Woessner, J., J. L. Hardebeck, and E. Haukkson, 2010, What is an instrumental seismicity catalog?, doi: 10.5078/CORSSA-38784307.

Woessner, J., and S. Wiemer, 2005, Assessing the Quality of Earthquake Catalogues: Estimating the Magnitude of Completeness and Its Uncertainty, Bull. Seismol. Soc. Am., 95, no. 2, 684–698, doi: 10.1785/0120040007.

Woo, G., and W. Marzocchi, 2014, Operational Earthquake Forecasting and Decision-Making, in *Early Warning for Geological Disasters* F. Wenzel, and J. Zschau (Editors), Springer Berlin Heidelberg, Berlin, Heidelberg, Advanced Technologies in Earth Sciences, 353–367.

Wyss, M., 1991, Evaluation of proposed earthquake precursors, AGU, United States.

Wyss, M., 1997, Second round of evaluations of proposed earthquake precursors, Pure Appl. Geophys. PAGEOPH, 149, no. 1, 3–16, doi: 10.1007/BF00945158.

Wyss, M., 2001, Why is earthquake prediction research not progressing faster?, Tectonophysics, 338, nos. 3–4, 217–223, doi: 10.1016/S0040-1951(01)00077-4.

Wyss, M., and D. C. Booth, 1997, The IASPEI procedure for the evaluation of earthquake precursors, Geophys. J. Int., 131, no. 3, 423–424, doi: 10.1111/j.1365-246X.1997.tb06587.x.

Wyss, M., A. Hasegawa, S. Wiemer, and N. Umino, 1999, Quantitative mapping of precursory seismic quiescence before the 1989, M 7.1 off-Sanriku earthquake, Japan, Ann. Geofis., 42, no. 5, 851–869.

Zechar, J. D., M. C. Gerstenberger, and D. A. Rhoades, 2010, Likelihood-Based Tests for Evaluating Space-Rate-Magnitude Earthquake Forecasts, Bull. Seismol. Soc. Am., 100, no. 3, 1184–1195, doi: 10.1785/0120090192.

Zechar, J. Douglas, M. C. Gerstenberger, and D. A. Rhoades, 2010, Likelihood-based tests for evaluating space-rate-magnitude earthquake forecasts, Bull. Seismol. Soc. Am., 100, no. 3, 1184–1195, doi: 10.1785/0120090192.

Zechar, J. D., and T. H. Jordan, 2008, Testing alarm-based earthquake predictions, Geophys. J. Int., 172, no. 2, 715–724, doi: 10.1111/j.1365-246X.2007.03676.x.

Zechar, J. D., and T. H. Jordan, 2010, The Area Skill Score Statistic for Evaluating Earthquake Predictability Experiments, Pure Appl. Geophys., 167, nos. 8–9, 893–906, doi: 10.1007/s00024-010-0086-0.

Zechar, J. D., D. Schorlemmer, M. Liukis, J. Yu, F. Euchner, P. J. Maechling, and T. H. Jordan, 2009, The Collaboratory for the Study of Earthquake Predictability perspective on computational earthquake science, Concurr. Comput. Pract. Exp., 22, no. 12, 1836–1847, doi: 10.1002/cpe.1519.

Zechar, J. D., and J. Zhuang, 2014, A parimutuel gambling perspective to compare probabilistic seismicity forecasts, Geophys. J. Int., 199, no. 1, 60–68, doi: 10.1093/gji/ggu137.

Zhuang, J., 2005, A study on the background and clustering seismicity in the Taiwan region by using point process models, J. Geophys. Res., 110, no. B5, B05S18, doi: 10.1029/2004JB003157.

Zhuang, J., 2010, Gambling scores for earthquake predictions and forecasts, Geophys. J. Int., 181, no. 1, 382–390, doi: 10.1111/j.1365-246X.2010.04496.x.

Zhuang, J., M. Murru, G. Falcone, and Y. Guo, 2019, An extensive study of clustering features of seismicity in Italy from 2005 to 2016, Geophys. J. Int., 216, no. 1, 302–318, doi: 10.1093/gji/ggy428.

Zhuang, J., Y. Ogata, and D. Vere-Jones, 2004, Analyzing earthquake clustering features by using stochastic reconstruction: RECONSTRUCTION OF CLUSTERING FEATURES, J. Geophys. Res. Solid Earth, 109, no. B5, doi: 10.1029/2003JB002879.

Zhuang, J., Y. Ogata, and D. Vere-Jones, 2002, Stochastic Declustering of Space-Time Earthquake Occurrences, J. Am. Stat. Assoc., 97, no. 458, 369–380, doi: 10.1198/016214502760046925.

Zhuang, J., M. J. Werner, S. Zhou, S. Hainzl, and D. Harte, 2012, Basic models of seismicity: temporal models, doi: 10.5078/CORSSA-79905851.

Zhuang, J., M. J. Werner, S. Zhou, D. Harte, and S. Hainzl, 2011, Basic models of seismicity: spatiotemporal models, Community Online Resour. Stat. Seism. Anal., doi: 10.5078/CORSSA-07487583.